Pharmakokinetische Charakterisierung D-enantiomerer Peptide zur Therapie der Alzheimer'schen Demenz

Inaugural-Dissertation

zur Erlangung des Doktorgrades
der Mathematisch-Naturwissenschaftlichen Fakultät
der Heinrich-Heine-Universität Düsseldorf

vorgelegt von

Anna Elena Schartmann
aus Stolberg Rhld.

Düsseldorf, Januar 2018

Aus dem Institut für Physikalische Biologie
der Heinrich-Heine-Universität Düsseldorf

Gedruckt mit der Genehmigung der
Mathematisch-Naturwissenschaftlichen Fakultät der
Heinrich-Heine-Universität Düsseldorf

1. Berichterstatter:	Prof. Dr. Dieter Willbold
2. Berichterstatter:	Prof. Dr. Karl-Josef Langen
3. Berichterstatter:	Prof. Dr. Peter Bayer
Tag der mündlichen Prüfung:	28.03.2018

I. Eidesstattliche Erklärung

Hiermit erkläre ich an Eides statt, dass ich die vorliegende Dissertation selbständig verfasst und keine anderen als die von mir angegebenen Quellen und Hilfsmittel verwendet und Zitate kenntlich gemacht habe.

Ferner erkläre ich, dass ich in keinem anderen Dissertationsverfahren mit oder ohne Erfolg versucht habe, diese Dissertation einzureichen.

Gesundheit ist nicht alles, aber ohne Gesundheit ist alles nichts.

Arthur Schopenhauer (1788-1860)

II. Danksagung

Bedanken möchte ich mich zunächst bei Prof. Dieter Willbold für die Möglichkeit, meine Promotion an seinen Instituten in Düsseldorf und Jülich durchführen zu dürfen und für seine bereichernde Betreuung meiner Projekte. Das Ziel, eine innovative Therapiestrategie gegen eine solch schwerwiegende Erkrankung wie die Alzheimer'sche Demenz zu optimieren, war sehr motivierend. Durch die zahlreichen Gelegenheiten, mit Wissenschaftlern, auch vieler anderer Fachrichtungen, zusammen zu arbeiten, habe ich in dieser Zeit viel dazulernen dürfen. Auch die Optionen, eigene Ergebnisse auf internationalen Konferenzen mit Wissenschaftlern aus aller Welt zu diskutieren, haben viele interessante Ideen hervorgebracht.

Meinem Zweitbetreuer Prof. Karl-Josef Langen möchte ich ebenfalls für die gute Zusammenarbeit und die Möglichkeiten danken, unzählige Experimente komplikationslos in seinem Institut durchführen zu dürfen.

Ein besonderer Dank geht an Dr. Antje Willuweit und Dr. Janine Kutzsche für ihre unermüdliche Betreuung, ihre vielen sehr hilfreichen Ratschläge, ihre guten Ideen und den herzlichen, persönlichen Kontakt.

Weiterhin bedanken möchte ich mich bei den vielen lieben Kolleginnen und Kollegen in Jülich und Düsseldorf für ihre Unterstützung sowie die schöne und häufig zum Glück auch sehr lustige Zusammenarbeit: Dr. Anne Elfgen, Dr. Tamar Ziehm, Markus Tusche, Dominik Honold, Julia Post-Schulz, Dr. Franziska Weirich, Michelle Hupert, Dr. Bea Santiago-Schübel, Alexandra Drechsel, Bettina Kass, Dr. Leonie Leithold, Dr. Nan Jiang, Dr. Oleksandr Brener, Dr. Lothar Gremer, Dr. Christian Zafiu, Dr. Andreas Kulawik, Dr. Dagmar Jürgens, Anne Cousin, Volker Söhnitz (für die geduldige technische Unterstützung), Caroline Folz, Michael Schöneck, Nicole Niemietz, Verena Graf, Dennis Oliveira, Dr. Carina Stegmayer und Arbia Khezami. Ein ganz besonderer Dank geht an Sarah Schemmert („Team ElSa") für die in vielerlei Hinsicht turbulenten 3,25 Jahre, in denen wir gemeinsam (der ein oder andere kann uns vermutlich immer noch nicht auseinander halten) so viel erlebt, durchgestanden, geschafft, neu gemacht, herausgefunden, optimiert, … und vor allem gelacht haben – es war mir eine Ehre und ein großer Spaß.

Vielen Dank auch an das Team des Tierhauses für ihre fortwährende tatkräftige Unterstützung bei all unseren Studien.

Vor allem möchte ich mich jedoch ganz besonders herzlich bei meiner Familie und meinen Freunden für ihre tatkräftige Unterstützung, Motivation und das große Verständnis sowie für ihre bereichernde Begleitung auf dem Weg hierher bedanken.

III. Inhaltsverzeichnis

III. Inhaltsverzeichnis

III. Inhaltsverzeichnis

IV. Publikationen & Konferenzbeiträge

a) Publikationen

2015:

- Jiang N, Leithold LHE, Post J, Ziehm T, Mauler J, Gremer L, Cremer M, **Schartmann E**, Shah NJ, Kutzsche J, Langen KJ, Breitkreutz J, Willbold D, Willuweit A (2015) Preclinical Pharmacokinetic Studies of the Tritium-Labelled D-Enantiomeric Peptide D3 Developed for the Treatment of Alzheimer's Disease. *PLoS One* **10**, e0128553.

2016:

- Leithold LHE, Jiang N, Post J, Ziehm T, **Schartmann E**, Kutzsche J, Shah NJ, Breitkreutz J, Langen KJ, Willuweit A, Willbold D (2016) Pharmacokinetic Properties of a Novel D-Peptide Developed to be Therapeutically Active Against Toxic beta-Amyloid Oligomers. *Pharm Res* **33**, 328-336.

- Leithold LHE, Jiang N, Post J, Niemietz N, **Schartmann E**, Ziehm T, Kutzsche J, Shah NJ, Breitkreutz J, Langen KJ, Willuweit A, Willbold D (2016) Pharmacokinetic properties of tandem D-peptides designed for treatment of Alzheimer's disease. *Eur J Pharm Sci* **89**, 31-38.

- Jiang N, Frenzel D, **Schartmann E**, van Groen T, Kadish I, Shah NJ, Langen KJ, Willbold D, Willuweit A (2016) Blood-brain barrier penetration of an Aβ-targeted, arginine-rich, D-enantiomeric peptide. *Biochim Biophys Acta* **1858**, 2717-2724.

2017:

- van Groen T, Schemmert S, Brener O, Gremer L, Ziehm T, Tusche M, Nagel-Steger L, Kadish I, **Schartmann E**, Elfgen A, Jurgens D, Willuweit A, Kutzsche J, Willbold D (2017) The Aβ oligomer eliminating D-enantiomeric peptide RD2 improves cognition without changing plaque pathology. *Sci Rep* 7, 16275.
- **Schartmann E**, Schemmert S, Ziehm T, Leithold LHE, Jiang N, Tusche M, Jon Shah N, Langen KJ, Kutzsche J, Willbold D, Willuweit A (2017) Comparison of

blood-brain barrier penetration efficiencies between linear and cyclic all-D-enantiomeric peptides developed for the treatment of Alzheimer's disease. *Eur J Pharm Sci* **114**, 93-102.

- Hupert M, Elfgen A, **Schartmann E**, Schemmert S, Buscher B, Kutzsche J, Willbold D, Santiago-Schubel B (2017) Development and validation of an UHPLC-ESI-QTOF-MS method for quantification of the highly hydrophilic amyloid-beta oligomer eliminating all-D-enantiomeric peptide RD2 in mouse plasma. *J Chromatogr B Analyt Technol Biomed Life Sci* **1073**, 123-129.

2018:

- Schemmert S, **Schartmann E**, Zafiu C, Kass B, Hartwig S, Lehr S, Bannach O, Langen KJ, Shah NJ, Kutzsche J, Willuweit A, Willbold D (2018, eingereicht) Aβ oligomer elimination restores cognition in transgenic Alzheimer's mice with full-blown pathology. *EMBO Rep, eingereicht*

- **Schartmann E**, Schemmert S, Niemietz N, Honold D, Ziehm T, Tusche M, Elfgen A, Gering I, Brener O, Shah NJ, Langen KJ, Kutzsche J, Willbold D, Willuweit A (2018, eingereicht) *In vitro* potency and preclinical pharmacokinetic comparison of all-D-enantiomeric peptides developed for the treatment of Alzheimer's disease. *J Alzheimers Dis, eingereicht*

IV. Publikationen & Konferenzbeiträge

b) Konferenzbeiträge

2016:

- **Schartmann E**, Schemmert S, Ziehm T, Leithold LHE, Jiang N, Kutzsche J, Willuweit A, Willbold D
  Raising available brain concentrations of a potential Alzheimer's disease drug candidate by peptide cyclization
  Alzheimer's Association International Conference (AAIC), Toronto 2016

- Schemmert S, **Schartmann E**, Willuweit A, Kutzsche J, Willbold D
  Therapeutic Treatment with a D-enantiomeric peptide improves cognitive impairment in aged APPswe/PS1 transgenic mice
  Alzheimer's Association International Conference (AAIC), Toronto 2016

2017:

- **Schartmann E**, Schemmert S, Ziehm T, Leithold LHE, Jiang N, Kutzsche J, Willuweit A, Willbold D
  The cyclized version of an all-D-enantiomeric peptide AD drug candidate reaches the brain more efficiently than its linear version
  The 13th International Conference on Alzheimer's & Parkinson's Diseases and Related Neurological Disorders (ADPD), Vienna 2017

- Schemmert S, **Schartmann E**, Willuweit A, Kutzsche J, Willbold D
  Therapeutic Treatment with a D-enantiomeric peptide improves cognitive impairment in aged APPswe/PS1 transgenic mice
  The 13th International Conference on Alzheimer's & Parkinson's Diseases and Related Neurological Disorders (ADPD), Vienna 2017

- **Schartmann E**, Schemmert S, Ziehm T, Leithold LHE, Jiang N, Kutzsche J, Willuweit A, Willbold D
  Cyclic D-enantiomeric peptide targeting Amyloid-beta in Alzheimer's disease
  Alzheimer's Association International Conference (AAIC), London 2017

IV. Publikationen & Konferenzbeiträge

- Schemmert S, **Schartmann E**, Willuweit A, Kutzsche J, Willbold D
  Treatment with an all-D-enantiomeric peptide improves cognitive and motoric impairment in two different Alzheimer mouse models
  Alzheimer's Association International Conference (AAIC), London 2017

- **Schartmann E**, Schemmert S, Ziehm T, Leithold LHE, Jiang N, Langen KJ, Kutzsche J, Willbold D, Willuweit A
  Comparison of blood-brain barrier penetration efficiencies between linear and cyclic all-D-enantiomeric peptides developed for the treatment of Alzheimer's disease
  Düsseldorf-Jülich Symposium on Neurodegenerative Diseases: Formation, aggregation and propagation of amyloids, Düsseldorf 2017

- Schemmert S, **Schartmann E**, Ziehm T, Kutzsche J, Kass B, Zafiu C, Willuweit A, Willbold D
  Treatment with the all-D-enantiomeric peptide RD2 improves cognitive and motor impairment in two different Alzheimer's disease mouse models
  Düsseldorf-Jülich Symposium on Neurodegenerative Diseases: Formation, aggregation and propagation of amyloids, Düsseldorf 2017

V. Abbildungs- und Tabellenverzeichnis

VI. Abkürzungsverzeichnis

%ID ..... *prozentualer Anteil der injizierten Dosis*
ABC ..... *ATP binding cassette*
AD ..... *Alzheimer'sche Demenz*
AICD ..... *APP intracellular domain*
AKH ..... *Amyloid Kaskaden Hypothese*
Apoε4 ..... *Apolipoprotein E4*
APP ..... *Amyloid Precursor Protein*
APP_{SL} ..... *transgene Mäuse, die das humane APP-Gen mit der Schweden- und der London-Mutation exprimieren*
AS ..... *Aminosäure*
AUC ..... *area under the curve*
AUMC ..... *Fläche unter der 1. Moment-Kurve*
Aβ ..... *Amyloid β*
BACE1 ..... *β-Sekretase*
BHS ..... *Blut-Hirn-Schranke*, *Blut-Hirn-Schranke*
c ..... *Plasmakonzentration*
CAA ..... *Cerebrale Amyloidangiopathie*
CBF ..... *muriner cerebraler Blutfluss*
CDK5 ..... *Cyclin-abhängige Kinase 5*
CL ..... *Clearance*
c_{max} ..... *Konzentrationsmaximum*
D ..... *Dosis*
D-Peptid ..... *D-enantiomeres Peptid*
F ..... *Bioverfügbarkeit*
fAD ..... *familiäre AD*
GSK3β ..... *Glykogen Synthase Kinase 3β*
HIV-1 Tat ..... *Humanen Immundefizienz-Virus Typ 1 Transkriptions-Transaktivator*
i.p. ..... *intraperitoneal*
K_D ..... *Dissoziationskoeffizient*
K_{in} ..... *einseitige Zuflussgeschwindigkeitskonstante*
logBB Wert ..... *Blut-Gehirn-Gleichgewichtsverteilung*
LRP1 ..... *Low Density Lipoprotein Receptor-related Protein 1*
MAP ..... *Mikrotubuli-assoziiertes Protein*
MIPD ..... *Mirror-Image Phage Display*
MRI ..... *Magnetresonanztomographie*
MRT ..... *mittlere Verweildauer*
MTT ..... *3-(4,5-Dimethylthiazol-2-yl)-2,5-diphenyltetrazoliumbromid*
NFT ..... *neurofibrillary tangles*
NMDA ..... *N-Methyl-D-Aspartat*
P ..... *Permeabilität*
p.o. ..... *per oral*
$pEA\beta_{3-42}$ ..... *Pyroglutamat-Aβ*
PET ..... *Positronenemissionstomographie*
Plaques ..... *Aβ Proteinablagerungen*
PS ..... *Permeability surface-area product*
PSD ..... *Postsynaptische Dichte*
PSEN1 ..... *Presenilin 1*

VI. Abkürzungsverzeichnis

PSEN2 ..... *Presenilin 2*
QIAD ..... *quantitative determination of interference with Aβ aggregate size distribution*
S ..... *Kapillar-Oberfläche*
sAD ..... *sporadische Alzheimer'sche Demenz*
sFIDA ..... *surface fluorescence intensity distribution anaylsis*
SPR ..... *Oberflächenresonanzspektroskopie*
t ..... *Zeit*
$t_{1/2}$ ..... *Eliminationshalbwertszeit*
ThT ..... *Thioflavin T*
t_{max} ..... *Zeit bis zum Erreichen des Konzentrationsmaximums*
V_0 ..... *intravaskuläres Volumen*
V_i ..... *initiales Verteilungsvolumen*
ZNS ..... *zentrales Nervensystem*
λ_z ..... terminale *Eliminationskonstante*

VII. Kurzfassung

Die Alzheimer'sche Demenz ist eine bislang unheilbare, progrediente neurodegenerative Erkrankung, die innerhalb weniger Jahre nach Ausbruch der ersten Symptome zum Tod führt. Sie ist die häufigste Form der Demenz und bis 2050 wird mit weltweit über 100 Millionen Patienten gerechnet. Die beiden pathologischen Hauptmerkmale der Erkrankung sind neurotoxische Proteinablagerungen im Gehirn: extrazelluläre Amyloid β (Aβ) Protein-Ablagerungen und intrazelluläre hyperphosphorylierte Tau Protein-Aggregate.

Ein aktueller therapeutischer Ansatz ist die Entwicklung D-enantiomerer Peptide, die die als besonders toxisch geltenden Aβ-Oligomere spezifisch und direkt eliminieren, um so deren Neurotoxizität zu verringern. Die Leitstruktur dieser Substanzklasse ist das aus 12 D-enantiomeren Aminosäure-Resten bestehende Peptid D3, dessen therapeutische Aktivität bereits in zahlreichen Studien in transgenen Mausmodellen der Alzheimer'schen Demenz bestätigt wurde. Zur D3-Optimierung wurden zahlreiche Derivate entwickelt. Die Tandem-Peptide RD2D3 und D3D3 bestehen beispielsweise aus 24 Aminosäure-Resten und zeigen *in vitro* hervorragendes Aβ-Oligomer-Eliminierungs-Potenzial, weisen jedoch unvorteilhafte pharmakokinetische Eigenschaften auf.

In dieser Arbeit wurde gezeigt, dass die pharmakokinetischen Eigenschaften der Tandem-Peptide, v.a. im Hinblick auf deren Blut-Hirn-Schranken (BHS)-Gängigkeit, durch N- zu C-terminale Zyklisierung effizienter gestaltet werden. Die Untersuchung verschiedener linearer D3-Derivate (D3, RD2D3, D3D3) und ihrer zyklischen Äquivalente (cD3r, cRD2D3, cD3D3) in Wildtyp-Mäusen zeigte, dass die Zyklischen, bei gleicher Plasma-Konzentration, deutlich höhere Gehirn-Konzentrationen aufwiesen als die Linearen. cRD2D3 wurde als D3-Derivat mit der effizientesten BHS-Gängigkeit selektiert und wies eine hohe proteolytische Stabilität sowie vorteilhafte pharmakokinetische Eigenschaften auf. Seine BHS-Durchlässigkeits-Parameter lagen in derselben Größenordnung wie die eines Heptapeptids, das als Positivkontrolle für BHS-Permeabilitäts-Studien in der Literatur beschrieben wird. Exemplarisch wurde für vier D3-Derivate gezeigt, dass die D-Peptid-Konzentrations-Zeit-Verläufe in Gehirn und CSF direkt korrelieren, während die Konzentrationen in Plasma und Gehirn bzw. CSF erst nach ca. 24 h ähnliche Werte annehmen.

Bei der Untersuchung von ANK6, eines *in vitro* optimierten D3-Derivats, das aus anderen Aminosäure-Resten als D3 besteht, und zwei seiner Derivate wurde erneut gezeigt, dass das *in vitro* Aβ-Oligomer-Eliminierungs-Potenzial für Tandem-Peptide (tANK6) größer ist als für die Einzel-Peptide, wobei das zyklische Derivat (cANK6r) ebenfalls hervorragende *in vitro* Eigenschaften aufwies. Auch die pharmakokinetischen Eigenschaften waren für die ANK6-Derivate effizienter als für das ANK6, wobei diese, v.a. in den nach oraler Gabe erreichten Plasma- und Gehirn-Konzentrationen, nicht mit denen der direkten D3-Derivate, RD2, cRD2D3 etc. mithalten konnten.

VIII. Abstract

Alzheimer's disease is a still incurable, progressive neurodegenerative disease causing death within a few years after symptom onset. It is the most common form of dementia and in 2050 more than 100 million Alzheimer's disease patients are expected. The two hallmarks of the disease are neurotoxic protein deposits in the brain: extracellular plaques consisting of amyloid β proteins, and intracellular tangles consisting of hyperphosphorylated Tau proteins.

One current therapeutic approach is the development of D-enantiomeric peptides that specifically and directly eliminate the, considered to be most neurotoxic, amyloid β oligomers to reduce their toxicity. The lead compound is named D3 and consists of 12 D-enantiomeric amino acid residues. Its therapeutic activity has already been confirmed in numerous studies in transgenic Alzheimer's disease mouse models. To optimize D3, several derivatives have been developed. The tandem D-peptides RD2D3 and D3D3 e.g. consist of 24 amino acid residues and show excellent amyloid β oligomer eliminating potential but only have disadvantageous pharmacokinetic characteristics.

In this work it could be shown that the tandem D-peptides' pharmacokinetic characteristics, especially with regard to their ability to permeate the blood-brain barrier (BBB), were enhanced by N- to C-terminal cyclization. Investigation of several linear D3-derivatives (D3, RD2D3, D3D3) and their cyclic equivalents (cD3r, cRD2D3, cD3D3) in wildtype mice showed that the cyclic D-peptides reached remarkably higher brain levels as compared to their linear equivalents, although their plasma levels were similar. cRD2D3 was selected to be the D3-derivative with the most efficient BBB permeability. It revealed high proteolytic stability, and advantageous pharmacokinetic characteristics. Its BBB permeability parameters were in the same order of magnitude as those of a heptapeptide that is described as positive control in literature. It could be shown exemplarily for four D3-derivatives that the D-peptide concentration-time curves in brain and CSF directly correlate while levels in plasma and brain respectively plasma and CSF only have similar values 24 h after administration.

Investigation of ANK6, an *in vitro* optimized D3-derivative consisting of different amino acid residues as compared to D3, and of two of its derivatives once again revealed that the tandem D-peptides' (tANK6) amyloid β oligomer elimination potential is more efficient than that of the single peptides, whereby the cyclic derivative (cANK6r) also shows excellent *in vitro* characteristics. The pharmacokinetic characteristics of the ANK6-derivatives were more favorable than those of ANK6. Still, plasma and brain levels, especially after oral administration, were remarkably lower than those of the direct D3-derivatives, e.g. RD2, cRD2D3.

1 Einleitung

1.1 Alzheimer'sche Demenz (AD)

Vor 110 Jahren stellte Alois Alzheimer bei seiner inzwischen weltberühmten, damals 51-jährigen Patientin Auguste Deter eine Persönlichkeitsveränderung fest, die mit zunehmendem Alter weiter fortschritt. Von anfänglichen „Eifersuchtsideen gegen den Mann", „Gedächtnisschwäche", absonderlichen Verhaltensweisen sowie von „zeitlich(er) und örtlich(er Desorientierung)" war in Alzheimers Krankheitsbeschreibung die Rede [1]. Vier Jahre nach Ausbruch der Erkrankung verstarb Auguste Deter in einer Frankfurter Psychiatrie, nachdem sie dort bettlägerig, inkontinent und wund gelegen war. Da ihm die Ursache ihres außergewöhnlichen Verhaltens unerklärlich war, untersuchte Alzheimer nach dem Tod der Patientin ihr Gehirn und diagnostizierte schon damals eben jene morphologischen Veränderungen, die noch heute als typisch für Patienten mit Alzheimer'scher Demenz (AD) gelten: Atrophie des Gehirngewebes, Anreicherungen intrazellulärer neurofibrillärer Bündel sowie extrazellulärer Plaques und eine Zunahme von Entzündungszellen [1, 2].

Die AD ist eine neurodegenerative Erkrankung, die durch Veränderungen im Gehirn mit einer allmählich fortschreitenden kognitiven Beeinträchtigung der Patienten einhergeht und die das alltägliche Leben nachhaltig negativ beeinflusst [3]. Sie ist mit ca. 60 % die häufigste Form aller Demenz-Erkrankungen [4]. Derzeit sind weltweit 47 Millionen Menschen erkrankt [5]. Prognosen der Vereinten Nationen zufolge steigt diese Zahl bis 2050 auf 106,8 Millionen an [6]. Hochrechnungen der „Alzheimer's Association" zufolge werden 2050 in den USA Kosten in Höhe von 1 Billion US$ für die Therapie und Versorgung aller über 65-jährigen AD-Patienten anfallen [7].

Während die Erkrankung einige Jahre bis Jahrzehnte symptomfrei und dadurch in der Regel unerkannt verläuft („Präklinischer Verlauf"), leiden die Patienten nach Ausbruch der Symptomatik zunächst an leichteren kognitiven und olfaktorischen Beeinträchtigungen, die im Laufe der Zeit zunehmen („moderate Demenz") und schließlich so weit führen, dass der Patient nicht mehr ohne Betreuung leben kann („schwere Demenz") [8-10]. Oftmals leiden die Patienten vor allem im fortgeschrittenen Stadium der Erkrankung zusätzlich an psychischen (Depression, Aggressivität etc.) und neurologischen (Sprachprobleme, Inkontinenz) Störungen. Die gesamte Symptomatik führt oft zur Bettlägerigkeit der Patienten und schreitet bis zum Tode der Patienten voran. Durch den stark geschwächten Allgemeinzustand wird dieser häufig durch Lungenentzündungen, kardiovaskuläre Ereignisse o.ä. ausgelöst [11].

Betrachtet man die 110 Jahre alten Beschreibungen Alois Alzheimers, wird deutlich, dass der AD-Krankheitsverlauf genauso noch heute in Erscheinung tritt, ohne dass es eine kurative Therapiemöglichkeit gibt. Dieser Umstand unterstreicht die Dringlichkeit der Entwicklung einer kausalen Therapie gegen die AD.

1.2 Formen der AD: sporadische und familiäre AD

1.2.1 Sporadische AD

Da die AD einen äußerst hohen Leidensdruck für die Patienten und deren Umfeld sowie enorm hohe Kosten für die Gesundheitssysteme erzeugt, forschen Wissenschaftler weltweit seit Jahrzehnten an Therapie-Optionen gegen das Fortschreiten bzw. den Ausbruch der Erkrankung. Ein großes Problem ist in diesem Zusammenhang, dass die Ursache der sog. **sporadischen AD** (sAD, > 95 % aller AD-Patienten), die in der Regel erst in einem Alter von über 65 Jahren auftritt (late-onset AD), bislang ungeklärt ist. Folglich ist es schwierig, geeignete Therapie-Ansätze zu entwickeln, die die Erkrankung kausal bekämpfen. Es ist jedoch bekannt, dass es Faktoren gibt, die das Risiko, an sAD zu erkranken, deutlich erhöhen. Hierzu gehören beispielsweise ein hohes Lebensalter, weibliches Geschlecht, Apolipoprotein E4 (Apoε4)-Polymorphismus, Hyperhomocysteinämie, niedriger Bildungsstand, geringe geistige und körperliche Aktivität im fortgeschrittenen Alter, Hypercholesterinämie, Bluthochdruck, Arteriosklerose, Metabolisches Syndrom, Adipositas und Kopfverletzungen [4, 12-18].

Der genaue Zusammenhang einiger der erwähnten Risikofaktoren und der tatsächlichen AD-Erkrankung ist noch nicht final geklärt. Es kann einerseits einen direkten Zusammenhang geben, bei dem die Bildung der im Folgenden noch genauer beschriebenen neurotoxischen Amyloid β (Aβ)-Proteinablagerungen (Plaques) und die Hyperphosphorylierung des Tau-Proteins, beides Hauptmerkmale der AD, beeinflusst werden [2]. Andererseits kann das erhöhte Risiko auch in einem indirekten Zusammenhang mit der Erkrankung stehen, wenn beispielsweise die Durchblutung des Gehirns negativ beeinflusst wird und es infolgedessen zu kognitiven Beeinträchtigungen kommt [4].

1.2.2 Familiäre AD

Im Gegensatz zur sAD tritt die auf vererbten Gendefekten beruhende **familiäre AD (fAD)** (weniger als 1 bis 5 % aller AD-Fälle) häufig schon ab einem Alter von etwa 50 Jahren oder früher auf (early-onset) [12]. Der fAD liegen hauptsächlich Mutationen in drei Genen (dem Amyloid Precursor Protein (APP)-Gen, dem Presenilin 1 (PSEN1)-Gen und dem Presenilin 2 (PSEN2)-Gen) zu Grunde, sodass die fAD an weiter vererbt werden kann. Als Folge dieser Mutationen kommt es zu einer vermehrten Bildung neurotoxischer Aβ-Proteinspezies im

Gehirn, die wiederum in direkten Zusammenhang mit dem Ausbruch der AD gebracht werden können (s. 1.4) [19-21].

1.3 Zugelassene Wirkstoffe zur symptomatischen AD-Therapie

Momentan gibt es nur zwei Wirkstoffklassen, die für die Behandlung der AD zugelassen sind. Mit ihrer Hilfe kann der progrediente neurodegenerative Verlauf der Erkrankung bestenfalls kurze Zeit herausgezögert werden, die Behandlung ist jedoch nicht ursächlich, sodass die Patienten nicht geheilt oder der Krankheitsfortschritt gebremst werden kann.

Patienten mit milder bis moderater AD werden mit Wirkstoffen aus der Klasse der **Acetylcholinesterase-Inhibitoren** (Donezepil, Galantamin und Rivastigmin) behandelt [22]. Normalerweise ist die Konzentration des Neurotransmitters Acetylcholin bei AD-Patienten durch die geringere Anzahl funktionstüchtiger Nervenzellen herabgesetzt, weshalb die Signalweiterleitung innerhalb des Gehirns vermindert wird. Durch Behandlung mit Acetylcholinesterase-Inhibitoren wird weniger Acetylcholin abgebaut, sodass mehr zur Signalweiterleitung im Gehirn der Patienten bleibt. Dieser Umstand sorgt kurzfristig zu einer geringen Steigerung der geistigen Leistungsfähigkeit [23].

Patienten mit moderater bis schwerer AD bekommen einen **N-Methyl-D-Aspartat (NMDA)-Rezeptor-Antagonisten** (Memantin). Eine Behandlung mit Memantin sorgt für einen verminderten Einstrom des exzitatorischen Neurotransmitters Glutamat in die Neuronen. Da auch dieser Glutamat-Einstrom neurotoxisch sein kann, führt eine Memantin-Behandlung zu einer kurzzeitigen Verzögerung der AD-Symptomatik [24].

Auch eine **Kombinationstherapie** aus einem Acetylcholinesterase-Inhibitor und einem NMDA-Antagonisten ist zur Behandlung der schweren AD geeignet [25]. Der Behandlungserfolg ist allerdings bei beiden Wirkstoffklassen nur von kurzer Dauer (ca. 9 bis 12 Monate) und geht z.T. mit erheblichen unerwünschten Arzneimittelwirkungen im Zusammenhang mit Funktionen des vegetativen Nervensystems einher [26], was die Dringlichkeit der Entwicklung eines neuen Therapieansatzes einmal mehr unterstreicht.

1.4 Pathophysiologie der AD

1.4.1 Hauptmerkmale der AD: Amyloid β und Tau

Um die Wirkansätze, aktuell in der Entwicklung befindlicher AD-Therapeutika, besser erläutern zu können, ist eine genauere Betrachtung des pathophysiologischen Verlaufs der Erkrankung hilfreich.

1.4.1.1 Amyloid β

Eines der beiden Hauptmerkmale der AD sind die eingangs erwähnten **neurotoxischen Aβ-Proteinspezies und Aβ-Aggregate** [27]. Sie sind größtenteils extrazellulär im Gehirn der AD-Patienten zu finden und entstehen sowohl bei der sAD als auch bei der fAD [3]. Bei Bildung des Aβ-Proteins aus seinem Vorläuferprotein APP, die in einem geringeren Ausmaß als bei AD-Patienten auch im gesunden Organismus stattfindet, können unterschiedlich lange Aβ-Moleküle aus i.d.R. 39 bis 43 Aminosäuren (AS) entstehen (z.B. 40 AS langes $Aβ_{1-40}$ und 42 AS langes $Aβ_{1-42}$) [15, 28]. Derzeit gelten **$Aβ_{1-42}$** (42 AS langes Aβ) und posttranslational, N-terminal modifiziertes Pyroglutamat-Aβ (**$pEAβ_{3-42}$**) aufgrund ihrer hohen Aggregationsneigung als toxischste Aβ-Varianten. Die N-terminale Modifikation des $pEAβ_{3-42}$ führt zu einer Zyklisierung des Glutamats an Position 3 oder 11 der Aβ-AS-Sequenz, welche mit einer erhöhten Tendenz zur β-Faltblatt-Struktur-Bildung in Verbindung gebracht wird [29]. **Aβ-Monomere, -Oligomere, -Protofibrillen, unlösliche Fibrillen und -Plaques** stehen in einem dynamischen Gleichgewicht miteinander (Abbildung 1) [15, 30].

Derzeit wird angenommen, dass die Bildung des Aβ-Proteins (auch Aβ-Prozessierung) folgendermaßen abläuft: Nach Proteinbiosynthese des auf **Chromosom 21 codierten APP-Gens** im Golgi-Apparat, werden die 753 AS langen Proteine in Endosomen oder an die Zelloberfläche transportiert. Den Großteil des Proteins stellt die N-terminale Ektodomäne dar. Sowohl in den Endosomen als auch an der Zelloberfläche wird APP mit unterschiedlichen Sekretasen gespalten. Auf dem **nicht-amyloidogenen Weg** wird APP mit der α-Sekretase inmitten der Aβ-AS-Sequenz gespalten, sodass im weiteren Verlauf der Prozessierung kein Aβ entstehen kann. Auf dem **amyloidogenen Weg**, wird APP durch die β-Sekretase (β-site of APP cleaving enzyme, BACE1) direkt oberhalb der N-terminalen Aβ-Sequenz gespalten, sodass im nächsten Schritt, durch Spaltung der γ-Sekretase am C-terminalen Ende der Aβ-Sequenz, **Aβ** entsteht. Findet die Spaltung des transmembranen Proteins an der Zelloberfläche statt, wird Aβ direkt in den Extrazellularraum freigegeben. Nach Prozessierung in den Endosomen verschmelzen diese im Anschluss mit der Zellmembran und sezernieren Aβ ebenfalls in den Extrazellularraum. Welche Aβ-Spezies (länge der AS-Sequenz) bei der Prozessierung entsteht, hängt davon ab, wo die γ-Sekretase APP schneidet (Abbildung 1) [31].

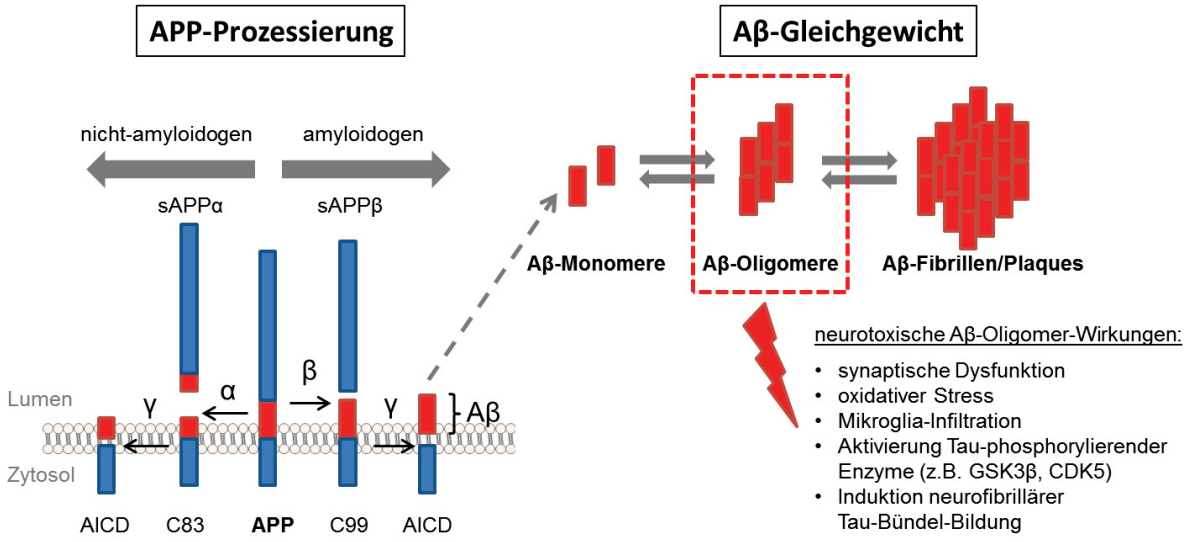

Abbildung 1: APP-Prozessierung, Aβ-Gleichgewicht und Aβ-Oligomer-Neurotoxizität

Nach O'Brien und Wong, 2011 [31]

Die sequentielle **Prozessierung** des „Amyloid Precursor Proteins" (APP) findet auf zwei Wegen statt: Bei der nicht-amyloidogenen Prozessierung (Pfeil nach links) sind die α- und die γ-Sekretase involviert. Bei der amyloidogenen Prozessierung (Pfeil nach rechts) sind die β- (auch BACE) und die γ-Sekretase involviert und es entsteht Aβ (rotes Rechteck). Beide Prozesse erzeugen lösliche Ektodomänen (sAPPα and sAPPβ) und identische intrazelluläre C-terminale Fragmente (AICD).

Aβ-Monomere, -Oligomere und lösliche -Fibrillen bzw. unlösliche -Plaques stehen miteinander im dynamischen **Gleichgewicht**. Aβ-Oligomere gelten derzeit als neurotoxischste Aβ-Spezies [31].

Während **Aβ-Monomere** vermutlich die Informationsübertragung an den Synapsen regulieren und damit eine hilfreiche Aufgabe im Organismus haben, interagieren die als toxisch geltenden, aggregierten **Aβ-Oligomere** nach aktuellem Wissensstand mit Neuronen und verändern pathologisch die Funktionen ihrer Membranproteine (Abbildung 1) [15, 32-35]. Die **Aβ-Aggregate (Fibrillen bzw. Plaques)** können vermutlich als Reservoir für die Bildung der toxischen Oligomere dienen und sind gleichzeitig raumfordernd, was ebenfalls negativ für das Fortbestehen der Neuronen ist [36, 37].

Bisher wurden unterschiedliche molekulare Mechanismen zur **Aβ-Neuro- bzw. Synaptotoxizität** aufgeklärt. Obwohl Aβ hauptsächlich extrazellulär auftritt, kann es in monomerer oder oligomerer Form auch über die Zellmembran in den **Intrazellularraum** gelangen. Intrazellulär kann Aβ die Mitochondrien hemmen, was letztlich zur Zellschädigung führen kann [38]. Aβ bzw. eine Domäne, die intrazellulär bei der APP-Prozessierung entsteht, die „APP intracellular domain" (AICD, Abbildung 1), kann die Calcium-Spiegel der Neuronen negativ verändern. Weitere, Neuronen-schädliche Einflüsse hat intrazelluläres Aβ auf die Konstitution des zweiten Hauptmerkmals der AD, das Mikrotubuli-assoziierte Protein (MAP) Tau (1.4.1.2). Aβ hemmt die Proteasomen, deren Aufgabe der Abbau

hyperphosphorylierten Taus ist, welches zur Bildung neurofibrillärer Bündel (neurofibrillary tangles (NFT)) führt. Folglich kommt es zur NFT-Bildung, zur Mikrotubuli-Depolymerisierung und dadurch zur Unterbrechung des axonalen Transports (s. 1.4.1.2). Außerdem können intrazelluläre Aβ-Dimere über Wechselwirkung mit unterschiedlichen Enzymen (z.B. Calcineurin, Proteinphosphatase 2A, Glykogen Synthase Kinase 3β (GSK3β), Cyclin-abhängige Kinase 5 (CDK5)) die Tau-Hyperphosphorylierung anregen, wodurch es schließlich zur Neurodegeneration kommt (Abbildung 1) [31, 39].

Um diesen neurotoxischen Prozessen vorzubeugen, werden Aβ, Aβ Oligomere und die AICD in funktionstüchtigen Neuronen normalerweise durch das Insulin-abbauende Enzym sowie durch Neprilysin abgebaut [40]. Folglich könnten auch Gen-Defekte, in den diese Proteine codierenden Enzymen, die Wahrscheinlichkeit, an AD zu erkranken, verändern [41].

Im **Extrazellularraum** bilden sich durch Aggregation toxische Aβ-Oligomere und -Plaques, die das Komplementsystem und die Astrozyten- bzw. Mikroglia-Aktivierung anregen. Hierdurch werden die für die AD typischen **Entzündungsreaktionen** im Gehirn ausgelöst [15] und die Bildung der **neurotoxischen NFT** (1.4.1.2) angeregt. Zusätzlich inhibieren Aβ-Oligomere die **Phagozytose**, was eine weitere Ansammlung neurotoxischer Aβ-Aggregate und -Plaques zur Folge hat [15]. Die raumfordernden Plaques und die NFT haben eine **Störung der Signalweiterleitung** zur Folge. Eine Aβ-Oligomer-Ansammlung im synaptischen Spalt hat negativen Einfluss auf die synaptischen Signalweiterleitungs-Funktionen, da so nikotinische Acetylcholinrezeptoren, NMDA-Rezeptoren und „α-amino-3-hydroxy-5-methyl-4-isoxazolepropionic acid“ Rezeptoren, eine Untergruppe der Glutamat-Rezeptoren, internalisiert bzw. inhibiert werden. Somit wird die **postsynaptische Dichte (PSD) verringert**, die Signalweiterleitung unterbrochen und es kommt zum Untergang der Neuronen (Abbildung 1) [42].

Eine weitere Begleiterscheinung der AD ist die **cerebrale Amyloidangiopathie** (CAA). Hierbei kommt es zur Ablagerung unlöslicher Aβ-Plaques an den Innenseiten der das Gehirn versorgenden Blutgefäße. Infolgedessen können Gefäße verstopfen und es kommt zur Unterversorgung gewisser Hirnregionen. Im schlimmsten Fall können Gefäße (bedingt durch den immer größer werdenden Blutdruck als Folge der immer kleiner werdenden Gefäßdurchmesser) sogar reißen, wodurch es zu Gehirnblutungen kommen kann. Durch die kaputten Gefäße und das austretende Blut werden Entzündungsmediatoren aktiviert, was letztlich zu einem hämorrhagischen Schlaganfall führen kann [43].

1.4.1.2 Mikrotubuli-assoziiertes Protein Tau

Das zweite Hauptmerkmal der AD, welches ebenfalls bei beiden Formen der AD, sAD und fAD, eine Rolle spielt, ist das intrazellulär vorkommende **MAP Tau** [3]. Im gesunden

Organismus ist es für die Stabilisierung axonaler Mikrotubuli und damit für die Aufrechterhaltung der Zellstruktur und des intrazellulären Verkehrs verantwortlich [3]. Bei AD-Patienten aggregiert das Tau-Protein durch außergewöhnliche Hyperphosphorylierung zu NFT, welche nicht mehr in der Lage sind, an die Mikrotubuli zu binden und diese so zu stabilisieren [3]. Daraufhin bricht der intrazelluläre Verkehr zusammen und es kommt zum Absterben neurologischer Axone und folglich ganzer Neurone [3]. Beim Untergang der Neuronen gelangen hyperphosphorylierte Tau-Proteine nicht nur ins Soma der Neuronen, wovon sie sonst durch die „Tau diffusion barrier“ abgehalten werden, und sorgen dort für einen Rückgang der Dendriten, sondern auch in den Extrazellularraum, von wo aus sie sich vermutlich zu anderen Zellen ausbreiten können [15, 44]. Dass die Hyperphosphorylierung des Tau-Proteins durch die Anwesenheit von Aβ-Oligomeren ausgelöst werden kann, wurde in 1.4.1.1 anhand mehrerer Mechanismen erläutert.

1.4.2 Entstehung der AD: Die „Amyloid Kaskaden Hypothese“

Bereits 1992 wurde die Amyloid Kaskaden Hypothese (AKH) postuliert. Darin wurde vermutetet, dass die Bildung der Aβ-Spezies (u.a. Plaques) bzw. ein **Ungleichgewicht im Aβ-Auf- und -Abbau** innerhalb des Gehirns der Ursprung der AD sind und dass alle weiteren pathologischen Veränderungen im Gehirn der AD-Patienten (Bildung der NFT, vaskuläre Schäden, Neurodegeneration, Entzündungsreaktionen) eine Folge dessen sind [28]. Ein stark für die AKH sprechendes und nicht widerlegtes Argument ist, dass Menschen, die an **Trisomie 21** leiden, schon in frühem Alter deutlich erhöhte Aβ-Spiegel aufweisen und die Wahrscheinlichkeit, an Demenz zu erkranken, für diese Menschen sehr hoch ist [28]. Da das APP-Gen auf dem bei dieser Erkrankung dreifach vorhandenen Chromosom 21 liegt, produzieren die Patienten deutlich mehr APP, und infolgedessen auch deutlich mehr Aβ [28]. Weiterhin wurde gezeigt, dass **Aβ die Bildung von Tau-Ablagerungen triggern kann**, während ein umgekehrter Mechanismus bislang nicht nachgewiesen werden konnte [45, 46]. Außerdem wird die AKH durch die Entdeckung einer **Missense-Mutation im APP-Gen (A673T) einer isländischen Kohorte** untermauert, die dafür sorgt, dass das APP möglicherweise weniger effizient von der β-Sekretase geschnitten werden kann und infolgedessen weniger Aβ entsteht. Träger dieser Mutation haben ein deutlich geringeres Risiko, an AD zu erkranken und sogar vergleichsweise weniger kognitive Beeinträchtigungen im Alter als andere gesunde Probanden, die diese Mutation nicht tragen [47]. Weiterhin für die AKH sprechen die erblich bedingte fAD, die aufgrund einer genetisch bedingten erhöhten Aβ-Produktion entsteht, sowie aktuelle klinische Studien mit drei verschiedenen **Aβ-Antikörpern** (1.5.3), die eine Verlangsamung der kognitiven Verschlechterung leicht kognitiv beeinträchtigter Patienten zeigt [48].

25 Jahre nach erstmaliger Postulierung der AKH wurde diese dahingehend erweitert, dass hauptsächlich die Aβ-Oligomeren für die die Aβ-vermittelte Neurotoxizität verantwortlich gemacht werden. Es wurde gezeigt, dass Aβ-Oligomere u.a. die synaptische Dichte verringern, die Langzeit-Potenzierung inhibieren, Tau-Proteine hyperphosphorylieren und Nervenzellen zerstören [45].

1.5 Verlauf, Diagnostik und Therapieansätze der AD

1.5.1 Zeitlicher Verlauf der AD

Möglicherweise gibt die zeitliche Abfolge, in der die oben genannten Hauptmerkmale und viele weitere, kleinere Merkmale der AD nachweisbar sind, Aufschluss über die Kausalität der Erkrankung und neue Therapie-Ansätze. Um den AD-Verlauf in Stadien einteilen zu können, haben Braak und Braak die Anatomie der Gehirne verstorbener AD-Patienten und gesunder Probanden verglichen, die extrazelluläre Aβ-Pathologie aufsteigend in die Stadien A bis C und die intrazellulären NFT-Veränderungen aufsteigend in die Stadien I bis VI eingeteilt [49]. Diese Einteilung gilt noch heute als Orientierung für den Schweregrad einer AD-Erkrankung, die *post mortem* diagnostiziert wird. Um jedoch auch bei lebenden Patienten eine Aussage über das Stadium der klinischen Erkrankung treffen bzw. überhaupt eine Diagnose stellen zu können, werden die Aβ-Akkumulation, die synaptische Dysfunktion, die durch Tau-vermittelten neuronalen Schäden, die Gehirn-Struktur, die Kognition und die klinischen Funktionen untersucht und ihr Verlauf von normalen zu abnormalen, pathologischen Werten eingeteilt (Abbildung 2).

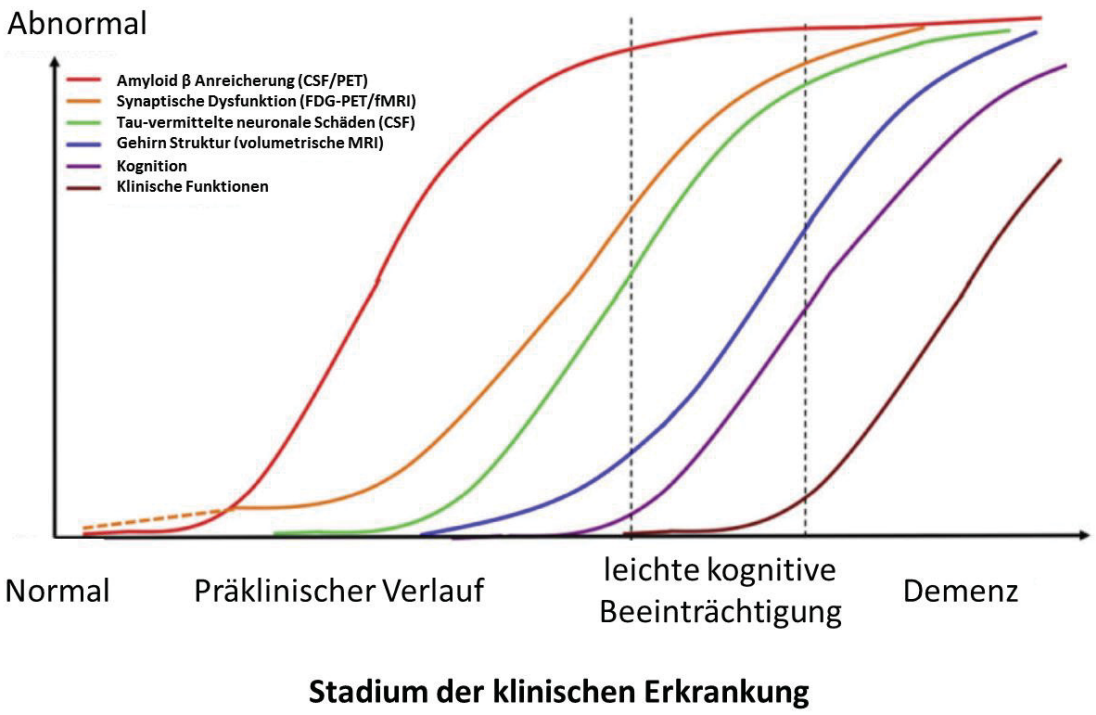

Abbildung 2: Zeitlicher Verlauf der AD

Nach Sperling et al., 2011 & Jack et al., 2010 [10, 50]

Erweitertes hypothetisches Modell dynamischer AD-Biomarker zur Erklärung des zeitlichen Verlaufs der präklinischen AD. $A\beta_{1-42}$-Anreicherung (rote Linie) in der Cerebrospinalflüssigkeit ($A\beta_{1-42}$-Assay) bzw. im Gehirn (Positronen-Emissions-Tomographie, PET). Synaptische Dysfunktion (orange Linie) nachgewiesen durch ^{18}F-2-Fluor-2-desoxy-D-glucose (FDG)-PET oder funktionelle Magnetresonanztomographie (fMRI). Die gestrichelte Linie zeigt, dass die synaptische Dysfunktion in ε4-Allel-Trägern des Apolipoprotein E-Gens evtl. noch vor der $A\beta_{1-42}$-Anreicherung detektierbar ist. Neuronale Schäden (grüne Linie) werden durch CSF-Tau oder CSF-Phospho-Tau nachgewiesen, während die Gehirn Struktur (blaue Linie) durch volumetrische MRI Messungen ermittelt wird. Die Biomarker verändern sich von „normal“ zu maximal „abnormal“ (y-Achse) als Funktion des Stadiums der klinischen Erkrankung (x-Achse). Der zeitliche Kurvenverlauf zweier Indikatoren des Stadiums der klinischen Erkrankung, Kognition (lila Linie) und klinische Funktionen (braune Linie), ist ebenfalls abgebildet [10, 50].

Folglich gelten sowohl Aβ als auch Tau inklusive ihrer Auf- und Abbaumechanismen seit vielen Jahren als Zielstrukturen für die Entwicklung neuer AD-Therapeutika (1.5.3).

1.5.2 AD-(Früh-)Diagnostik

Sobald eine AD-Therapie entwickelt worden ist, hat eine frühzeitige AD-Diagnose den Vorteil, dass noch vor Beginn der irreversiblen Schädigung zahlreicher Neurone mit einer Therapie begonnen werden kann [10]. Im Idealfall kann so künftig der Ausbruch der AD-Symptomatik komplett verhindert werden. Da inzwischen bekannt ist, dass sowohl Aβ- als auch Tau-Ablagerungen im Gehirn der AD-Patienten bereits einige Jahre vor Äußerung der typischen kognitiven Symptome entstehen (Abbildung 2), werden Aβ und Tau als Biomarker zur AD-Diagnose verwendet und sollen künftig auch zur Früherkennung der präklinischen

AD dienen [51]. Um **Aβ bzw. Tau zu diagnostischen Zwecken** im Gehirn potentieller AD-Patienten nachweisen zu können, gibt es zwei Möglichkeiten: die Cerebrospinalflüssigkeit (CSF) kann mit Assays (z.B. sFIDA, 1.5.2.1) auf den Aβ- bzw. Tau-Gehalt untersucht werden und bildgebende Verfahren (z.B. Positronenemissionstomographie (PET) und Magnetresonanztomographie (magnetic resonance imaging, MRI),) können zeigen, wie viel Aβ bzw. Tau in bestimmten Gehirnregionen vorhanden ist bzw. wie sich das Gehirn strukturell verändert (Abbildung 2).

1.5.2.1 Entwicklung eines Diagnose-Verfahrens zur selektiven Aβ-Oligomer-Detektion in CSF und Plasma: sFIDA

Da Aβ-Oligomere derzeit als toxischste und am frühesten nachweisbare Aβ-Spezies im Organismus der AD-Patienten gelten, zielt der im Arbeitskreis um Professor Willbold entwickelte „**s**urface **f**luorescence **i**ntensity **d**istribution **a**naylsis **(sFIDA)-Assay“** auf eine möglichst genaue Differenzierung zwischen löslichen Aβ-Monomeren und -Oligomeren in der CSF bzw. im Plasma potentieller AD-Patienten ab [30].

1.5.3 Übersicht aktueller Therapieansätze in der Forschung

Auf der Suche nach neuen AD-Wirkstoffen werden zahlreiche Therapieansätze verfolgt und in klinischen Studien getestet. Zahlreiche Wirkstoffkandidaten haben es dabei in klinische Studien der Phase III (letzte Phase vor der Zulassung) geschafft, bislang sind dort jedoch alle mangels nachweisbarer Wirksamkeit in großen AD-Patienten-Kohorten ausgeschieden.

Der derzeit vielversprechendste **antikörperbasierte** Ansatz beruht auf einem humanen monoklonalen Antikörper (**Aducanumab**), der sowohl mit löslichen Aβ-Oligomeren als auch mit unlöslichen Aβ-Fibrillen interagiert. Nach einmal monatlicher Gabe über den Gesamtzeitraum eines Jahres konnte mittels PET-Messungen eine deutliche Aβ-Plaque-Reduktion im Vergleich zu vorher sowie eine deutlich verlangsamte Progredienz der kognitiven Beeinträchtigung, verglichen mit Placebo-behandelten Probanden, gezeigt werden [52]. Der therapeutische Erfolg der Aducanumab-Studien bestätigt zugleich, dass Aβ-Oligomere ein vielversprechendes Target für die Entwicklung neuartiger AD-Wirkstoffe sind. Bei der Entwicklung immunotherapeutischer Ansätze ist allerdings zu beachten, dass die Patienten für eine erfolgreiche passive Immunisierung ein intaktes Immunsystem brauchen, was v.a. bei älteren Menschen oft problematisch ist. Folglich ist eine frühe AD-Diagnose, gefolgt von einer frühen Behandlung, voraussichtlich vorteilhaft. Neben weiteren Ansätzen zur **Aβ-Eliminierung** durch **passive Immunisierung** (z.B. Crenezumab, Solanezumab [53]) und **aktive Immunisierung** (z.B. CAD106 [54]) wird durch **β- und γ-Sekretase-Inhibitoren** (z.B. MK8931 [55]) probiert, die Aβ-Produktion zu verringern (Abbildung 3). Dieser Ansatz löste allerdings häufig unerwünschte Arzneimittelwirkungen

aus, da beide Sekretasen auch physiologische Funktionen haben, deren Hemmung sich negativ auf die Funktionen des Organismus auswirken kann [56].

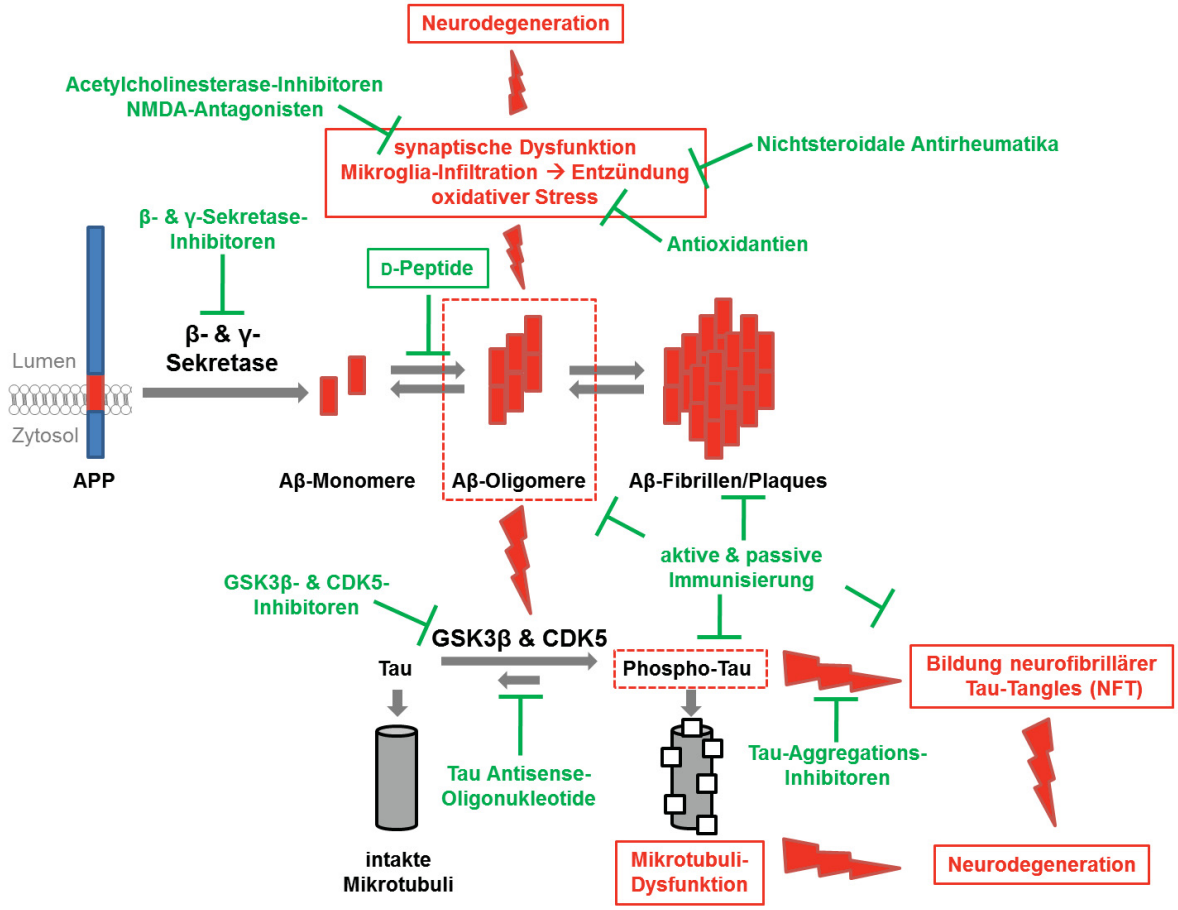

Abbildung 3: Therapieansätze gegen die Alzheimer'sche Demenz

Im Zentrum zahlreicher Therapieansätze (grüne Beschriftung) gegen die Alzheimer'sche Demenz steht die Amyloid β (Aβ)-Prozessierung und das dynamische Aβ-Gleichgewicht. Die direkten und indirekten neurotoxischen Auswirkungen (rote Blitze) der Aβ-Oligomere sollen auf zahlreichen Wegen wiederum direkt und indirekt inhibiert werden. Im grünen Kasten hervorgehoben sind D-Peptide, die toxische Aβ-Oligomere direkt und spezifisch eliminieren sollen, indem sie Aβ-Monomere in nicht-toxischen, nicht-amyloidogenen Komplexen abfangen und so das Aβ-Gleichgewicht weg von toxischen Aβ-Oligomeren, hin zu neuroprotektiven Aβ-Monomeren verschieben (1.6). Dies ist der im Arbeitskreis um Professor Willbold entwickelte Therapieansatz, um dessen pharmakokinetische und pharmakodynamische Untersuchung es in dieser Arbeit geht.

Auch der **Tau-Metabolismus** wird in einigen Ansätzen gezielt beeinflusst (Abbildung 3). Der **Tau-Aggregations-Inhibitor** TRx0237 ist ein weniger toxischer und höher bioverfügbarer Abkömmling des Methylenblaus und wurde bereits in klinischen Studien der Phase III untersucht [57]. Ebenfalls von aktuellem Interesse ist der aktive **Tau-Impfstoff** AADvac-1, der bereits in transgenen AD-Ratten eine Verbesserung des klinischen Phänotyps erzielen konnte [58]. Bis Februar 2019 läuft eine klinische Studie Phase II zu diesem Impfstoff (NCT02579252) [59]. **Tau Antisense-Oligonucleotide** wurden erfolgreich in transgenen

Mäusen getestet, die humanes Tau exprimieren. Sie verringerten dort selektiv die Tau-mRNA sowie die Tau-Proteine [60].

Weiterhin gibt es zahlreiche Wirkansätze, die nicht auf den Aβ- oder Tau-Metabolismus abzielen und in unterschiedlichen AD-Tiermodellen vielversprechende Wirkung zeigten: Levetiracetam [61], Fyn-Kinase-Hemmstoffe [62], intranasale Insulingabe [63], Nahrungsergänzungsmittel [64], körperliche Aktivität im aeroben Bereich [65] u.v.a. mehr.

1.6 Entwicklung D-enantiomerer Peptide zur selektiven Eliminierung toxischer Aβ-Oligomere

Grundlage der AD-Wirkstoff-Entwicklung im Arbeitskreis um Professor Willbold war das so genannte „**M**irror-**I**mage **P**hage **D**isplay“ **(MIPD) Peptid-Selektionsverfahren** [66]. Es basiert auf dem Prinzip des Phagen-Displays, soll aber, anders als beim „normalen“ Phagen-Display, ein **D-enantiomeres Peptid** (D-Peptid) hervorbringen, das an ein natürlich vorkommendes (L-enantiomeres) Zielmolekül (z.B. Aβ), bindet. Vorzüge der D-Peptide gegenüber L-Peptiden als Therapeutika oder Diagnostika sind u.a. eine deutlich **geringere Immunogenität** und **höhere proteolytische Stabilität**, wodurch sie z.T. sogar oral verabreicht werden können [67-70].
In der MIPD-Selektion zur AD-Wirkstoff-Entwicklung wurde gegen **Aβ-Monomere** selektiert, um diese in nicht-toxischen, nicht-amyloidogenen, höhermolekularen Komplexen abzufangen und so das dynamische Gleichgewicht der verschiedenen Aβ-Spezies (Abbildung 1) von den toxischen Aβ-Oligomeren, hin zu den als neuroprotektiv geltenden Aβ-Monomeren [33], zu verschieben. Aus einer solchen Selektion wurde u.a. das aus 12 AS-Resten bestehende D-Peptid **D3** (rprtrlhthrnr) hervorgebracht, welches nach wie vor als Leitstruktur für die Entwicklung weiterer AD-Wirkstoff-Kandidaten gilt.

1.6.1 *In vitro*-Untersuchungen zur D-Peptid-Selektion und Optimierung der Leitstruktur

In zahlreichen *in vitro*-Tests mit $A\beta_{1-40}$ und $A\beta_{1-42}$ wurde zunächst für D3, und später auch für andere D-Peptide, ihre **Aβ-Interaktion**, ihre **Aβ-Aggregations-inhibierende Wirkung** sowie ihre **Aβ-Oligomer-reduzierende Wirkung** gezeigt [71-75]. Mittels Oberflächenresonanzspektroskopie **(SPR)**-Messungen wurde die D-Peptid-Aβ-Interaktion getestet [76] und dabei deren Dissoziationskoeffizienten **(K_D)** an Aβ-Monomere, -Oligomere und -Fibrillen ermittelt [77]. Mittels Thioflavin T **(ThT)**-Test und dem sog. „Seeding-Assay“ wurde untersucht, in wie weit die D-Peptide die Aβ-Aggregation verzögern bzw. verhindern [78]. Zellviabilitäts-Tests, nach dem im Test verwendeten gelben Farbstoff 3-(4,5-Dimethylthiazol-2-yl)-2,5-diphenyltetrazoliumbromid **(MTT)** auch MTT-Tests genannt,

zeigten, dass die D-Peptide den zytotoxischen Einfluss von Aβ-Oligomeren verringern [71, 79]. Der „**q**uantitative determination of **i**nterference with Aβ **a**ggregate size **d**istribution“ **(QIAD)-Assay** untersucht den Einfluss von Wirkstoffen auf die natürliche Aβ-Aggregat-Größenverteilung (Monomere, Oligomere, höhermolekulare Aggregate) nach Inkubation in physiologischem Puffer. Mit Hilfe dieses Assays konnte bestätigt werden, dass die D-Peptide einen Aβ-Oligomer-reduzierenden Einfluss haben, was im Hinblick auf die Aβ-Oligomer-Toxizität von besonderer Bedeutung ist [74, 80]. Zusätzlich zu Tests, die auf die Interaktion der D-Peptide mit Aβ abzielen, wurden die D-Peptide auf unterschiedliche Weise auf ihre proteolytische Stabilität und ihre Bindung an humane Plasmaproteine untersucht [81-86].

Erst wenn die D-enantiomeren Peptid-Wirkstoffkandidaten in diesen *in vitro* Tests erfolgreich waren, wurden mit ihnen weitere pharmakokinetische und pharmakodynamische *in vivo* Studien durchgeführt (1.6.2).

Um die Aβ-Spezifität und somit die pharmakodynamischen Eigenschaften (1.6.2.2) der D3-Leitstruktur zu verbessern, wurden unterschiedliche D3-Derivate entwickelt. Hierzu wurde zunächst die AS-Sequenz der Leitstruktur nach rationalem Ansatz umsortiert und dabei die D-Peptide selektiert, die großes Aβ-Interaktionspotenzial aufwiesen. **RD2** (ptlhthnrrrrr) stellte sich, mit allen fünf Arginin-Resten kumuliert am C-Terminus, dabei als vielversprechender Wirkstoffkandidat heraus [78, 80, 87]. Im nächsten Optimierungsschritt wurden so genannte *head-to-tail* Tandempeptide aus den beiden zuvor genannten Peptiden, D3 und RD2, gebildet (**D3D3, RD2D3**) und untersucht [74, 84, 87, 88]. Weiterhin wurde der Einfluss der Nettoladung sowie der konformativen Starrheit auf das Vermögen, Aβ-Oligomere zu reduzieren bzw. die Aβ-induzierte Zytotoxizität zu verringern untersucht, wobei **cD3r** (N- zu C-terminal zyklisiertes D3 mit einem zusätzlich eingebauten Arginin) sich als effizientester Kandidat herausstellte [89]. In einem weiteren Optimierungsansatz wurde jeder AS-Rest der D3-Leitstruktur gegen 19 proteinogene (alle außer Zystein) und 13 nicht-proteinogene AS-Reste ausgetauscht und die entstandenen D-Peptide nach ihrer spezifischen Bindung an Aβ-Monomeren selektiert, wobei ANK6 als vielversprechendster Kandidat benannt wurde [90].

1.6.2 *In vivo*-Untersuchungen zur pharmakokinetischen und pharmakodynamischen Eignung der *in vitro* selektierten D-Peptide

Da neu entwickelte Wirkstoffkandidaten nicht direkt in erkrankten Menschen auf ihre Verträglichkeit und Wirksamkeit getestet werden dürfen, werden diese, nach zahlreichen *in vitro*-Tests, in Tiermodellen auf die beiden Parameter untersucht. Ist ein Wirkstoffkandidat in einem Tiermodell verträglich, wird er im Anschluss (ebenfalls in einem Tiermodell) auf seine **pharmakokinetische** und **pharmakodynamische** Eignung (1.7) getestet [91]. Während pharmakokinetische Studien zunächst in nicht genetisch modifizierten Wildtyp-Tieren

durchgeführt werden, wird die Wirksamkeit in pharmakodynamischen Studien in genetisch modifizierten Tiermodellen untersucht, die ein dem Menschen ähnliches Krankheitsbild aufweisen. Zeigt der Wirkstoffkandidat geeignete pharmakologische Eigenschaften und beeinflusst nach einer Therapie die pathologische Symptomatik positiv, wird er in einem weiteren Tiermodell auf seine Verträglichkeit und Wirksamkeit untersucht. Das erste Tiermodell, in dem ein neuer Wirkstoff getestet wird, ist i.d.R. ein Nagetier-Modell, das zweite Tiermodell ein „Nicht-Nager"-Tiermodell. All diese Schritte zählen zur präklinischen Wirkstoff-Entwicklung, bei der – im Gegensatz zur klinischen Wirkstoff-Entwicklung – noch keine Anwendung im Menschen stattfindet.

1.6.2.1 Pharmakokinetische Untersuchungen zuvor *in vitro* selektierter D-Peptide

Um einen Wirkstoff mit überzeugenden *in vitro*-Eigenschaften in Wildtyp-Mäusen auf seine pharmakokinetischen Eigenschaften untersuchen zu können, wird dieser den Mäusen zunächst auf unterschiedlichen Applikationswegen verabreicht. Im Anschluss wird die Konzentration des Wirkstoffs im Plasma sowie unterschiedlichen Organen (z.B. Gehirn, Leber und Niere) zu unterschiedlichen Zeitpunkten nach der Applikation gemessen und auf Basis dieser Daten Konzentrations-Zeit-Profile erstellt. Daraus können weiterhin zahlreiche pharmakokinetische Parameter berechnet werden. Da das Gehirn der Wirkort für AD-Wirkstoffe ist, ist deren **Blut-Hirn-Schranken (BHS)-Gängigkeit** besonders wichtig. Diese wurde für D3 zunächst in einem Zellkultur-Modell bestimmt.

1.6.2.2 Pharmakodynamische Untersuchungen zuvor *in vitro* selektierter D-Peptide

Um die D-Peptide, die die vorherigen *in vitro*-Tests und pharmakokinetischen *in vivo*-Studien erfolgreich durchlaufen haben, auch auf ihre pharmakodynamische Eignung zu untersuchen, werden therapeutische *in vivo*-Studien in unterschiedlichen Mausmodellen durchgeführt. Zur Testung neu entwickelter, potentieller AD-Wirkstoffkandidaten machen sich Forscher die oben (1.2) beschriebenen genetischen fAD-Mutationen zu Nutze, indem sie diese Mutationen in Form eines Transgens ins Genom von Mäusen einführen. Da es bislang kein allumfassendes AD-Mausmodell gibt, können immer nur Teilaspekte der AD untersucht werden. Die pharmakodynamische Studie, die im Rahmen dieser Arbeit durchgeführt wurde, wurde in folgendem transgenen Mausmodell durchgeführt:

1.6.2.2.1 APPswe/PS1dE9-Mausmodell mit **kognitiven** Defiziten

Sog. **APPswe/PS1dE9** Mäusen wurde ein Transgen mit APP und der sog. „Swedish"-Mutation, die bei einer schwedischen Familie, in der überdurchschnittlich viele Mitglieder in verhältnismäßig jungem Alter an AD erkranken, entdeckt wurde, ins murine Genom inseriert. Gleichzeitig wurde eine Mutation im Presenilin 1-Gen, welche durch Deletion des Exons 9 zustande kommt, inseriert. Durch die Insertionen entwickeln die Mäuse bereits ab einem

Alter von 6 Monaten eine Astrogliose, ab 9 Monaten eine Aβ-Pathologie (Amyloidose) in Hippocampus und Cortex und ab 8 bis 10 Monaten leichte neuronale Verluste. Diese pathologischen Veränderungen des Gehirns haben kognitive Defizite zur Folge [92-94]. Infolgedessen können mit therapeutischen Behandlungsstudien in diesem Mausmodell die Einflüsse eines AD-Wirkstoffkandidaten auf kognitive Defizite untersucht werden.

1.6.2.2.2 Durchgeführte therapeutische *in vivo* Behandlungsstudien mit D-Peptiden

Für D3 und einige seiner Derivate wurden bereits zahlreiche therapeutische *in vivo*-Behandlungsstudien in transgenen AD-Mäusen erfolgreich durchgeführt. Hierbei wurden die D-Peptide auf unterschiedlichen Wegen appliziert: **intraperitoneal** (i.p.) mit einer Pumpe, die operativ in die Bauchhöhle der Mäuse eingesetzt wurde und kontinuierlich für bis zu vier Wochen das D-Peptid freisetzte [74, 89]; **per oral** (p.o.) täglich mit einer Fütternadel, über das Trinkwasser [75, 87]; **intrakraniell** über eine Kanüle direkt in den Hippocampus aus einer Pumpe, die den Mäusen subkutan implantiert wurde [71, 72, 95, 96]. Die Behandlungsdauer und das Alter der Mäuse zu Beginn der Behandlung variierten dabei deutlich. Kurz vor dem Ende der Behandlungsstudien wurden Verhaltenstests durchgeführt, die, abhängig vom Mausmodell, die kognitiven oder motorischen Fähigkeiten der Mäuse untersuchten. In allen Studien konnte eine signifikante Erhöhung der kognitiven bzw. motorischen Fähigkeiten durch die D-Peptid-Behandlung, im Vergleich zu den mit Placebo behandelten Mäusen, gezeigt werden. Nach Abschluss der Behandlung wurden die Gehirne (Zielwirkort) der Mäuse untersucht: immunhistochemische Färbungen (Aβ-Plaques, aktivierte Astrozyten und Mikroglia, Neurone etc.) oder immunbiochemische Untersuchung mittels ELISA oder Western Blot zur Bestimmung des Aβ-Gehalts wurden durchgeführt. In diesen Untersuchungen konnte eine D-Peptid-vermittelte Reduktion des Aβ-Gehalts bzw. der Aβ-vermittelten Entzündungsreaktionen im Gehirn der Mäuse gezeigt werden.

Zusammenfassend belegen die Ergebnisse der *in vitro*-Tests, der pharmakokinetischen und pharmakodynamischen *in vivo*-Studien das therapeutische Potenzial der D-Peptide zur AD-Therapie. Folglich ist es nicht verwunderlich, dass der derzeit vielversprechendste D-Peptid-Wirkstoffkandidat kurz davor steht, in einer klinischen Studie Phase I getestet zu werden.

1.7 Pharmakologie

„Sola dosis facit venenum.“ – „Allein die Dosis macht das Gift.“ (nach Paracelsus, *1493)

Die Pharmakologie wird i.d.R. in zwei Teilbereiche, Pharmakokinetik und Pharmakodynamik unterteilt. Während die Pharmakokinetik sich damit auseinandersetzt, was ein Organismus mit einem Wirkstoff macht, befasst sich die Pharmakodynamik damit, welche Auswirkung ein Wirkstoff auf einen Organismus hat (Abbildung 4) [97]. Neuerdings gibt es noch eine weitere

Subkategorie, die Pharmakogenetik, die sich mit der genetischen Ausstattung eines Organismus und dem daraus resultierenden Einfluss auf die Wirkung eines Wirkstoffs beschäftigt [98].

1.7.1 Pharmakokinetik

Da es in dieser Arbeit hauptsächlich um die pharmakokinetische Charakterisierung D-enantiomerer Peptide geht, wird dieser Teilbereich der Pharmakologie im Folgenden genauer erläutert. Um eine Wirkung erzielen zu können, muss der Wirkstoff zunächst verabreicht werden. Dies ist durch zahlreiche Applikationsarten (z.B. intravenös, oral, subkutan, transdermal, etc.) und Darreichungsformen möglich. Alleine für die orale Applikation gibt es unzählige Darreichungsformen (z.B. Tabletten, Kapseln mit modifizierter Wirkstofffreisetzung, Säfte, Tropfen, u.v.m.). Ein Wirkstoff durchläuft nach der Applikation im Organismus mehrere Schritte, bis er letztlich am Ziel, seinem Wirkort, ankommt bzw. den Organismus wieder verlässt. Die im Folgenden beschriebenen Abläufe werden häufig unter dem Überbegriff „**LADME**“ zusammengefasst (Abbildung 4) [99].

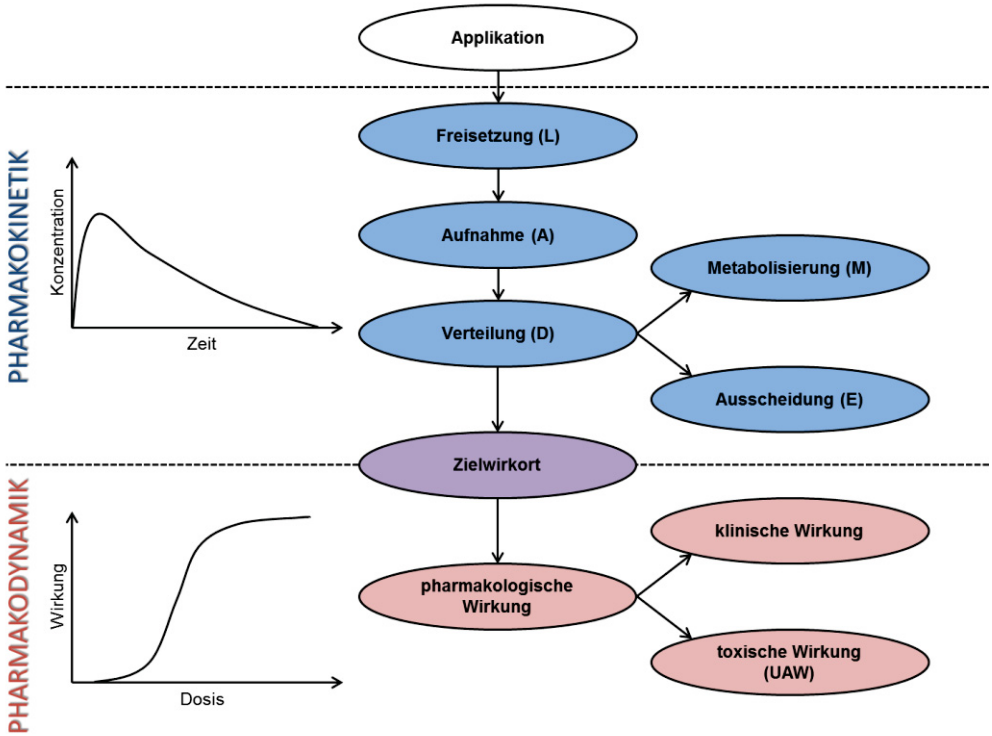

Abbildung 4: Pharmakokinetik und Pharmakodynamik

Nach Hein, 2011 und Herdegen, 2013 [97, 100]

Die Pharmakologie kann in die Teilgebiete der Pharmakokinetik und der Pharmakodynamik unterteilt werden. Die Pharmakokinetik beschreibt, was ein Organismus mit einem Wirkstoff macht (z.B. Plasmakonzentrations-Zeit-Verlauf), während die Pharmakodynamik beschreibt, welche Wirkung ein Wirkstoff auf einen Organismus hat (z.B. Dosis-Wirkungs-Kurve) [97, 100].

Freisetzung („**L**iberation“): Der Wirkstoff wird aus der Applikationsform, z.B. im Gastrointestinaltrakt aus einer Tablette, freigesetzt. Es gibt zahlreiche Applikationsformen mit modifizierter Wirkstofffreisetzung. Ist ein Wirkstoff beispielsweise säureinstabil, soll jedoch oral verabreicht werden, kann eine Darreichungsform gewählt werden, die den Wirkstoff erst im Darm (ca. pH 6-8) und nicht bereits im Magen (ca. pH 1-2) freisetzt.

Aufnahme („**A**bsorption“): Der Wirkstoff gelangt z.B. aus dem Gastrointestinaltrakt über die Schleimhäute in die Blutbahn. Dies kann auf verschiedenste Arten (passiver und aktiver Transport, Diffusion etc.) stattfinden. Allgemein gelangen kleine, lipophile Wirkstoffe besser über Zellmembranen als große, hydrophile Wirkstoffe.

Verteilung („**D**istribution“): Der Wirkstoff verteilt sich hauptsächlich über die Blutbahn im gesamten Organismus und tritt an gewissen Stellen über Blut-Gewebe-Schranken (z.B. der BHS) hin zu seinem Zielwirkort. Gleichzeitig ist es möglich, dass der Wirkstoff zu Orten gelangt, an denen er gewünschte Nebenwirkungen oder unerwünschte Arzneimittelwirkungen hervorruft. Eine weitere Möglichkeit ist die Ablagerung in Geweben (z.B. dem Fettgewebe), wo der Wirkstoff zwar keinen pharmakodynamischen Effekt hervorruft, jedoch durch die dortige Ansammlung auch nicht an seinen Zielwirkort gelangt.
Außerdem kann es sein, dass der Wirkstoff, während er sich im Blut befindet, dort an Plasmaproteine bindet **(Plasmaproteinbindung)**. Dies kann wiederum zur Folge haben, dass weniger Wirkstoff frei im Blut bzw. Organismus zirkuliert, wodurch die Wirkung weniger stark ausgeprägt ist. Umgekehrt wird das Risiko für unerwünschte Nebenwirkungen gemindert und ein relativ konstanter Wirkspiegel, durch das dynamische Gleichgewicht zwischen gebundenem und ungebundenem Wirkstoff, erreicht. Nimmt ein Patient gleichzeitig zwei Wirkstoffe ein, die an das gleiche Plasmaprotein binden, kann es zu Veränderungen der ungebundenen Wirkstoffkonzentration kommen, da die Wirkstoffe sich gegenseitig aus den Bindungen an den Plasmaproteinen verdrängen. In diesem Fall spricht man von einer Wechselwirkung (Interaktion).

Metabolisierung („**M**etabolization“): Da der Körper Wirkstoffe i.d.R. als „körperfremd“ erkennt, werden diese v.a. in der Leber, die hauptsächlich für den Metabolismus zuständig ist, chemisch so verändert (häufig durch enzymatisch katalysierte Reaktionen), dass sie hydrophiler und damit der Ausscheidung über Leber und Niere zugänglicher gemacht werden. Oftmals hat diese Veränderung auch einen Verlust der Wirksamkeit zur Folge. Vereinzelt gibt es jedoch Wirkstoffe, die durch eine bestimmte metabolische Reaktion erst in ihre wirksame Form umgewandelt werden, diese heißen „Prodrugs“. Levodopa wird z.B. gegen Morbus Parkinson verabreicht, der durch Metabolisierung im Gehirn wirksame Metabolit ist jedoch Dopamin.

Eliminierung („**E**limination“): Der Wirkstoff oder dessen Metabolit wird z.B. über Leber, Galle und Darm, im Stuhl, oder die Niere, im Urin, ausgeschieden. Andere Wege, z.B. über die Atemluft oder die Haut, sind ebenfalls möglich. Wie groß der Zeitraum zwischen der Wirkstoff-Applikation und seiner Ausscheidung ist, kann von wenigen Sekunden oder Minuten bis hin zu Tagen oder sogar Wochen und Monaten variieren.
Stoffe, die dem sog. „**First-Pass-Effekt“** unterliegen, gelangen nach der Aufnahme über den Gastrointestinaltrakt über die Pfortader zur Leber und werden dort so metabolisiert, dass sie umgehend über die Galle zurück in den Darm gelangen und (zum Großteil) ausgeschieden werden. Dieser Vorgang wird auch als „**präsystemische Elimination“** bezeichnet und kann dazu führen, dass über 95 % eines per oral verabreichten Wirkstoffs ausgeschieden werden, ohne jemals über die Blutbahn in den Organismus zu gelangen.
Bei Stoffen, die dem sog. **„enterohepatischen Kreislauf“** unterliegen, sieht es zunächst ähnlich aus wie bei denen, die dem First-Pass-Effekt unterliegen. Allerdings werden die Metabolite aus der Leber, die über die Galle in den Darm gelangen, dort nicht sofort ausgeschieden, sondern durch Darmbakterien wiederum chemisch so verändert, dass sie rückresorbiert werden und erneut über die Pfortader zur Leber transportiert werden können. Folglich werden diese Wirkstoffe nur sehr langsam ausgeschieden.

Um die komplexen Vorgänge, die für jeden Wirkstoff im Zusammenhang mit jedem Organismus anders verlaufen können, genauer beschreiben und vergleichbar machen zu können, wird der Wirkstoffkonzentrations-Zeit-Verlauf in einem bestimmten Organismus häufig durch **pharmakokinetische Parameter** beschrieben. Hierzu wird, wenn ein Wirkstoff in einem Tier oder einem Menschen pharmakokinetisch untersucht werden soll, zunächst die **Plasmakonzentrations-Zeit-Kurve des Wirkstoffs** aufgezeichnet. Diese kann, abhängig von der Applikationsart und der Darreichungsform, sehr unterschiedlich verlaufen (Abbildung 5).

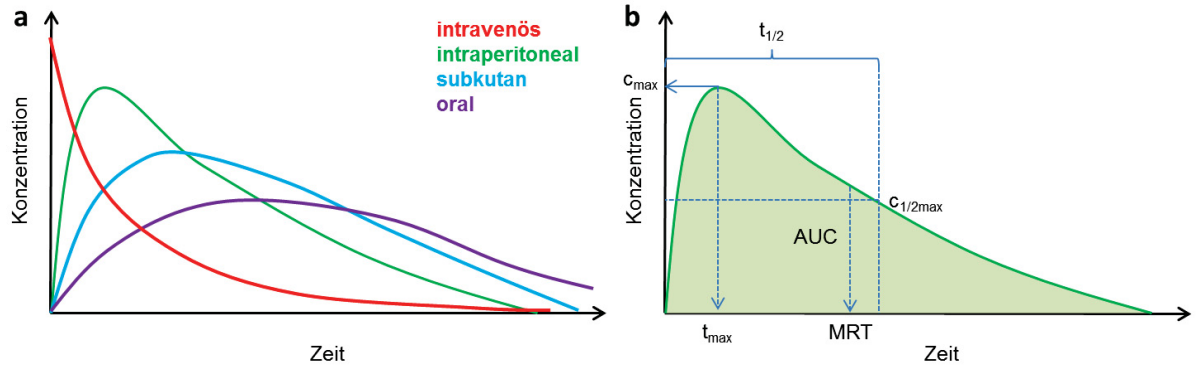

Abbildung 5: Plasmakonzentrations-Zeit-Kurven
(a) nach Lüllmann, Mohr, Hein, 2008 [101]

(a) Der Verlauf einer Plasmakonzentrations-Zeit-Kurve hängt stark von der jeweiligen Applikationsart ab. Die Geschwindigkeit des initialen Plasmakonzentrations-Anstiegs nimmt von intravenöser (rot), über intraperitoneale (grün) und subkutane (blau) bis hin zu oraler (lila) Applikation ab [101].
(b) Pharmakokinetische Parameter können direkt aus dem Verlauf der Plasmakonzentrations-Zeit-Kurve abgelesen oder indirekt aus ihr berechnet werden. Die Fläche unter der Plasmakonzentrations-Zeit-Kurve (hellgrün) wird dabei häufig als *„area under the curve (AUC)“* bezeichnet. Die mittlere Verweildauer des Wirkstoffs im Organismus (MRT), die maximale Plasmakonzentration (c_{max}), die halbmaximale Plasmakonzentration ($c_{1/2max}$) und die Halbwertszeit ($t_{1/2}$) sind Beispiele für pharmakokinetische Parameter.

Abhängig davon, ob der Wirkstoff einmal oder mehrmals (z.B. während einer Therapie, bei der täglich ein oder zwei Mal Wirkstoff eingenommen wird) verabreicht wird, variiert der Plasmakonzentrations-Zeit-Verlauf ebenfalls. Im Folgenden werden einige pharmakokinetische Parameter erläutert, die im Rahmen dieser Arbeit für D-enantiomere Peptid-Wirkstoffkandidaten gegen die AD experimentell ermittelt wurden:

1.7.1.1 Plasmakonzentrationsmaximum (c_{max})

Maximale Plasmakonzentration, die nach (einmaliger) Wirkstoffapplikation erreicht wird.

Einheit: $\frac{\text{mg}}{\text{L}}$ oder $\frac{\%\text{ID}}{\text{L}}$, dabei ist %ID = prozentualer Anteil der injizierten Dosis

Formel: wird direkt aus der Plasmakonzentrations-Zeit-Kurve abgelesen

1.7.1.2 Zeit bis zum Erreichen des Plasmakonzentrationsmaximums (t_{max})

Zeit, die zwischen Applikation und Erreichen der maximalen Plasmakonzentration vergeht. Diese kann abhängig von der jeweiligen Darreichungsform zwischen wenigen Sekunden (i.v. Applikation) und mehreren Stunden (retardierte orale Darreichungsformen, subkutane Injektion, o.ä.) variieren.

Einheit: h

Formel: wird aus der Plasmakonzentrations-Zeit-Kurve abgelesen

1.7.1.3 Terminale Eliminationskonstante (λ_z)

I.d.R. findet die Wirkstoffelimination nach einer Kinetik 1. Ordnung (exponentieller Konzentrationsabfall) statt, d.h. „Die Konzentrationsänderung zum Zeitpunkt t hängt von der aktuellen Konzentration (c_t) ab.“ [102]. Hierbei beschreibt die terminale Eliminationskonstante (λ_z) den Konzentrationsabfall eines Wirkstoffs, welcher alle für dessen Ausscheidung aus dem Blutkompartiment verantwortlichen Prozesse (z.B. Metabolisierung und Eliminierung) umfasst [102].

Einheit: $\frac{1}{\text{h}}$

Formeln: $c_t = c_0 \cdot e^{-\lambda_z \cdot t} \Leftrightarrow \lambda_z = -\frac{\ln\left(\frac{c_t}{c_0}\right)}{t}$

$\lambda_z = \left|\frac{\ln c_1 - \ln c_2}{t_2 - t_1}\right| = \frac{\ln 2}{t_{\frac{1}{2}}} = \frac{CL}{V}$

c_0 = Plasmakonzentration zum Zeitpunkt 0

c_1 = Plasmakonzentration zum Zeitpunkt 1

c_2 = Plasmakonzentration zum Zeitpunkt 2

t_1 = Zeitpunkt 1

t_2 = Zeitpunkt 2

1.7.1.4 Eliminationshalbwertszeit ($t_{1/2}$)

Die Eliminationshalbwertszeit ($t_{1/2}$) ist die Zeitspanne, nach der die Hälfte der zu Beginn der Zeitmessung (t_0) im Organismus vorhandenen Wirkstoffmenge metabolisiert bzw. eliminiert wurde. Bei einer Wirkstoffelimination nach einer Kinetik 1. Ordnung ist diese dosisunabhängig. Üblicher Weise wird die terminale Eliminationshalbwertszeit angegeben, bei der die Wirkstoffaufnahme abgeschlossen ist und lediglich die Metabolisierung und Elimination eine Rolle spielen. Ein durch Einmalgabe applizierter Wirkstoff ist nach fünf Halbwertszeiten zu mehr als 95 % metabolisiert bzw. eliminiert [97].

Einheit: h

Formeln: $t_{1/2} = \frac{\ln 2}{\lambda_z} = \frac{\ln 2 \cdot V}{CL}$

V = Verteilungsvolumen

CL = Clearance

1.7.1.5 Clearance (CL)

Die Clearance beschreibt das formale Blut- bzw. Plasmavolumen, das pro Zeiteinheit durch Ausscheidung über die Niere (renale Clearance), Leber (hepatische Clearance), Haut, Lunge, etc. sowie durch Metabolisierung vollständig vom Wirkstoff befreit wird [97].

Einheit: $\frac{l}{h}$

Formel: $CL = \lambda_z \cdot V = \frac{D \cdot F}{AUC}$

D = Dosis

AUC = Fläche unter der Konzentrations-Zeit-Kurve

1.7.1.6 Fläche unter der Konzentrations-Zeit-Kurve (Area under the curve, AUC)

Die Fläche unter der Plasmakonzentrations-Zeit-Kurve (AUC) ist gleich der Wirkstoffmenge, die den Kreislauf erreicht, geteilt durch die Clearance. Sie spiegelt wider, in welchem Ausmaß ein Organismus dem Wirkstoff über einen gewissen Zeitraum (t) in Abhängigkeit der CL ausgesetzt ist [103].

Einheit: $\frac{\mathrm{mg \cdot h}}{\mathrm{l}}$

Formel: intravenöse Applikation: $\mathrm{AUC} = \frac{\mathrm{D}}{\mathrm{CL}} = \frac{\mathrm{c_0}}{\lambda_\mathrm{z}}$

extravaskuläre Applikation (z.B. p.o.): $\mathrm{AUC} = \frac{\mathrm{D \cdot F}}{\mathrm{CL}}$

allgemein (mathematisch, grafisch): sog. Trapezregel $\mathrm{AUC} = \int_0^\infty c dt$

1.7.1.7 Fläche unter der 1. Moment-Kurve (Area under the first moment curve, AUMC)

Die Fläche unter der 1. Moment-Kurve (AUMC) ist die Fläche unter der Kurve des Produktes aus der Zeit (t) und der Plasmakonzentration (c) von t = 0 bis unendlich. Sie wird z.B. zur Bestimmung der mittleren Verweildauer und des Verteilungsvolumens im „Steady State“ (Kumulationsgleichgewicht, wenn Resorption und Elimination gleich schnell ablaufen) verwendet [103].

Einheit: $\frac{\mathrm{h \cdot h \cdot mg}}{\mathrm{l}}$

Formel: $\mathrm{AUMC} = \int_0^\infty \mathrm{t} \cdot c dt$

1.7.1.8 Mittlere Verweildauer (Mean Residence Time, MRT)

Die mittlere Verweildauer (MRT) entspricht der Zeit, die ein verabreichtes Wirkstoffmolekül durchschnittlich im Organismus verweilt [104].

Einheit: h

Formel: i.v. Applikation: $\mathrm{MRT} = \frac{\mathrm{AUMC}}{\mathrm{AUC}}$

extravaskuläre Applikation (z.B. p.o.): $\mathrm{MRT} = \frac{\mathrm{AUMC}}{\mathrm{AUC}} - \mathrm{MIT}$

(MIT = mean input time → Zeit, die nach extravaskulärer Applikation durchschnittlich vergeht, bis ein Wirkstoffmolekül im Organismus ankommt.)

1.7.1.9 Bioverfügbarkeit (F)

Die Bioverfügbarkeit (F) beschreibt den prozentualen Anteil, zu dem die nicht i.v. verabreichte Dosis (D) eines Wirkstoffs aus der jeweiligen Darreichungsform, relativ zur gleichen i.v. verabreichten Dosis, systemisch verfügbar wird. Die Bioverfügbarkeit kann beispielsweise durch unvollständige Freisetzung aus der Arzneiform, unvollständige Resorption am Applikationsort oder präsystemische Elimination (z.B. First-Pass-Effekt im Gastrointestinaltrakt) vermindert werden [97].

Einheit: %

Formel: $$F = \frac{AUC_{extravasculär} \cdot D_{intravenös}}{AUC_{intravenös} \cdot D_{extravasculär}}$$

1.7.2 Blut-Hirn-Schranke

Die das Gehirn durchblutenden Gefäße sind von besonders dichten, kontinuierlichen Endothel- und Gliazellen umgeben, die durch so genannte „*tight junctions*“ verbunden sind, um v.a. hydrophilen Substanzen den Übertritt aus dem Blut ins Gehirngewebe und damit ins zentrale Nervensystem (ZNS) zu erschweren. Auf diese Weise sollen unerwünschte Arzneimittelwirkungen im ZNS vermieden werden, was im Gegenzug die erwünschte Wirkung eines Wirkstoffs im ZNS (z.B. bei der AD) erschwert. Für Moleküle mit einem Molekulargewicht kleiner 60-600 Da ist die Blut-Hirn-Schranke (BHS) durchlässig [97], wobei es eine Reihe spezifischer Transporter gibt, die dafür sorgen, dass größere Moleküle, die ins ZNS gelangen sollen, die BHS passieren können. Für Moleküle, die fälschlicher Weise ins ZNS gelangt sind oder solche, die wieder ausgeschleust werden sollen, weil sie ihren Zweck erfüllt haben, gibt es ebenso spezifische Transporter, die bestimmte Substanzklassen aus dem ZNS über die BHS zurück in den Blutkreislauf transportieren. Hierzu zählen u.a. die ABC (ATP binding cassette)-Transporter und die Low Density Lipoprotein Receptor-related Protein 1 (LRP1)-Transporter (auch CD91 genannt), die u.a. das Aβ-Protein aus dem ZNS transportieren und dadurch mit der AD in Zusammenhang gebracht werden [105, 106]. Da diese Transporter spezifisch für Peptide bzw. Proteine sind, spielen sie möglicherweise ebenfalls eine Rolle beim ZNS-Auswärts-Transport der gegen die AD entwickelten D-Peptide [85].

Da eine effiziente BHS-Gängigkeit für die AD-Therapie besonders wichtig ist, wird diese im Rahmen dieser Arbeit für die gegen die AD entwickelten D-Peptide untersucht. Hierzu werden unterschiedliche BHS-Durchlässigkeits-Parameter bestimmt, sodass die erhaltenen Werte mit denen anderer Peptide aus einer internationalen Peptid-Datenbank [107]

verglichen werden können. In diesem Zusammenhang wurden die folgenden vier BHS-Durchlässigkeits-Parameter ermittelt [107].

1.7.2.1 Blut-Gehirn-Gleichgewichtsverteilung (logBB Wert)

Die Blut-Gehirn-Gleichgewichtsverteilung (logBB Wert) beschreibt das Verhältnis der Konzentrationen in Blut und Gehirn nach Einstellen des „Steady States“ (bei Mehrfachgabe) bzw. das Verhältnis der AUCs in Blut und Gehirn (bei Einfachgabe). Der Wert ist zusätzlich sowohl von der Plasmaproteinbindung des Wirkstoffs als auch von Bindung des Wirkstoffs an das Gehirngewebe abhängig [107].

Einheit: ohne Einheit

Formel: $\mathrm{logBB} = \log\left(\frac{AUC_{Gehirn}}{AUC_{Plasma}}\right)$

1.7.2.2 Einseitige Zuflussgeschwindigkeitskonstante (K_{in})

Die einseitige Zuflussgeschwindigkeitskonstante (K_{in}) beschreibt die Kinetik der BHS-Gängigkeit (vom Blut ins Gehirn) eines Wirkstoffes und kann mit Hilfe der Daten der Plasma- und Gehirnkonzentrations-Zeit Kurven graphisch bestimmt werden. Sie beschreibt wie viel Plasma- bzw. Blut-Volumen durch eine Gehirnpassage pro Zeiteinheit vom applizierten Wirkstoff befreit wird [108, 109].

Einheit: mL/(g*min)

Formel: graphische Bestimmung durch $\frac{C_b(t)}{C_p(t)} = K_{in} * \frac{AUC_p(t)}{C_p(t)} + V_i$ (K_{in} = Steigung)

1.7.2.3 Initiales Verteilungsvolumen (V_i)

Das initiale Verteilungsvolumen (V_i) umfasst das intravaskuläre Volumen (V_0) sowie das Volumen sämtlicher Kompartimente des Gehirns, die in einem sich schnell einstellenden, reversiblen Gleichgewicht mit dem Plasma stehen, und ist eine funktionelle Größe. [109, 110]

Einheit: mL/g

Formel: graphische Bestimmung durch $\frac{C_b(t)}{C_p(t)} = K_{in} * \frac{AUC_p(t)}{C_p(t)} + V_i$ (V_i = Achsenabschnitt)

1.7.2.4 Permeabilitäts-Oberflächen-Produkt (permeability surface-area product, PS)

Das Permeabilitäts-Oberflächen-Produkt (PS) ist das Produkt aus der Permeabilität (P) und der Kapillar-Oberfläche (S). Es gibt an, wie viel Wirkstoff nach einmaliger i.v.-Bolusinjektion

aus einem bestimmten Volumen Blut pro Zeiteinheit in eine bestimmte Masse Gehirngewebe übergeht und wird auch als „uptake clearance from blood to brain“ (Beseitigung durch Aufnahme vom Blut ins Gehirn [107]) definiert [109].

Wenn die BHS-Permeabilität im Vergleich zum cerebralen Blutfluss (CBF) relativ gering ist (≤ 0,2 * CBF), ist PS ≈ K_{in} [109].

Der logarithmische PS-Wert (logPS) korreliert oftmals mit dem Oktanol/Wasser-Verteilungskoeffizienten ($logP_{Oktanol/Wasser}$) [109].

Einheit: mL/(g*min)

Formel: $PS = (-CBF)* \ln(1-K_{in}/CBF)$
wobei CBF = muriner cerebraler Blutfluss = 1,07 mL/(g*min) [111]

Nach Renkin-Crone-Gleichung: $PS = (-CBF) * (1-Hct) * \ln(1-E)$ [112]

Hct = Hämatokritwert [%]

E = Extraktionskonstante: Anteil des Wirkstoffes, der den Blutgefäßinnenraum beim ersten Durchfluss nach einer Bolusinjektion durch das Blutgefäßsystem (ins Gehirngewebe) verlässt

2 Zielsetzung der Arbeit

Ziel dieser Arbeit war die pharmakokinetische und pharmakodynamische Untersuchung Aβ-Oligomer eliminierender D-enantiomerer Peptide, die zur AD-Therapie entwickelt wurden. Während die pharmakokinetischen Studien, mit besonderem Augenmerk auf die BHS-Gängigkeit der D-Peptide, in Wildtyp-Mäusen durchgeführt werden sollten, sollten für die pharmakodynamische Therapie-Studie transgene Mäuse eines AD-Mausmodells mit kognitiven (1.6.2.2.1) Defiziten behandelt und untersucht werden.

2.1 Untersuchung der pharmakokinetischen Eigenschaften sowie der Blut-Hirn-Schranken-Gängigkeit D-enantiomerer Peptide

Damit ein gegen die AD entwickelter Wirkstoff im Gehirn der Patienten seine Wirkung entfalten kann, muss dieser geeignete pharmakokinetische Eigenschaften aufweisen, die BHS überwinden und therapeutisch wirksam sein. In dieser Arbeit sollten u.a. die pharmakokinetischen Eigenschaften D3‘s und zahlreicher seiner Derivate, die zuvor *in vitro*, und z.T. auch therapeutisch *in vivo* [74, 88] getestet wurden, untersucht werden. Ein besonderes Augenmerk sollte dabei auf die zuvor für die D-Peptide nur *in vitro* untersuchte BHS-Gängigkeit gelegt werden.

In Studien zu Beginn dieser Arbeit stellte sich heraus, dass Tandem-D-Peptide, die in vorherigen Behandlungsstudien eine hohe therapeutische Effizienz aufgewiesen hatten, keine vorteilhaften pharmakokinetischen Eigenschaften zeigten. Daher sollten deren pharmakokinetische Eigenschaften optimiert und in weiteren Studien dieser Arbeit untersucht werden, um das hohe Aβ-Oligomer-Eliminierungspotenzial der Tandem-D-Peptide effizienter nutzen zu können. Außerdem sollte eine wirksame Konzentration im Gehirn auch nach oraler Gabe erreicht werden, um so das Nutzen-Risiko-Verhältnis bei einer Langzeit-Therapie zu optimieren. Je geringer die nötige zu applizierende Dosis eines Wirkstoffes ist, desto geringer ist das Risiko unerwünschter Arzneimittelwirkungen und desto geringer sind langfristig die Therapie-Kosten.

Um herauszufinden, ob eine N- zu C-terminale Zyklisierung die BHS-Gängigkeit der D-Peptide effizienter macht, sollten ein lineares (RD2) und drei *head-to-tail* zyklisierte (cD3r, cD3D3, cRD2D3), direkte D3-Derivate (Sequenz bestehend aus den gleichen AS-Resten wie D3, z.T. jedoch abweichende AS-Reste-Anzahl) pharmakokinetisch in Wildtyp-Mäusen untersucht und miteinander verglichen werden. Das D3-Derivat mit der effizientesten BHS-Gängigkeit sollte dabei selektiert und detaillierteren pharmakokinetischen Untersuchungen

unterzogen werden, um seine Eignung für den Einsatz in einer therapeutischen Studie in transgenen AD-Mäusen zu überprüfen. Mithilfe der D-Peptid-Konzentrations-Zeit-Profile in Plasma und Gehirn sollten außerdem BHS-Durchlässigkeits-Parameter des selektierten D-Peptids berechnet werden, um einen Vergleich mit anderen, z.T. bereits als Wirkstoffe zugelassenen, Peptiden zu ermöglichen.

Die Gehirn-Konzentration eines Wirkstoffs kann im Rahmen klinischer Studien (in Menschen) nicht direkt ermittelt werden, die Konzentration des Wirkstoffs in der das Gehirn umgebenden CSF jedoch schon. Folglich sollte anhand der für die D-Peptid-Selektion erhobenen Daten überprüft werden, ob die Konzentrations-Zeit-Verläufe in Gehirn und CSF von Wildtyp-Mäusen direkt miteinander korrelieren. Weiterhin sollte die Korrelation der Konzentrations-Zeit-Verläufe in Gehirn und CSF mit denen im Plasma der Mäuse untersucht werden.

2.2 *In vitro* und *in vivo* Vergleich dreier D-enantiomerer Peptide gegen die AD

In einer weiteren Studie sollte ein *in vitro* gegen Aβ-Monomere selektiertes D3-Derivat der zweiten Generation (andere AS-Reste-Zusammensetzung als D3), ANK6, sowie zwei seiner Derivate, Tandem-ANK6 (tANK6) und zyklisches ANK6 (cANK6r), untersucht und miteinander verglichen werden. Dabei sollten unterschiedliche *in vitro* Tests zur Aβ-Interaktion und zum Aβ-Oligomer-Eliminierungspotenzial der D-Peptide sowie pharmakokinetische *in vivo* Untersuchungen in Wildtyp-Mäusen zur Ermittlung der Konzentrations-Zeit-Profile und der BHS-Durchlässigkeits-Parameter durchgeführt werden. Auch hier sollte eine mögliche Eignung der D-Peptide für den Einsatz in therapeutischen Studien in transgenen AD-Mäusen überprüft werden.

2.3 Untersuchung der pharmakodynamischen Eignung eines D-enantiomeren Peptids in einem transgenen AD-Mausmodell

Um die zuvor *in vitro* auf ihre Aβ-Interaktion und *in vivo* auf ihre pharmakokinetische Eignung untersuchten D-Peptide pharmakodynamisch *in vivo* in einer mehrwöchigen, oralen Therapiestudie in transgenen AD-Mausmodellen auf ihre Wirksamkeit testen zu können, sollte eine orale Darreichungsform gefunden werden, die die tägliche orale Gabe eines D-Peptid-Kandidaten minimalinvasiv gewährleistet.

Mit dieser Darreichungsform sollte eine 12-wöchige Therapiestudie (tägliche orale Wirkstoff-Gabe) in einem transgenen Mausmodell mit kognitiven Defiziten (APP/PS1dE9) mit dem D3-

Derivat RD2 durchgeführt werden. Um zu testen, ob die tägliche orale D-Peptid-Behandlung den AD-Phänotyp der transgenen Mäuse (verglichen mit Placebo-behandelten transgenen Mäusen) verringert, sollten zu Beginn und am Ende der Behandlung Verhaltenstests durchgeführt werden. Nach Abschluss der Behandlung sollten die Gehirne (Zielwirkort) der Mäuse immunhistochemisch und immunbiochemisch auf ihren Aβ-Gehalt sowie auf Entzündungsmarker untersucht werden.

3 Publikationen

3.1 Preclinical Pharmacokinetic Studies of the Tritium Labelled D-Enantiomeric Peptide D3 Developed for the Treatment of Alzheimer's Disease

Autoren:	Jiang N, Leithold LH, Post J, Ziehm T, Mauler J, Gremer L, Cremer M, **Schartmann E**, Shah NJ, Kutzsche J, Langen KJ, Breitkreutz J, Willbold D, Willuweit A
Journal:	PLoS One
	veröffentlicht am 05.06.2015
DOI:	10.1371/journal.pone.0128553
Impact Factor:	3,057 (2015)
Beitrag:	Beteiligung an der Durchführung der pharmakokinetischen Experimente
	Unterstützung bei der Auswertung der pharmakokinetischen Experimente

PLOS | ONE

RESEARCH ARTICLE

Preclinical Pharmacokinetic Studies of the Tritium Labelled D-Enantiomeric Peptide D3 Developed for the Treatment of Alzheimer´s Disease

Nan Jiang[1], Leonie H. E. Leithold[1], Julia Post[1], Tamar Ziehm[1], Jörg Mauler[2], Lothar Gremer[1], Markus Cremer[3], Elena Schartmann[1], N. Jon Shah[2], Janine Kutzsche[1], Karl-Josef Langen[2,4], Jörg Breitkreutz[5], Dieter Willbold[1,6]*, Antje Willuweit[2]*

1 Structural Biochemistry, Institute of Complex Systems (ICS-6), Forschungszentrum Jülich GmbH, Jülich, Germany, **2** Medical Imaging Physics, Institute of Neuroscience and Medicine (INM-4), Forschungszentrum Jülich GmbH, Jülich, Germany, **3** Structural and functional organisation of the brain, Institute of Neuroscience and Medicine (INM-1), Forschungszentrum Jülich GmbH, Jülich, Germany, **4** Department of Nuclear Medicine, Universitätsklinikum der RWTH Aachen, Aachen, Germany, **5** Institute of Pharmaceutics and Biopharmaceutics, Heinrich-Heine-Universität Düsseldorf, Düsseldorf, Germany, **6** Institut für Physikalische Biologie, Heinrich-Heine-Universität Düsseldorf, Düsseldorf, Germany

* D.Willbold@fz-juelich.de (DW); A.Willuweit@fz-juelich.de (AW)

OPEN ACCESS

Citation: Jiang N, Leithold LHE, Post J, Ziehm T, Mauler J, Gremer L, et al. (2015) Preclinical Pharmacokinetic Studies of the Tritium Labelled D-Enantiomeric Peptide D3 Developed for the Treatment of Alzheimer´s Disease. PLoS ONE 10(6): e0128553. doi:10.1371/journal.pone.0128553

Academic Editor: Riqiang Yan, Cleveland Clinic Foundation, UNITED STATES

Received: March 4, 2015

Accepted: April 28, 2015

Published: June 5, 2015

Data Availability Statement: All relevant data are within the paper and its Supporting Information files.

Funding: DW was supported by grants from the "Portfolio Technology and Medicine" and the Helmholtz-Validierungsfonds of the Impuls und Vernetzungs-Fonds der Helmholtzgemeinschaft; KJL and DW were supported by the "Portfolio Drug Design" of the Impuls und Vernetzungs-Fonds der Helmholtzgemeinschaft (http://www.helmholtz.de/ueber_uns/impuls_und_vernetzungsfonds; no grant numbers available). The funders had no role in study

Abstract

Targeting toxic amyloid beta (Aβ) oligomers is currently a very attractive drug development strategy for treatment of Alzheimer´s disease. Using mirror-image phage display against Aβ1-42, we have previously identified the fully D-enantiomeric peptide D3, which is able to eliminate Aβ oligomers and has proven therapeutic potential in transgenic Alzheimer´s disease animal models. However, there is little information on the pharmacokinetic behaviour of D-enantiomeric peptides in general. Therefore, we conducted experiments with the tritium labelled D-peptide D3 (^{3}H-D3) in mice with different administration routes to study its distribution in liver, kidney, brain, plasma and gastrointestinal tract, as well as its bioavailability by i.p. and p.o. administration. In addition, we investigated the metabolic stability in liver microsomes, mouse plasma, brain, liver and kidney homogenates, and estimated the plasma protein binding. Based on its high stability and long biological half-life, our pharmacokinetic results support the therapeutic potential of D-peptides in general, with D3 being a new promising drug candidate for Alzheimer´s disease treatment.

Introduction

After the initial description by Alois Alzheimer in 1906 [1], Alzheimer's disease (AD), a progressive neurodegenerative disorder, has become nowadays the most common form (60–80%) of dementia [2]. According to the World Alzheimer Report 2014, nearly 36 million people worldwide are suffering from AD or related dementia. Even after years of intensive

design, data collection and analysis, decision to publish, or preparation of the manuscript.

Competing Interests: The authors have declared that no competing interests exist.

investigation and research, it is still an incurable disease [3]. Current treatments are only supportive against some of its symptoms. Clinical duration of AD varies from one to 25 years, typically eight to ten years [4].

Amyloid beta (Aβ) is produced by sequential cleavage of a type I integral transmembrane protein, called amyloid precursor protein (APP) by β- and γ-secretases. Variable lengths of Aβ isomers differing at the C-terminus are produced due to imprecise cleavage by γ-secretase [5, 6]. The most abundant isomers are Aβ1–40 (approximately 80–90%) and Aβ1–42 (approximately 5–10%). Aβ1–42 is more hydrophobic and fibrillogenic, and therefore the main component of Aβ plaques in the brain of AD patients [7]. It also aggregates readily into oligomers, which are considered to be the most toxic form of Aβ [8–10].

In recent years, many substances have been developed targeting Aβ production and clearance [11], including peptide-based drugs [12, 13]. In spite of the many advantages of peptide drugs, for example high specificity and low toxicity, their short half-life time *in vivo* due to rapid degradation by proteases, and low bioavailability by oral administration, restrict their clinical usage. In comparison to naturally occurring L-form peptides, peptides derived from partial D-amino acid substitutions or D-enantiomeric peptides, which are composed entirely of D-amino acids, have advantages over L-enantiomers. Because of the stereoisomeric selectivity of proteolytic enzymes they are less prone to proteolysis, therefore longer half-lives and higher bioavailability after oral administration are to be expected [14–16]. Furthermore, they are less or even not immunogenic at all [13].

The fully D-enantiomeric peptide D3, which was identified by mirror-image phage display [17, 18] for binding to Aβ (1–42), has been shown to have interesting properties. D3 inhibits Aβ fibril formation and eliminates Aβ-oligomers *in vitro*. *Ex vivo*, D3 has been shown to specifically bind to amyloid plaques in transgenic mice [19]. *In vivo*, D3 was able to reduce plaque load and inflammation markers in the brains of treated transgenic mice, as well as improve their cognition even after oral administration [20–23]. Here we investigate the pharmacokinetic properties of D3 in mice.

We present the first comprehensive preclinical pharmacokinetic study of a peptide consisting solely of D-enantiomeric amino acid residues in general and in particular for such a D-peptide developed for the treatment of Alzheimer's disease.

Materials and Methods

Materials

^{3}H-D3 (rprtr-(4,5-^{3}H-Leu)-hthrnr) and its L-form enantiomer ^{3}H-(L)-D3 (RPRTR-(4,5-^{3}H-Leu)-HTHRNR) were purchased from Quotient Bioresearch (Radiochemicals) Ltd. (Cardiff, United Kingdom) with 10–100 Ci/mmol, 1 mCi/ml and purity >95%.

All chemicals were supplied by Fluka Chemie AG (Buchs, Switzerland), Merck (Darmstadt, Germany), AppliChem (Darmstadt, Germany) and VWR (Darmstadt, Germany) in research grade. Micro-osmotic pumps (model 1007D) were purchased from Alzet DURECT Corporation, (Cupertino, CA, USA).

Animals

Male C57Bl/6 mice (Charles River, Sulzfeld Germany) with an average age of 13 weeks and body weight of 28.5 g were used in this study. For micro-osmotic pump i.p. implantation experiment, 19 months old mice were used with average body weight of 34 g. The mice were hosted in the animal facility of the Forschungszentrum Juelich under standard housing conditions with free access to food and water for at least 2 weeks before experiment. All animal experiments were approved by the Animal Protection Committee of the local government

(LANUV (Landesamt für Natur, Umwelt und Verbraucherschutz), North-Rhine-Westphalia, Germany, AZ84-02.04.2011. A359 and AZ84-02.04.2011. A356) according to the Deutsche Tierschutzgesetz). All sections of this study adhere to the ARRIVE Guidelines for reporting animal research [24]. A completed ARRIVE guidelines checklist was included in Supporting Information (S1 File).

Pharmacokinetic studies

Mice were administered with 100 µl radioactive working solution consisting of 5 µCi ^{3}H-D3 in 5 µl with 95 µl buffer (0.1 M phosphate buffer, pH 8) as a single bolus dose either i.v. (tail vein), i.p. or p.o. (gavaging). In order to achieve the desired total D3 concentration, non-radioactive D3 was added to a concentration of 1 mg/ml (i.v.) or 3 mg/ml (i.p. and p.o.). Doses were selected from previous tolerability studies and were not causing any adverse effects. I.v. injections and i.p micro-osmotic pump implantations were performed under anaesthesia with ketamine/medetomidine per i.p. administration. Antisedan was administered s.c. to reverse the anaesthesia directly after the intervention, which took about 10 min. Sampling times were chosen depending on the route of administration (i.p.: 10, 20, 30, 60, 120, 240, 360, 1440 and 2880 min.; p.o.: 10, 20, 30, 60, 120, 240, 360, 1080, 1440, 2880 and 4320 min.; i.v.: 3, 5, 10, 15, 30, 60, 240, 1440 and 2880 min.; 3 animals per time point). For i.p. micro-osmotic pump implantation, delivery dose of pumps was set to 5 µCi ^{3}H-D3 plus 0.3 mg non-radioactive D3 per 24 hours per mouse. Sampling times were 2, 4 and 6 days after implantation (3 mice per time point).

Upon sampling time, blood was drawn per heart puncture under isoflurane anaesthesia and heparinized plasma was isolated. A small piece of liver (approx. 0.2 g), the left kidney and the right brain hemisphere were sampled. To study the gastrointestinal absorption and elimination by p.o. administration, mice were fasted 18 hours before the experiment and their complete gastrointestinal tracts were prepared. Small intestine was dissected into 4 equal parts and marked from oral to aboral as 1 to 4, respectively. Organ samples were weighted and homogenized in homogenizer tubes (Precellys Ceramic Kit 1.4 mm, Precellys 24, Bertin technologies SAS, Montigny le Bretonneux, France) with 500 µl PBS. 10 ml scintillation cocktail (Ultima Gold XR, PerkinElmer, Waltham, Massachusetts, USA) was added to 100 µl of each organ homogenate or plasma (diluted 1:1 with PBS) and mixed well. Disintegrations per unit time (dpm) were obtained in triplicates with a liquid scintillation counter (Packard Tri-Carb 2100TR Liquid Scintillation Analyser, PerkinElmer, Waltham, MA, USA). Blank values of each sample were obtained by omitting radioactive substance following the same protocol.

Radioactivity counted in each sample was adjusted (subtraction of the blank value) and was expressed as percentage injected dose per gram tissue or millilitre plasma (%ID/g or %ID/ml), or as milligram of total D3 per gram tissue or millilitre plasma (mg/g or mg/ml).

Pharmacokinetic analysis

Pharmacokinetic parameters were calculated with non-compartmental analysis using Phoenix WinNonlin, version 6.3 (Pharsight Corp., St. Louis, USA). Mean D3 concentrations per time point were used to calculate the PK parameters (model type: plasma (200–202); calculation method: linear trapezoidal linear interpolation; dose options: "IV Bolus" for i.v. or "Extravascular" for i.p. and p.o. administration). The same model setting was used to estimate pharmacokinetic parameters of brain. For i.v. administration, plasma concentration at time zero (C0) was back extrapolated with a log-linear regression of the first two observed plasma concentrations, while brain C0 was set to be zero. For the i.p. and p.o. administrations, all concentrations at time zero were set to be zero.

The last three to five observed mean plasma concentrations were used to estimate the first order rate constant in the terminal elimination phase (Lambda_z) based on the largest adjusted square of the correlation coefficient (R^2) of the log-linear regression lines. The area under the curve (AUC) from C0 extrapolated to infinity ($AUC_{C0\text{-}inf}$) was calculated as the sum of $AUC_{C0\text{-}last}$+(Clast/Lambda_z), calculated from the last determined concentration derived by Lambda_z, and $AUC_{C0\text{-}last}$ representing the AUC from time point zero to the last observed concentration (Clast). Parameters that do not require Lambda_z were calculated for brain data: time of maximal observed concentration (Tmax), maximal observed concentration (Cmax), maximal observed concentration normalized to dose (Cmax/D), $AUC_{C0\text{-}last}$ and mean residence time from the time of dosing to the last time point ($MRT_{C0\text{-}last}$). Additional parameters requiring estimated Lambda_z were calculated for plasma data: Lambda_z, terminal half-life (HL_Lambda_z), $AUC_{C0\text{-}inf}$, terminal volume of distribution (Vz), plasma clearance (Cl), $MRT_{C0\text{-}inf}$ and volume of distribution at steady state (Vss). Absolute bioavailability of i.p. and p.o. administration was calculated with $AUC_{C0\text{-}inf}$ by: F(bioavailability) = [AUC(non-iv)*Dose (iv)]/[AUC(iv)*Dose(non-iv)]*100.

To minimize the time dependence of brain-plasma ratio by bolus dosing, brain-plasma ratio was calculated from the areas under the brain and plasma concentration curves in the terminal elimination phase starting from 4 hours to infinity (brain_$AUC_{4h\text{-}inf}$/plasma_$AUC_{4h\text{-}inf}$).

Plasma protein binding

Plasma protein binding was estimated by incubation of D3 with varying concentrations of protein using TRANSIL^{XL} binding kits (Sovicell GmbH, Leipzig, Germany). K_D values were determined by titrating a constant drug concentration against different concentrations of human serum albumin (HSA) and α_1-acid glycoprotein (AGP). Experiments were performed as recommended for the kit. To obtain the desired D3 stock solution of 80 μM, non-radioactively labelled D3 was dissolved in PBS and 5% ^{3}H-labelled D3 solution was added for detection purposes. A final concentration of 5 μM D3 was applied in the assay. After incubation and centrifugation 15 μl supernatant were taken and scintillation cocktail was added. This was done in triplicate. Radioactivity was then quantified using liquid scintillation counting. After measuring the disintegrations per minute (dpm) of the supernatant containing the unbound peptide, the D3 fraction bound to the titrated protein was calculated and plotted against the protein concentrations. The curves were fitted to the Michaelis Menten ligand binding equation (SigmaPlot 11.0, Systat Software, Inc., San Jose, California, USA) to obtain the K_D. Mean and relative standard error (%) of multiple measurements are given (AGP n = 3, HSA n = 2).

For bioavailability determination, the unbound fraction of D3 (f_u) was calculated using the equation below:

$$f_u = 100 * \frac{\frac{C_{D3}-K_D-C_{physiol}}{2} + \sqrt{K_D * C_{D3} + \left(\frac{C_{D3}-K_D-C_{physiol}}{2}\right)^2}}{C_{D3}} \quad (1)$$

For very low D3 concentrations in blood (C_{D3}), Eq (1) can be simplified by Eq (2), where the unbound fraction of D3 can be calculated independently of the applied D3 concentration. Since this is true for our *in vivo* experiments we used Eq (2) for the total free fraction of D3, combining the binding of D3 to HSA and AGP. For calculation of the overall unbound fraction according to Eq (2), physiological concentrations ($C_{physiol}$) of 0.65 mM HSA and 0.02 mM

AGP were assumed.

$$f_{u,total} = 100 * \frac{1}{1 + \frac{C_{physiolHSA}}{K_D HSA} + \frac{C_{physiolAGP}}{K_D AGP}} \quad (2)$$

Calibration curves and internal standard

Calibration curves were prepared by adding a corresponding ^{3}H-D3 dilution series with certain dpm range to plasma or organ homogenates in comparison to those diluted in PBS. The dpm ranges of each ^{3}H-D3 dilution series were set to cover the measured dpm ranges of each sample (for plasma 400–40000; for brain 100–1200; for liver 3000–15000; for kidney 40000–400000). Plasma and organ homogenates obtained from C57Bl/6 mice were prepared following the same procedure as outlined above.

No differences were found comparing the calibration curves of ^{3}H-D3 in organ homogenates or plasma to those in PBS. The measured dpm values of the internal standard with ^{3}H-D3 in PBS matched closely the expected ones.

Thin layer chromatography

In order to study the proteolytic stability of peptides in biological extracts, tritium labelled peptides were incubated with liver microsomes (pooled from mouse (CD-1), Sigma-Aldrich), freshly prepared mouse plasma or extracts of brain, liver and kidney at 37°C for different time periods (from 0 min to 2 days). 1 μCi (approx. 0.08–0.8 μg) radioactive labelled peptide was mixed with 1 μl microsomes stock solution, plasma or organ extracts, respectively (in great excess to peptide). Mixtures containing tritium-labelled peptides were applied onto HPTLC Silica Gel 60 plates (OMNILAB, Essen, Germany) for thin layer chromatography (TLC) with a mobile solvent (2-Butanol/Pyridine/Ammonia(28%)/Water(39/34/10/26)). After development, a phosphor imaging plate for ^{3}H-autoradiography (FUJIFILM, Tokyo, Japan) was exposed to the TLC plates for 3 days. Images were acquired with a BAS reader and AIDA software (Raytest, Freiburg, Germany). Retardation factor (Rf) of each substance was defined as the ratio of the migration distance of the centre of a separated spot to the migration distance of the solvent front.

Results

Proteolytic stability of D3 in comparison to its L-enantiomer

Before meaningful pharmacokinetic studies could be performed with ^{3}H-D3, it was essential to show that the D-peptide is stable under near *in vivo* conditions. First, we compared the stability of ^{3}H-D3 with its exact enantiomer, ^{3}H-(L)-D3 in plasma (Fig 1). ^{3}H-(L)-D3 shows significant degradation already after 60 min incubation in plasma as concluded by the appearance of additional bands as compared to the mixture at 0 min on the TLC plate after detection by autoradiography. In contrast, ^{3}H-D3 did not show any degradation products even after 2 d incubation in the same plasma preparation.

More importantly, ^{3}H-D3, was neither degraded after 2 h incubation in liver microsomes nor after 2 days incubation in homogenates of kidney, brain and liver as shown by TLC and detection by autoradiography (Fig 2). Microsomes were checked for proteolytic activity using L-peptide substrates.

Due to high but unspecific affinity of D3 and (L)-D3 to the TLC plate support material (glass), artefacts were observed at the starting points of the TLC as well as light smears

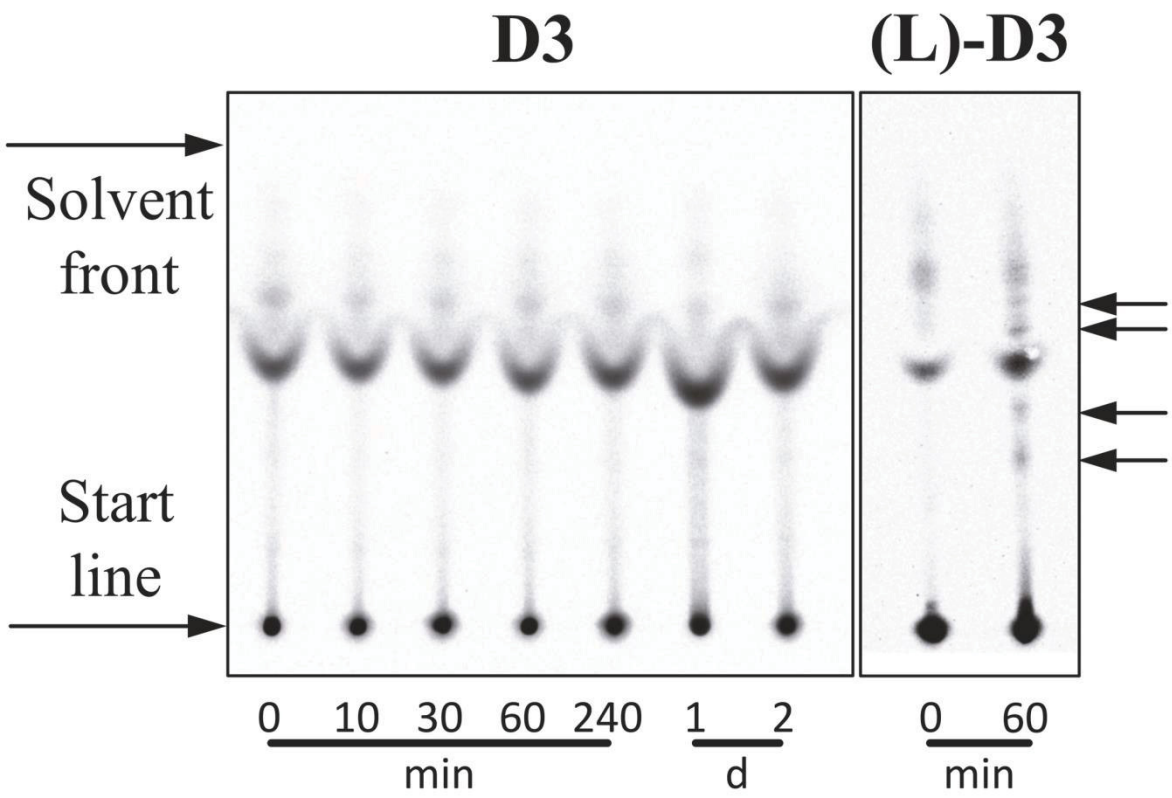

Fig 1. Autoradiogram demonstrating proteolytic stability of ^{3}H labelled peptides in plasma. ^{3}H-D3 was incubated with plasma for different times at 37°C and developed on TLC plates. For comparison, the exact enantiomer of D3, (L)-D3, was used in this stability assay. ^{3}H-(L)-D3 was incubated with plasma for 0 and 60 min at 37°C. Please note that free ^{3}H-(L)-D3 and free ^{3}H-D3 are perfect enantiomers to each other and because the TLC material is not chiral, both compounds show identical Rf values. Additional bands in the 0 min lanes of ^{3}H-(L)-D3 and ^{3}H-D3 that arise from binding and co-migration of ^{3}H-D3 and ^{3}H-(L)-D3 to plasma components do not necessarily have identical Rf values in the 0 min lanes of ^{3}H-(L)-D3 and ^{3}H-D3, because some of the plasma components are enantiomers themselves. Therefore, any effect of degradation will lead to extra additional bands as compared to the 0 min lane of the very same compound. Obvious proteolytic degradation can be observed for ^{3}H-(L)-D3 already after 60 min incubation with plasma leading to additionally appearing bands (black arrows) as compared to the 0 min lane ^{3}H-(L)-D3. Additionally appearing bands as compared to 0 min incubation are not observed for ^{3}H-D3 even after 2 days incubation.

doi:10.1371/journal.pone.0128553.g001

originating thereof. To prove that these compounds were not located in the layer of the TLC matrices, a control experiment was performed by placing a new TLC plate to a freshly developed plate to transfer only the ^{3}H-peptides within matrices, but not those on the glass surface support (Fig 3). Artefacts could thus be eliminated.

Pharmacokinetics

Time dependent distribution of D3 in organs and plasma after different administration routes was analysed using tritium labelled D3 (^{3}H-D3) as shown in Fig 4. The corresponding pharmacokinetic parameters calculated with non-compartmental analysis based on the absolute amount of administered D3 are shown in Tables 1 and 2.

After i.v. and i.p. administration, pharmacokinetic curves showed similar patterns with highest concentration of tritium per gram tissue found in kidney, followed by liver and plasma.

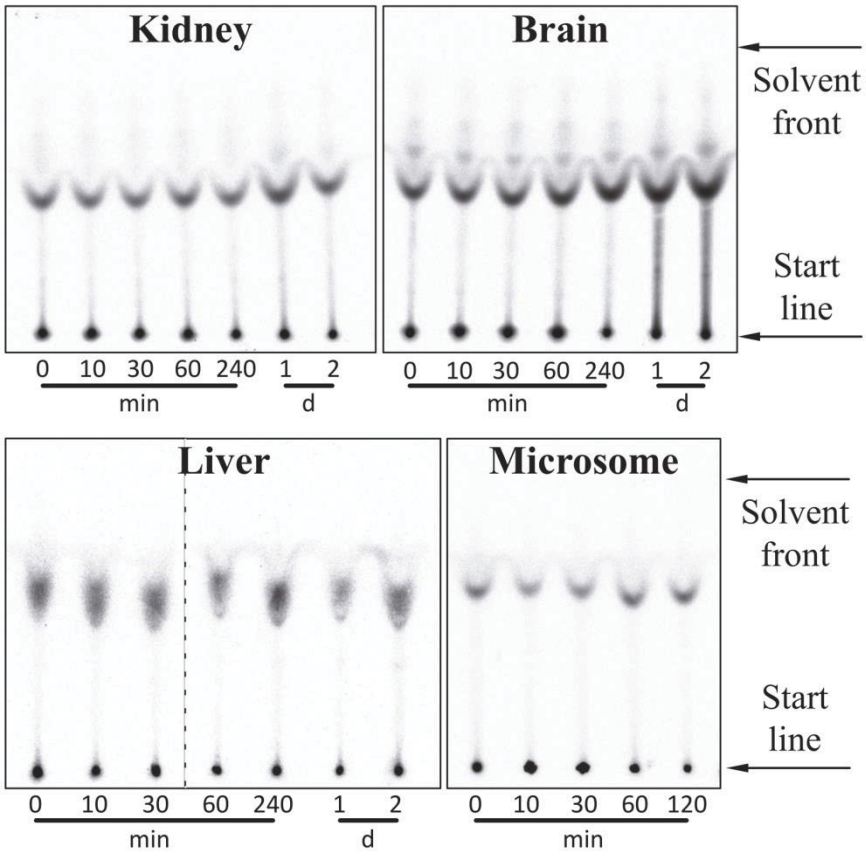

Fig 2. Autoradiogram demonstrating proteolytic stability of ^{3}H labelled peptides in liver microsomes and organ homogenates. ^{3}H-D3 was incubated with kidney, brain and liver homogenate for 0, 10, 30, 60, 240 min and 1, 2 days at 37°C and developed on TLC plates. For liver microsomes, the incubation time was 0, 10, 30, 60 and 120 min. Slight difference in Rf values of ^{3}H-D3 in liver homogenate might be due to incompletely homogenized liver tissues, which was not observed after incubation with liver microsomes. (Two autoradiograms of liver homogenate were presented in one image and separated through a dashed line.) No obvious proteolytic degradation of D3 can be observed in all the organ homogenates with up to two days' incubation.

doi:10.1371/journal.pone.0128553.g002

However, after oral administration ^{3}H-D3 concentrations measured in kidney and liver did not exceed concentrations in plasma (Fig 4). Plasma Cmax/D after i.v. administration reached 78 μg/ml/mg at Tmax 3 min (the first sampling time point), while after i.p. and p.o. administration plasma Cmax/D were 47 μg/ml/mg at 10 min and 1.5 μg/ml/mg at 240 min (Table 1). In brain, the Cmax/D and their corresponding Tmax values for i.v., i.p. and p.o. administration were 2.8, 2.2 and 1.3 μg/ml/mg at 3, 20 and 240 min, respectively (Table 2). However, after 4 hours concentrations in brain reached similar concentrations irrespectively of the administration route (Fig 4). Although plasma concentrations after p.o. administration appeared to be very low in comparison to i.v. and i.p. administration, comparable concentrations of ^{3}H-D3 were found in the brain resulting in high brain/plasma ratio after 4 h (Fig 5).

4 hours after a ^{3}H-D3 bolus dose, brain/plasma ratio of all administration routes reached a plateau between 0.7 and 1.0 (Fig 5). To minimize the time dependence of brain/plasma ratio, the absolute ratios were calculated from the area under the brain and plasma concentration

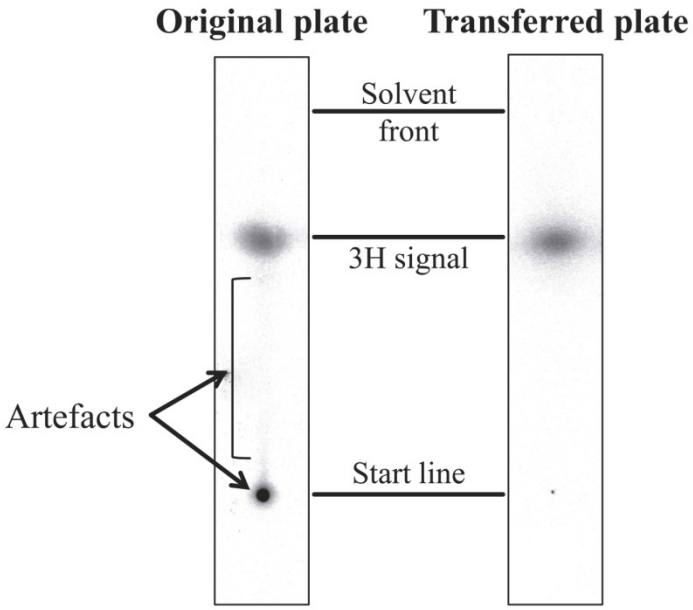

Fig 3. Plate-transfer of ^{3}H-D3 in TLC matrices. A control experiment was performed by placing a new TLC plate to a freshly developed plate to transfer only the ^{3}H-D3 within matrices. On the mirror image of the transferred plate, the ^{3}H signals at the start points as well as the smears were obviously reduced, while the intensity of separated ^{3}H-D3 did only change slightly. This result suggests that the observed artefacts arise from unspecific ^{3}H-D3 binding to the glass surface.

doi:10.1371/journal.pone.0128553.g003

curves from 4 hours to infinity (brain_$AUC_{4h\text{-}inf}$/plasma_$AUC_{4h\text{-}inf}$) with 1.07 for i.v., 0.69 for i.p., and 0.85 for p.o. administration.

After bolus administration, D3 showed relatively long elimination half-lives in plasma of 31.8 h, 41.2 h and 40.7 h after i.v., i.p. and p.o. administration, respectively. Plasma clearance was 0.12 ml/min after i.v. administration. Apparent volumes of distribution were different among i.v., i.p. and p.o. administration with 316, 444 and 684 ml, respectively (Table 1).

Absolute bioavailability was high with 92.2% after i.p. administration and 58.3% after p.o. administration (Table 1). When studying gastrointestinal distribution of D3 after p.o. administration (Fig 6), most of the radioactivity was found in the lower intestinal tract after 4 hours, which suggested that the majority of D3 did not enter the system circulation within 4 hours. Still, the AUC of D3 in brain after p.o. administration was comparable to those after i.p. and i.v. administration (Table 2).

We were also interested in answering the question, whether continuous dosing over several days using an i.p. implanted osmotic pump is showing specific effects in D3 distribution. We found linearly increasing D3 concentrations in plasma and all tested organs over 6 days (Fig 7). Although D3 highly accumulated in liver and kidney at day 6, the mice did not show any obvious signs of intoxication. The brain/plasma ratio increased with time from 0.53 at day 2 to 0.77 at day 6.

Plasma protein binding of D3

To estimate the free fraction of D3 in plasma *in vivo* ($f_{u,total}$), D3 was incubated with human serum albumin (HSA) and α_1-acid glycoprotein (AGP) in an *in vitro* assay (Fig 8). The plasma

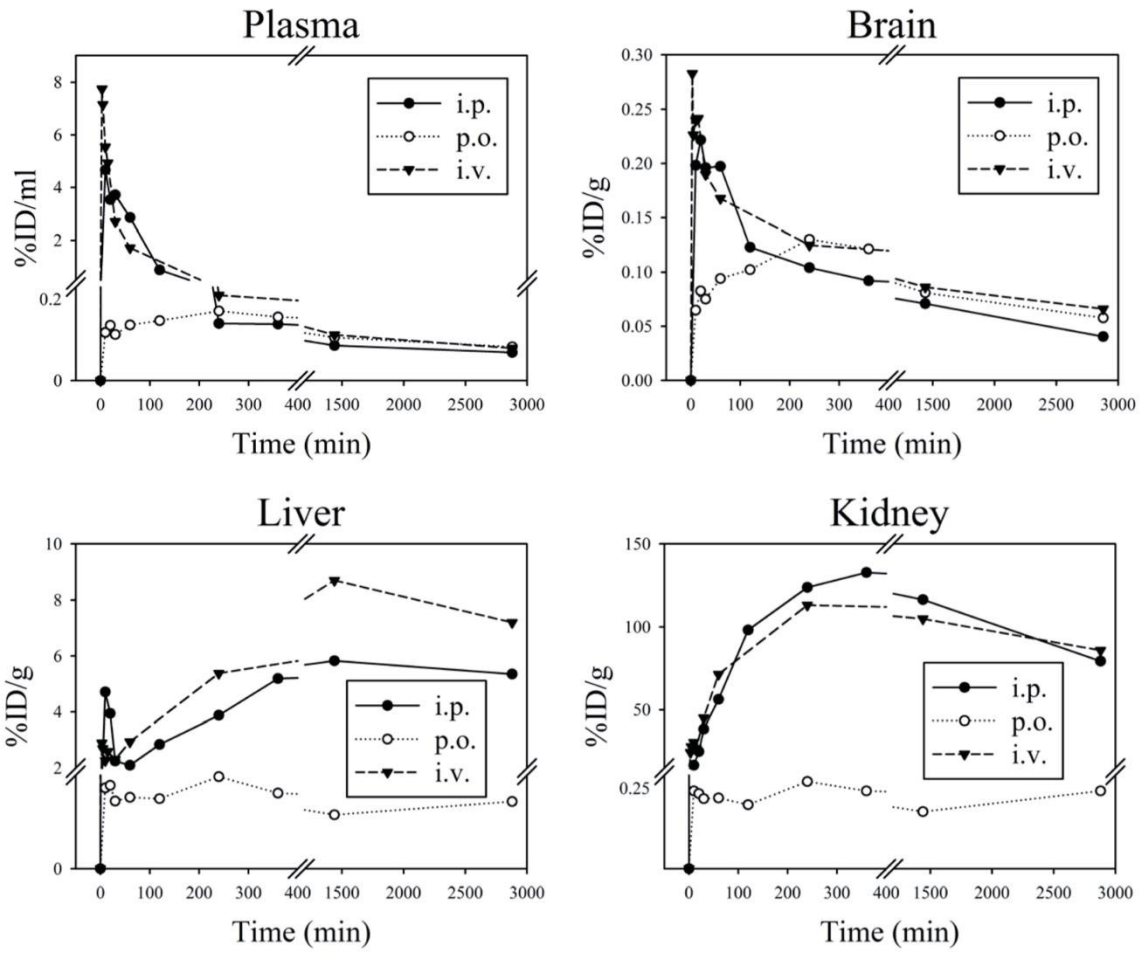

Fig 4. Mean pharmacokinetic profiles of ^{3}H-D3 in organs and plasma after i.p., p.o. and i.v. administration. ^{3}H-D3 (5 μCi) mixed with D3 in a total concentration of 3.5 mg/kg (i.v.) or 10.5 mg/kg (i.p. and p.o.) was applied per mouse. D3 concentrations are shown as percentage of injected dose per gram tissue or milliliter plasma (%ID/g or %ID/ml) dependent of time after administration. Mean values from 3 mice are shown.

doi:10.1371/journal.pone.0128553.g004

protein binding assay for AGP resulted in a K_D of 1.8 μM ± 7.9%. Assuming a D3 concentration in blood of 0.1 μM (C_{D3}, measured 4 h after i.p. injection) calculation of binding to AGP according to Eq (1) predicts a free fraction of 8.3%. For HSA, the K_D was above the detection limit of the kit (> 1.4 mM) indicating very low affinity of D3 to HSA. Nevertheless, calculation of the free fraction with an assumed K_D of 1.4 mM resulted in 68.3% free D3. Taken together, using Eq (2), the estimated free fraction of D3 in plasma was calculated to be approximately 8%.

Discussion

In the current study we have analysed the distribution of the D-enantiomeric peptide D3 after single intravenous, intraperitoneal and per oral administration, as well as continuous dosing

Table 1. Pharmacokinetic parameters for D3 from noncompartmental analysis of plasma.

Parameter	Units	i.v. (3.5 mg/kg)	i.p. (10.5 mg/kg)	p.o. (10.5 mg/kg)
Tmax	min	3	10	240
Cmax	µg/ml	7.75	14	0.45
Cmax/D	µg/ml/mg	77.5	46.7	1.48
$AUC_{C0\text{-}last}$	min*µg/ml	679	1763	1095
$MRT_{C0\text{-}last}$	min	547	527	1718
Lambda_z	1/min	0.00036	0.00028	0.00028
HL_Lambda_z	min	1907	2471	2439
$AUC_{C0\text{-}inf}$	min*µg/ml	869	2404	1521
$MRT_{C0\text{-}inf}$	min	1658	2104	3430
Vz	ml	317	445	684
Cl	ml/min	0.115	N.A.	N.A.
Vss	ml	190	N.A.	N.A.
Bioavailability	%	N.A.	92.2	58.3

N.A.: Parameters not applicable for this administration route. For abbreviations see methods section.

doi:10.1371/journal.pone.0128553.t001

via intraperitoneally implanted osmotic pumps. To the best of our knowledge, this is the first report of a comprehensive pharmacokinetic study of a peptide consisting solely of D-enantiomeric amino acid residues in rodents demonstrating excellent proteolytic stability, long plasma half-life and very high oral bioavailability.

D3 showed high proteolytic resistance exactly as it was shown *in vitro* previously with other all-D-peptides [14–16]. Thanks to this stability, metabolites can be neglected and the measured ^{3}H radioactivity represents the concentration of D3 after administration *in vivo*.

Estimated terminal plasma half-lives of D3 were between 32 and 41 h and were thus much higher than those reported for L-enantiomeric peptides which are typically only a few minutes [25]. Four hours after administration, irrespective of the administration routes, the temporal distribution of D3 in brain closely followed that in plasma resulting in brain/plasma ratios between 0.7 and 1.0 (Fig 5). While substances with a brain/plasma ratio larger than 0.3 are considered to have sufficient access to the central nervous system [26], our results suggest that D3 efficiently overcomes the blood-brain barrier.

Interestingly, by p.o. administration of D3, in spite of only a small rate of D3 being absorbed via the enteric tract, the bioavailability was 58.3% (Table 1), which is relatively high in comparison to that of L-peptide drugs, which were described to be less than 1% without delivery enhancement [27–30]. This finding can be explained by slow oral absorption of D3 and particularly long terminal half-life in plasma resulting in high AUC-values after p.o.

Table 2. Pharmacokinetic parameters for D3 from noncompartmental analysis of brain.

Parameter	Units	i.v. (3.5 mg/kg)	i.p. (10.5 mg/kg)	p.o. (10.5 mg/kg)
Tmax	min	3	20	240
Cmax	µg/g	0.283	0.665	0.390
Cmax/D	µg/g/mg	2.83	2.22	1.30
$AUC_{C0\text{-}last}$	min*µg/g	275	643	935
$MRT_{C0\text{-}last}$	min	1173	1108	1693

For abbreviations see methods section.

doi:10.1371/journal.pone.0128553.t002

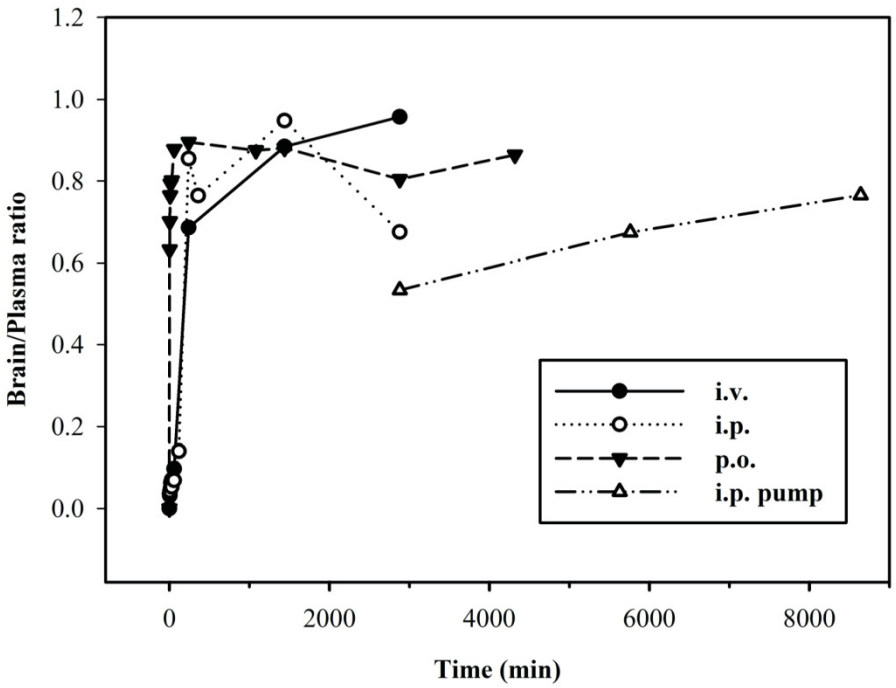

Fig 5. Temporal distribution of brain/plasma ratio of ^{3}H-D3 after different administration routes. Following bolus dose administration, low brain/plasma ratios were found at the starting time points. After 4 hours, the ratios reached relative high values and varied between 0.7–1.0. Upon i.p. pump implantation the ratio increased constantly with time.

doi:10.1371/journal.pone.0128553.g005

administration (Table 1). Low concentrations of D3 as found in kidney and liver after p.o. administration are desirable because this lowers the risk of possible intoxication of important organs. With absorption enhancers and a more suitable formulation of D3, even higher oral bioavailabilities seem to be feasible. Due to the observed high stability of D3 against proteolysis under biological conditions and its hydrophilic properties, elimination via biliary excretion (without re-absorption) and renal clearance in unchanged form could be expected.

Estimated volumes of distribution were 11.1 (i.v.), 15.6 (i.p.) and 24.0 l/kg (p.o.), respectively considering the body weight of the mice (28.5 g in average). The total body water in C57Bl/6 mice is approximately 0.6 l/kg [31], suggesting a distribution of D3 beyond the body fluid and some uptake in peripheral tissues.

Plasma volume of distribution at steady state was also high with 191 ml and 6.69 l/kg considering the body weight of the mice and the fraction of unbound D3 in plasma was predicted to be around 8%. High volume of distribution promotes low plasma clearance, which in our study was approximately between 0.12–0.19 ml/min observed in all routes of administration.

In summary, the current study demonstrates high proteolytic stability for the D-enantiomeric peptide D3. Furthermore, D3 enters the brain very efficiently and shows high oral bioavailability. The terminal half-life in mice after p.o. administration was approximately 41 hours with a brain/plasma ratio between 0.7 and 1.0, and a bioavailability of about 60%.

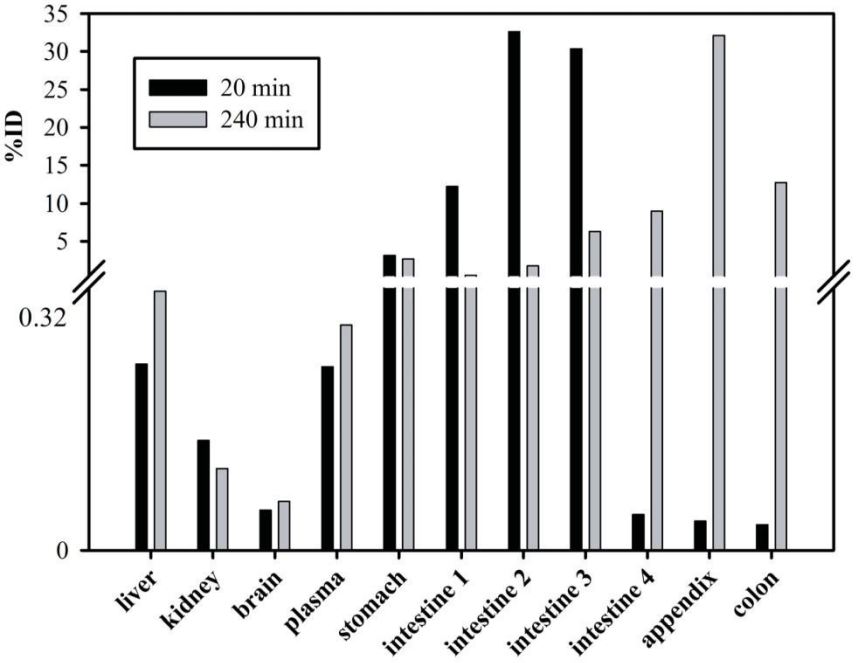

Fig 6. Distribution of ^{3}H-D3 after p.o. administration in organs and plasma. 20 min after gavaging of 100 µl, 5 µCi ^{3}H-D3 with a total D3 concentration of 10.5 mg/kg, most of the radioactivity was located in the middle of small intestine (intestine 2 and 3); 4 hours later, it spread to the lower intestinal tract. Of note is the high concentration of D3 observed in the appendix. At this time point, D3 could already be detected in feces. In comparison to the gastrointestinal tract, the amount of D3 in other organs or plasma after p.o. administration was very low.

doi:10.1371/journal.pone.0128553.g006

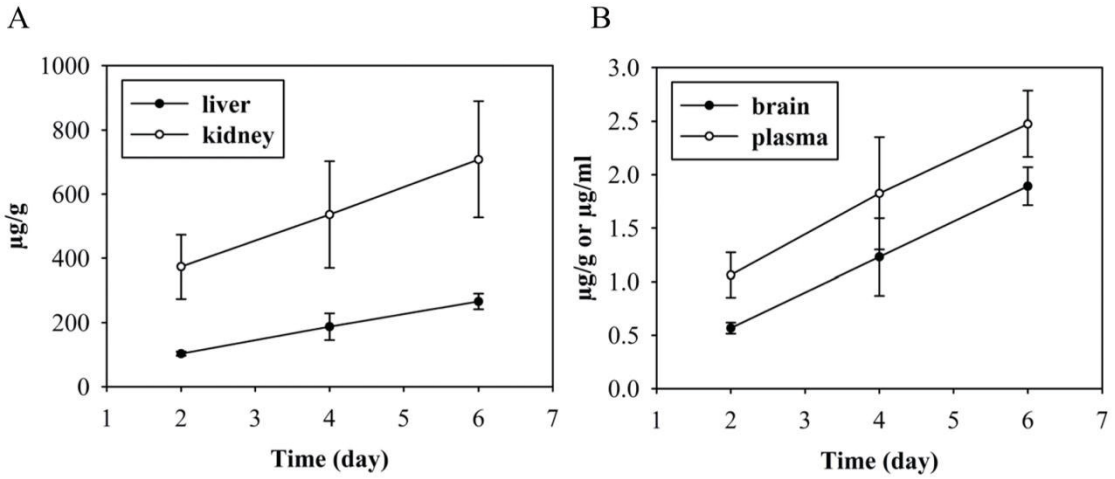

Fig 7. Concentration of ^{3}H-D3 in kidney, liver, brain and plasma administered via i.p. implanted osmotic pump. Alzet mini pumps with a delivery rate of 0.3 mg D3 (plus 5 µCi ^{3}H-D3) per 24 hours were implanted i.p. and organs were sampled after 2 to 6 days. Similar to bolus i.p. administration, more ^{3}H-D3 was found in kidney than in liver (A), whereas D3 concentrations in plasma and brain were considerably lower (B). The concentration of D3 was increasing linearly over time suggesting that the saturation concentration in the respective organs and plasma was not reached by 6 days of continuous dosing.

doi:10.1371/journal.pone.0128553.g007

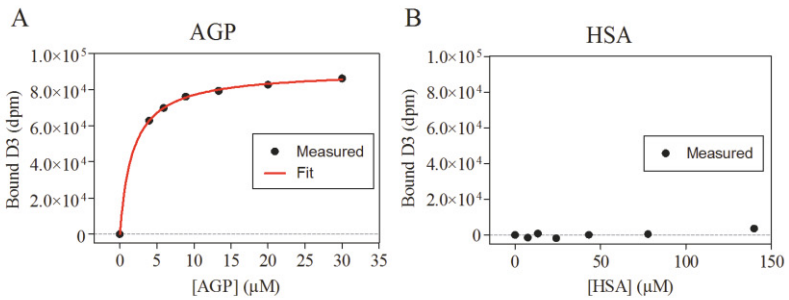

Fig 8. The bound D3 (in dpm) over the protein concentration as determined using the TRANSIL^{XL} kits. Each sample contained 5 μM D3 added to varying concentrations of AGP or HSA. (A) AGP fitted to the Michaelis Menten equation (red). (B) The binding of D3 to HSA was below the detection limit of the kit (K_D > 1.4 mM).

doi:10.1371/journal.pone.0128553.g008

In our previous studies, D3 already proved to be therapeutically active in reversing cognitive deficits and amyloid plaque load *in vivo*. Given its high oral bioavailability, suitably formulated D3 with multiple dosing might be a promising drug candidate against Alzheimer's disease.

Supporting Information

S1 File. ARRIVE Checklist. Completed "The ARRIVE Guidelines Checklist" for reporting animal data in this manuscript.
(DOCX)

Acknowledgments

We thank Michael Schöneck, Nicole Niemietz and Daniela Schumacher for excellent technical assistance and Dr. Dagmar Jürgens for discussions on the data analysis.

Author Contributions

Conceived and designed the experiments: NJ LL JB LG MC NJS JK KJL DW AW. Performed the experiments: NJ LL JP ES. Analyzed the data: NJ LL JP TZ JM DW AW. Wrote the paper: NJ LL NJS JB DW AW.

References

1. Berchtold NC, Cotman CW. Evolution in the conceptualization of dementia and Alzheimer's disease: Greco-Roman period to the 1960s. Neurobiology of aging. 1998; 19(3):173–89. Epub 1998/07/14. PMID: 9661992.
2. Fletcher LC, Burke KE, Caine PL, Rinne NL, Braniff CA, Davis HR, et al. Diagnosing Alzheimer's disease: are we any nearer to useful biomarker-based, non-invasive tests? GMS health technology assessment. 2013; 9:Doc01. Epub 2013/06/12. doi: 10.3205/hta000107 PMID: 23755087; PubMed Central PMCID: PMC3677379.
3. Nygaard HB. Current and emerging therapies for Alzheimer's disease. Clinical therapeutics. 2013; 35 (10):1480–9. Epub 2013/10/22. doi: 10.1016/j.clinthera.2013.09.009 PMID: 24139420.
4. TD B. Alzheimer Disease Overview. 1993. In: GeneReviews(R) [Internet]. University of Washington, Seattle.
5. Mikulca JA, Nguyen V, Gajdosik DA, Teklu SG, Giunta EA, Lessa EA, et al. Potential novel targets for Alzheimer pharmacotherapy: II. Update on secretase inhibitors and related approaches. Journal of clinical pharmacy and therapeutics. 2014; 39(1):25–37. Epub 2013/12/10. doi: 10.1111/jcpt.12112 PMID: 24313554.

6. Stockley JH, O'Neill C. Understanding BACE1: essential protease for amyloid-beta production in Alzheimer's disease. Cellular and molecular life sciences: CMLS. 2008; 65(20):3265–89. Epub 2008/08/13. doi: 10.1007/s00018-008-8271-3 PMID: 18695942.

7. Selkoe DJ. Alzheimer's disease: genes, proteins, and therapy. Physiological reviews. 2001; 81(2):741–66. Epub 2001/03/29. PMID: 11274343.

8. Bitan G, Kirkitadze MD, Lomakin A, Vollers SS, Benedek GB, Teplow DB. Amyloid beta-protein (Abeta) assembly: Abeta 40 and Abeta 42 oligomerize through distinct pathways. Proceedings of the National Academy of Sciences of the United States of America. 2003; 100(1):330–5. Epub 2002/12/31. doi: 10.1073/pnas.222681699 PMID: 12506200; PubMed Central PMCID: PMC140968.

9. Kayed R, Lasagna-Reeves CA. Molecular mechanisms of amyloid oligomers toxicity. Journal of Alzheimer's disease: JAD. 2013; 33 Suppl 1:S67–78. Epub 2012/04/26. doi: 10.3233/JAD-2012-129001 PMID: 22531422.

10. Tamaoka A. [The pathophysiology of Alzheimer's disease with special reference to "amyloid cascade hypothesis"]. Rinsho byori The Japanese journal of clinical pathology. 2013; 61(11):1060–9. Epub 2014/01/24. PMID: 24450113.

11. Schenk D, Basi GS, Pangalos MN. Treatment strategies targeting amyloid beta-protein. Cold Spring Harbor perspectives in medicine. 2012; 2(9):a006387. Epub 2012/09/07. doi: 10.1101/cshperspect.a006387 PMID: 22951439; PubMed Central PMCID: PMC3426815.

12. Citron M. Alzheimer's disease: strategies for disease modification. Nature reviews Drug discovery. 2010; 9(5):387–98. doi: 10.1038/nrd2896 PMID: 20431570

13. Sun N, Funke SA, Willbold D. A Survey of Peptides with Effective Therapeutic Potential in Alzheimer's Disease Rodent Models or in Human Clinical Studies. Mini-Rev Med Chem. 2012; 12(5):388–98. PMID: ISI:000303103600005.

14. Liu M, Li C, Pazgier M, Mao Y, Lv Y, Gu B, et al. D-peptide inhibitors of the p53-MDM2 interaction for targeted molecular therapy of malignant neoplasms. Proceedings of the National Academy of Sciences of the United States of America. 2010; 107(32):14321–6. Epub 2010/07/28. doi: 10.1073/pnas.1008930107 PMID: 20660730; PubMed Central PMCID: PMC2922601.

15. Zawadzke LE, Berg JM. A Racemic Protein. Journal of the American Chemical Society. 1992; 114 (10):4002–3. doi: 10.1021/Ja00036a073 PMID: ISI:A1992HT80100073.

16. Milton RCD, Milton SCF, Kent SBH. Total Chemical Synthesis of a D-Enzyme—the Enantiomers of Hiv-1 Protease Show Demonstration of Reciprocal Chiral Substrate-Specificity. Science. 1992; 256 (5062):1445–8. doi: 10.1126/science.1604320 PMID: ISI:A1992HX33700036.

17. Wiesehan K, Willbold D. Mirror-image phage display: aiming at the mirror. Chembiochem: a European journal of chemical biology. 2003; 4(9):811–5. Epub 2003/09/10. doi: 10.1002/cbic.200300570 PMID: 12964153.

18. Schumacher TN, Mayr LM, Minor DL Jr., Milhollen MA, Burgess MW, Kim PS. Identification of D-peptide ligands through mirror-image phage display. Science. 1996; 271(5257):1854–7. PMID: 8596952

19. van Groen T, Kadish I, Wiesehan K, Funke SA, Willbold D. In vitro and in vivo staining characteristics of small, fluorescent, Abeta42-binding D-enantiomeric peptides in transgenic AD mouse models. ChemMedChem. 2009; 4(2):276–82. Epub 2008/12/17. doi: 10.1002/cmdc.200800289 PMID: 19072935.

20. van Groen T, Kadish I, Funke SA, Bartnik D, Willbold D. Treatment with D3 removes amyloid deposits, reduces inflammation, and improves cognition in aged AbetaPP/PS1 double transgenic mice. J Alzheimers Dis. 2013; 34(3):609–20. Epub 2012/12/29. doi: 10.3233/JAD-121792 PMID: 23271316.

21. van Groen T, Kadish I, Funke A, Bartnik D, Willbold D. Treatment with Abeta42 binding D-amino acid peptides reduce amyloid deposition and inflammation in APP/PS1 double transgenic mice. Advances in protein chemistry and structural biology. 2012; 88:133–52. Epub 2012/07/21. doi: 10.1016/B978-0-12-398314-5.00005-2 PMID: 22814708.

22. Aileen Funke S, van Groen T, Kadish I, Bartnik D, Nagel-Steger L, Brener O, et al. Oral treatment with the d-enantiomeric peptide D3 improves the pathology and behavior of Alzheimer's Disease transgenic mice. ACS chemical neuroscience. 2010; 1(9):639–48. Epub 2010/09/15. doi: 10.1021/cn100057j PMID: 22778851; PubMed Central PMCID: PMC3368690.

23. van Groen T, Wiesehan K, Funke SA, Kadish I, Nagel-Steger L, Willbold D. Reduction of Alzheimer's disease amyloid plaque load in transgenic mice by D3, A D-enantiomeric peptide identified by mirror image phage display. ChemMedChem. 2008; 3(12):1848–52. Epub 2008/11/19. doi: 10.1002/cmdc.200800273 PMID: 19016284.

24. Kilkenny C, Browne WJ, Cuthill IC, Emerson M, Altman DG. Improving Bioscience Research Reporting: The ARRIVE Guidelines for Reporting Animal Research. Plos Biol. 2010; 8(6). ARTN e1000412 doi: 10.1371/journal.pbio.1000412 PMID: ISI:000279355600022.

25. Pollaro L, Heinis C. Strategies to prolong the plasma residence time of peptide drugs. MedChemComm. 2010; 1(5):319–24. doi: 10.1039/c0md00111b

26. Reichel A. The role of blood-brain barrier studies in the pharmaceutical industry. Current drug metabolism. 2006; 7(2):183–203. Epub 2006/02/14. PMID: 16472107.

27. Wong TW. Design of oral insulin delivery systems. Journal of drug targeting. 2010; 18(2):79–92. Epub 2009/12/09. doi: 10.3109/10611860903302815 PMID: 19968567.

28. Takagi H, Hiroi T, Hirose S, Yang L, Takaiwa F. Rice seed ER-derived protein body as an efficient delivery vehicle for oral tolerogenic peptides. Peptides. 2010; 31(8):1421–5. Epub 2010/05/12. doi: 10.1016/j.peptides.2010.04.032 PMID: 20457197.

29. Mason JM. Design and development of peptides and peptide mimetics as antagonists for therapeutic intervention. Future medicinal chemistry. 2010; 2(12):1813–22. Epub 2011/03/25. doi: 10.4155/fmc.10.259 PMID: 21428804.

30. Lalatsa A, Garrett NL, Ferrarelli T, Moger J, Schatzlein AG, Uchegbu IF. Delivery of Peptides to the Blood and Brain after Oral Uptake of Quaternary Ammonium Palmitoyl Glycol Chitosan Nanoparticles. Molecular pharmaceutics. 2012; 9(6):1764–74. doi: 10.1021/Mp300068j PMID: ISI:000304728700022.

31. Chapman ME, Hu L, Plato CF, Kohan DE. Bioimpedance spectroscopy for the estimation of body fluid volumes in mice. American journal of physiology Renal physiology. 2010; 299(1):F280–3. Epub 2010/05/14. doi: 10.1152/ajprenal.00113.2010 PMID: 20462974; PubMed Central PMCID: PMC2904176.

3.2 Pharmacokinetic Properties of a Novel D-Peptide Developed to be Therapeutically Active Against Toxic beta-Amyloid Oligomers

Autoren:	Leithold LH, Jiang N, Post J, Ziehm T, **Schartmann E**, Kutzsche J, Shah NJ, Breitkreutz J, Langen KJ, Willuweit A, Willbold D
Journal:	Pharmaceutical Research
	veröffentlicht im Februar 2016
DOI:	10.1007/s11095-015-1791-2
Impact Factor:	3,952 (2013)
Beitrag:	Beteiligung an der Durchführung der pharmakokinetischen Experimente
	Unterstützung bei der Auswertung der pharmakokinetischen Experimente

Pharm Res (2016) 33:328–336
DOI 10.1007/s11095-015-1791-2

RESEARCH PAPER

Pharmacokinetic Properties of a Novel D-Peptide Developed to be Therapeutically Active Against Toxic β-Amyloid Oligomers

Leonie H. E. Leithold[1] · Nan Jiang[1] · Julia Post[1] · Tamar Ziehm[1] · Elena Schartmann[1] · Janine Kutzsche[1] · N. Jon Shah[2] · Jörg Breitkreutz[3] · Karl-Josef Langen[2,4] · Antje Willuweit[2] · Dieter Willbold[1,5]

Received: 29 April 2015 / Accepted: 8 September 2015 / Published online: 17 September 2015

ABSTRACT

Purpose It has been shown that amyloid β (Aβ) oligomers play an important role in the pathology of Alzheimer's disease (AD). D3, a peptide consisting solely of D-enantiomeric amino acid residues, was developed to specifically eliminate Aβ oligomers and is therapeutically active in transgenic AD mice. D-peptides have several advantages over L-peptides, but little is known about their pharmacokinetic potential *in vivo*. Here, we analysed the pharmacokinetic properties of RD2, a rationally designed and potent D3 derivative.

Methods The pharmacokinetic analysis was performed using ^{3}H-RD2 after administration via several routes in mice. The time dependent amount of radiolabelled RD2 was measured in plasma and several organ homogenates by liquid scintillation counting. Furthermore, binding to plasma proteins was estimated.

Results RD2 penetrates into the brain, where it is thought to implement its therapeutic function. All administration routes result in a maximal brain concentration per dose (C_{max}/D) of 0.06 (μg/g)/(mg/kg) with brain/plasma ratios ranging between 0.7 and 1.0. RD2 shows a small elimination constant and a long terminal half-life in plasma of more than 2 days. It also exhibits high bioavailability after i.p., s.c. or p.o. administration.

Conclusions These excellent pharmacokinetic properties confirm that RD2 is a very promising drug candidate for AD.

KEY WORDS Alzheimer's disease · D-enantiomer · peptide · pharmacokinetics · preclinical

ABBREVIATIONS

%ID	Relative injected dose
AD	Alzheimer's disease
AGP	α_1-acid glycoprotein
AUC	Area under the concentration-time curve
AUMC	Area under the moment curve
Aβ	Amyloid β
C	Concentration
Cl	Clearance
D	Dose
dpm	Disintegrations per minute
F	Bioavailability
f_u	Unbound fraction
HSA	Human serum albumin
i.p.	Intraperitoneal
i.v.	Intravenous
inf	Infinity
MAT	Mean absorption time
MRT	Mean residence time
n.i.v.	Non-intravenous
p.o.	*per os*, oral delivery
r^2	Correlation coefficient
s.c.	Subcutaneous
$t_{1/2}$	Terminal half-life
TLC	Thin layer chromatography

✉ Antje Willuweit
a.willuweit@fz-juelich.de

✉ Dieter Willbold
d.willbold@fz-juelich.de

1 Institute of Complex Systems, Structural Biochemistry (ICS-6), Forschungszentrum Jülich GmbH, 52425 Jülich, Germany

2 Institute of Neuroscience and Medicine, Medical Imaging Physics (INM-4), Forschungszentrum Jülich GmbH, 52425 Jülich, Germany

3 Institute of Pharmaceutics and Biopharmaceutics, Heinrich-Heine-Universität Düsseldorf, Düsseldorf, Germany

4 Clinic for Nuclear Medicine, RWTH Aachen University, Aachen, Germany

5 Institut für Physikalische Biologie, Heinrich-Heine-Universität Düsseldorf, Düsseldorf, Germany

V_{ss} Distribution volume in steady state
V_z Terminal distribution volume
λ_z Terminal elimination rate constant

INTRODUCTION

Alzheimer's disease (AD) is a progressive neurodegenerative disorder and the most common form of dementia. It currently affects about 24 million people worldwide, but to date, no curative treatment exists (1,2).

The pathology of Alzheimer's disease is mainly characterised by extracellular amyloid plaques and intracellular neurofibrillary tangles. Research suggests that amyloid β (Aβ) aggregation plays a major role in the development of AD (3,4), while Aβ oligomers are thought to be the most toxic species (5–7). Therefore, various strategies to develop AD therapeutics address Aβ, trying to reduce its formation, inhibit aggregation to fibrils or enhance its clearance (3,8). Several studies on potential therapeutics considered peptides, e.g. designed to prevent β-sheet conformation (3,9). However, peptide drugs show several disadvantages since they can be immunogenic, instable due to degradation by proteases and often show rapid clearance (10). Additionally, they generally have a very low oral bioavailability and short *in vivo* half-lives (11).

D-peptides, which are entirely composed of D-amino acids, are more protease resistant than L- peptides, due to the stereoisomeric selectivity of most proteolytic enzymes (12,13). As a result, system elimination is slower and they remain stable in the body for longer periods of time than L-peptides, thereby providing more time to be therapeutically active *in vivo* (14,15). This was for instance shown for all D-enantiomeric peptides in rat plasma and Rhesus monkey cerebrospinal fluid (16,17). In addition it has been shown that they are not immunogenic or at least significantly less than L-peptides (15).

Previously, a D-peptide, called D3, has been identified by mirror image phage display for binding to Aβ (18,19). It has been shown that it is able to improve both pathology and cognition of AD transgenic mice e.g. after 4 weeks of i.p. treatment or after 8 weeks of oral delivery (20–24).

RD2 is a derivative of D3 consisting of a rationally repositioned sequence, resulting in improved binding to Aβ oligomers (25) which are currently widely believed to be the most toxic Aβ species (26,27).

Here, we determined and compared the pharmacokinetic properties of RD2 in mice after intraperitoneal, subcutaneous, oral and intravenous delivery. This is the first systematic preclinical pharmacokinetic study of a D-enantiomeric peptide to such an extent.

METHODS

Peptides

RD2 (H-ptlhthnrrrrr-NH_2, all amino acid residues are D-enantiomers, 1.6 kDa) was purchased from Cambridge Peptides Ltd. (Birmingham, United Kingdom). The Lewis structure of RD2 can be found in Fig. 1.

Radioactively labelled peptides were purchased from Quotient Bioresearch (Radiochemicals) Ltd. (Cardiff, United Kingdom) containing 1 mCi/ml and were supplied as solution in water:ethanol (1:1). RD2 (H-pt-[4,5-^{3}H-D-Leu]-hthnrrrrr-NH_2) was supplied with > 95% purity, containing 124 Ci/mmol. Radioactively labelled L-peptide (H-RPRTR-[4,5-^{3}H-Leu]-HTHRNR-NH_2), 103 Ci/mmol was used as control for stability assessment.

Animals

C57BL/6 mice (Charles River Laboratories, Sulzfeld, Germany) were housed in groups of up to four mice in standard mouse individually ventilated cages with standard chip aspen bedding, a nestlet was provided as cage enrichment. Water as well as food were available *ad libitum*. Housing rooms were maintained on a 12/12 h light–dark cycle (7 a.m. – 7 p.m.), with a temperature of 22°C and approx. 54% humidity. All animal experiments were carried out in conformance with the German Protection of Animals Act (TierSchG §§ 7–9) and with permit of an Animal Protection Committee (AZ84-02.04.2011.A356).

Proteolytic Stability

To assess the stability of RD2 in different organs, thin layer chromatography (TLC) was applied using the ^{3}H-radioactively labelled RD2. As positive control an L-peptide was included. Blood and organs were sampled from C57BL/6 mice (25 g body weight). The animal was anaesthetised with isoflurane (Actavis Deutschland GmbH & Co. KG, Langenfeld, Germany) and blood was taken by cardiac puncture with a heparin containing needle before the mouse was sacrificed by cervical dislocation. Blood was spun down at 4°C and 1200 g for 15 min and plasma was taken. A small piece of liver (approx. 0.2 g), the left kidney and the right brain hemisphere were taken. All organ weights were measured and homogenised with 500 µl PBS per 0.2 g organ weight. Afterwards, organ homogenates were centrifuged at 4°C and 1200 g for 10 to 15 min and supernatant was taken off. 5 µl radioactively labelled peptide (5 µCi) were then added to 1 µl mouse plasma or organ homogenate supernatant. After different incubation times the reaction was stopped by adding 4 µl mobile solvent (2-butanol/pyridine/ammonia (28%)/water, 39/34/10/26 ml respectively) to each sample which was

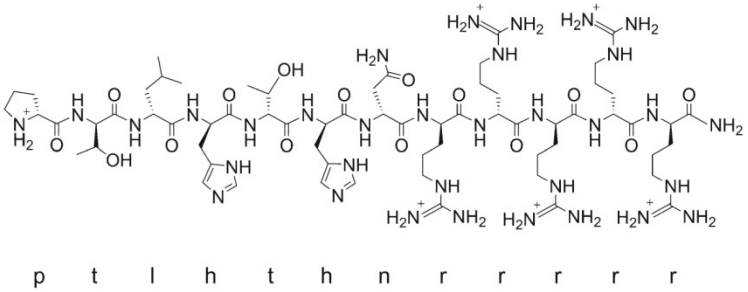

Fig. 1 Lewis structure and single letter amino acid code of the D-enantiomeric peptide RD2 (1.6 kDa).

then stored at - 20°C until further use. Samples were then dotted on the TLC membrane (HPTLC Silica 60 gel plates, Merck, Darmstadt, Germany) and placed into the solvent. Upon drying, start- and endpoint were marked with spots of ^{3}H-labelled peptide. For ^{3}H detection plates were then placed on phosphor imaging plates (Fujifilm, Tokyo, Japan) for 3 days and afterwards detected using a BAS reader with AIDA software (Raytest GmbH, Freiburg, Germany).

Pharmacokinetic Studies

Pharmacokinetic properties of ^{3}H-radioactively labelled RD2 in male C57BL/6 mice were studied using different administration routes. The applied amount contained 10 mg/kg for subcutaneous (s.c.) and intraperitoneal (i.p.) injection as well as oral gavage (p.o.) and 3.3 mg/kg for intravenous (i.v.) injection.

To achieve sufficiently high total concentrations of RD2, a combination of ^{3}H-labelled "hot" RD2 and non-radioactive "cold" RD2 was used, as detailed below. The working solution was prepared in phosphate buffer (0.1 M, pH 8.0). To achieve the appropriate dose each mouse received ^{3}H-labelled RD2 together with non-radioactive "cold" RD2, resulting in a total dose of 10 mg/kg (i.p., p.o., s.c.) or 3.3 mg/kg (i.v.) RD2 per mouse. I.v. injection was given into the tail vain under anaesthesia. Animals were sacrificed after different incubation times as detailed in Table I, for each time point three mice were used. Just before sampling time, the animal was anaesthetised with isoflurane and blood was taken by cardiac puncture with a heparin containing needle before the mouse was sacrificed by cervical dislocation. Blood was spun down at 4°C and 1200 g for 15 min and plasma was taken. A small piece of liver, the left kidney and the right brain hemisphere were taken at all time points. Additionally, at the late time points of 7 and 28 days, the spleen and the inguinal lymph nodes were harvested (spleen all administration routes, lymph nodes i.p. and i.v. only). 24 h after i.v. and i.p. administration urine and faeces were taken freshly (urine $n=2$ (i.p.) $n=4$ (i.v.), faeces $n=5$). All weights were measured and organs were homogenised with 500 µl PBS. After mixing with 10 ml scintillation cocktail (Ultima Gold XR, PerkinElmer, Waltham, MA, USA) ^{3}H-radioactivity was then measured in triplicate with a liquid scintillation analyser beta radiation counter (PerkinElmer, Waltham, MA, USA) in form of disintegrations per minute (dpm). The same procedure was performed on three animals without RD2 application, thereby creating blank reference values for each organ that were subtracted from all dpm values.

From the activity of the working solution subtracted with blank values and the organ weight the relative injected dose (%ID/g or %ID/ml) and total amount of RD2 (mg/g or mg/ml) per gram organ or millilitre plasma were calculated. All calculations of pharmacokinetic parameters were based on the total RD2 concentration. For calculation of pharmacokinetic parameters of the brain the radioactivity resulting from residual blood was subtracted assuming a plasma fraction of 1.5% in brain. The relative injected dose was only used for presentation purposes of the time dependent distribution in organs and plasma and displayed as mean and standard error of the mean where numbers are given.

Calculation of Pharmacokinetic Parameters

A non-compartmental analysis of pharmacokinetic parameters was performed. The area under the curve (AUC) as well as the area under the moment curve (AUMC) for the total RD2 concentrations was calculated (SigmaPlot 11.0, Systat Software, Inc., San José, CA, USA). The mean residence time (MRT) was calculated according to MRT = AUMC/AUC. The RD2 concentration at time zero was assumed to be zero for all applications except for plasma after i.v. delivery where it was back extrapolated from the first two observed concentrations in the semi-logarithmic time-concentration plot (SigmaPlot). The terminal elimination rate constant (λ_z) was obtained by logarithmic extrapolation based on the last observed concentrations starting from 2 days post administration (the correlation coefficient (r^2) was between 0.92 and 1.0 for all extrapolations). Parameters containing the suffix "0–28" were calculated from the measured data points while "0-inf" denotes values reaching into infinity being calculated based on λ_z. The AUC and AUMC reaching into infinity were

Table I Pharmacokinetic Experiments were Performed According to this Scheme

Administration method	Time points	RD2 dose
i.v.	3 min, 5 min, 10 min, 15 min, 30 min, 1 h, 4 h, 1 d, 2 d, 7 d, 28 d	3.3 mg/kg
i.p.	10 min, 20 min, 30 min, 1 h, 2 h, 4 h, 6 h, 1 d, 2 d, 7 d, 28 d	10 mg/kg
s.c.	10 min, 20 min, 30 min, 1 h, 2 h, 4 h, 6 h, 1 d, 2 d, 7 d, 28 d	10 mg/kg
p.o.	30 min, 1 h, 2 h, 4 h, 6 h, 8 h, 18 h, 1 d, 2 d, 3 d, 7 d, 28 d	10 mg/kg

Assessed durations post administration and concentrations of RD2 per route of administration are given. For each time point three mice were used

calculated by $AUC_{0\ inf} = AUC_{0-28} + C_{28}/\lambda_z$ and $AUMC_{0\ inf} = AUMC_{0-28} + (C_{28}*t_{28})/\lambda_z + C_{28}/\lambda_z^2$. The bioavailability (F) was calculated on the basis of the respective AUC according to $F = 100*(D_{i.v.}*AUC_{n.i.v.})/(D_{n.i.v.}*AUC_{i.v.})$ with n.i.v. denoting the respective extravascular administration route. Parameters describing the terminal elimination phase were calculated based on λ_z: the terminal half-life ($t_{1/2} = \ln 2/\lambda_z$) and clearance ($Cl_{i.v.} = \lambda_z * V_z$), the terminal distribution volume ($V_z = D/(\lambda_z * AUC_{inf})$ (for n.i.v. Cl and V_z were calculated including the bioavailability: $Cl_{n.i.v.} = \lambda_z * V_z/F$ and $V_z = (D*F)/(\lambda_z * AUC_{inf})$) was calculated as well as the distribution volume in steady state ($V_{ss} = (D*AUMC)/AUC^2$).

The overall brain/plasma ratio was determined using the respective AUC_{0-28} whereas the brain/plasma ratio over time was calculated from the individual values of each time point, both with subtracted radioactivity from residual blood, assuming a plasma fraction of 1.5% in brain (28).

Plasma Protein Binding

Plasma protein binding was estimated by incubation of RD2 with varying concentrations of protein using TRANSIL^{XL} binding kits (Sovicell GmbH, Leipzig, Germany). K_D values were determined by titrating a constant drug concentration against different concentrations of human serum albumin (HSA) and α_1-acid glycoprotein (AGP). Experiments were performed as recommended for the kit. To obtain the desired RD2 stock solution of 80 µM, non-radioactively RD2 was dissolved in PBS and 5% ^{3}H-labelled RD2 solution was added for detection purposes. A final concentration of 5 µM RD2 was applied in the assay. After incubation and centrifugation 15 µl supernatant were taken and scintillation cocktail was added for detection using liquid scintillation counting. This was done in triplicate. After measuring the disintegrations per minute (dpm) of the supernatant containing the unbound RD2, the fraction bound to the titrated protein was calculated and plotted against the protein concentrations. The curves were fitted to the Michaelis Menten ligand binding equation (SigmaPlot) to obtain a K_D. Mean and relative standard error (%) of multiple measurements are given where applicable (AGP $n = 2$).

For determination of the unbound fraction of RD2 (f_u) Eq. (1) was used:

$$f_u - 100* \frac{\frac{C_{RD2} - K_D - C_{physiol}}{2} + \sqrt{K_D * C_{RD2} + \left(\frac{C_{RD2} - K_D - C_{physiol}}{2}\right)^2}}{C_{RD2}} \quad (1)$$

For very low RD2 concentrations in blood (C_{RD2}), Eq. (1) can be simplified by Eq. (2), where the unbound fraction of RD2 can be calculated independently of the applied RD2 concentration. Since this is true for our *in vivo* experiments we used Eq. (2) for the total free fraction of RD2, combining the binding of RD2 to HSA and AGP. For calculation of the unbound fraction according to Eq. (2), physiological concentrations ($C_{physiol}$) of 0.65 mM HSA and 0.02 mM AGP were assumed.

$$f_{u,total} = 100* \frac{1}{1 + \frac{C_{physiol,HSA}}{K_{D,HSA}} + \frac{C_{physiol,AGP}}{K_{D,AGP}}} \quad (2)$$

RESULTS

Proteolytic Stability of RD2

To confirm stability of ^{3}H-labelled RD2 in mouse plasma, thin layer chromatography (TLC) was performed after incubation of ^{3}H-RD2 with plasma for up to 1 day and detected via autoradiography. This experiment was essential to consider potential metabolites in later pharmacokinetic analyses. TLC results showed that RD2 remained stable in mouse plasma (Fig. 2) for at least 24 h while a comparable L-peptide was proteolytically degraded within 2 h as is deduced from the appearance of additional bands at that time (marked by arrows) in comparison to those present at 0 h. Similarly, the pattern of RD2 after incubation with organ homogenates did not change over time, indicating that no proteolytic degradation took place (Fig. 2). Of note, the peptides bind to different components of the plasma and organ samples resulting in different patterns and intensities for each peptide.

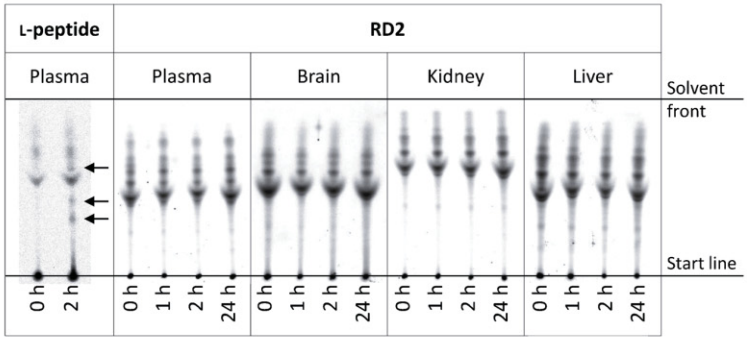

Fig. 2 Autoradiography of thin layer chromatogram demonstrating proteolytic stability of ^{3}H-labelled RD2 in mouse plasma, brain, kidney and liver. ^{3}H-RD2 was incubated at 37°C with mouse plasma for different durations and developed on TLC plates. For comparison, a very similar L-peptide was also incubated with mouse plasma. Multiple bands in the 0 h lanes arise from binding and co-migration of the ^{3}H-peptides with plasma and tissue components. Therefore, any effect of degradation will lead to extra additional bands as compared to the 0 h lane of the very same compound. Obvious proteolytic degradation can be observed for the ^{3}H-L-peptide already after 2 h of incubation with plasma leading to additionally appearing bands (*black arrows*) as compared to the 0 h lane. Additionally appearing bands as compared to 0 h incubation are not observed for ^{3}H-RD2 even after 24 h of incubation in plasma and tissue homogenates.

However, since the overall composition did not change with time, it can be concluded that RD2 was not subject to proteolytic degradation. The L-peptide showed appearance of additional bands after 2 h incubation, while the pattern of RD2 remained unchanged. Therefore, metabolites were considered negligible and the measured radioactivity was used to back calculate the total RD2 concentration.

Pharmacokinetic Properties

Pharmacokinetic analyses were performed using ^{3}H-labelled RD2 after i.v., i.p., s.c. or oral administration in mice. Graphs showing the relative injected dose per organ weight over time of the different administration routes can be found in Fig. 3.

Significant amounts of ^{3}H-RD2 were found in the analysed organs after i.v., i.p. or s.c. injection with highest concentrations present in kidney, followed by liver and plasma (Fig. 3). Oral administration resulted in very low ^{3}H-RD2 levels in liver, kidney and plasma. Interestingly, in brain ^{3}H-RD2 was found in amounts similar to the other administration routes. Exposure to all analysed organs was quite stable for a couple of days and declined gradually until 28 days after injection where it was still detectable in very low amounts.

Additionally, ^{3}H-RD2 amounts in urine and faeces were evaluated 24 h post i.p. and i.v. injection, showing only low doses in faeces (0.28±0.05 (i.p.) and 0.35±0.02%ID/g (i.v.), n=5). The amount of ^{3}H-RD2 in urine was higher, following i.p. administration it reached 2.3±0.09%ID/ml and 4.3±0.07%ID/ml upon i.v. administration (i.p. n=2; i.v. n=4). Furthermore, at 7 and 28 days post injection the presence of ^{3}H-RD2 in spleen and lymph nodes was determined, showing only low concentrations at 7 days (0.4 – 0.6±0.11%ID/g) decreasing with time (0.01 – 0.2±0.02%ID/g, except spleen i.v. 0.6 ±0.02%ID/g). Remarkably, upon oral application nearly no ^{3}H-RD2 was found in the spleen at 7 days post injection (0.04±0.004%ID/g).

Plasma Pharmacokinetic Parameters

A summary of all pharmacokinetic parameters in mouse plasma can be found in Table II, parameters were determined based on the back-calculated total RD2 concentration from measured radioactivity.

In contrast to the other administration routes, i.v. injection was performed with 3.3 mg/kg body weight. Results show low rate of terminal plasma clearance with Cl/F=1.68 ml/(kg*min) and a relatively long terminal half-life ($t_{1/2}$) of 59 h. Since the extrapolated part of the area under the curve (AUC) is small (≤1%) the AUC_{0-28} and $AUC_{0\text{-inf}}$ are very similar with $AUC_{0\text{-inf}}$=1.97 mg/ml*min.

Upon extravascular administration, absorption happened rapidly, as t_{max} was between 0.5 and 1 h, with oral administration showing the slowest absorption. The maximal observed concentration relative to the dose (C_{max}/D) was highest for i.v. administration (3.04 (µg/ml)/(mg/kg)), lower after i.p. and s.c. injection (0.79 and 0.98 (µg/ml)/(mg/kg)) and lowest following oral administration (0.09 (µg/ml)/(mg/kg)). The drug exposure in plasma, calculated as $AUC_{0\text{-inf}}$, showed the highest values after s.c. injection (5.42 mg/ml*min) and similar values upon i.p. and p.o. administration (4.57 and 4.54 mg/ml*min). The mean residence time (MRT), however, appeared to be comparable between all administration routes. The terminal half-life was about 60 h and independent of the administration route. The bioavailability (F) was similar for i.p. and p.o. administration (approx. 76%) and even higher upon s.c. injection (91%).

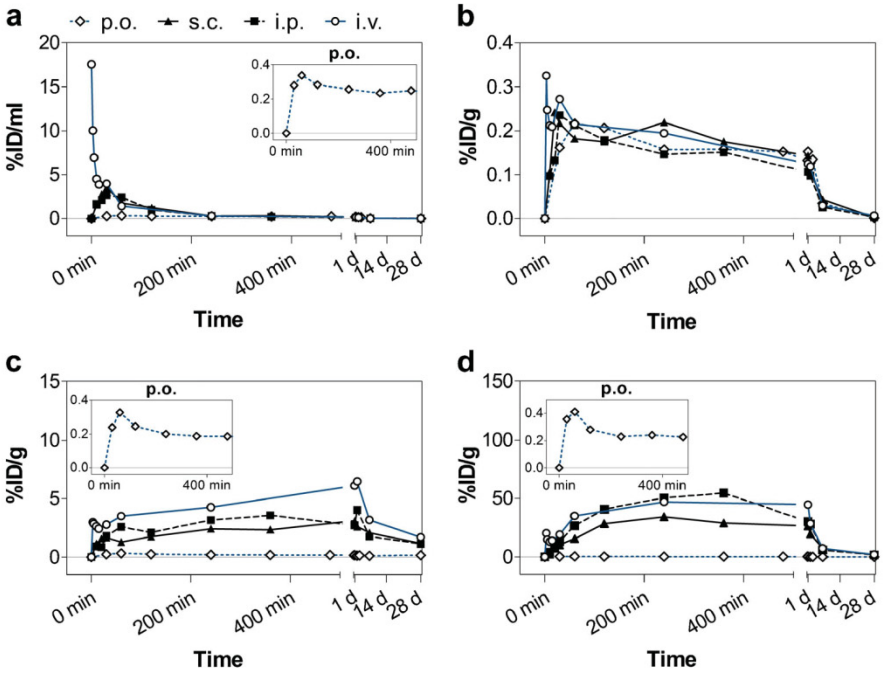

Fig. 3 Time dependent distribution of ^{3}H-RD2 in mouse organs and plasma after different administration routes. ^{3}H-RD2 was administered together with non-radioactive RD2 via different routes at 10 mg/kg or 3.3 mg/kg (i.v.). The concentration of ^{3}H-RD2 as expressed in relative injected dose per gram organ (%ID/g) or millilitre plasma (%ID/ml) is shown for plasma (**a**), brain (**b**), liver (**c**) and kidney (**d**) over time after different administration routes (p.o. *dashed line, open square*; s.c. *triangle*; i.p. *dashed line, closed square*; i.v. *open circle*). Graphs show the mean of three mice per time point.

Pharmacokinetic Parameters of RD2 in the Brain

Table III shows a summary of parameters calculated for the brain as this is expected to be the therapeutically relevant organ. The present study was performed in healthy C57BL/6 mice. The resulting pharmacokinetic parameters may be different in transgenic AD mouse models. Measured ^{3}H-RD2 radioactivity was used to extrapolate the total RD2 concentration in brain.

Brain/plasma ratios increased over time for i.v., i.p. and s.c. injection (Fig. 4), whereas for oral administration it remained relatively stable, all delivery routes almost reaching

Table II Determined Pharmacokinetic Parameters in Mouse Plasma for Different Administration Routes, based on Measured ^{3}H-RD2

Parameter	Units	i.v.	i.p.	s.c.	p.o.
Dose (D)	mg/kg	3.3	10	10	10
t_{max}	min	3	30	30	60
C_{max}/D	(μg/ml)/(mg/kg)	3.04	0.79	0.98	0.09
AUC_{0-28}	mg/ml*min	1.95	4.54	5.39	4.51
$AUMC_{0-28}$	min^2*mg/ml	9908	22,154	26,169	23,355
MRT_{0-28}	h	84.8	81.4	80.9	86.3
λ_z	min^{-1}	0.00020	0.00019	0.00019	0.00020
$t_{1/2}$	h	59	62	60	58
AUC_{0-inf}	mg/ml*min	1.97	4.57	5.42	4.54
$AUMC_{0-inf}$	min^2*mg/ml	10,794	23,676	27,514	24,748
MRT_{0-inf}	h	91.4	86.4	84.6	90.8
V_z	l/kg	8.57	8.95	8.77	8.46
Cl/F	ml/(min*kg)	1.68	2.19	1.84	2.20
V_{ss}	l/kg	9.20			
F_{AUC-28}	%		76.9	91.4	76.5
% AUC extrapolated	%	1.0	0.7	0.5	0.7

For comparison of absolute values, note that i.v. was administered at lower dose than extravascular administration. Clear fields are not applicable for this respective administration route. For abbreviations please refer to the abbreviation and methods sections

Table III Calculated Pharmacokinetic Parameters in Mouse Brains for Different Administration Routes, based on Measured ^{3}H-RD2

Parameter	Units	i.v.	i.p.	s.c.	p.o.
Dose (D)	mg/kg	3.3	10.0	10.0	10.0
t_{max}	min	3	30	20	60
C_{max}/D	(μg/g)/(mg/kg)	0.06	0.06	0.06	0.06
AUC_{0-28}	mg/g*min	1.48	3.37	4.51	4.49
$AUMC_{0-28}$	min^2*mg/g	11,408	22,656	31,419	27,039
MRT_{0-28}	h	128.4	111.9	116.1	100.3
λ_z	min^{-1}	0.00019	0.00019	0.00012	0.00016
$t_{1/2}$	h	60	61	94	73
F_{AUC-28}	%		75.2	100.6	100.1
Brain/plasma ratio AUC_{0-28}		0.8	0.7	0.8	1.0

Clear fields are not applicable for this respective administration route. For abbreviations please refer to the abbreviation and methods sections

1 at 2 days post administration. Overall, a good penetration of the brain was reached with AUC-based brain/plasma ratios reaching 0.8 (i.v. and s.c.) and even 1.0 (p.o.). Interestingly, C_{max}/D in brain was similar for all administration routes (0.06 (μg/ml)/(mg/kg)). The AUC_{0-28} was high for s.c. and p.o. administration (4.5 mg/g*min) but lower following i.p. injection (3.4 mg/g*min). After i.v. injection the AUC_{0-28} was found to be 1.5 mg/g*min but was performed using a lower dose of RD2. The terminal half-life of ^{3}H-RD2 in brain was very comparable to that in plasma, i.e. 61 h (i.v. and i.p.), 73 h (p.o.) and 94 h (s.c.). The bioavailability in the brain was calculated to be 75% for i.p. injection and 100% for s.c. and oral administration.

Plasma Protein Binding

For estimation of the *in vivo* free fraction of RD2 in blood ($f_{u,total}$), an *in vitro* assay was used, incubating RD2 with human serum albumin (HSA) and α_1-acid glycoprotein (AGP) (Fig. 5). For AGP this assay resulted in a K_D of 2.77 μM ± 9.97% (r^2 = 99.4%). The fraction unbound to AGP (f_u) was estimated using Eq. (1) under assumption of a RD2 blood concentration of 0.23 μM (C_{RD2}, measured 4 h after p.o. administration). This predicts a free fraction of 12.3%. For HSA, the K_D was above the detection limit of the kit (≥1.4 mM) indicating a very low affinity for HSA and leaving AGP as the main binding partner. Nevertheless, calculation of the RD2 fraction unbound to HSA with an assumed K_D of 1.4 mM results in 68.3% free RD2. Taken together, using Eq. (2), the estimated free fraction of RD2 in plasma was calculated to be approximately 11.5%.

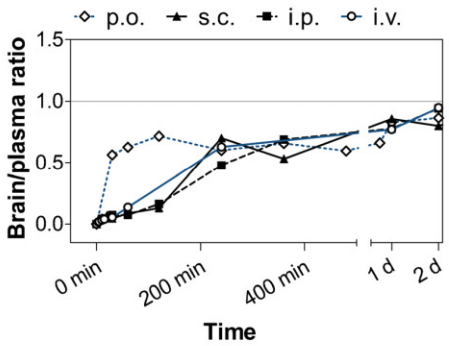

Fig. 4 Time dependent development of the brain/plasma ratio for different administration routes, corrected for residual blood in the brain.

DISCUSSION

In the present study we have analysed the pharmacokinetic properties of the D-peptide RD2, an improved derivative of D3, which has previously been shown to be therapeutically active *in vivo* (20,22).

It has previously been shown *in vivo* for rat plasma and rhesus monkey CSF that D-peptides are proteolytically more stable than their L-forms (16,17). Here, we also demonstrated that RD2 remains intact in mouse plasma and organ homogenates for at least 24 h. Thus, we considered metabolites negligible and used the measured ^{3}H-radioactivity to calculate the RD2 concentrations *in vivo*. Nevertheless, it needs to be clearly stated that all obtained pharmacokinetic values are based on the assumption that the measured radioactivity represents the non-metabolised RD2. Although we have shown that RD2 is stable for at least 24 h in plasma and tissue homogenates, we cannot exclude for later time points partial conversion of RD2 into metabolites that may or may not have reduced therapeutic activities. However, because we did not see any RD2 metabolism at 24 h, there was no reason to expect significant metabolism at 48 h or even 7 days. Furthermore, incubation in organ homogenates or plasma beyond 24 h appeared not to be meaningful because after longer incubation times enzymes

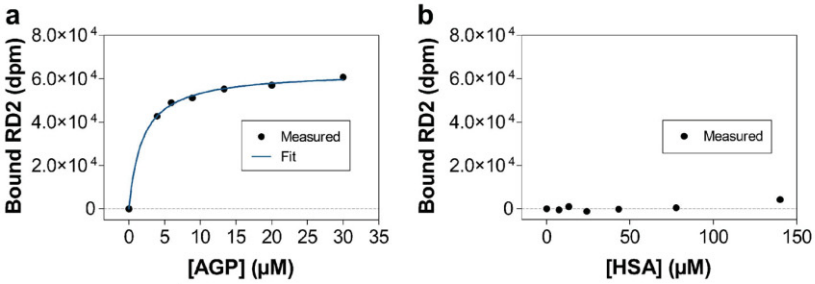

Fig. 5 Plasma protein binding of RD2. Bound ^{3}H-RD2 (in dpm) dependent on AGP (**a**) and HSA (**b**) concentration (*dots*). For binding of RD2 to AGP the fit according to the Michaelis Menten binding equation (*line*) is shown, indicating an almost perfect fit ($r^2 = 99.4\%$, **a**). Binding of RD2 to HSA was below the detection limit of the applied kit ($K_D \geq 1.4$ mM).

in those biological samples will have digested themselves leading to artefacts.

In the present study non-compartmental analysis was performed because a simplistic analysis of the data at hand is possible without making assumptions regarding the number of compartments as is necessary for other analyses such as compartmental or physiologically based models. We quantified RD2 in plasma and brain by measuring the radioactivity and assumed based on the 24 h stability data in plasma and organ homogenates that the measured radioactivity parallels RD2 concentration. Any minor metabolite would influence a more complex model, e.g. a minimal physiologically based model, to produce inaccurate data. However, non-compartmental analysis assumes linear kinetics and may therefore not be the optimal model for pharmacokinetic analysis of RD2. This may result in over- or under-estimation of certain values. Nevertheless, non-compartmental analysis is often used to give an indication of the pharmacokinetic properties of a candidate. Therefore, the more simple non-compartmental analysis was used to avoid additional over-interpretation of our data towards the pharmacokinetic properties of RD2.

Summarised, the pharmacokinetic results yielded a low terminal plasma clearance (Cl/F = 1.68 ml/(min*kg)) of RD2 resulting in long terminal half-lives of about 60 h upon all assessed administration routes. Since L-peptides are typically cleared from the blood relatively fast after administration, often within minutes, this long half-life represents a major advantage of RD2 since it provides more time to reach the target tissue and to be therapeutically active (10,29). The plasma bioavailability was exceptionally high following extravascular administration, with 77% upon intraperitoneal and oral administration and 91% after subcutaneous injection. In comparison to other peptide drugs especially the bioavailability upon oral application is very high (11,30).

It is noteworthy that irrespective of the administration route similar concentrations of RD2 reached the brain where it is thought to be therapeutically active. Irrespective of the administration route an overall brain/plasma ratio of 1 was reached. This indicates sufficient transport of RD2 into the target organ.

RD2 levels found in urine at 24 h post injection agree with the relatively high values obtained at the 24 h time point in the kidney. In general, values are higher upon i.v. injection than those obtained following i.p. administration. Hence, even 1 day after dosing the kidney still seems to be a major excretion route, illustrated also by the high RD2 concentrations observed in the kidney for at least 2 days. Additionally, excretion of RD2 also appears to take place via faeces although rather low doses of RD2 are measured at 24 h post i.v. or i.p. administration, indicating that this excretion pathway is not the dominating one for these administration routes. Furthermore, measurements of RD2 in spleen and inguinal lymph nodes indicate that after 28 days post administration only very low amounts of RD2 remain in the lymphatic system.

Prediction of plasma protein binding based on binding to HSA and AGP suggested a plasma free fraction of about 12%, which is also a very favourable property of RD2 as potential AD drug candidate. It has been reported that only the minority of the examined drugs developed for the central nervous system exhibit free plasma fractions above 10% (31).

Here, we compare RD2 distribution after different administration routes as well as the predicted plasma protein binding. In this pharmacokinetic study we were able to demonstrate high stability, long plasma half-life of several days and favourable oral and subcutaneous bioavailability of this all D-enantiomeric peptide in mice.

CONCLUSION

Taken together, the current study demonstrates favourable pharmacokinetic properties of the D-enantiomeric peptide RD2. Based on the long terminal half-life, high oral bioavailability and drug exposure to the brain it can be concluded, that D-peptides in general may be very well suited as drug candidates. Particularly, providing therapeutic efficiency

in vivo, RD2 may be a very promising candidate for the treatment of Alzheimer's disease.

ACKNOWLEDGMENTS AND DISCLOSURES

We thank Daniela Schumacher, Elias Bissong and Nicole Niemietz for the excellent technical assistance. Additionally, we thank Jörg Mauler for helping with the data analysis. D.W. was supported by grants from the "Portfolio Technology and Medicine" and the Helmholtz-Validierungsfonds of the Impuls und Vernetzungs-Fonds der Helmholtzgemeinschaft; K.J.L. and D.W. were supported by the "Portfolio Drug Research" of the Impuls und Vernetzungs-Fonds der Helmholtzgemeinschaft. The authors declare that they have no conflict of interest.

REFERENCES

1. Reitz C, Mayeux R. Alzheimer disease: epidemiology, diagnostic criteria, risk factors and biomarkers. Biochem Pharmacol. 2014;88(4):640–51.
2. Alzheimer's Association. 2014 Alzheimer's disease facts and figures. Alzheimers Dement. 2014;10(2):e47–92.
3. Soto C. Plaque busters: strategies to inhibit amyloid formation in Alzheimer's disease. Mol Med Today. 1999;5(8):343–50.
4. Hardy JA, Higgins GA. Alzheimer's disease: the amyloid cascade hypothesis. Science. 1992;256(5054):184–5.
5. Benilova I, Karran E, De Strooper B. The toxic a beta oligomer and Alzheimer's disease: an emperor in need of clothes. Nat Neurosci. 2012;15(3):349–57.
6. DaRocha-Souto B, Scotton TC, Coma M, Serrano-Pozo A, Hashimoto T, Serenó L, *et al.* Brain oligomeric beta-amyloid but not total amyloid plaque burden correlates with neuronal loss and astrocyte inflammatory response in amyloid precursor protein/tau transgenic mice. J Neuropathol Exp Neurol. 2011;70(5):360–76.
7. Decker H, Lo KY, Unger SM, Ferreira ST, Silverman MA. Amyloid-beta peptide oligomers disrupt axonal transport through an NMDA receptor-dependent mechanism that is mediated by glycogen synthase kinase 3 beta in primary cultured hippocampal neurons. J Neurosci. 2010;30(27):9166–71.
8. Hardy J, Selkoe DJ. The amyloid hypothesis of Alzheimer's disease: progress and problems on the road to therapeutics. Science. 2002;297(5580):353–6.
9. Sun N, Funke SA, Willbold D. A survey of peptides with effective therapeutic potential in Alzheimer's disease rodent models or in human clinical studies. Mini Rev Med Chem. 2012;12(5):388–98.
10. Sato AK, Viswanathan M, Kent RB, Wood CR. Therapeutic peptides: technological advances driving peptides into development. Curr Opin Biotechnol. 2006;17(6):638–42.
11. Pauletti GM, Gangwar S, Siahaan TJ, Aubé J, Borchardt RT. Improvement of oral peptide bioavailability: peptidomimetics and prodrug strategies. Adv Drug Deliv Rev. 1997;27(2–3):235–56.
12. van Regenmortel MHV, Muller S. D-peptides as immunogens and diagnostic reagents. Curr Opin Biotechnol. 1998;9(4):377–82.
13. Soto C, Kindy MS, Baumann M, Frangione B. Inhibition of Alzheimer's amyloidosis by peptides that prevent beta-sheet conformation. Biochem Biophys Res Commun. 1996;226(3):672–80.
14. Sela M, Zisman E. Different roles of D-amino acids in immune phenomena. FASEB J. 1997;11(6):449–56.
15. Dintzis HM, Symer DE, Dintzis RZ, Zawadzke LE, Berg JM. A comparison of the immunogenicity of a pair of enantiomeric proteins. Proteins Struct Funct Genet. 1993;16(3):306–8.
16. Findeis MA, Musso GM, Arico-Muendel CC, Benjamin HW, Hundal AM, Lee JJ, *et al.* Modified-peptide inhibitors of amyloid beta-peptide polymerization. Biochemistry. 1999;38(21):6791–800.
17. Poduslo JF, Curran GL, Kumar A, Frangione B, Soto C. beta-sheet breaker peptide inhibitor of Alzheimer's amyloidogenesis with increased blood–brain barrier permeability and resistance to proteolytic degradation in plasma. J Neurobiol. 1999;39(3):371–82.
18. Schumacher TNM, Mayr LM, Minor DL, Milhollen MA, Burgess MW, Kim PS. Identification of D-peptide ligands through mirror-image phage display. Science. 1996;271(5257):1854–7.
19. Wiesehan K, Willbold D. Mirror-image phage display: aiming at the mirror. Chembiochem. 2003;4(9):811–5.
20. Funke SA, van Groen T, Kadish I, Bartnik D, Nagel-Steger L, Brener O, *et al.* Oral treatment with the D-enantiomeric peptide D3 improves the pathology and behavior of Alzheimer's disease transgenic mice. ACS Chem Neurosci. 2010;1(9):639–48.
21. van Groen T, Kadish I, Funke A, Bartnik D, Willbold D. Treatment with a beta 42 binding D-amino acid peptides reduce amyloid deposition and inflammation in APP/PS1 double transgenic mice. Adv Protein Chem Struct Biol. 2012;88:133–52.
22. van Groen T, Wiesehan K, Funke SA, Kadish I, Nagel-Steger L, Willbold D. Reduction of Alzheimer's disease amyloid plaque load in transgenic mice by D3, a D-enantiomeric peptide identified by mirror image phage display. ChemMedChem. 2008;3(12):1848–52.
23. van Groen T, Kadish I, Wiesehan K, Funke SA, Willbold D. In vitro and in vivo staining characteristics of small, fluorescent, Aβ42-binding D-enantiomeric peptides in transgenic AD mouse models. ChemMedChem. 2009;4(2):276–82.
24. van Groen T, Kadish I, Funke SA, Bartnik D, Willbold D. Treatment with D3 removes amyloid deposits, reduces inflammation, and improves cognition in aged AbetaPP/PS1 double transgenic mice. J Alzheimers Dis. 2013;34(3):609–20.
25. Olubiyi OO, Frenzel D, Bartnik D, Glück JM, Brener O, Nagel-Steger L, *et al.* Amyloid aggregation inhibitory mechanism of arginine-rich D-peptides. Curr Med Chem. 2014;21(12):1448–57.
26. Larson ME, Lesne SE. Soluble Abeta oligomer production and toxicity. J Neurochem. 2012;120 Suppl 1:125–39.
27. Ferreira ST, Klein WL. The Abeta oligomer hypothesis for synapse failure and memory loss in Alzheimer's disease. Neurobiol Learn Mem. 2011;96(4):529–43.
28. Brown RP, Delp MD, Lindstedt SL, Rhomberg LR, Beliles RP. Physiological parameter values for physiologically based pharmacokinetic models. Toxicol Ind Health. 1997;13(4):407–84.
29. Pollaro L, Heinis C. Strategies to prolong the plasma residence time of peptide drugs. Med Chem Commun. 2010;1(5):319–24.
30. Renukuntla J, Vadlapudi AD, Patel A, Boddu SH, Mitra AK. Approaches for enhancing oral bioavailability of peptides and proteins. Int J Pharm. 2013;447(1–2):75–93.
31. Kratochwil NA, Huber W, Muller F, Kansy M, Gerber PR. Predicting plasma protein binding of drugs: a new approach. Biochem Pharmacol. 2002;64(9):1355–74.

3.3 Pharmacokinetic properties of tandem D-peptides designed for treatment of Alzheimer's disease

Autoren:	Leithold LH, Jiang N, Post J, Ziehm T, **Schartmann E**, Kutzsche J, Shah NJ, Breitkreutz J, Langen KJ, Willuweit A, Willbold D
Journal:	European Journal of Pharmaceutical Sciences
	veröffentlicht am 30.06.2016
DOI:	10.1016/j.ejps.2016.04.016
Impact Factor:	3,756 (2016)
Beitrag:	Beteiligung an der Durchführung der pharmakokinetischen Experimente und der Stabilitätstests
	Unterstützung bei der Auswertung der pharmakokinetischen Experimente und der Stabilitätstests

European Journal of Pharmaceutical Sciences 89 (2016) 31–38

Contents lists available at ScienceDirect

European Journal of Pharmaceutical Sciences

journal homepage: www.elsevier.com/locate/ejps

Pharmacokinetic properties of tandem D-peptides designed for treatment of Alzheimer's disease

Leonie H.E. Leithold [a,1], Nan Jiang [a,1], Julia Post [a], Nicole Niemietz [b], Elena Schartmann [a], Tamar Ziehm [a], Janine Kutzsche [a], N. Jon Shah [b,c], Jörg Breitkreutz [d], Karl-Josef Langen [b,e], Antje Willuweit [b,*], Dieter Willbold [a,f,**]

[a] Institute of Complex Systems, Structural Biochemistry, Forschungszentrum Jülich GmbH, 52425 Jülich, Germany
[b] Institute of Neuroscience and Medicine, Medical Imaging Physics, Forschungszentrum Jülich GmbH, 52425 Jülich, Germany
[c] Department of Neurology, Universitätsklinikum der RWTH Aachen, 52074 Aachen, Germany
[d] Institute of Pharmaceutics and Biopharmaceutics, Heinrich-Heine-Universität Düsseldorf, 40225 Düsseldorf, Germany
[e] Department of Nuclear Medicine, Universitätsklinikum der RWTH Aachen, 52074 Aachen, Germany
[f] Institut für Physikalische Biologie, Heinrich-Heine-Universität Düsseldorf, 40225 Düsseldorf, Germany

ARTICLE INFO

Article history:
Received 19 November 2015
Received in revised form 6 April 2016
Accepted 12 April 2016
Available online 13 April 2016

Keywords:
Pharmacokinetics
Alzheimer's disease
D-enantiomeric peptide
Beta amyloid ligand
Therapy

ABSTRACT

Peptides are more and more considered for the development of drug candidates. However, they frequently exhibit severe disadvantages such as instability and unfavourable pharmacokinetic properties. Many peptides are rapidly cleared from the organism and oral bioavailabilities as well as *in vivo* half-lives often remain low. In contrast, some peptides consisting solely of D-enantiomeric amino acid residues were shown to combine promising therapeutic properties with high proteolytic stability and enhanced pharmacokinetic parameters. Recently, we have shown that D3 and RD2 have highly advantageous pharmacokinetic properties. Especially D3 has already proven promising properties suitable for treatment of Alzheimer's disease. Here, we analyse the pharmacokinetic profiles of D3D3 and RD2D3, which are head-to-tail tandem D-peptides built of D3 and its derivative RD2. Both D3D3 and RD2D3 show proteolytic stability in mouse plasma and organ homogenates for at least 24 h and in murine and human liver microsomes for 4 h. Notwithstanding their high affinity to plasma proteins, both peptides are taken up into the brain following i.v. as well as i.p. administration. Although both peptides contain identical D-amino acid residues, they are arranged in a different sequence order and the peptides show differences in pharmacokinetic properties. After i.p. administration RD2D3 exhibits lower plasma clearance and higher bioavailability than D3D3. We therefore concluded that the amino acid sequence of RD2 leads to more favourable pharmacokinetic properties within the tandem peptide, which underlines the importance of particular sequence motifs, even in short peptides, for the design of further therapeutic D-peptides.

1. Introduction

Despite remarkable efforts to develop curative and disease modifying treatments against Alzheimer's disease (AD), thus far only symptomatic treatment is available (Nygaard, 2013). Among other substance classes, peptides are being investigated as promising drug candidates (Sun et al., 2012). Currently, however, most peptides have shown severe disadvantages due to their immunogenicity and instability as well as unfavourable pharmacokinetic properties such as rapid clearance, low oral bioavailability and short *in vivo* half-lives (Pauletti et al., 1997; Sato et al., 2006).

To overcome those disadvantages, D-enantiomeric peptides are being developed. They combine high protease resistance due to stereoisomeric selectivity of mammalian proteolytic enzymes with low, if any, immunogenicity, leading to slower system elimination and thereby providing more time for therapeutic activity (Dintzis et al., 1993; van Regenmortel and Muller, 1998).

Abbreviations: %ID, relative injected dose; AD, Alzheimer's disease; AGP, α_1-acid glycoprotein; AUC, area under the concentration-time curve; AUMC, area under the moment curve; Aβ, β-amyloid; C, concentration; Cl, clearance; D, dose; dpm, disintegrations per minute; F, bioavailability; f_u, unbound fraction; HSA, human serum albumin; i.p., intraperitoneal; i.v., intravenous; inf, infinity; K_D, dissociation constant; MRT, mean residence time; r^2, correlation coefficient; $t_{1/2}$, terminal half-life; TLC, thin layer chromatography; V_{ss}, distribution volume in steady state; V_z, terminal distribution volume; λ_z, terminal elimination rate constant.

* Correspondence to: A. Willuweit, Institute of Neuroscience and Medicine, Medical Imaging Physics (INM-4), Forschungszentrum Jülich GmbH, 52425 Jülich, Germany.
** Correspondence to: D. Willbold, Institute of Complex Systems, Structural Biochemistry (ICS-6), Forschungszentrum Jülich GmbH, 52425 Jülich, Germany.
E-mail addresses: l.hofmann@fz-juelich.de (L.H.E. Leithold), n.jiang@fz-juelich.de (N. Jiang), j.post@fz-juelich.de (J. Post), n.niemietz@fz-juelich.de (N. Niemietz), e.schartmann@fz-juelich.de (E. Schartmann), t.ziehm@fz-juelich.de (T. Ziehm), j.kutzsche@fz-juelich.de (J. Kutzsche), n.j.shah@fz-juelich.de (N.J. Shah), joerg.breitkreutz@uni-duesseldorf.de (J. Breitkreutz), kj.langen@fz-juelich.de (K.-J. Langen), a.willuweit@fz-juelich.de (A. Willuweit), d.willbold@fz-juelich.de (D. Willbold).
[1] Authors contributed equally.

http://dx.doi.org/10.1016/j.ejps.2016.04.016
0928-0987/

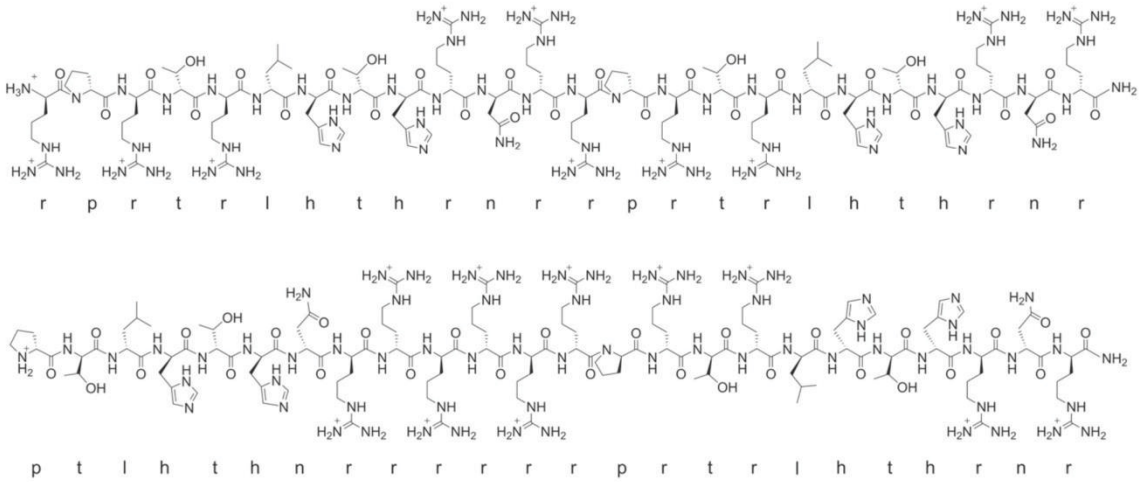

Fig. 1. Lewis structure and single letter amino acid code of D3D3 (top) and RD2D3 (bottom). Both peptides are D-enantiomeric peptides (3.2 kDa).

Using mirror image phage display against β-amyloid (Aβ) monomers as target (Schumacher et al., 1996; Wiesehan and Willbold, 2003), we have previously identified the D-peptide D3 which has been shown to improve pathology and cognition in transgenic AD mice (Funke et al., 2010; van Groen et al., 2012; van Groen et al., 2013; van Groen et al., 2008). Additionally, a number of derivatives have also been designed. Among those, RD2 has shown enhanced properties *in vitro* and *in silico*, while containing the same D-amino acid residues in a rationally reordered sequence (Olubiyi et al., 2014). Studies assessing pharmacokinetic properties of both D3 (Jiang et al., 2015)

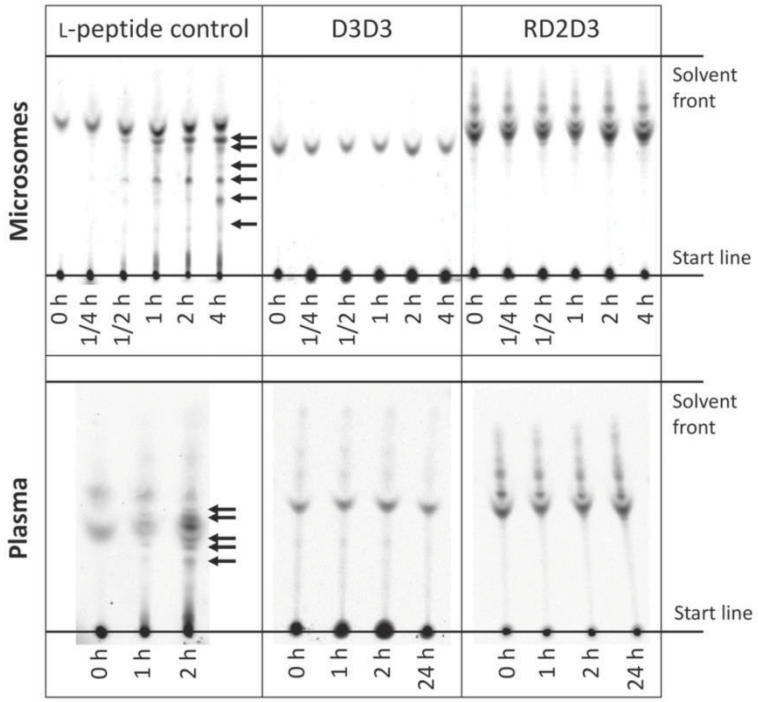

Fig. 2. Autoradiography of thin layer chromatogram, showing proteolytic stability of ^{3}H-D3D3 and ^{3}H-RD2D3 in mouse plasma and liver microsomes in comparison to an L-peptide control. The peptides were incubated with plasma or microsomes at 37 °C for the given amount of time and applied to thin layer chromatography plates. Proteolytic degradation is apparent from time dependent appearance of additional bands, as was obvious for the L-peptide control (arrows). In contrast, D3D3 and RD2D3 remained stable for 4 h in liver microsomes and plasma for up to 24 h of incubation.

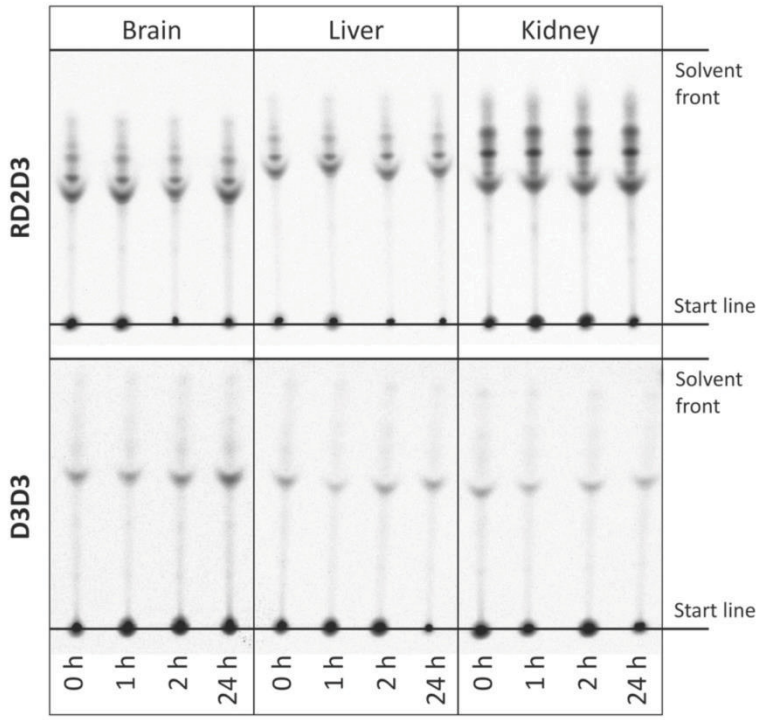

Fig. 3. Autoradiography of thin layer chromatogram, showing proteolytic stability of ^{3}H-D3D3 and ^{3}H-RD2D3 in mouse organ homogenates. The peptides were incubated with brain, liver and kidney homogenates at 37 °C for the given amount of time and applied to thin layer chromatography plates. No proteolytic degradation is apparent for both peptides for up to 24 h of incubation.

and RD2 (Leithold et al., 2015) have demonstrated auspicious characteristics such as long half-lives and high oral bioavailability.

Here, we determined the pharmacokinetic properties of D3D3 and RD2D3, which can be thought of as head-to-tail tandem homo- and heteropeptides made of D3 and RD2. The rationale behind the design of the tandem peptides is that multivalent D-peptides can be expected to target their multivalent target molecules, here Aβ oligomers, with increased efficiency. Recently, this was shown to be true for D3D3 *in vitro* and *in vivo* (Brener et al., 2015).

2. Methods

2.1. Peptides

D3D3 (H-rprtrlhthrnrrprtrlhthrnr-NH_2, 3.2 kDa) and RD2D3 (H-ptlhthnrrrrrrprtrlhthrnr-NH_2, 3.2 kDa) were purchased from peptides&elephants GmbH (Potsdam, Germany). All peptides consist solely of D-enantiomeric amino acids. The Lewis structures of both peptides can be found in Fig. 1.

The tritium-labelled peptides ^{3}H-D3D3 (H-rprtrlhthrnrrprtrlhthrnr-NH_2, 110 Ci/mmol) and ^{3}H-RD2D3 (H-ptlhthnrrrrrrprtrlhthrnr-NH_2, 73 Ci/mmol) were purchased from Quotient Bioresearch (Radiochemicals) Ltd. (Cardiff, United Kingdom) to contain 1 mCi/ml respectively 37 MBq/ml and were supplied as solution in water and ethanol (1:1). The radioactively labelled L-enantiomer of D3 (H-RPRTRLHTHRNR-NH_2, 103 Ci/mmol, Quotient Bioresearch), was used as control peptide for stability assessment.

2.2. Proteolytic stability

Proteolytic stability of ^{3}H-D3D3 and ^{3}H-RD2D3 in mouse organ homogenates was assessed as described previously (Leithold et al., 2015). Additionally, 2 µl of a ^{3}H-L-peptide were incubated with 1 µl mouse plasma as control.

Furthermore, proteolytic stability of all peptides against degradation by microsomes was analysed using microsomes from mouse and human liver (pooled from CD-1 mice; pooled from male human liver; protein content approx. 20 mg/ml, Sigma-Aldrich). 6 µl ^{3}H-peptide were added to 4 µl pre-warmed microsome solution and incubated at 37 °C. After different incubation times the reaction was stopped by addition of 6 µl mobile solvent (2-butanol/pyridine/ammonia (28%)/water, 39/34/10/26 ml respectively) and samples were stored at −20 °C until further use. For detection, thin layer chromatography and autoradiography were performed as described before (Leithold et al., 2015).

2.3. Pharmacokinetic studies

Pharmacokinetic analysis of the ^{3}H-peptides was assessed as previously described, with the exceptions explained below (Leithold et al., 2015). For pharmacokinetic analysis different doses and time points of organ harvesting were chosen per route of administration: i.v. injection 3.3 mg/kg, 3 min, 5 min, 10 min, 15 min, 30 min, 1 h, 4 h, 18 h, 1 d, 2 d; i.p. administration 10 mg/kg, 10 min, 20 min, 30 min, 1 h, 2 h, 4 h, 6 h, 1 d, 2 d. For each time point three mice were administered with the respective dose. The terminal elimination rate constant (λ_z) was obtained

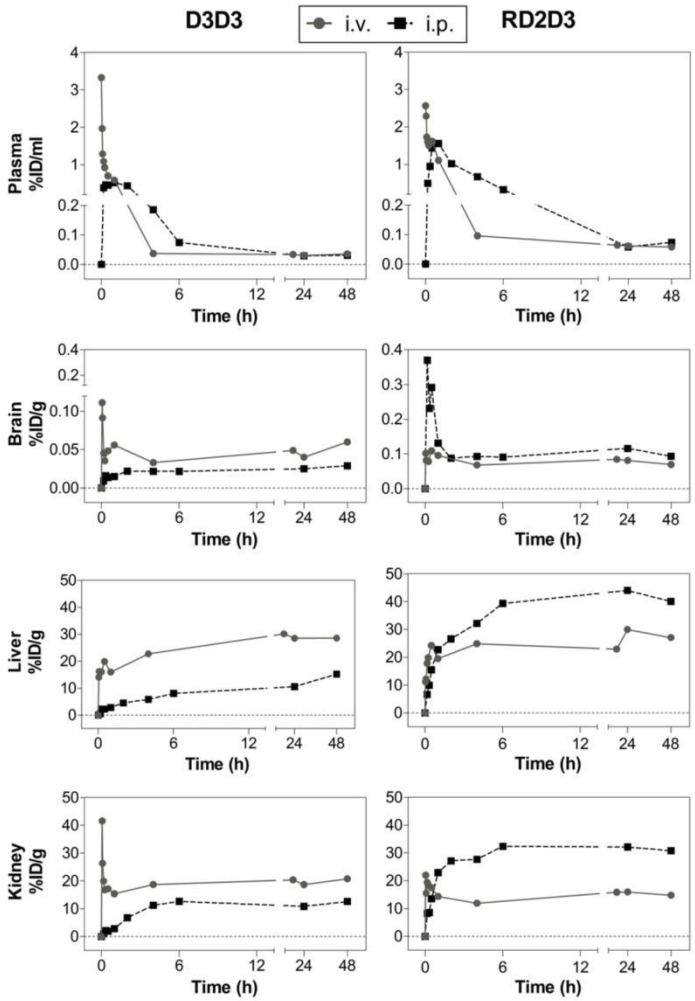

Fig. 4. Time-dependent distribution of ^{3}H-D3D3 and ^{3}H-RD2D3 in mouse plasma, brain, liver and kidney after i.v. and i.p. administration. Radioactively labelled D3D3 or RD2D3 was administered together with non-labelled peptide at total concentrations of 10 mg/kg (i.p.) or 3.3 mg/kg (i.v.). The concentration of D3D3 and RD2D3 is shown as percent of the injected dose per millilitre plasma (%ID/ml) or gram organ (%ID/g). Graphs show the means of three mice per time point.

by logarithmic extrapolation of the last five to six observed concentrations based on the highest correlation coefficient obtained ($r^2 = 0.99$ for all calculations).

2.4. Plasma protein binding

The plasma protein binding assay was performed twice per peptide as described previously (Leithold et al., 2015).

2.5. Animals

C57BL/6 mice were used for plasma extraction and pharmacokinetic studies. All animal experiments were carried out in conformance with the German Protection of Animals Act (TierSchG §§ 7–9) and with permit from an Animal Protection Committee (AZ84-02.04.2011.A356).

3. Results

3.1. Proteolytic stability

It was shown previously that both D3 and RD2 are proteolytically stable in organ homogenates and plasma (Jiang et al., 2015; Leithold et al., 2015). To confirm the proteolytic stability for both tandem peptides, ^{3}H-D3D3 and ^{3}H-RD2D3 were incubated with mouse plasma (Fig. 2) and organ homogenates (Fig. 3) for up to 24 h and analysed by thin layer chromatography (TLC). It is noteworthy that under TLC conditions the peptides bound differently to plasma and organ constituents, thereby exhibiting different patterns and intensities on the TLC plate as detected by autoradiography. Results show that overall composition of both D3D3 and RD2D3 did not change over time, but remained stable for at least 24 h. In contrast, the L-peptide used for control was proteolytically degraded within 2 h as visible by the time dependent appearance of additional bands (Fig. 2).

Table 1
Pharmacokinetic parameters determined from mouse plasma for i.v. and i.p. administration. Clear fields are not applicable for the respective administration route. For abbreviations please refer to the abbreviations section.

Parameter	Units	D3D3		RD2D3	
		i.v.	i.p.	i.v.	i.p.
Dose (D)	mg/kg	3.3	10	3.3	10
t_{max}	min	3	60	3	60
C_{max}/D	(μg/ml)/(mg/kg)	0.54	0.16	0.58	0.47
$AUC_{0\text{-}last}$	mg/ml * min	0.18	0.61	0.32	1.82
$AUMC_{0\text{-}last}$	min^2 * mg/ml	131	424	229	1091
$MRT_{0\text{-}last}$	h	11.9	11.6	11.9	10.0
λ_z	min^{-1}	0.0155	0.0075	0.0137	0.0050
$t_{1/2}$	h	0.7	1.5	0.8	2.3
$AUC_{0\text{-}inf}$	mg/ml * min	0.18	0.62	0.32	1.87
$AUMC_{0\text{-}inf}$	min^2 * mg/ml	137	461	240	1225
$MRT_{0\text{-}inf}$	h	12.3	12.3	12.3	10.9
V_z	l/kg	1.15	2.37	0.74	1.99
Cl/F	ml/(min * kg)	17.9	16.1	10.2	5.4
V_{ss}	l/kg	13.2		7.5	
$F_{AUC\text{-}last}$	%		110		187
% AUC extrapolated	%	1.1	1.9	1.2	2.3

Moreover, neither D-peptide was degraded after 4 h incubation with liver microsomes, in contrast to the L-peptide (Fig. 2). Confirmation of proteolytic stability of D3D3 and RD2D3 was important to ensure that measured radioactivity in the pharmacokinetic studies correlated with ^{3}H-D3D3 and ^{3}H-RD2D3 total concentrations.

3.2. Pharmacokinetic properties

To assess pharmacokinetic parameters ^{3}H-labelled D3D3 and RD2D3 were used for i.p. and i.v. administration in mice. Following the radioactive label, both peptides were successfully quantitated in all analysed organs and upon all administration routes. Fig. 4 shows the relative injected dose per millilitre plasma or gram brain, liver and kidney over the time course of two days as well as the brain/plasma ratio.

Remarkably, for RD2D3 intraperitoneal rather than intravenous administration resulted in higher values in all organs, whereas this was the opposite for D3D3 where i.v. resulted in higher amounts present in all assessed organs. Higher concentration of D3D3 and RD2D3 in the liver as compared to the kidney suggests the liver as the major pathway for excretion for both peptides. It is noteworthy that after 2 days post administration both peptides were still present in all organs and especially high in liver and kidney. RD2D3 reached higher levels than D3D3 in the brain as well as in liver and kidney (Fig. 4), which is most prominent following i.p. administration.

3.2.1. Plasma pharmacokinetic parameters

Plasma pharmacokinetic parameters were calculated based on back calculated peptide concentrations from measured radioactivity in plasma and are summarised in Table 1. The maximally observed concentration relative to the Dose (C_{max}/D) was similar for i.v. injection (D3D3 0.54 and RD2D3 0.58 (μg/ml)/(mg/kg)) but differed upon i.p. administration between 0.16 (μg/ml)/(mg/kg) for D3D3 and 0.47 (μg/ml)/(mg/kg) for RD2D3. For both D-peptides the areas under the curve $AUC_{0\text{-}last}$ and $AUC_{0\text{-}inf}$ do not differ much, which is due to the very low extrapolated part of the $AUC_{0\text{-}inf}$ (< 3%). RD2D3 showed higher plasma $AUC_{0\text{-}inf}$ for both administration routes (i.v. 0.32 mg/ml * min and i.p. 1.87 mg/ml * min) as compared to D3D3 (i.v. 0.18 mg/ml * min and i.p. 0.62 mg/ml * min). The mean retention time ($MRT_{0\text{-}inf}$) was around 11 and 12 h and similar for all administration routes and both peptides. The rate of i.v. terminal plasma clearance was higher for D3D3 with Cl/F = 17.9 ml/(min * kg) than for RD2D3 with Cl/F = 10.2 ml/(min * kg). Additionally, upon i.p. administration the clearance was found to be lower than after i.v. administration for both peptides. This results in longer half-lives ($t_{1/2}$) for RD2D3 (i.v. 0.8 h and i.p. 2.3 h) compared to D3D3 (i.v. 0.7 h and i.p. 1.5 h). Furthermore, the bioavailability (F) upon i.p. administration of RD2D3 was very high with about 190%, while D3D3 reached 110%.

3.2.2. Brain pharmacokinetic parameters

Since the brain is thought to be the therapeutically relevant target organ, pharmacokinetic parameters were also calculated for the brain (Table 2). Both peptides showed an increasing brain/plasma ratio over time, reaching 1 after about 6 to 12 h (Fig. 5), which resulted in an overall brain/plasma ratio based on the $AUC_{0\text{-}last}$ of 0.6 (i.v.) and 0.3 (i.p.) for D3D3 and 0.6 (i.v.) and 0.5 (i.p.) for RD2D3. The time-dependent The brain exposure ($AUC_{0\text{-}last}$) was higher for RD2D3 than for D3D3, especially upon i.p. administration (RD2D3 i.v. 0.19 and i.p. 0.88 mg/g * min and D3D3 i.v. 0.12 and i.p. 0.20 mg/g * min). The C_{max}/D was 0.02 (μg/g)/(mg/kg) for i.v. administration. I.p. injection lead to a C_{max}/D of 0.01 for D3D3 and was higher for RD2D3 with 0.11 (μg/g)/(mg/kg). The MRT was calculated to be about one day for both peptides and administration routes. Furthermore, the bioavailability of the i.p. administration was low for D3D3 with 55% and very high for RD2D3 with 157%.

3.3. Plasma protein binding

In vivo plasma protein binding was estimated by *in vitro* incubation of ^{3}H-labelled D3D3 and RD2D3 with human serum albumin (HSA) and α_1-acid glycoprotein (AGP) (Fig. 6). For AGP the binding curves of both peptides reached saturation even at the lowest AGP concentration. This indicates strong binding affinities to AGP. Results yielded for RD2D3 a K_D of 0.04 μM ± 18% and for D3D3 a K_D of 0.03 μM ± 18%. Binding to HSA did not reach saturation and could therefore not be determined reliably, with K_D values being in the hundreds micromolar range. It could be deduced that both peptides showed much higher affinity to AGP than to HSA and plasma protein binding therefore is mainly determined by AGP binding. The expected free fraction in plasma was calculated disregarding HSA binding and under the assumption of peptide concentrations in plasma of C_{RD2D3} = 0.027 μM and C_{D3D3} = 0.013 μM (concentrations 24 h after administration). Results showed a fraction unbound (f_u) for RD2D3 of 0.20% and for D3D3 of 0.16%.

3.4. Proteolytic stability in human samples

To confirm that the peptides are not only stable in mouse tissue, proteolytic stability was additionally assessed and ^{3}H-D3D3 and ^{3}H-RD2D3 and the ^{3}H-L-peptide control were incubated with human liver microsomes and analysed by TLC (Fig. 7). Results show that overall composition of both D3D3 and RD2D3 remained stable for at least 24 h both in human microsomes. In contrast, the L-peptide used for control was quickly proteolytically degraded.

Table 2
Brain pharmacokinetic parameters determined for i.v. and i.p. administration. Clear fields are not applicable for the respective administration route. For abbreviations please refer to the abbreviations section.

Parameter	Units	D3D3		RD2D3	
		i.v.	i.p.	i.v.	i.p.
Dose (D)	mg/kg	3.3	10	3.3	10
t_{max}	min	3	2880	30	10
C_{max}/D	(μg/g)/(mg/kg)	0.02	0.01	0.02	0.11
$AUC_{0\text{-}last}$	mg/g * min	0.12	0.20	0.19	0.88
$AUMC_{0\text{-}last}$	min^2 * mg/g	189	315	269	1264
$MRT_{0\text{-}last}$	h	26.8	26.5	24.2	23.8
$F_{AUC\text{-}last}$	%		55		157
Brain/plasma ratio $AUC_{0\text{-}last}$		0.6	0.3	0.6	0.5

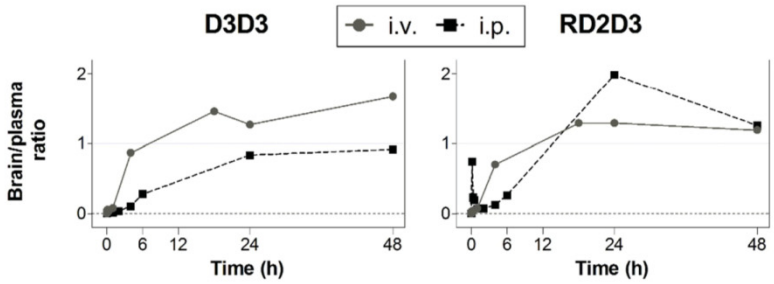

Fig. 5. Time-dependent development of ^{3}H-D3D3 and ^{3}H-RD2D3 brain/plasma ratio after i.v. and i.p. administration. Graphs show the means of three mice per time point, corrected for residual blood in the brain.

4. Discussion

Here, we have assessed the pharmacokinetic properties of two D-peptides which are head-to-tail tandem derivatives of the previously described peptides D3 and its derivative RD2. D3 has been selected by mirror image phage display for binding against Aβ(1–42) and both D3 and RD2 have demonstrated therapeutic potential *in vitro* and *in vivo* (Bartnik et al., 2010; Funke et al., 2010; Olubiyi et al., 2014; van Groen et al., 2008). Furthermore, D3 and RD2 exhibited excellent pharmacokinetic properties as has been shown previously (Jiang et al., 2015; Leithold et al., 2015). In a next step, tandem peptides were created in order to enhance the affinity to Aβ (Brener et al., 2015). Thereafter, pharmacokinetic assessment was performed to determine their ability to reach the target organ brain.

For both D3 and RD2 it could previously be shown that they remain stable in mouse organ homogenates and plasma (Jiang et al., 2015; Leithold et al., 2015). Here, we demonstrated that the homo- and heteropeptides D3D3 and RD2D3 are likewise proteolytically stable for at least 24 h in mouse plasma, organ homogenates and liver microsomes. We used the measured ^{3}H-radioactivity of the administered peptides in the pharmacokinetic study to calculate the peptide concentrations. This assumes that the non-metabolised peptides are represented by the measured radioactivity which is then used to obtain the pharmacokinetic parameters. Although we have shown that the peptides are stable in mouse plasma for 24 h we cannot exclude partial metabolism at later time points which might or might not influence their therapeutic effectivity. Incubation in plasma and organ homogenates beyond 24 h and microsomes beyond 4 h appeared not to be meaningful since enzyme activities in biological samples cannot be expected to last for long incubation times at 37 °C. Furthermore, due to the complete lack of metabolism of RD2D3 and D3D3 after 24 h incubation with organ homogenates as well as after incubation with microsomes there was no reason to expect significant metabolism at 48 h. Nevertheless, for pharmacokinetic assessment we performed a non-compartmental analysis since this is a simplistic analysis without the need for assumptions regarding the number of compartments. Any minor metabolite would influence more complex pharmacokinetic models and would lead to inaccurate data. The authors are aware that non-compartmental analysis may not be the optimal model for the pharmacokinetic analysis. It assumes linear kinetics and may therefore result in over- or under-estimation of certain parameters. However, it is often used as an initial indication of the pharmacokinetic properties of a substance and avoids additional over-interpretation of the data at hand. The present study was performed in healthy C57BL/6 mice. The

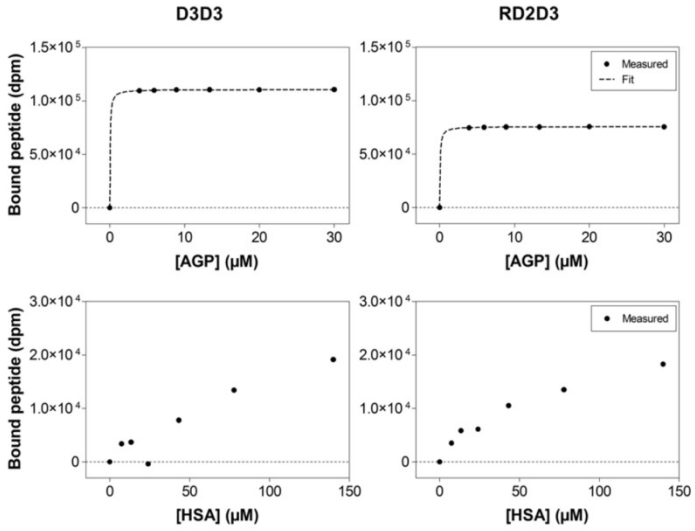

Fig. 6. Plasma protein binding of ^{3}H-D3D3 and ^{3}H-RD2D3. Graphs display the determined amount of D-peptide bound (in dpm) to α_1-acid glycoprotein (AGP) or human serum albumin (HSA) at different concentrations. Binding affinity to AGP was roughly estimated based on the Michaelis Menten binding equation (dotted lines). Dissociation constants for binding to HSA could be estimated to be in the hundreds μM range as the saturation was not reached even above 100 μM.

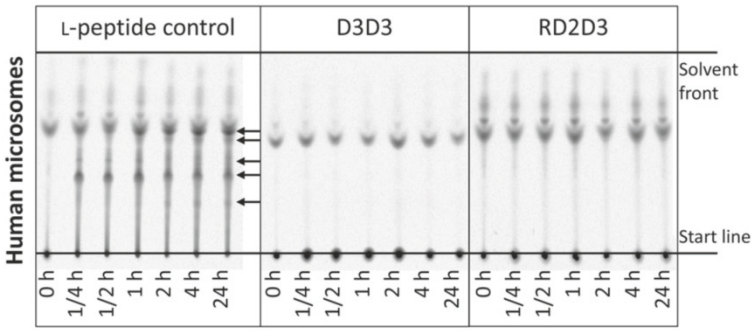

Fig. 7. Autoradiography of thin layer chromatogram, showing proteolytic stability of ^{3}H-D3D3 and ^{3}H-RD2D3 in human liver microsomes. The peptides were incubated with human liver microsomes at 37 °C for the given amount of time and applied to thin layer chromatography plates. No proteolytic degradation is apparent for both peptides for up to 24 h of incubation whereas the L-peptide control is degraded rapidly as indicated by the appearance of additional bands (arrows).

resulting pharmacokinetic parameters may be different in transgenic AD mouse models. Existing preliminary pharmacokinetic data for D3, however, does not suggest any significant difference in pharmacokinetic properties between wild type mice and transgenic AD mice.

To summarise, the pharmacokinetic analysis showed that RD2D3 has a lower clearance than D3D3, resulting in higher drug exposure in plasma and brain as well as a high bioavailability after i.p. administration. Both peptides have higher AUC values upon i.p. administration compared to i.v. administration. However, both D3D3 and RD2D3 have relatively high elimination rate constants and therefore short half-lives of only few hours that are in the same range as other peptides assessed as potential drugs (Pollaro and Heinis, 2010). Furthermore, D3D3 and RD2D3 have a low predicted free fraction in plasma and may therefore only be available for therapeutic action in the target organ in small amounts. However, it was shown that high plasma protein binding does not necessarily impede drug efficacy, and newly approved drugs often show high plasma protein binding (Liu et al., 2014; Smith et al., 2010; Zhang et al., 2012). This is also the case for the available drugs indicated for the central nervous system, Kratochwil et al. (2002) found no general preference for high or low HSA binding.

The i.p. plasma drug exposure especially of RD2D3 is considerably higher than upon i.v. administration. This could possibly be explained by the higher rate of clearance observed for i.v. administration. Entero-hepatic recirculation or renal reabsorption can lead to a prolonged presence of the peptide in the organism (Bendayan, 1996; Roberts et al., 2002). This is underlined by the results showing no apparent decrease of the peptide concentration in liver and kidney after 2 days (Fig. 4). For RD2D3 the concentration in both organs is higher than for D3D3, indicating that this effect is more pronounced for RD2D3, explaining the much higher bioavailability of RD2D3 than D3D3. The bioavailability upon oral administration for the tandem peptides remains to be analysed, however, both monovalent peptides D3 and RD2 were shown to exhibit promising pharmacokinetic properties for oral application (Jiang et al., 2015; Leithold et al., 2015).

It was shown that D3 itself has a half-life in plasma of 32 h for i.v. and >40 h upon i.p. or oral administration (Jiang et al., 2015). Remarkably, RD2 showed a plasma half-life of about 60 h for all assessed administration routes (Leithold et al., 2015). In contrast, both tandem peptides have remarkably short half-lives of only few hours. This is also reflected in the clearance, with D3D3 exhibiting the highest rate, followed by RD2D3, D3 and RD2 having the slowest clearance. Interestingly, the MRT in both plasma and brain was higher for the tandem peptides than for D3 for both i.p. and i.v. administration, while RD2 had much higher MRT values for all administration routes. RD2 also showed the highest brain/plasma ratio when calculated using the $AUC_{0\text{-last}}$ of all peptides. Since also the drug exposure in plasma, as calculated by plasma $AUC_{0\text{-inf}}$, is highest in RD2 and D3, it is concluded that the larger size of the tandem peptides results in less favourable pharmacokinetic parameters. Furthermore, resorption from the peritoneum into the blood seems to be least effective for the tandem peptides. Plasma levels of D3D3 are very low, higher for RD2D3 followed by D3, while RD2 is resorbed very efficiently. Similarly, peptide levels in the brain are highest for RD2, followed by D3 and the tandem peptides with RD2D3 exhibiting higher levels than D3D3. Considering the brain/plasma ratios which do not differ much, the low brain levels of the tandem peptides may result primarily from their insufficient resorption rather than from an inferior ability to enter the brain.

Additionally, we were able to show that D3D3 and RD2D3 are proteolytically stable in human liver microsomes for at least 24 h. The stability in human tissue is important knowledge for the further development of these D-peptides into clinical application.

5. Conclusions

Taken together, the tandem peptides exhibit less favourable pharmacokinetic properties than the single peptides. Resorption of D3D3 and RD2D3 is less effective, resulting in lower brain concentrations as compared to the single peptides D3 and RD2. This disadvantage of the tandem peptides could possibly be outweighed by higher efficiency of the tandem compounds as was indicated by recent data for D3D3 (Brener et al., 2015). Furthermore, it is concluded that the sequence order of the D-enantiomeric amino acid residues has a considerable impact on pharmacokinetic properties of the peptide. Peptides harbouring the amino acid residue sequence of RD2 were found to exhibit enhanced pharmacokinetic properties than those harbouring the D3 sequence. This can be seen both in RD2 alone when compared to D3 and similarly within RD2D3 in comparison to D3D3.

Conflict of interest

The authors declare that they have no conflict of interest.

Acknowledgements

We thank Jörg Mauler for helping with the data analysis. D.W. and N.J.S. were supported by grants from the "Portfolio Technology and Medicine" of the Impuls und Vernetzungs-Fonds der Helmholtzgemeinschaft. D.W. was supported by the Helmholtz-Validierungsfonds of the Impuls und Vernetzungs-Fonds der Helmholtzgemeinschaft; K.J.L. and D.W. were supported by the "Portfolio Drug Research" of the Impuls und Vernetzungs-Fonds der Helmholtzgemeinschaft.

References

Bartnik, D., Funke, S.A., Andrei-Selmer, L.C., Bacher, M., Dodel, R., Willbold, D., 2010. Differently selected D-enantiomeric peptides act on different Abeta species. Rejuvenation Res. 13, 202–205.

Bendayan, R., 1996. Renal drug transport: a review. Pharmacotherapy 16, 971–985.

Brener, O., Dunkelmann, T., Gremer, L., van Groen, T., Mirecka, E.A., Kadish, I., Willuweit, A., Kutzsche, J., Jurgens, D., Rudolph, S., Tusche, M., Bongen, P., Pietruszka, J., Oesterhelt, F., Langen, K.J., Demuth, H.U., Janssen, A., Hoyer, W., Funke, S.A., Nagel-Steger, L., Willbold, D., 2015. QIAD assay for quantitating a compound's efficacy in elimination of toxic Abeta oligomers. Sci. Rep. 5, 13222.

Dintzis, H.M., Symer, D.E., Dintzis, R.Z., Zawadzke, L.E., Berg, J.M., 1993. A comparison of the immunogenicity of a pair of enantiomeric proteins. Protein Struct. Funct. Genet. 16, 306–308.

Funke, S.A., van Groen, T., Kadish, I., Bartnik, D., Nagel-Steger, L., Brener, O., Sehl, T., Batra-Safferling, R., Moriscot, C., Schoehn, G., Horn, A.H.C., Mueller-Schiffmann, A., Korth, C., Sticht, H., Willbold, D., 2010. Oral treatment with the D-enantiomeric peptide D3 improves the pathology and behavior of Alzheimer's disease transgenic mice. ACS Chem. Neurosci. 1, 639–648.

Jiang, N., Leithold, L.H.E., Post, J., Ziehm, T., Mauler, J., Gremer, L., Cremer, M., Schartmann, E., Shah, N.J., Kutzsche, J., Langen, K.-J., Breitkreutz, J., Willbold, D., Willuweit, A., 2015. Preclinical pharmacokinetic studies of the tritium labelled D-enantiomeric peptide D3 developed for the treatment of Alzheimer's disease. PLoS One 10, e0128553.

Kratochwil, N.A., Huber, W., Muller, F., Kansy, M., Gerber, P.R., 2002. Predicting plasma protein binding of drugs: a new approach. Biochem. Pharmacol. 64, 1355–1374.

Leithold, L.H.E., Jiang, N., Post, J., Ziehm, T., Schartmann, E., Kutzsche, J., Shah, N.J., Breitkreutz, J., Langen, K.J., Willuweit, A., Willbold, D., 2015. Pharmacokinetic Properties of a Novel D-Peptide Developed to Be Therapeutically Active Against Toxic β-Amyloid Oligomers. Pharm. Res.

Liu, X., Wright, M., Hop, C.E.C.A., 2014. Rational use of plasma protein and tissue binding data in drug design. J. Med. Chem. 57, 8238–8248.

Nygaard, H.B., 2013. Current and emerging therapies for Alzheimer's disease. Clin. Ther. 35, 1480–1489.

Olubiyi, O.O., Frenzel, D., Bartnik, D., Glück, J.M., Brener, O., Nagel-Steger, L., Funke, S.A., Willbold, D., Strodel, B., 2014. Amyloid aggregation inhibitory mechanism of arginine-rich D-peptides. Curr. Med. Chem. 21, 1448–1457.

Pauletti, G.M., Gangwar, S., Siahaan, T.J., Aubé, J., Borchardt, R.T., 1997. Improvement of oral peptide bioavailability: peptidomimetics and prodrug strategies. Adv. Drug Deliv. Rev. 27, 235–256.

Pollaro, L., Heinis, C., 2010. Strategies to prolong the plasma residence time of peptide drugs. Medchemcomm 1, 319–324.

Roberts, M.S., Magnusson, B.M., Burczynski, F.J., Weiss, M., 2002. Enterohepatic circulation: physiological, pharmacokinetic and clinical implications. Clin. Pharmacokinet. 41, 751–790.

Sato, A.K., Viswanathan, M., Kent, R.B., Wood, C.R., 2006. Therapeutic peptides: technological advances driving peptides into development. Curr. Opin. Biotechnol. 17, 638–642.

Schumacher, T.N.M., Mayr, L.M., Minor, D.L., Milhollen, M.A., Burgess, M.W., Kim, P.S., 1996. Identification of D-peptide ligands through mirror-image phage display. Science 271, 1854–1857.

Smith, D.A., Di, L., Kerns, E.H., 2010. The effect of plasma protein binding on in vivo efficacy: misconceptions in drug discovery. Nat. Rev. Drug Discov. 9, 929–939.

Sun, N., Funke, S.A., Willbold, D., 2012. A survey of peptides with effective therapeutic potential in Alzheimer's disease rodent models or in human clinical studies. Mini Rev. Med. Chem. 12, 388–398.

van Groen, T., Wiesehan, K., Funke, S.A., Kadish, I., Nagel-Steger, L., Willbold, D., 2008. Reduction of Alzheimer's disease amyloid plaque load in transgenic mice by D3, a D-enantiomeric peptide identified by mirror image phage display. ChemMedChem 3, 1848–1852.

van Groen, T., Kadish, I., Funke, A., Bartnik, D., Willbold, D., 2012. Treatment with a beta 42 binding D-amino acid peptides reduce amyloid deposition and inflammation in APP/PS1 double transgenic mice. Adv. Protein Chem. Struct. Biol. 88, 133–152.

van Groen, T., Kadish, I., Funke, S.A., Bartnik, D., Willbold, D., 2013. Treatment with D3 removes amyloid deposits, reduces inflammation, and improves cognition in aged AbetaPP/PS1 double transgenic mice. J. Alzheimers Dis. 34, 609–620.

van Regenmortel, M.H.V., Muller, S., 1998. D-peptides as immunogens and diagnostic reagents. Curr. Opin. Biotechnol. 9, 377–382.

Wiesehan, K., Willbold, D., 2003. Mirror-image phage display: aiming at the mirror. Chembiochem 4, 811–815.

Zhang, F., Xue, J., Shao, J., Jia, L., 2012. Compilation of 222 drugs' plasma protein binding data and guidance for study designs. Drug Discov. Today 17, 475–485.

3.4 Blood-brain barrier penetration of an Aβ-targeted, arginine-rich, D-enantiomeric peptide

Autoren: Jiang N, Frenzel D, **Schartmann E**, van Groen T, Kadish I, Shah NJ, Langen KJ, Willbold D, Willuweit A

Journal: Biochimica et Biophysica Acta

veröffentlicht im November 2016

DOI: 10.1016/j.bbamem.2016.07.002

Impact Factor: 4,702 (2016)

Beitrag: Beteiligung an der Durchführung der pharmakokinetischen Experimente

Beteiligung an der Diskussion und Formulierung der Ergebnisse

Prüfung des Manuskripts

Biochimica et Biophysica Acta 1858 (2016) 2717–2724

Contents lists available at ScienceDirect

Biochimica et Biophysica Acta

journal homepage: www.elsevier.com/locate/bbamem

Blood-brain barrier penetration of an Aβ-targeted, arginine-rich, D-enantiomeric peptide

Nan Jiang [a], Daniel Frenzel [a,b], Elena Schartmann [a], Thomas van Groen [c], Inga Kadish [c], N. Jon Shah [d], Karl-Josef Langen [d,e], Dieter Willbold [a,f,*], Antje Willuweit [d,**]

[a] Forschungszentrum Jülich, Institute of Complex Systems, Structural Biochemistry, 52428 Jülich, Germany
[b] European Molecular Biology Laboratory, Meyerhofstraße 1, 69117 Heidelberg, Germany
[c] Department of Cell, Developmental and Integrative Biology, University of Alabama at Birmingham, Birmingham, AL 35294, USA
[d] Forschungszentrum Jülich, Institute of Neuroscience and Medicine, Medical Imaging Physics, 52428 Jülich, Germany
[e] Department of Neurology, Faculty of Medicine, JARA, RWTH Aachen University, Aachen, Germany
[f] Heinrich-Heine-Universität Düsseldorf, Institut für Physikalische Biologie, 40225 Düsseldorf, Germany

ARTICLE INFO

Article history:
Received 11 February 2016
Received in revised form 1 July 2016
Accepted 12 July 2016
Available online 14 July 2016

Keywords:
Blood-brain barrier penetration
Arginine-rich motif of HIV-Tat protein
D-Enantiomeric peptide
Alzheimer's disease
Amyloid beta
Transgenic mouse models

ABSTRACT

The application of small peptides targeting amyloid beta (Aβ) is one of many drug development strategies for the treatment of Alzheimer's disease (AD). We have previously identified several peptides consisting solely of D-enantiomeric amino acid residues obtained from mirror-image phage display selection, which bind to Aβ in different assembly states and eliminate toxic Aβ aggregates. Some of these D-peptides show both diagnostic and therapeutic potential *in vitro* and *in vivo*. Here we have analysed the similarity of the arginine-rich D-peptide D3 to the arginine-rich motif (ARM) of the human immunodeficiency virus type 1 transactivator of transcription (HIV-Tat) protein, and examined its *in vivo* blood-brain barrier (BBB) permeability using wild type mice and transgenic mouse models of Alzheimer's disease. We are able to demonstrate that D3 rapidly enters the brain where it can be found associated with amyloid plaques suggesting a direct penetration of BBB.

1. Introduction

Currently, two molecular weight categories classify drugs into conventional "small molecule" drugs (<500 Da) and "biologics" which are generally referred to as protein-based drugs (>5000 Da) [1]. Small molecules are often associated with favorable oral bioavailability and their production is considered scalable and economical. During drug discovery, they can be rationally designed, for example, altering the structure to optimize physiochemical properties for enhanced brain delivery [2,3]. Frequently, however, small molecules show low target selectivity, which may ultimately result in side effects. Protein-based drugs, for example antibodies, possess high selectivity, mainly because their large size allows formation of specific and high affinity binding sites for their target molecules. Usually they have poor oral bioavailability due to low membrane permeability and proteolytic instability [4]. Small peptide based molecules consisting of 5 to 50 amino acid residues may fill the molecular weight gap and combine the advantages o small molecules and protein based drugs.

Well-known examples of peptide-based drugs with high medica and economic impact are the peptide hormones insulin and glucagon Diseases like diabetes, cancer, inflammation and cardiovascular diseases, are strong drivers for the development of peptide based drugs [5]. Peptide drugs have the potential for high substrate specificity and affinity. Their degradation usually doesn't lead to toxic metabolites They are smaller than proteins and thus can be obtained synthetically by well-established and cost-efficient methods [6]. A drawback of peptide drugs is their relatively low bioavailability due to degradation and the resulting short half-lives. Several approaches have been developed to enhance the bioavailability of peptide based drug candidates. The application of D-enantiomeric amino acids is an effective way to enhance the resistance to degradation, because most proteolytic enzymes have substrate specificity for L-peptide bonds. This even allows the oral administration of D-enantiomeric peptides [7,8]. Furthermore, D-peptides are less, if at all, immunogenic [9].

The application of peptide based drugs for the treatment of central nervous system (CNS) diseases is hindered by the blood-brain barrier (BBB) [10,11]. Blood capillaries at the BBB have specialized structures and are characterized by the i) absence of fenestrae, ii) the presence o tight intercellular junctions, iii) low pinocytotic activity, and iv) high

* Corresponding author at: Forschungszentrum Jülich, Institute of Complex Systems, Structural Biochemistry, 52428 Jülich, Germany.
** Corresponding author.
E-mail addresses: D.Willbold@fz-juelich.de (D. Willbold), A.Willuweit@fz-juelich.de (A. Willuweit).

http://dx.doi.org/10.1016/j.bbamem.2016.07.002
0005-2736/

levels of efflux transporters at their luminal endothelial surface. This efficiently limits the penetration potential of 95% of all known drugs into the brain [12]. In the absence of active transport mechanisms, the ability of peptides to permeate through membranes usually decreases with increasing mass and hydrophilicity. Studies have shown that most drugs with molecular weights above 500 Da already show poor brain penetration potential and compounds with molecular weights above 1000 Da are usually widely excluded from the passive transmembrane transport system [13,14]. In spite of poor BBB permeability in general, some peptides can be transported into the brain *via* specific transporters expressed in brain endothelium under physiological or pathological conditions [15,16]. Furthermore, several BBB penetration mechanisms such as receptor-mediated, adsorptive-mediated or carrier-mediated mechanism are intensively studied [17]. Properties such as the presence of basic clusters have been found to trigger the uptake of compounds into the cell by an as yet unresolved mechanism. A well-known example is the human immunodeficiency virus type 1 (HIV-1) transactivator of transcription (Tat) [18–20]. The HIV-1 Tat is a regulatory protein with 86 to 101 amino acids depending on the subtype. It is produced in the very early stages of viral infection and greatly enhances the transcriptional rates which result in high viral gene expression. It also mediates viral spreading in disease progression [21]. The basic region of HIV-1 Tat protein involved in RNA binding is rich in arginines and lysines, and thus belongs to the family of arginine-rich motif (ARM) RNA binding proteins [22]. Such ARMs have been identified first in lentiviral Tat proteins, *e.g.* from HIV and equine infectious anaemia virus (EIAV), and later in a variety of nucleic acid binding proteins. Functional and structural details have been described for Tat proteins [23–26]. Currently there are several hypotheses about the potential mechanism for HIV-1 Tat uptake; these all incorporate the fact that HIV-1 Tat binds negatively-charged targets such as heparane sulfate/glycosaminoglycans, sialic acid and phospholipids, and traverses the plasma-membranes passively. Furthermore, recent *in vitro* experiments based on artificial membrane systems suggest the formation of plasma-membrane pores [18–20,27]. The exact mechanism of ARM transduction is still unknown, but the relative abundance of arginines is suggested to play a decisive role [28,29]. Although lysine presents the same positive net charge as arginine, the substitution of arginines with lysines decreases the transduction efficiency [30,31]. Studies show that arginine-rich peptides, which demonstrate membrane permeation, lack secondary structure, and D-enantiomeric arginine as well as guanidino peptoids work equivalently [28,31,32], which demonstrate that the guanidinium groups are the critical structural component responsible for the transduction [28,30,33]. Such mechanisms may be beneficial for peptide design.

We have identified several D-peptides by mirror-image phage display [34] for binding to Aβ [35,36]. They show promising abilities, *e.g.* elimination of Aβ oligomers and inhibition of Aβ fibril formation *in vitro* [37], and fluorescently labelled D-peptides bind to amyloid plaques in transgenic mice after direct brain infusion. [38]. One of those D-peptides, D3, was able to reduce plaque load and inflammation markers in the brains of aged APP/PS1 double transgenic mice and improved cognition even after oral administration [39–42]. Recently, the first comprehensive preclinical pharmacokinetic study of D3 was reported [7] and its BBB permeability was evaluated in an *in vitro* cell culture model [43].

D3 (rprtrlhthrnr) is an arginine-rich peptide containing five arginines out of twelve amino acid residues and shares sequence homology to ARM of HIV-1 Tat (HXB2) [44] (Fig. 1). HXB2 is a recombinant inbred strain derived from a cross of SHR/OlaIpcv with BN-Lx/Cub (HXB) of the first HIV-1 isolate, regarding as a standard reference strain [45,46]. The ARM mediates HIV-1 Tat's activity to overcome plasma membranes. Given the amino acid sequence similarity of D3 to the ARM of HIV-1 Tat, the ability of D3 to penetrate the BBB may be based on the same mechanism.

```
HIV-1 (HXB2) Tat 53-64:  RQRRRAHQNSQT
D3 1-12:                 rprtrlhthrnr
                         *  *  *  *
```

Fig. 1. Alignment of D3 with human immunodeficiency virus type 1 (HIV-1), strain HXB2, transactivator (Tat) protein. D3 shows sequence similarity to the arginine-rich motif (ARM) of a recombinant inbred strain (HXB2) of HIV-1 Tat protein.

To test this hypothesis, we have studied the *in vivo* localization of D3 in the CNS and its potential to pass the BBB as well as to bind amyloid plaques *in vivo* and *in vitro* in mouse brain sections.

Our results suggest that the BBB penetration of D3 may indeed have the same mechanism as HIV-1 Tat. This may offer a strategy to design and select peptide-based drugs and suggests that D3 and its derivatives are promising candidates for the future treatment of Alzheimer's disease.

2. Materials and methods

2.1. Peptides and other chemicals

^{3}H-D3 (rprtr-(4,5-^{3}H-Leu)-hthrnr) was purchased from Quotient Bioresearch (Radiochemicals) Ltd. (Cardiff, United Kingdom) with 10–100 Ci/mmol, 1 mCi/ml and purity >95%. D3 (rprtrlhthrnr), FAM-D3 (H-rprtrlhthrnr-Lys(5(6)-carboxyfluorescein)-NH2) and FAM-LP (LRMMLQIKRIPR-Lys(5(6)-carboxyfluorescein)-NH2) was purchased from JPT peptide Technologies GmbH (Berlin, Germany). Molecular weight of D3 is 1599, while FAM-D3 is 2086; The FAM tagging through 5-FAM lysine introduced one negative charge to D3 from a carboxylic acid at 5-FAM molecule. Thioflavine S was from Sigma-Aldrich (Munich, Germany). All other chemicals were supplied by Fluka Chemie AG (Buchs, Switzerland), Merck (Darmstadt, Germany), AppliChem (Darmstadt, Germany) and VWR (Darmstadt, Germany) in research grade.

2.2. Animals

To study the distribution of ^{3}H-D3, male C57Bl/6 mice (Charles River, Sulzfeld Germany) with an average body weight of 33.4 g were used. The mice were hosted in our animal facility under standard housing conditions for at least 2 weeks before experiment. All animal experiments were approved by the Animal Protection Committee of the local government (LANUV, North-Rhine-Westphalia, Germany, AZ84-02.04.2011. A359 and AZ84-02.04.2011. A356) according to the German Protection of Animals Act.).

For the experiment of FAM-D3 oral administration, seven male four-month old APP and PS1 double transgenic mice (APPswe/PS1ΔE9) were used in the present study. It has been shown that animals from this line exhibit numerous plaques and cerebral amyloid angiopathy within the brain, especially within cortex and hippocampus but also in other brain areas including the cerebellum [47–49]. The APPswe/PS1ΔE9 mice were acquired from JAX at the age of six weeks and housed in 4/cage in a controlled environment (temperature 22 °C, humidity 50–60%, and light from 07:00–19:00) until the treatments; food and water were available *ad libitum*. The experiment was conducted in accordance with the local Institutional Animal Care and Use Committee (IACUC) guidelines. All animal studies comply with the ARRIVE guidelines [50]. A completed ARRIVE guidelines checklist was included in S1 ARRIVE Checklist.

2.3. ^{3}H-D3 distribution in brain, plasma and CSF

^{3}H-D3 was mixed with non-radioactive D3 in a 0.1 M phosphate buffer (pH 8) to a total D3 concentration of 3 mg/ml with a specific radioactivity of 16.7 μCi per mg D3. 5 μCi D3 (100 μl) were administered as a single bolus intraperitoneally. Doses were selected according to

tolerability studies and did not cause adverse reactions. The total D3 concentration was calculated through 3H radioactivity assuming radioactive/non-radioactive ratio of the working solution stays the same during bio-distribution. Sampling times were 30, 60, 240 and 1440 min after administration (3 mice per time point). The administration method and the sampling time were selected based on our previous pharmacokinetic study [7]. Mice were anaesthetized with ketamine/medetomidine 10 min before samples were collected. Cerebrospinal fluid (CSF) was collected with a glass capillary tube (Round Boro Capillaries, CM Scientific, New Jersey, USA) from the *cisterna magna* as described by Liu and Duff [51]. About 8 to 9 μl CSF was obtained from each mouse. Blood was drawn by heart puncture and heparinized to isolate blood plasma. The right brain hemisphere was isolated directly after euthanasia through cervical dislocation.

The brain hemisphere was weighed and homogenized in homogenizer tubes (Precellys Ceramic Kit 1.4 mm, Precellys 24, Bertin technologies SAS, Montigny le Bretonneux, France) with 500 μl PBS. 10 ml scintillation cocktail (Ultima Gold XR, PerkinElmer, Waltham, Massachusetts, USA) was added to 100 μl of brain homogenate or plasma (diluted 1:1 with PBS) and mixed well. Disintegrations per unit time (dpm) were obtained in triplicates with a liquid scintillation counter (Packard Tri-Carb 2100TR Liquid Scintillation Analyser, PerkinElmer, Waltham, MA, USA). CSF was mixed directly with 10 ml scintillation cocktail.

Radioactivity was quantified in each sample as the percentage of injected dose (ID) per weight unit for brain tissue (%ID/g), or dose per volume unit for plasma/CSF samples (%ID/ml). Analogously, for cold material the concentration was expressed as weight unit of total D3 per weight unit of brain tissue (μg/g), or as weight unit per volume unit for plasma/CSF samples (μg/ml). Ratios were calculated from the values of brain, CSF and plasma, respectively. Mean values with standard error (SEM) of three mice were presented.

2.4. In vitro autoradiography (^3H) with mouse brain sections

Brain from a homozygous 18.5 months old APP/PS1 (ARTE 10) transgenic mouse is a generous gift from Andre Manook (Nuklearmedizinische Klinik und Poliklinik, Klinikum rechts der Isar, Technische Universität München, Munich, Germany). Homozygous ARTE10 mice of this age exhibit extensive plaque load and to a lesser extent cerebral amyloid angiopathy especially in cortex and hippocampus, but also in other areas except the cerebellum [42,52]. The brain was fixed in 4% formaldehyde (Carl Roth, Karlsruhe, Germany) in PBS for one week at room temperature then transferred into 30% sucrose in PBS for 2 days at 4 °C. A series of 30 μm free floating cryosections were cut sagittal and post-fixed in 4% paraformaldehyde for 30 min at room temperature. After washing and 10 min permeabilization with 1% Triton X-100 in Tris-buffered saline (TBS), sections were transferred into a staining dish containing ^{3}H-D3 solution in 1% Triton-TBS (2.5 k-becquerel (kBq) per section) and incubated for 3 days at room temperature. After washing in TBS and a rapid washing step in H_2O, sections were mounted on glass slides and dried at 37 °C for 2 h, then exposed against a phosphor-imaging plate for ^{3}H-autoradiography (FUJIFILM, Tokyo, Japan) in an autoradiography cassette for 7 days. The imaging plate was scanned with a phosphor film imager (Fujifilm BAS-5000, FUJIFILM Life Science, Japan) and images were acquired with BAS reader and AIDA software (Raytest, Freiburg, Germany).

2.5. Thioflavine S staining

Sections from *in vitro* autoradiography were immersion-fixed in 4% paraformaldehyde for 20 min, and then equilibrated in water twice for 2 min. After incubation in freshly filtrated 1% (w/v in water) Thioflavine S for 30 min at RT in a dark chamber, sections were washed twice for 2 min in $_{dd}H_2O$, and differentiated in two changes of 80% ethanol for 5 and 1 min, respectively. After washing three times in water (2 min per iteration), sections were covered with a glass slide and Aqua Poly/Mount (Polysciences, Warrington, US). Images were acquired with a Lumar V12 SteREO microscope (Zeiss, Oberkochen, Germany) with AxioCamMR3 camera (Zeiss, Oberkochen, Germany) and processed with AxioVs40 software (Release 4.5 SP1) and ImageJ (1.48 s).

2.6. Oral administration of D3 and FAM-D3

We chose oral administration for this long term experiments as it is favorable for animals. In order to achieve the desired total D3 concentration, non-labelled D3 (90%) was added to FAM-D3 (10%) with a final concentration of 0.25 mg/ml. Seven four-month old APPswe/PS1ΔE9 transgenic mice were treated for eight weeks with FAM-D3 and D3 in the drinking water. On average, the mouse drank ca. 2 to 3 ml water per day. The stability of D3 in water containing mouse saliva was verified using reversed phase HPLC analysis. Briefly, D3 was dissolved in double-distilled water, drinking water and drinking water containing 0.05% (v/v) mouse saliva to a final concentration of 27 μM. Freshly prepared solution and solution incubated for 24 h at 37 °C were analysed through reversed phase HPLC with a C18 column (Phenomenex Aschaffenburg, Germany) and compared. No obvious degradation was observed. Eight weeks after the start of treatment, the mice were sacrificed for histopathological analysis (see below).

2.7. Immunohistochemistry and immunofluorescence

Brain sections from the transgenic mouse orally administered with FAM-D3 were treated with a monoclonal mouse anti-Aβ(4–10) (W0-2) antibody (EMD Millipore). The sections were incubated overnight in a solution of TBS; then the sections were treated for 30 min in a heated (85 °C) sodium citrate solution (0.05 M, pH 6.0) and allowed to cool down. Afterwards, the series of sections were transferred into TBS-T (TBS with 0.5% Triton X-100) containing the primary antibody (mouse anti-Aβ(4–10), USA) for 24 h at 20 °C in a dark room. The sections were washed three times in TBS-T and transferred into a solution containing the secondary antibody (biotinylated goat anti mouse; Sigma) for 2 h. Again, the sections were washed three times with TBS-T and transferred to a solution containing ExtrAvidin for 2 h. Then the sections were incubated for approximately 3 min with Ni-enhanced diaminobenzidine (DAB) (12.5 mg DAB in 25 ml 0.1 M phosphate buffer pH 7.4, 30 μl H_2O_2 (30%), with 1 ml of a 15% ammonium Ni-sulfate solution added). The stained sections were mounted on gelatinized slides and coverslipped.

Cerebral blood vessels were visualized with GLUT-1 antibody (rabbit anti-GLUT-1 antibody EMD Millipore). The staining was performed exactly as described for Aβ, with the exception that no pretreatment was performed and a fluorescent secondary antibody (goat anti rabbit, Jackson ImmunoResearch) was applied. The stained sections were mounted on gelatinized slides and coverslipped.

2.8. Thin layer chromatography

Untreated wildtype mouse brain was homogenized with the same method as described above. After centrifuge at 20,000 ×*g* for 15 min at 4 °C to clarify the homogenate, extract of mouse brain was obtained from supernatant. FAM labelled peptide was incubated with the brain extract at 37 °C for different time periods (from 0 to 2 days). 2 μg FAM labelled peptide was mixed with 1 μl brain extract (in excess to peptide [53,54]). Mixtures containing FAM-labelled peptides were applied onto a HPTLC cellulose plate (OMNILAB, Essen, Germany) for thin layer chromatography (TLC) with mobile solvent (2-butanol/pyridine/acetic acid/water (30/20/6/24)). Images were acquired using the ChemDoc MP imaging system (Bio-RAD, Munich, Germany) under the fluorescein channel. The retardation factor (R_f) of each substance was defined as the ratio of the migration distance of the centre of a separated spot to the migration distance of the solvent front.

3. Results

3.1. Temporal distribution of ^{3}H-D3 in brain, plasma and CSF after intraperitoneal administration

To study the temporal and spatial distribution of D3 *in vivo*, we have analysed the concentrations of radioactively labelled D3 in brain, plasma and CSF. The time-concentration profiles of ^{3}H-D3 in whole brain, plasma and CSF after *i.p.* administration are shown in Fig. 2. Brain/plasma, CSF/plasma and brain/CSF ratios are shown in Fig. 3.

As expected, the highest concentration of D3 was measured in plasma shortly after administration with 8.4 μg/ml after 4 h and subsequently decreased to 0.53 μg/ml, whereas the concentration of D3 in brain and CSF started at about 0.6 μg/ml and decreased only slightly (Fig. 2). The brain/plasma ratio reached 0.8 to 0.9 after 4 h. D3 concentration in CSF remained slightly higher in comparison to that in the brain at all four time points, resulting in a relatively constant brain/CSF ratio of about 0.8 (Fig. 3).

3.2. Binding of ^{3}H-D3 on Aβ plaques by in vitro autoradiography

In order to study the influence of ^{3}H-D3 within cerebral blood vessels on the total radioactivity detected in the whole brain, brain slices of a transgenic APP/PS1 (ARTE 10) mouse were incubated with ^{3}H-D3 and subsequently developed by *in vitro* autoradiography (Fig. 4A). Additionally, the same slices were stained with Thioflavine S to stain beta-sheet rich structure elements (Fig. 4B), which is regarded as a robust and easy method for Aβ plaque quantification in this mouse model [55]. Co-localization of ^{3}H-D3 and Thioflavine S is an indicator of the specific binding of D3 to the amyloid plaques (Fig. 4C). Furthermore, the use of 1% Thioflavine S causes the strong non-specific staining of blood vessels [56], which also visualizes cerebral blood vessels on the section (Fig. 4D).

The APP/PS1 (ARTE 10) mouse model used is characterized by the lack of Aβ plaques in the cerebellum [55], which is in agreement with the Thioflavine S stain, as well as the autoradiography with ^{3}H-D3 in this study. No ^{3}H-D3 labelled structures of blood vessels in either the cerebrum or cerebellum could be observed in the autoradiogram, even though some of the vessels were clearly stained by Thioflavine S (Fig. 4D). This shows that ^{3}H-D3 bound specifically to Aβ plaques in the parenchyma and any specific binding of ^{3}H-D3 to cerebral blood vessels was negligible.

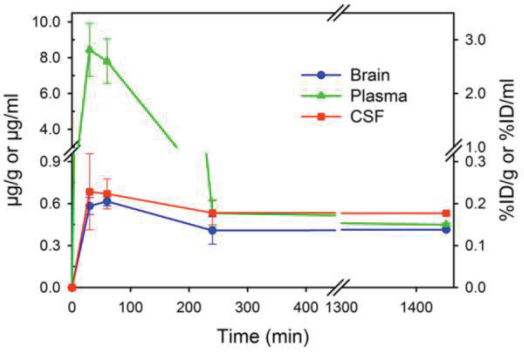

Fig. 2. Temporal distribution of ^{3}H-D3 in brain, plasma and cerebrospinal fluid (CSF) after *i.p.* administration in C57Bl/6 mice. ^{3}H-D3 (5 μCi) mixed with non-radioactive D3 to a total amount of 0.3 mg D3 was applied as single bolus per mouse. The concentration of D3 is shown as the mean value ± SEM (n = 3) at each time point. Units are given in μg/g (left Y-axis) or %ID/g (percentage of injected dose per gram tissue, right Y-axis) for brain, μg/l or %ID/ml (percentage of injected dose per milliliter) for CSF and plasma. ^{3}H-D3 concentration in brain and CSF were quite stable (about 0.6 μg/ml), whereas plasma concentration dropped rapidly initially until it reached similar levels to those in brain and CSF 4 h post injection (from 8.4 μg/ml to 0.53 μg/ml).

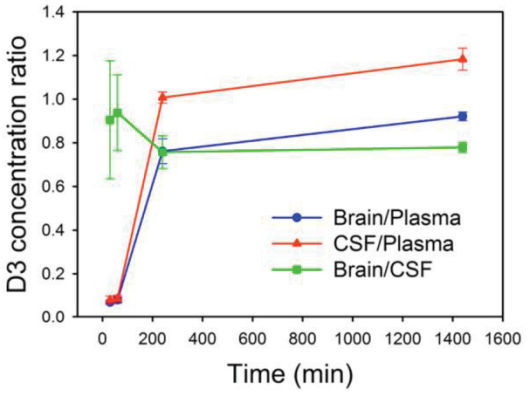

Fig. 3. Temporal development of ^{3}H-D3 concentration ratios after *i.p.* administration in C57Bl/6 mice. Illustrated are the brain/plasma, cerebrospinal fluid (CSF)/plasma, and brain/CSF ratios as the mean value ± SEM (n = 3) at different time points post injection. Following bolus dose administration, low brain/plasma and CSF/plasma ratios were found at the starting time points (about 0.1), whereas the brain/CSF ratio was high with about 0.9. After 4 h, all the ratios reached relative stable values.

3.3. Oral administration of FAM-D3

As demonstrated recently in a pharmacokinetic study, oral administration yielded similar D3 concentrations after 4 h in the brain as *i.p.* and *i.v.* administrations did [7]. Here we used fluorescently labelled D3 for the purpose of direct visualization. After eight weeks of oral administration of 5(6)-carboxyfluorescein labelled D3 (FAM-D3) in an APPswe/PS1ΔE9 transgenic mouse, fluorescence was observed associated with Aβ plaques in brain parenchyma (Fig. 5A). Colocalization of FAM-D3 fluorescence with Aβ aggregates was validated by immunohistochemistry using anti-Aβ antibody (W0-2) based staining on adjacent sections (Fig. 5B and C). Cerebral blood vessels were visualized using an *anti*-glucose transporter GLUT-1 antibody (Fig. 5D). No specific binding of FAM-D3 on cerebral blood vessels was observed (Fig. 5E). An anti-GLUT-1 positive structure was found in the middle of an Aβ deposition, suggesting this plaque was formed around the blood vessel (Fig. 5D and E, white arrows).

3.4. Proteolytic stability of FAM-D3 in comparison to FAM labelled L-enantiomeric peptide

In order to support the interpretation that FAM fluorescence correlates with binding of intact FAM-D3, an *ex vivo* stability test was performed with brain homogenate. The proteolytic stability of D3 peptide within its amino acid sequence has been reported earlier [7]. In this study, the stability of D3 bound to FAM *via* an L-Lys linker was tested additionally. As a control, a 12-mer peptide consisting of L-enantiomeric amino acid residues (LP) coupled to FAM was used. FAM-D3 and FAM-LP were incubated with brain homogenate at 37 °C and applied to thin layer chromatography (TLC) (Fig. 6). Under the same experimental conditions, Rf values of FAM-D3 and FAM-LP were different due to their different amino acid sequences. Most of the FAM-LP was degraded in brain homogenate after 2 h, whereas FAM-D3 was resistant to proteolysis within the same time frame.

4. Discussion

The all-D-enantiomeric peptide D3 contains five arginines out of twelve amino acid residues. Three arginines at the N-terminus and two at C-terminus are separated by single spacing amino acids, respectively. This arginine arrangement in peptide backbone may increase its

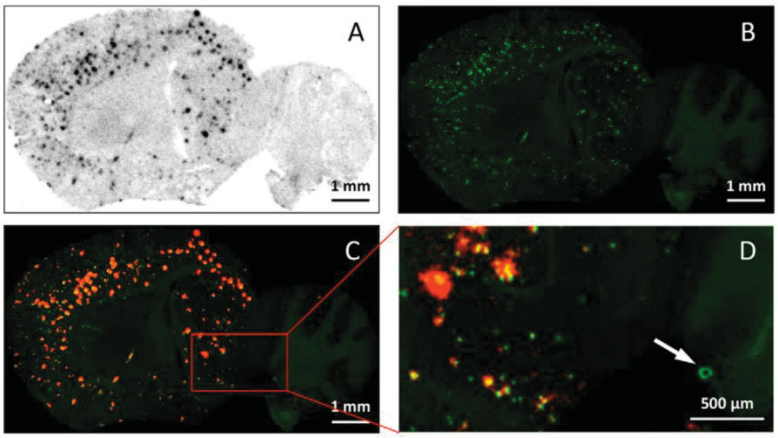

Fig. 4. *In vitro* autoradiography of ^{3}H-D3 on mouse brain cross-sections. (A) Autoradiogram of an APP/PS1 (ARTE 10) transgenic mouse brain section (sagittal) incubated with ^{3}H-D3. A stronger ^{3}H-signal correlates to a higher blackening of the image. (B) Thioflavine S staining for amyloid of section A performed after autoradiography. (C) Merged image based on the fluorescence signal after Thioflavine S staining (green) and autoradiography (converted to red). Yellow indicates colocalization of Thioflavine S and ^{3}H-D3. (D) Merged image with higher magnification. White arrow points to a blood vessel in cerebellum which is not positive for ^{3}H-D3. Other small spots that only showed Thioflavine S positive stain but were no stained by ^{3}H-D3 could be either plaques that were only weakly stained by ^{3}H-D3 or small cerebral blood vessels.

cellular uptake as studies have shown that increase of the distance between arginine residues enhances the uptake of ARMs [57,58]. The arrangement of arginines at the C-terminus may contribute to the overall similarity of D3 to ARM of HIV-1 Tat, which may lead to the ability to penetrate plasma membranes and the BBB. In order to elucidate this observation, further *in vivo* experiments using tritium labelled (^{3}H-D3) and fluorescently labelled (FAM-D3) peptide were carried out.

The systemic administration of ^{3}H-D3 (*i.p.*) led to similar concentrations of radioactivity in CSF, plasma and whole brain after 4 h. As ^{3}H-D3 has been shown to be proteolytically stable, D3 concentrations can be calculated from measured radioactivity and its metabolites can be neglected [7]. Also, temporal distribution of ^{3}H-D3 in the plasma and brain fitted well with recently reported pharmacokinetic data [7]. The fast appearance and constant presence of D3 in the brain suggests direct penetration into brain parenchyma via the blood brain barrier. It must be noted that, as radioactivity from CSF remained in the ventricles or from the blood in the cerebrovasculature, this may have contributed to the radioactivity detected in the whole brain to some extent. But because the CSF space was destroyed during preparation of the brain hemispheres, the amount of remaining CSF in the brain hemisphere was considered negligible. Since we could not detect specific binding of ^{3}H-D3 to cerebral blood vessels in *in vitro* autoradiography, it is unlikely that radioactivity bound to the vessel walls contributed significantly to the amount detected in the whole brain. Furthermore, the cerebral blood volume decreases dramatically in the absence of any cardiac activity once the mouse is euthanized [59]. Derivation of theoretical concentration in intact brain assuming well preserved cerebral blood and CSF volume was also performed. When maximal blood and CSF compartments (using measured plasma and CSF concentrations) were excluded, there was still about half of the concentration left in the brain. Thus, the ^{3}H-D3 concentration detected in the brain likely represents its real concentration in the brain parenchyma and the vascular fraction is negligible.

The amount of ^{3}H-D3 measured up to 4 h post-administration in the brain is 0.14% to 0.21% of the total administered dose, which is clearly above the known bias concentration of 0.10% for BBB permeating agents [60]. Clinically applied CNS drugs consisting of L-polypeptides with proven BBB penetration potential, like Colistin, have CSF/serum ratios in the range of 0.051 to 0.057, or 0.16 [61]. In contrast, the CSF/plasma ratio of D3 started at 0.1 and reached 1.2 after 4 h post-administration, suggesting distribution in brain parenchyma. Even if drug entry into the CSF alone is not a proper measure of BBB permeability [62], CSF concentrations o

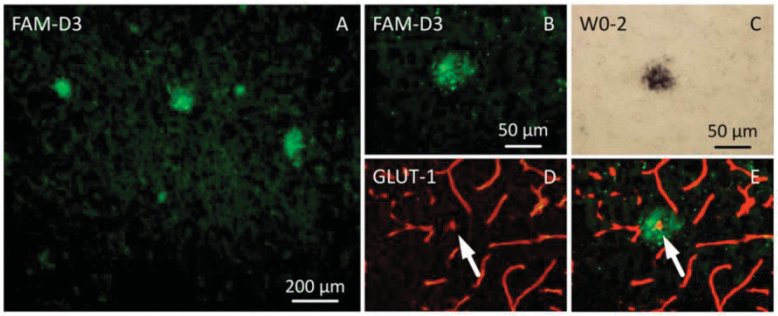

Fig. 5. Colocalization of FAM-D3 and Aβ in APPswe/PS1ΔE9 transgenic mouse brain sections after eight weeks' oral administration of FAM-D3. (A and B) Fluorescence images detecting FAM-D3 in cortex with low-magnification (A) and high-magnification (B), respectively. (C) High-magnification of photomicrograph showing adjacent section of B stained with anti Aβ antibody (W0-2). (D) Microvasculature stained with anti-GLUT-1 antibody on the same section of B. (E) Merged image of B and D. White arrows highlight anti-GLUT-1 positive structure in the center of Aβ aggregate.

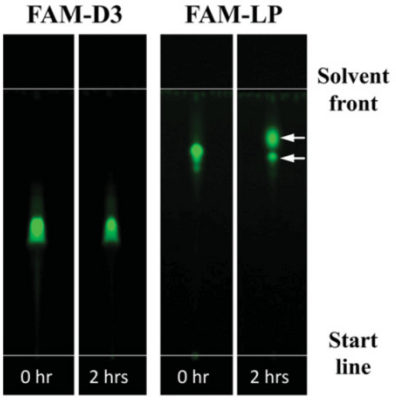

Fig. 6. Comparison of the proteolytic stability of FAM-D3 in comparison to a FAM labelled L-peptide (LP) of similar molecular weight as D3. FAM-D3 and FAM-LP were incubated in brain homogenate at 37 °C for 0 and 2 h and developed on TLC plate. Degradation of FAM-LP but not FAM-D3 is indicated by formation of additional bands and change in intensity and retardation factor (Rf) value (white arrows).

drugs are still considered as discriminating factors of drugs and their bioavailabilities in the CNS, especially for hydrophilic or large molecular weight compounds [63,64].

BBB permeability of D3 was demonstrated and further confirmed by oral administration of FAM labelled D3 in a transgenic AD mouse model. Aβ plaques in the brain were visualized under fluorescent light indicating FAM-D3 entered the brain parenchyma and bound to Aβ plaques. Together with the proteolytic stability test, results showed that D3 was orally active. D3 is selected to specifically bind to Aβ(1–42) [7], which is the major component of parenchymal Aβ, whereas the major Aβ species in cerebral amyloid angiopathy (CAA) is Aβ(1–40) (however, upon aging, more and more Aβ1–42 can be found in CAA) [65,66]. No specific binding of FAM-D3 on cerebral blood vessels was found, which is in accordance with our observations during the study when incubating ^{3}H-D3 with mouse brain sections. We also detected blood vessels in close proximity to Aβ plaques (Fig. 5E), supporting the hypothesis that every plaque seems to be associated with a vessel [67,68].

In our study, BBB penetration of D3 was quantified by measuring its brain concentration after *i.p.* administration (using ^{3}H-D3) and visualized through its binding to Aβ plaques inside the brain (using FAM-D3 and ^{3}H-D3). However, all those methods have their restrictions and thus needed to be validated by each other: D3 concentration in brain was calculated from radioactivity of tritium labelled D3, assuming that ^{3}H-D3 is proteolytically stable as shown previously [7]. Also, we showed that D3 did not bind to the CNS vasculature, which otherwise would have lead us to misinterpreted brain levels (Fig. 4). In addition, labelling with a bulky, hydrophobic 5-FAM lysine molecule adding one extra negative charge to D3 could have an influence on its BBB penetration and Aβ binding. Thus combination of experiments in Figs. 2 and 4 demonstrated that ^{3}H-D3, which preserves the original physical and chemical properties of D3 to the fullest extent, could pass the BBB and bind Aβ plaques.

Re-analysis and interpretation of the data reported previously [7] and in combination with Figs. 2 and 3, suggests that high concentrations of D3 in plasma do not directly translate into similarly high D3 concentrations either in brain or in CSF. After *i.p.* administration the plasma concentration of D3 rises rapidly to reach its maximum before dropping away within the first hours. In contrast, brain concentrations do not follow the same pattern but rise until certain and very stable levels are reached. Similar brain levels could previously be found after *i.v.* and even after *p.o.* administration despite huge differences by the order of several magnitudes in the initial plasma levels after *i.v.*, *i.p.* and *p.o.* administration. Those obviously constant brain levels may suggest that the responsible transport mechanism from plasma into the CNS is kinetically limited and that elevating the plasma concentration dose not directly lead to a proportional increase of brain concentration. This is in perfect agreement with a previous report on the permeability of D3 in an *in vitro* BBB model [43]. On a co-culture of rat brain microvascular endothelial cells and rat astrocytes in a transwell filter system, D3 passed through the *in vitro* BBB model and showed a partially saturated apical-to-basolateral (blood to brain) transport pattern, whereas another D-peptide (qshyrhispaqv) used as a control containing only one arginine did not pass the *in vitro* BBB model. This pattern was further investigated and it was suggested that D3 might be transported *via* adsorptive-mediated transcytosis [43,69].

Arginine-rich HIV-Tat-like peptides were suggested to bind negatively-charged cell membrane embedded molecules such as heparan sulfate and sialinic acid [70–72]. If the cell membrane-permeating property of Tat is independent of cell surface receptor proteins, it is likely that this process is rather dependent on the overall charge density, than on the presence of any specific sequence or secondary structure elements. Thus, the configuration of peptides (chirality) should not be relevant for cell membrane penetration. In the study of Tünnemann et al., D-enantiomeric arginine-rich peptides showed improved ability to cross the cell membrane as compared to their L-enantiomers, which was explained as a result of difference in proteolytic stability [73]. The observed BBB permeability of D3 in the hereby presented *in vivo* study is in agreement with this concept. Tünnemann et al. also investigated the cell penetration ability of oligo-arginines (with 5 to 12 arginine residues) coupled directly to fluorescein or 5,6-carboxytetramethylrhodamine (TAMRA). Their results show that the transduction ability of arginines increase with the number of consecutive residues and the best performance associated with a tolerable toxicity is achieved with 9 and 10 arginines [73]. Other studies reported that not only linear peptides but also branched-chain peptides show efficient transduction with an optimum number of approximately 8 arginines [74,75]. In this study, D3 achieved the *in vivo* BBB permeability through 5 arginine residues almost equally distributed over the whole molecule, which suggests a cation (guanidinium) dependent and sequence/structure related electrostatic interaction of D3. This special feature not only enables protease-resistant D3 to interact with Aβ, but also has advantage over the strategy to add extra arginine-rich peptides to achieve BBB permeability, as more arginine residues are usually accompanied with increased toxicity and production costs [73,76].

Another study showed that arginine-rich peptides are able to directly penetrate the plasma membrane independent of endocytosis [77]. The formation of nonselective pores was also excluded, because simultaneously added fluorophores were not taken up together with the arginine-rich peptides. BBB penetration of D3 might follow a similar mechanism as HIV-Tat assuming the limited transport pattern mentioned above. In fact, no complex transport mechanism is necessary to explain the distribution pattern of D3 in the body. It could be described as a rapid absorption phase from peritoneal cavity into systemic circulation followed by slower passive entry into intracellular compartments of brain and other organs, after which the proteolytically stable D3 remains equilibrated throughout the body. Remarkably, our results showed a relatively constant brain/CSF ratio over all time points, which also indicated a distribution equilibrium of D3 between brain and CSF. The most straight forward explanation would be that this equilibrium, as well as differences in brain/plasma and CSF/plasma ratios may simply reflect reduced distribution to non-aqueous compartments in brain that do not exist in CSF. In addition, this constant brain/CSF ratio might also provide a possibility to monitor D3 concentrations in brain, because CSF sampling can be performed several times or even continuously in living animals.

Taken together, our results strongly suggest that D3 penetrates the blood brain barrier and specifically binds to Aβ plaques after systemic administration. Being orally active, D3 might be a promising drug

candidate for therapeutic intervention in Alzheimer's disease. Additionally, being a middle-sized peptide of synthetic origin, D3 allows easy chemical modifications *e.g.* radiolabelling for early diagnosis of the disease.

Supplementary data to this article can be found online at http://dx.doi.org/10.1016/j.bbamem.2016.07.002.

Conflict of interest

There is no conflict of interest regarding this manuscript.

Author contributions

Conceived and designed the experiments: NJ, DF, TVG, IK, NJS, KJL, DW, AW
Performed the experiments: NJ, ES, TVG, IK
Analysed the data: NJ, TVG, IK, DW, AW
Wrote the paper: NJ, TVG, IK, KJL, DW, AW

Transparency document

The Transparency document associated with this article can be found, in the online version.

Acknowledgements

D.W. was supported by grants from the "Portfolio Technology and Medicine" and the Helmholtz-Validierungsfonds of the Impuls und Vernetzungs-Fonds der Helmholtzgemeinschaft; K.J.L. and D.W. were supported by the "Portfolio Drug Design" of the Impuls und Vernetzungs-Fonds der Helmholtzgemeinschaft. We thank Ashish Kumar and Monique Dozier-Sharpe for the excellent technical assistance.

References

[1] D.J. Craik, D.P. Fairlie, S. Liras, D. Price, The future of peptide-based drugs, Chem. Biol. Drug Des. 81 (2013) 136–147.
[2] C.A. Lipinski, F. Lombardo, B.W. Dominy, P.J. Feeney, Experimental and computational approaches to estimate solubility and permeability in drug discovery and development settings, Adv. Drug Deliv. Rev. 64 (2012) 4–17.
[3] J.L. Mikitsh, A.M. Chacko, Pathways for small molecule delivery to the central nervous system across the blood-brain barrier, Perspect. Med. Chem. 6 (2014) 11–24.
[4] M.T. Weinstock, J.N. Francis, J.S. Redman, M.S. Kay, Protease-resistant peptide design-empowering nature's fragile warriors against HIV, Biopolymers 98 (2012) 431–442.
[5] Watching peptide drugs grow up, Chem. Eng. News Arch. 83 (2005) 17–24.
[6] D. Goodwin, P. Simerska, I. Toth, Peptides as therapeutics with enhanced bioactivity, Curr. Med. Chem. 19 (2012) 4451–4461.
[7] N. Jiang, L.H.E. Leithold, J. Post, T. Ziehm, J. Mauler, et al., Preclinical pharmacokinetic studies of the tritium labelled D-enantiomeric peptide D3 developed for the treatment of Alzheimer's disease, PLoS One 10 (2015), e0128553.
[8] L. Leithold, N. Jiang, J. Post, T. Ziehm, J. Kutzsche, et al., Pharmacokinetic properties of a novel D-peptide developed to be therapeutically active against toxic β-amyloid oligomers, Pharm. Res. (2015).
[9] P. Chong, C. Sia, B. Tripet, O. James, M. Klein, Comparative immunological properties of enantiomeric peptides, Lett. Pept. Sci. 3 (1996) 99–106.
[10] B.V. Zlokovic, M.B. Segal, D.J. Begley, H. Davson, L. Rakic, Permeability of the blood cerebrospinal-fluid and blood-brain barriers to thyrotropin-releasing-hormone, Brain Res. 358 (1985) 191–199.
[11] B.V. Zlokovic, D.J. Begley, D.G. Chaineliash, Blood-brain barrier permeability to leucine-enkephalin, D-Alanine2-D-Leucine5-enkephalin and their N-terminal amino-acid (tyrosine), Brain Res. 336 (1985) 125–132.
[12] A. Lalatsa, V. Lee, J.P. Malkinson, M. Zloh, A.G. Schatzlein, et al., A prodrug nanoparticle approach for the oral delivery of a hydrophilic peptide, leucine(5)-enkephalin, to the brain, Mol. Pharm. 9 (2012) 1665–1680.
[13] W.M. Pardridge, CNS drug design based on principles of blood-brain barrier transport, J. Neurochem. 70 (1998) 1781–1792.
[14] W.M. Pardridge, Drug targeting to the brain, Pharm. Res. 24 (2007) 1733–1744.
[15] B.V. Zlokovic, S. Hyman, J.G. Mccomb, M.N. Lipovac, G. Tang, et al., Kinetics of arginine-vasopressin uptake at the blood-brain-barrier, Biochim. Biophys. Acta 1025 (1990) 191–198.
[16] B.V. Zlokovic, R. Deane, A.P. Sagare, R.D. Bell, E.A. Winkler, Low-density lipoprotein receptor-related protein-1: a serial clearance homeostatic mechanism controlling Alzheimer's amyloid beta-peptide elimination from the brain, J. Neurochem. 115 (2010) 1077–1089.
[17] J.A. Vazquez, M. Raghunath, S.A. Adibi, Uptake and hydrolysis of Glycylglutamine a the blood-brain-barrier, Metab. Clin. Exp. 41 (1992) 121–124.
[18] E. Vives, P. Brodin, B. Lebleu, A truncated HIV-1 Tat protein basic domain rapidly translocates through the plasma membrane and accumulates in the cell nucleus, J Biol. Chem. 272 (1997) 16010–16017.
[19] H. Brooks, B. Lebleu, E. Vives, Tat peptide-mediated cellular delivery: back to basics Adv. Drug Deliv. Rev. 57 (2005) 559–577.
[20] F. Salomone, F. Cardarelli, M. Di Luca, C. Boccardi, R. Nifosi, et al., A novel chimeri cell-penetrating peptide with membrane-disruptive properties for efficien endosomal escape, J. Control. Release 163 (2012) 293–303.
[21] M. Zeitler, J.P. Steringer, H.M. Muller, M.P. Mayer, W. Nickel, HIV-Tat form phosphoinositide dependent membrane pores implicated in unconventional protein secretion, J. Biol. Chem. (2015).
[22] T.H. Tahirov, N.D. Babayeva, K. Varzavand, J.J. Cooper, S.C. Sedore, et al., Crystal structure of HIV-1 Tat complexed with human P-TEFb, Nature 465 (2010) 747–751.
[23] M.J. Seewald, A.U. Metzger, D. Willbold, P. Rosch, H. Sticht, Structural model of the HIV-1 Tat(46-58)-TAR complex, J. Biomol. Struct. Dyn. 16 (1998) 683–692.
[24] A.U. Metzger, T. Schindler, D. Willbold, M. Kraft, C. Steegborn, et al., Structural rearrangements on HIV-1 Tat (32-72) TAR complex formation, FEBS Lett. 384 (1996) 255–259.
[25] D. Willbold, R. Rosin-Arbesfeld, H. Sticht, R. Frank, P. Rosch, Structure of the equine infectious anemia virus Tat protein, Science 264 (1994) 1584–1587.
[26] P. Bayer, M. Kraft, A. Ejchart, M. Westendorp, R. Frank, et al., Structural studies of HIV-1 Tat protein, J. Mol. Biol. 247 (1995) 529–535.
[27] D. Sun, J. Forsman, M. Lund, C.E. Woodward, Effect of arginine-rich cell penetrating peptides on membrane pore formation and life-times: a molecular simulation study Phys. Chem. Chem. Phys. 16 (2014) 20785–20795.
[28] J.B. Rothbard, T.C. Jessop, R.S. Lewis, B.A. Murray, P.A. Wender, Role of membrane potential and hydrogen bonding in the mechanism of translocation of guanidinium-rich peptides into cells, J. Am. Chem. Soc. 126 (2004) 9506–9507.
[29] I. Nakase, T. Takeuchi, G. Tanaka, S. Futaki, Methodological and cellular aspects that govern the internalization mechanisms of arginine-rich cell-penetrating peptides Adv. Drug Deliv. Rev. 60 (2008) 598–607.
[30] D.J. Mitchell, D.T. Kim, L. Steinman, C.G. Fathman, J.B. Rothbard, Polyarginine enter cells more efficiently than other polycationic homopolymers, J. Pept. Res. 56 (2000) 318–325.
[31] P.A. Wender, D.J. Mitchell, K. Pattabiraman, E.T. Pelkey, L. Steinman, et al., The design, synthesis, and evaluation of molecules that enable or enhance cellular uptake Peptoid molecular transporters, Proc. Natl. Acad. Sci. U. S. A. 97 (2000) 13003–13008.
[32] D. Derossi, S. Calvet, A. Trembleau, A. Brunissen, G. Chassaing, et al., Cell internalization of the third helix of the antennapedia homeodomain is receptor-independent, J Biol. Chem. 271 (1996) 18188–18193.
[33] M. Rizzuti, M. Nizzardo, C. Zanetta, A. Ramirez, S. Corti, Therapeutic applications of the cell-penetrating HIV-1 Tat peptide, Drug Discov. Today 20 (2015) 76–85.
[34] T.N.M. Schumacher, L.M. Mayr, D.L. Minor, M.A. Milhollen, M.W. Burgess, et al., Identification of D-peptide ligands through mirror-image phage display, Science 271 (1996) 1854–1857.
[35] K. Wiesehan, D. Willbold, Mirror-image phage display: aiming at the mirror Chembiochem 4 (2003) 811–815.
[36] S.A. Funke, T. van Groen, I. Kadish, D. Bartnik, L. Nagel-Steger, et al., Oral treatment with the D-enantiomeric peptide D3 improves the pathology and behavior of Alzheimer's disease transgenic mice, ACS Chem. Neurosci. 1 (2010) 639–648.
[37] T. van Groen, K. Wiesehann, S.A. Funke, I. Kadish, L. Nagel-Steger, et al., Reduction of Alzheimer's disease amyloid plaque load in transgenic mice by D3, a D-enantiomeric peptide identified by mirror image phage display, ChemMedChem 3 (2008) 1848–1852.
[38] T. van Groen, I. Kadish, K. Wiesehan, S.A. Funke, D. Willbold, In vitro and in vivo staining characteristics of small, fluorescent, Abeta42-binding D-enantiomeric peptides in transgenic AD mouse models, ChemMedChem 4 (2009) 276–282.
[39] T. van Groen, I. Kadish, S.A. Funke, D. Bartnik, D. Willbold, Treatment with D3 removes amyloid deposits, reduces inflammation, and improves cognition in aged AbetaPP/PS1 double transgenic mice, J. Alzheimers Dis. 34 (2013) 609–620.
[40] T. van Groen, I. Kadish, A. Funke, D. Bartnik, D. Willbold, Treatment with Abeta42 binding D-amino acid peptides reduce amyloid deposition and inflammation in APP/PS1 double transgenic mice, Adv. Protein Chem. Struc. Biol. 88 (2012) 133–152
[41] S. Aileen Funke, T. van Groen, I. Kadish, D. Bartnik, L. Nagel-Steger, et al., Oral treatment with the d-enantiomeric peptide D3 improves the pathology and behavior of Alzheimer's disease transgenic mice, ACS Chem. Neurosci. 1 (2010) 639–648.
[42] T. van Groen, K. Wiesehan, S.A. Funke, I. Kadish, L. Nagel-Steger, et al., Reduction of Alzheimer's disease amyloid plaque load in transgenic mice by D3, a D-enantiomeric peptide identified by mirror image phage display, ChemMedChem 3 (2008) 1848–1852.
[43] H.M. Liu, S.A. Funke, D. Willbold, Transport of Alzheimer disease amyloid-beta-binding D-amino acid peptides across an in vitro blood-brain barrier model, Rejuvenation Res. 13 (2010) 210–213.
[44] A.G. Fisher, E. Collalti, L. Ratner, R.C. Gallo, F. Wong-Staal, A molecular clone of HTLV III with biological activity, Nature 316 (1985) 262–265.
[45] B. Korber, B. Gaschen, K. Yusim, R. Thakallapally, C. Kesmir, et al., Evolutionary and immunological implications of contemporary HIV-1 variation, Br. Med. Bull. 58 (2001) 19–42.
[46] B.H. Hahn, G.M. Shaw, S.K. Arya, M. Popovic, R.C. Gallo, et al., Molecular cloning and characterization of the HTLV-III virus associated with AIDS, Nature 312 (1984) 166–169.

[47] J.L. Jankowsky, D.J. Fadale, J. Anderson, G.M. Xu, V. Gonzales, et al., Mutant presenilins specifically elevate the levels of the 42 residue beta-amyloid peptide in vivo: evidence for augmentation of a 42-specific gamma secretase, Hum. Mol. Genet. 13 (2004) 159–170.
[48] T. Malm, J. Koistinaho, K. Kanninen, Utilization of APPswe/PS1dE9 transgenic mice in research of Alzheimer's disease: focus on Gene therapy and cell-based therapy applications, Int. J. Alzheimers Dis. 2011 (2011) 517160.
[49] M. Garcia-Alloza, E.M. Robbins, S.X. Zhang-Nunes, S.M. Purcell, R.A. Betensky, et al., Characterization of amyloid deposition in the APPswe/PS1dE9 mouse model of Alzheimer disease, Neurobiol. Dis. 24 (2006) 516–524.
[50] C. Kilkenny, W.J. Browne, I.C. Cuthill, M. Emerson, D.G. Altman, Improving bioscience research reporting: the ARRIVE guidelines for reporting animal research, PLoS Biol. 8 (2010).
[51] L. Liu, K. Duff, A technique for serial collection of cerebrospinal fluid from the cisterna magna in mouse, J. Vis. Exp. (2008).
[52] A. Willuweit, J. Velden, R. Godemann, A. Manook, F. Jetzek, et al., Early-onset and robust amyloid pathology in a new homozygous mouse model of Alzheimer's disease, PLoS One 4 (2009).
[53] V. Vergote, S. Van Dorpe, K. Peremans, C. Burvenich, B. De Spiegeleer, In vitro metabolic stability of obestatin: kinetics and identification of cleavage products, Peptides 29 (2008) 1740–1748.
[54] S. Stalmans, N. Bracke, E. Wynendaele, B. Gevaert, K. Peremans, et al., Cell-penetrating peptides selectively cross the blood-brain barrier in vivo, PLoS One 10 (2015), e0139652.
[55] A. Manook, B.H. Yousefi, A. Willuweit, S. Platzer, S. Reder, et al., Small-animal PET imaging of amyloid-beta plaques with [11C]PiB and its multi-modal validation in an APP/PS1 mouse model of Alzheimer's disease, PLoS One 7 (2012), e31310.
[56] A. Sun, X.V. Nguyen, G. Bing, Comparative analysis of an improved thioflavin-s stain, Gallyas silver stain, and immunohistochemistry for neurofibrillary tangle demonstration on the same sections, J. Histochem. Cytochem. 50 (2002) 463–472.
[57] J.B. Rothbard, E. Kreider, C.L. VanDeusen, L. Wright, B.L. Wylie, et al., Arginine-rich molecular transporters for drug delivery: role of backbone spacing in cellular uptake, J. Med. Chem. 45 (2002) 3612–3618.
[58] G. Lattig-Tunnemann, M. Prinz, D. Hoffmann, J. Behlke, C. Palm-Apergi, et al., Backbone rigidity and static presentation of guanidinium groups increases cellular uptake of arginine-rich cell-penetrating peptides, Nat. Commun. 2 (2011) 453.
[59] A.J. de Crespigny, J. Rother, C. Beaulieu, T. Neumann-Haefelin, M.E. Moseley, Comparison of diffusion, blood oxygenation, and blood volume changes during global ischemia in rats, Magn. Reson. Med. 45 (2001) 10–16.
[60] A. Lalatsa, A.G. Schatzlein, I.F. Uchegbu, Strategies to deliver peptide drugs to the brain, Mol. Pharm. 11 (2014) 1081–1093.
[61] R. Nau, F. Sorgel, H. Eiffert, Penetration of drugs through the blood-cerebrospinal fluid/blood-brain barrier for treatment of central nervous system infections, Clin. Microbiol. Rev. 23 (2010) (858−+).
[62] W.M. Pardridge, Drug transport in brain via the cerebrospinal fluid, Fluids Barriers CNS, 8, 2011, p. 7.
[63] D.D. Shen, A.A. Artru, K.K. Adkison, Principles and applicability of CSF sampling for the assessment of CNS drug delivery and pharmacodynamics, Adv. Drug Deliv. Rev. 56 (2004) 1825–1857.
[64] J.H. Lin, CSF as a surrogate for assessing CNS exposure: an industrial perspective, Curr. Drug Metab. 9 (2008) 46–59.
[65] C.L. Joachim, L.K. Duffy, J.H. Morris, D.J. Selkoe, Protein chemical and immunocytochemical studies of meningovascular beta-amyloid protein in Alzheimer's disease and normal aging, Brain Res. 474 (1988) 100–111.
[66] F. Prelli, E. Castano, G.G. Glenner, B. Frangione, Differences between vascular and plaque core amyloid in Alzheimers-disease, J. Neurochem. 51 (1988) 648–651.
[67] C. Humpel, Organotypic vibrosections from whole brain adult Alzheimer mice (overexpressing amyloid-precursor-protein with the Swedish-Dutch-Iowa mutations) as a model to study clearance of beta-amyloid plaques, Front. Aging Neurosci. 7 (2015) 47.
[68] L. Bouman, Über die entwicklung der senilen plaques, Zeitschrift für Die Gesamte Neurologie Und Psychiatrie, 94, 1925, pp. 267–274.
[69] B.V. Zlokovic, Cerebrovascular permeability to peptides - manipulations of transport-Systems at the Blood-Brain-Barrier, Pharm. Res. 12 (1995) 1395–1406.
[70] P. Chiodelli, C. Urbinati, S. Mitola, E. Tanghetti, M. Rusnati, Sialic acid associated with alphavbeta3 integrin mediates HIV-1 Tat protein interaction and endothelial cell proangiogenic activation, J. Biol. Chem. 287 (2012) 20456–20466.
[71] M. Tyagi, M. Rusnati, M. Presta, M. Giacca, Internalization of HIV-1 tat requires cell surface heparan sulfate proteoglycans, J. Biol. Chem. 276 (2001) 3254–3261.
[72] C. Urbinati, S. Nicoli, M. Giacca, G. David, S. Fiorentini, et al., HIV-1 Tat and heparan sulfate proteoglycan interaction: a novel mechanism of lymphocyte adhesion and migration across the endothelium, Blood 114 (2009) 3335–3342.
[73] G. Tunnemann, G. Ter-Avetisyan, R.M. Martin, M. Stockl, A. Herrmann, et al., Live-cell analysis of cell penetration ability and toxicity of oligo-arginines, J. Pept. Sci. 14 (2008) 469–476.
[74] S. Futaki, S. Goto, Y. Sugiura, Membrane permeability commonly shared among arginine-rich peptides, J. Mol. Recognit. 16 (2003) 260–264.
[75] T. Suzuki, S. Futaki, M. Niwa, S. Tanaka, K. Ueda, et al., Possible existence of common internalization mechanisms among arginine-rich peptides, J. Biol. Chem. 277 (2002) 2437–2443.
[76] S.W. Jones, R. Christison, K. Bundell, C.J. Voyce, S.M. Brockbank, et al., Characterisation of cell-penetrating peptide-mediated peptide delivery, Br. J. Pharmacol. 145 (2005) 1093–1102.
[77] G. Ter-Avetisyan, G. Tunnemann, D. Nowak, M. Nitschke, A. Herrmann, et al., Cell entry of arginine-rich peptides is independent of endocytosis, J. Biol. Chem. 284 (2009) 3370–3378.

3.5 The Aβ oligomer eliminating D-enantiomeric peptide RD2 improves cognition without changing plaque pathology

Autoren:	van Groen T, Schemmert S, Brener O, Gremer L, Ziehm T, Tusche M, Nagel-Steger L, Kadish I, **Schartmann E**, Elfgen A, Juergens D, Willuweit A, Kutzsche J, Willbold D
Journal:	Scientific Reports
	veröffentlicht am 24.11.2017
DOI:	10.1038/s41598-017-16565-1
Impact Factor:	4,259 (2016)
Beitrag:	Beteiligung an der Diskussion und Formulierung der Ergebnisse
	Prüfung des Manuskripts

www.nature.com/scientificreports

SCIENTIFIC REPORTS

OPEN

The Aβ oligomer eliminating D-enantiomeric peptide RD2 improves cognition without changing plaque pathology

Received: 18 July 2017
Accepted: 15 November 2017
Published online: 24 November 2017

Thomas van Groen[1], Sarah Schemmert[2], Oleksandr Brener[2,3], Lothar Gremer[2,3], Tamar Ziehm[2], Markus Tusche[2], Luitgard Nagel-Steger[2,3], Inga Kadish[1], Elena Schartmann[2], Anne Elfgen[2], Dagmar Jürgens[2], Antje Willuweit[4], Janine Kutzsche[2] & Dieter Willbold[2,3]

While amyloid-β protein (Aβ) aggregation into insoluble plaques is one of the pathological hallmarks of Alzheimer's disease (AD), soluble oligomeric Aβ has been hypothesized to be responsible for synapse damage, neurodegeneration, learning, and memory deficits in AD. Here, we investigate the *in vitro* and *in vivo* efficacy of the D-enantiomeric peptide RD2, a rationally designed derivative of the previously described lead compound D3, which has been developed to efficiently eliminate toxic Aβ42 oligomers as a promising treatment strategy for AD. Besides the detailed *in vitro* characterization of RD2, we also report the results of a treatment study of APP/PS1 mice with RD2. After 28 days of treatment we observed enhancement of cognition and learning behaviour. Analysis on brain plaque load did not reveal significant changes, but a significant reduction of insoluble Aβ42. Our findings demonstrate that RD2 was significantly more efficient in Aβ oligomer elimination *in vitro* compared to D3. Enhanced cognition without reduction of plaque pathology in parallel suggests that synaptic malfunction due to Aβ oligomers rather than plaque pathology is decisive for disease development and progression. Thus, Aβ oligomer elimination by RD2 treatment may be also beneficial for AD patients.

Alzheimer's disease (AD) is the most common form of dementia in the elderly[1]. The main characteristic pathological hallmarks of AD are neurodegeneration, neurofibrillary tangles (NFTs), and neuritic plaques in the brain[2]. Intracellular neurofibrillary tangles consist of hyperphosphorylated, twisted filaments of the cytoskeletal protein tau, whereas extracellular plaques are primarily made up of amyloid-β (Aβ)[3], a 39 to 43 amino acid long peptide derived from the proteolytic processing of the amyloid protein precursor (APP)[4]. When APP is cleaved by β- and γ-secretases, the resulting breakdown product is Aβ[5].

Most cases of AD are sporadic, while a small percentage of AD cases are familial[6,7]. These cases are related to mutations in the genes coding for APP, presenilin 1 and 2 (PS1 and PS2)[7]. In general, the mutations influence APP metabolism such that the ratio of Aβ42/Aβ40 is often shifted to higher values[8,9]. Further, it has been shown that duplication of the APP gene[10,11] also results in early AD. Finally, a recent study has demonstrated that a novel mutation in the APP gene protects against the development of AD[12]. Together, these findings imply a central role for APP and its processing for the pathological changes occurring during AD[13,14].

The original amyloid cascade hypothesis[15] postulated that overproduction of Aβ would lead to Aβ deposition in neuritic plaques, which were supposed to be the cause of cognitive deficits. Nowadays, it is thought that soluble Aβ oligomers are the main etiologic agent for pathology and cognitive decline in AD[16–18]. The Aβ oligomers are hypothesized to cause a series of molecular events centring on disrupting the maintenance of synapse structure and function and thus leading to dysfunctional synapses, which are associated with memory loss[19,20].

[1]Department of Cell, Developmental and Integrative Biology, University of Alabama at Birmingham, Birmingham, AL, 35294, USA. [2]Institute of Complex Systems (ICS-6), Structural Biochemistry, Forschungszentrum Jülich GmbH, 52425, Jülich, Germany. [3]Institut für Physikalische Biologie, Heinrich-Heine-Universität Düsseldorf, 40225, Düsseldorf, Germany. [4]Institute of Neuroscience and Medicine (INM-4), Medical Imaging Physics, Forschungszentrum Jülich GmbH, 52425, Jülich, Germany. Correspondence and requests for materials should be addressed to T.G. (email: vangroen@uab.edu) or D.W. (email: d.willbold@fz-juelich.de)

Nowadays, the inhibition of the formation of Aβ oligomers and the elimination of already present Aβ oligomers is thought to be one of the most promising strategies to modify disease progression according to the modified amyloid cascade hypothesis. Currently registered drugs can only ameliorate symptoms and cannot slow down disease progression. Previously, we have reported about a D-enantiomeric peptide, named "D3", which was identified by mirror image phage display and solely consists of D-enantiomeric amino acid residues[21,22]. D3 inhibits the formation of regular Aβ fibrils, eliminates directly and specifically Aβ oligomers and reduces Aβ cytotoxicity *in vitro*[23,24]. *In vivo*, D3 binds to amyloid plaques[25], reduces Aβ plaque load, decreases inflammation and enhances cognition in various transgenic AD mouse models even after oral administration[24,26–28]. In order to enhance D3's potential to remove Aβ oligomers, we have used systematic approaches to identify derivatives with increased Aβ monomer binding activity and increased Aβ oligomer elimination properties[23,29–31]. In parallel, we also tried an additional rational approach to identify more efficient derivatives of D3 and learn more about important sequence motifs. We have identified a compound within this rational design series by the rearrangement of the amino acid residue sequence that showed very promising properties, termed "RD2" (abbreviation for "rational design 2"). In previous studies, we examined the pharmacokinetic characteristics of D3 and RD2[32,33]. These analyses have revealed a higher bioavailability of RD2 compared to D3, indicating improved pharmacokinetic characteristics.

In this study, we examined the *in vitro* profile of RD2 by various analyses to prove our hypothesis whether the rational design enhances the potential of our compound to remove Aβ oligomers. Moreover, we intraperitoneally treated APP/PS1 transgenic mice for only 28 days with RD2 compared to placebo and examined the treatment's influence on cognitive deficits at the end of the treatment period.

Material and Methods

Ethics statement. All experiments were carried out in compliance with the USPHS Guide for Care and Use of Laboratory Animals and approved by the Institutional Animal Care and Use Committee (IACUC; approval number 09457).

Peptides. The compounds D3 (rprtrlhthrnr) and RD2 (ptlhthnrrrrr) with amidated C-termini were purchased as lyophilized powder with >95% purity from JPT Peptide Technologies (JPT, Germany) and Cambridge peptides (Cambridge peptides, United Kingdom), respectively.

Synthetic and recombinant Aβ(1-42) with >95% purity was purchased as lyophilized powder from Bachem (Germany) and Isoloid (Germany), respectively. Biotinylated Aβ(1-42) was also purchased from Bachem (Germany).

Preparation of Aβ(1-42) stock solutions. Lyophilized Aβ(1-42) was dissolved overnight in HFIP (1,1,1,3,3,3-hexafluoro-2-propanol, Sigma-Aldrich, Germany). Aliquots were stored at −20 °C until further processing. Before usage, Aβ(1-42) was lyophilized and dissolved in 10 mM sodium phosphate buffer, pH 7.4.

Surface plasmon resonance measurements. The dissociation constants (K_D) of the compounds binding to Aβ(1-42) were determined by surface plasmon resonance (SPR) measurements using a T200 device (Biacore, GE Healthcare, Sweden). Because of the aggregation tendency of Aβ, especially under the binding assay conditions at neutral pH, Aβ was used solely as a ligand rather than as an analyte. Also, in order to avoid blockage of the microfluidic channels of the SPR device, we have refrained from using larger Aβ assemblies or fibrils as ligands or analytes. Immobilization was performed as described by Frenzel *et al.*[34] with minor modifications. 8 µM N-terminally biotinylated Aβ(1-42) was dissolved in 10 mM sodium phosphate buffer and monomers were separated via density gradient centrifugation as described in the QIAD section. The gradient was fractionated into 14 fractions à 140 µl. Aβ(1-42) monomers from fraction 1 were directly immobilized onto a series S sensor chip SA (Biacore, GE Healthcare, Sweden) by biotin-streptavidin coupling to a final level of 600 RU. The ligand flow cell and a reference flow cell were quenched with 10 µg/ml biotin for 7 min. For affinity determination of RD2 and D3, single cycle kinetic experiments were applied at 25 °C and 30 µl/min flow rate. 0.6 µM, 1.9 µM, 5.6 µM, 16.7 µM, and 50 µM of RD2 or D3 were diluted in 20 mM sodium phosphate buffer including 50 mM sodium chloride, pH 7.4 and injected over the flow cells for 180 s. The reference flow cell and buffer cycles were used for double referencing of the sensorgrams. For evaluation, the sensorgrams were fitted applying the steady state Langmuir 1:1 fit model of the Biacore T200 Evaluation Software 2.0 and the offset was constantly set to zero.

Quantitative determination of interference with Aβ aggregate size distribution (QIAD). For the evaluation of Aβ oligomer elimination of RD2, a QIAD assay (quantitative determination of interference with Aβ aggregate size distribution) was performed according to Brener *et al.*[23]. Briefly, 80 µM Aβ(1-42) was pre-incubated for 4.5 h to enrich Aβ oligomers. Then either RD2 or D3 were added to the pre-incubated solution with the resulting concentration of 20 µM RD2 or D3 and co-incubated for further 40 min. The samples were loaded on top of a density gradient containing 5 to 50% (w/v) iodixanol (OptiPrep, Axis-Shield, Norway) and centrifuged for 3 h at 4 °C and 259.000 × g (Optima TL-100, Beckman Coulter, USA). After centrifugation, 14 fractions à 140 µl were harvested by upward displacement. Fraction 1 from the top of the gradient was the least dense fraction while fraction 14 from just above the bottom was the densest fraction. The pellet of each tube was mixed with 60 µl of a 6 M guanidine hydrochloride solution and boiled for 10 min. The resulting solution represents fraction 15. All fractions were analysed with respect to their Aβ(1-42) content by analytical RP-HPLC (reversed phase-high performance liquid chromatography) and UV absorbance detection at 214 nm. The data for the D3 values and the Aβ(1-42) controls without compounds were already previously used in Brener *et al.*[23]. Analyses were done at least in quadruplicates (D3 and RD2 n = 4, Aβ(1-42) n = 11).

In a second experiment we investigated, whether RD2 eliminates Aβ(1-42) oligomers in a dose-dependent manner. Therefore, the QIAD assay was performed with minor modifications. Instead of 15 single fractions the

fractions 1 to 3, 4 to 6, 7 to 9, 10 to 11 and 12 to 14 have been pooled resulting in a total of six fractions. RD2 was added to 80 µM Aβ(1-42) after the 4.5 h incubation step at 1 µM, 5 µM, 10 µM, 20 µM, 30 µM, and 40 µM final concentrations. As described already above for the QIAD, the resulting mixtures were incubated for further 40 min before being applied to density gradient centrifugation. The half-maximal inhibitory concentration (IC_{50}) resulted from the compound concentration at the inflection point obtained by a logistic fit of the data (OriginPro 8.5 G, OriginLab, USA) obtained for fraction 2 (pooled fractions 4 to 6 of the above described QIAD), which contains the pooled oligomers of interest. The experiment has been performed in triplicate (n = 3).

Thioflavin T assay. The Thioflavin T (ThT) assay is a commonly used assay to visualize and quantify the fibrilisation of Aβ, since this dye binds to amyloidogenic cross-β-sheet structures. While Aβ aggregates into fibrils, the ThT fluorescence intensities increase until a saturation level is accomplished. Within this test, we analysed the inhibitory function of RD2 on the Aβ(1-42) fibril formation. 20 µM Aβ(1-42) was incubated with 5 µM ThT and different concentrations of RD2 (serial dilution from 80 µM till 1.25 µM) for IC_{50} calculation. ThT fluorescence was monitored over 21 h every 5 min at $\lambda_{ex} = 440$ nm and $\lambda_{em} = 490$ nm in a fluorescence plate reader (Polarstar Optima, Germany) at 37 °C. Correction was done using all supplements without Aβ. For data evaluation, the fibril masses were determined by subtracting the baseline fluorescence intensities from the top and normalised to the Aβ control to calculate the inhibition in percent. The IC_{50} resulted from the compound concentration at the inflection point obtained by a logistic fit of the data (OriginPro 8.5 G, OriginLab, USA).

Seeding assay. A seeding assay with RD2 was performed to investigate whether RD2 can inhibit the potential of preformed Aβ(1-42) seeds to accelerate the aggregation of monomeric Aβ(1-42). The seeds were prepared by incubating 200 µM monomeric Aβ(1-42) in 10 mM sodium phosphate buffer, pH 7.4, for three days at 37 °C with slight shaking. Afterwards, the sample was centrifuged at 14,000 × g at 4 °C for 45 min. The supernatant was discarded and the loose pellet, which contained the insoluble fibrils, was resuspended in buffer. The sample was sonicated for 2 min in an ultrasonic bath to disperse large Aβ aggregates. The concentration of Aβ seeds according to the monomers was determined by RP-HPLC[23]. The seeds were incubated with or without RD2 in a molar ratio of 1:1 for 24 h at 37 °C with slight shaking. The samples were sonicated again for 2 min. Lyophyllised monomeric Aβ(1-42) was dissolved at a concentration of 15 µM in buffer immediately before the measurement and was mixed with 1.9 µM seeds (molar ratio of 8:1 monomers:seeds) or 1.9 µM seed-RD2-mix (molar ratio of 8:1:1 of monomers:seeds:RD2). As a control, monomeric Aβ without seeds was used. Every sample was mixed with 20 µM ThT to monitor Aβ aggregation. The ThT fluorescence was monitored for 24 h at 24 °C. Samples were measured in triplicate. The resulting ThT fluorescence intensities were fitted with 5-parametrical logistic fits and the amplitude as well as the half-life was calculated in each case. The amplitude of the fluorescence intensities of the Aβ aggregation alone was set to 100% and the amplitude of the seeded Aβ aggregation with and without RD2 was normalised to it. The measurements were performed in three independent experiments (n = 9).

Cell viability assay (MTT test). MTT (3-(4,5-Dimethylthiazol-2-yl)-2,5-diphenyl-tetrazolium bromide) based cell viability assays were accomplished to examine the cytotoxicity of Aβ(1-42) in the presence of RD2 on two different cell lines, PC-12 (rat pheochromocytoma cell line), and SH-SY5Y (human neuroblastoma cell line) cells[35].

PC-12 cells (DSMZ, Germany) were cultured in DMEM medium supplemented with 10% fetal calf serum, 1% antibiotics (Penicillin/Streptomycin) (all Sigma-Aldrich, USA), and 5% horse serum (PAA Laboratories GmbH, Germany) on collagen A-coated (Biochrom GmbH, Germany) tissue culture flasks (SPL Life Sciences Co., Korea). SH-SY5Y cells (DSMZ, Germany) were cultured in DMEM medium supplemented with 20% fetal calf serum and 1% antibiotics (Penicillin/Streptomycin) (all Sigma-Aldrich, USA) on tissue culture flasks (SPL Life Sciences Co., Korea). Cells were allowed to grow in a humidified incubator with 5% CO_2 at 37 °C and a maximum of 12 (PC-12 cells) or 21 (SH-SY5Y cells) passages. Medium was changed every two days and cells were passaged every three to five days, according to their confluence.

MTT test was performed according to the manufacturer's protocol (CellProliferation Kit I; Roche, Switzerland). PC-12 or SHSY-5Y cells were seeded in clear, collagen-coated 96-well flat bottom microwell plates (Life Technologies Inc., USA) at a density of 1×10^4 cells in a volume of 100 µl per well and incubated for 24 h. For both cell lines, compounds were prepared in the following way as a fivefold determination in three independent experiments. 51 µM Aβ(1-42) was incubated for 4.5 h at 37 °C shaking at 600 rpm. Afterwards, 255 µM RD2 was added and incubated for another 40 min. Throughout the test, cells were exposed to 1 µM Aβ with or without 5 µM RD2. The arithmetic mean of all measurements per approach was calculated. Results are represented as the percentage of MTT reduction, assuming that the absorbance of control cells was 100%.

Animals. For this study, 21 APP/PS1 double transgenic mice (APPSwedish/PS1ΔE9)[36] were used. The very well characterized APP/PS1 mouse model develops cognition deficits and abundant Aβ deposits already at early age. The original mice were purchased from JAX (The Jackson Laboratory, USA) and maintained in our own colony at the University of Alabama in Birmingham. Before treatment, the mice were housed in a controlled environment (humidity 50–60%, temperature 22 °C, light from 06:00 a.m. to 6:00 p.m.) with 4 animals per cage in our facility with food and water available *ad libitum*. After the implantation of the Alzet minipumps the mice were housed individually.

Treatment of APP/PS1 mice. In this study, we treated seven months old female APP/PS1 mice intraperitoneally by use of Alzet osmotic minipumps (Alzet osmotic mini pumps, model #1004, Alzet, USA). Mice were either treated with 5.3 mg/kg/day RD2 (n = 11) or placebo (0.9% sodium chloride solution) (n = 10) as control group. The Alzet minipumps were soaked in sterile 0.9% sodium chloride solution for 24 h before implantation. The next day, the pumps were filled with the appropriate solution and implanted intraperitoneally. In short, mice

were anesthetised with isoflurane, the skin and the muscle layer below were cut in the midline and the pump was inserted in the abdominal cavity. Following placement of the pump, the wound was sutured. Three weeks after the implantations, the mice were tested in different behavioural set ups. 28 days after the implantations, the mice were sacrificed for histopathological analysis. All mice of both groups were included in the experiments described below.

Behavioural tests. The mice were tested at the end of the treatment period in different behavioural tests.

Open field test. The open field test was performed to evaluate the activity and anxiety behaviour of the mice. The arena (42 cm × 42 cm surrounded with clear Plexiglass sides (20 cm high)) was subdivided into two areas: border and centre. The mice were observed with a camera driven tracker system (Ethovision XT10, Noldus, The Netherlands) for 4 min. Time spent in both areas was analysed. After each testing day and in between the mice, the apparatus was wiped out with chlorhexidine and 70% ethanol and allowed to air-dry.

Zero maze. Similar to the open field test, the zero maze was used to assess the anxiety behaviour of the mice. The maze consisted of a circular arena (65 cm diameter) that is raised 40 cm above the table. The maze was separated into four equal parts, with two parts with 15 cm high walls of opaque material and two only 0.5 cm high walls. Therefore, it consisted of two open and two closed areas. The mice were put into the circle and observed for 4 min with a camera driven tracker system (Ethovision XT10, Noldus, The Netherlands). Analysed was the time mice spent in the open and closed arms. After each testing day and in between mice, the apparatus was wiped out with chlorhexidine solution and 70% ethanol and allowed to air-dry.

Morris water maze (MWM). The mice were tested daily for one week in a water maze. Our version of the Morris water maze consists of a blue circular tank (120 cm diameter) filled with clear water (22 °C ± 1 °C). In short, the mice were placed into the water at the edge of the pool and allowed to swim in order to find a hidden but fixed escape platform (0.5 cm below the water surface) by orientating themselves with the help of extramaze cues. The mice were allowed to swim freely for a maximum of 60 s to re-find the hidden platform (or until they climbed onto the hidden platform). If they had not found it, they were placed on the platform for 20 s. Each mouse was tested for three trials per day with inter-trial intervals of 60 s and varying starting positions in a pseudo random order. The platform was placed in the middle of one of the quadrants (south-east) of the pool approximately 30 cm from the edge of the pool. The task of the mice throughout the experiment was to find and escape on the hidden platform. Once the mouse had learned the task (day 6, trial 18), a probe trial was performed immediately following the last trial of acquisition on day 6. In the probe trial (i.e. trial 19), the platform was removed from the pool and animals were allowed to swim for 60 s. Mice were recorded with a camera driven tracker system (Ethovision XT10, Noldus, The Netherlands). It was analysed the time the mice needed to escape to the hidden platform (escape latency) and the time they spent in the target quadrant (probe trial).

Histopathology. In short, mice were anesthetized, transcardially perfused with ice-cold saline and the brains were removed. The brain was cut in half through the midline. One hemisphere was frozen for biochemical analysis and the other half was fixed overnight in 4% paraformaldehyde. Following overnight postfixation and cryoprotection in 30% sucrose, six series (1 in 6) of coronal sections were cut through the brain. One half of the first series of sections was mounted unstained, the other half was stained for Aβ using the W0-2 antibody (mouse anti-human Aβ4-10, Merck, Germany), as described in detail below. The second series was stained immunohistochemically according to published protocols[37]. One half of the second series was stained for GFAP (mouse anti-GFAP; Sigma-Aldrich, USA), a marker for astrocytes, whereas the other half was stained for Iba-1 (rabbit anti-Iba-1; WAKO, USA), a marker for microglia. Some of the stained sections were double stained with either Congo red, Thioflavin S or Thiazine red. The other three series were stored at −20 °C in antifreeze for future analyses.

The sections from the first series which had been destined for Aβ staining were pre-treated for 30 min with hot citrate buffer (85 °C). The series of sections was transferred into a tris-buffered saline (TBS) solution containing 0.5% Triton X-100 (TBS-T) and the primary antibody. 18 h after incubation in this solution at room temperature (20 °C) on a shaker table in the dark, the sections were rinsed three times with TBS-T and transferred into a solution with the secondary antibody (goat anti-mouse*biotin (Sigma-Aldrich, Germany), or sheep anti-rat Ig*biotin (Biorad, USA)) and incubated for two hours. Then, the sections were rinsed three times with TBS-T and transferred into a solution with mouse ExtrAvidin (Sigma-Aldrich, Germany). Following rinsing, the sections were incubated for approximately 3 min with a 3,3′-Diaminobenzidine (DAB) solution enhanced with a saturated nickel ammonium sulphate solution. All stained sections were mounted on slides and coverslipped.

Plaque quantification. The plaque load of the appropriate areas (dorsal hippocampus and parietal cortex) of the brains was determined as described previously[28].

Biochemistry. Diluted brain samples were assayed for Aβ(x-40) and Aβ(x-42) as described previously[24,26,28].

Statistics. All statistical calculations were performed using GraphPad Prism 5 (GraphPad Software, Inc., USA) or SigmaPlot Version 11 (Systat Software, Germany). Data is represented as mean ± SD (SPR, QIAD, ThT assay, seeding assay, MTT test) or SEM (behavioural tests, histochemical and biochemical analysis), $p > 0.05$ was considered as not significant (n.s.). Normal distribution of data was either tested by use of Shapiro-Wilk normality test or by use of a normal probability plot (InVivoStat, Version 3.4.0.0, UK)[38]. Normal distributed data was analysed with one-way ANOVA with Bonferroni post hoc analysis (QIAD assay, seeding assay, MTT test). Two-way ANOVA with Bonferroni post hoc analysis was used to analyse the results of the *in vivo* study (open

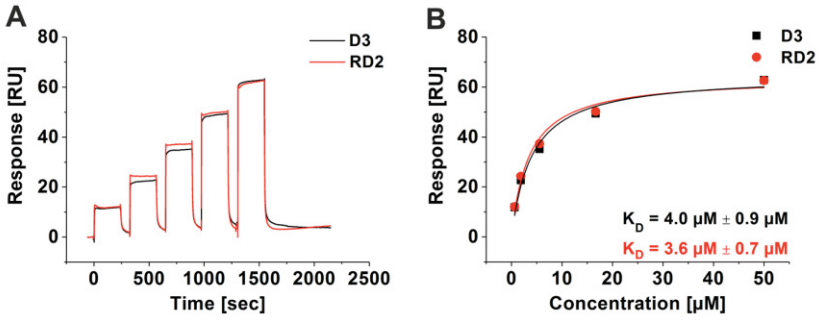

Figure 1. Affinity determination of D3 and RD2 by SPR. N-terminally biotinylated Aβ(1-42) was immobilised on a streptavidin sensor chip and the binding of different D3 (black) and RD2 (red) concentrations was analysed in a single cycle (**A**). For evaluation, the steady-state binding signals were plotted over the concentrations and fitted using a Langmuir 1:1 binding model (**B**). Data is represented as values ± errors of the fit.

field test, zero maze, probe trial Morris water maze, ELISA). Escape latency to the platform within the Morris water maze was considered as not normally distributed and therefore analysed by Friedman Repeated Measures ANOVA on Ranks with Dunn's post hoc analysis.

Results

RD2 and D3 bound to Aβ(1-42) with similar affinities. Binding affinities of D3 and RD2 were determined using surface plasmon resonance (SPR). Monomeric N-terminally biotinylated Aβ(1-42) was immobilized on the surface and concentration dependent series with the respective compound were injected (Fig. 1A). Steady-state analysis of the data revealed similar dissociation constants (K_D) for both peptides which were 4.0 µM ± 0.9 µM for D3 and 3.6 µM ± 0.7 µM for RD2 (Fig. 1B).

RD2 eliminated Aβ oligomers. *In vitro*, the influence of RD2 and D3 on the Aβ aggregate size distribution was tested by the assay for quantitative determination of interference with Aβ aggregate size distribution (Aβ QIAD)[23] (Fig. 2A). Aβ species located in fractions 4 to 6 of the density gradient were efficiently eliminated by RD2 and D3 (Fig. 2B). Aβ species located in these fractions are Aβ oligomers, which were previously characterised in detail[23]. They have a molecular weight of about 100 kDa, corresponding to about 23 monomeric units. Both, RD2 and D3 significantly reduced the amount of Aβ oligomers in fractions 4 to 6 by 71% and 51%, respectively (Fig. 2B, one-way ANOVA, $p \leq 0.001$, Bonferroni post hoc analysis, Aβ(1-42) vs. D3 or RD2 in fractions 4–6, $p \leq 0.001$, fraction 4 D3 vs RD2, $p = 0.019$, fraction 5 D3 vs RD2, $p = 0.025$, fraction 6 D3 vs RD2, $p = 0.045$) without causing a significant change of the Aβ monomer amount in the first fractions of the density gradient (one-way ANOVA, $p = 0.19$). Although RD2 and D3 have the same qualitative effect on Aβ oligomers, RD2 was found to be significantly more efficient in Aβ oligomer elimination (Fig. 2B). Furthermore, a QIAD assay for Aβ(1-42) size distributions was performed in dependence of different RD2 concentration (Fig. 2C). Based on the results of the performed assay it could be shown that RD2 eliminates Aβ(1-42) oligomers in a dose-dependent manner with a resulting half-maximal inhibition concentration (IC_{50}) of 8.4 µM (Fig. 2D).

Aβ fibril formation was inhibited by RD2 in a dose-dependent manner. Investigation of the functional effect of RD2 on Aβ(1-42) fibril formation was accomplished by Thioflavin T (ThT). As demonstrated in Fig. 3A, RD2 inhibited the formation of Aβ(1-42) fibrils in a dose-dependent manner and a half-maximal inhibition concentration (IC_{50}) of 7.7 µM was determined (Fig. 3B). Thus, the IC_{50} value is in very good agreement with the K_D value obtained by SPR, indicating that the binding event is responsible for the inhibitory function of RD2.

RD2 reduced the catalytic effect of preformed seeds on Aβ aggregation. To investigate whether RD2 can inhibit the seeding potential of Aβ, a seeding assay was performed. The aggregation of monomeric Aβ(1-42) alone or together with preformed Aβ(1-42) seeds incubated with and without RD2 was monitored. The resulting intensities were fitted and the amplitude and the half-life ($t_{1/2}$) were calculated. For monomeric Aβ(1-42) without seeds $t_{1/2}$ was 11.6 h, whereas the aggregation of seeded monomeric Aβ(1-42) was significantly ($p \leq 0.001$) accelerated to a half-life of 1 h (one-way ANOVA with Bonferroni post hoc analysis) (Fig. 4A). 24 h incubation of RD2 with seeds decelerated the aggregation of monomeric Aβ significantly ($p \leq 0.001$) by factor of 5 (4.6 h) compared to seeded Aβ without RD2. This indicates that RD2 lowers the catalytic effect of the seeds on Aβ aggregation *in vitro*. The amplitude of seeded Aβ was not affected by the pre-treatment of the seeds with RD2 (Fig. 4B). This observation supports the hypothesis that the observed effect in Fig. 4A was indeed due to the potential of RD2 to reduce the seeding potential of the seeds during the pre-treatment rather than due to any remaining free RD2, which would reduce also the overall fibril formation as shown in Fig. 3A.

Increased cell viability after pre-incubation of Aβ(1-42) assemblies with RD2. The MTT cell viability test was performed to survey the effects of RD2 co-incubated with Aβ(1-42) on PC-12 and SH-SY5Y cells. PC-12 cells are extensively used to study Aβ induced neurotoxicity, because this cell type is vulnerable to Aβ. Additionally, we have used SH-SY5Y cells in addition to study the effects on a more appropriate neuronal cell

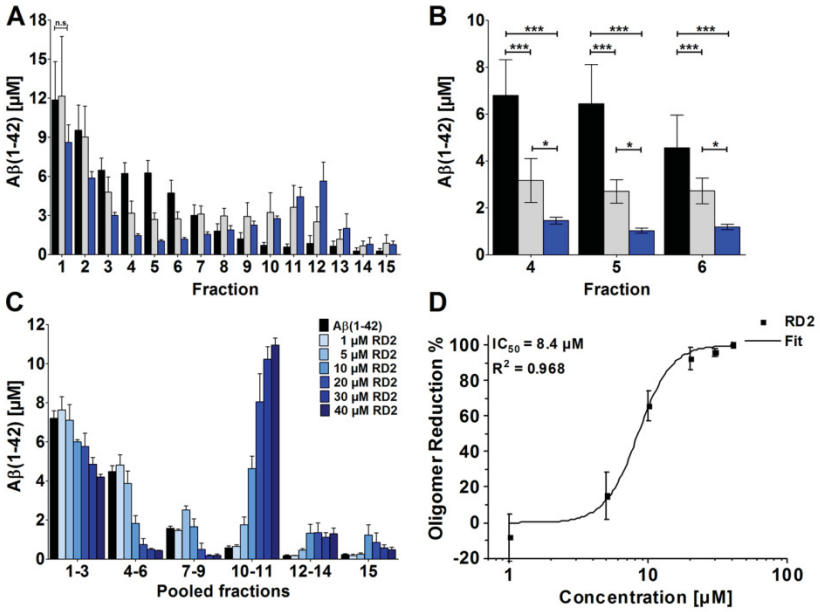

Figure 2. RD2 eliminated Aβ(1-42) oligomers in a concentration dependent manner. Aβ(1-42) size distributions without D-peptide (black in **A**–**C**) and in the presence of compounds were analysed by density gradient centrifugation. Aβ(1-42) concentrations for each fraction were determined by UV absorption during RP-HPLC. Aβ(1-42) oligomers of interest are located in fractions 4 to 6 (**A**–**C**). Comparison of 20 µM D3 (grey) and 20 µM RD2 (blue) (**A**,**B**) revealed the superior oligomer elimination efficacy of RD2. In (**C**) the QIAD assay for Aβ(1-42) size distributions in dependence of different RD2 concentrations (0 µM black, 1 µM till 40 µM, from light to dark blue) are shown. Graphical representation of the measured decrease in oligomer concentration in % of the amount of oligomers found in the control with 0 µM RD2 in dependence of the different RD2 concentration. The curve was fitted according to a logistic fit function yielding an IC_{50} value (**D**). In each experiment, data is represented as mean ± SD; A: one-way ANOVA, with Bonferroni post hoc analysis, Aβ(1-42) vs. D3 or RD2 in fractions 4–6, ***$p \leq 0.001$, fraction 4 D3 vs RD2, *$p = 0.019$, fraction 5 D3 vs RD2, *$p = 0.025$, fraction 6 D3 vs RD2, *$p = 0.045$. Data of Aβ(1-42) and D3 were taken from Brener *et al.*[23].

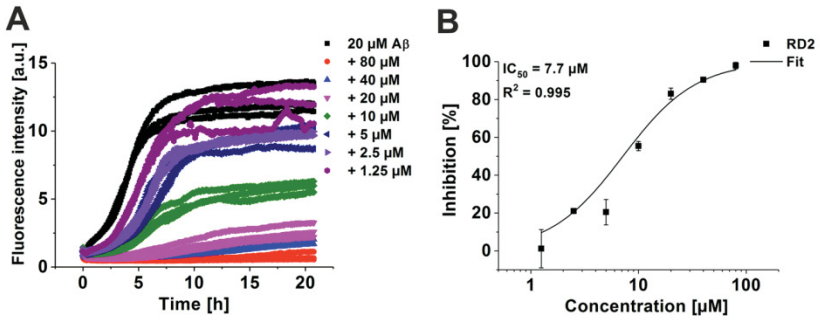

Figure 3. Inhibitory function of RD2 for Aβ(1-42) fibril formation. Aβ(1-42) fibril formation was monitored by Thioflavin T (ThT) in the absence or presence of different RD2 concentrations (0 µM black, 80 µM red, 40 µM light blue, 20 µM pink, 10 µM green, 5 µM blue, 2.5 µM lilac, 1.25 µM purple) (**A**). Fibril mass was normalised to the Aβ control and the inhibition in % was calculated. The curve was fitted according to a logistic fit function yielding an IC_{50} value (**B**). The data represent three replicates.

type. We incubated Aβ(1-42), at a final concentration of 1 µM, with and without 5 µM RD2 on PC-12 or SH-SY5Y cells. We found a significant increase of cell viability of PC-12 and SH-SY5Y cells after pre-incubation of Aβ with RD2 from 25% to 76% (Fig. 5A) and 65% to 94% (Fig. 5B), respectively (both: one-way ANOVA, $p \leq 0.001$ with

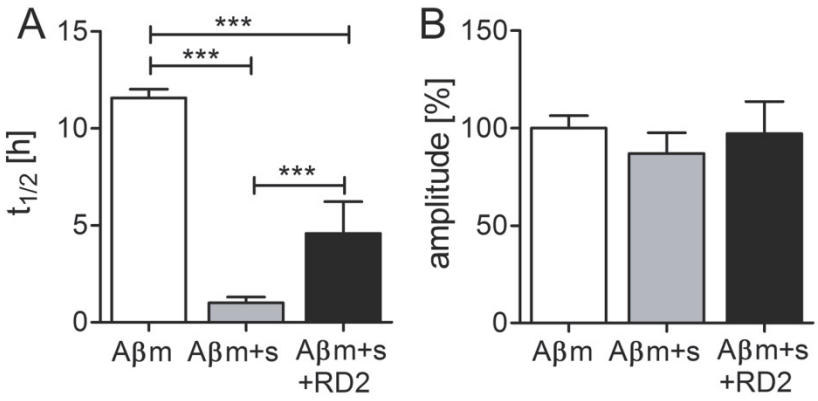

Figure 4. Influence of RD2 on the seeded Aβ(1-42) aggregation. The aggregation of monomeric Aβ without (m, white), and with preformed seeds (s, grey) incubated with or without RD2 (black) was monitored and the half-life ($t_{1/2}$) (**A**) as well as the amplitude (**B**) of the aggregation was determined. In (**B**) the amplitude of monomeric Aβ without seeds was set to be 100% and the amplitudes of the other samples were normalized accordingly. Data is represented as mean ± SD, one-way ANOVA with Bonferroni post hoc analysis, ***$p \leq 0.001$.

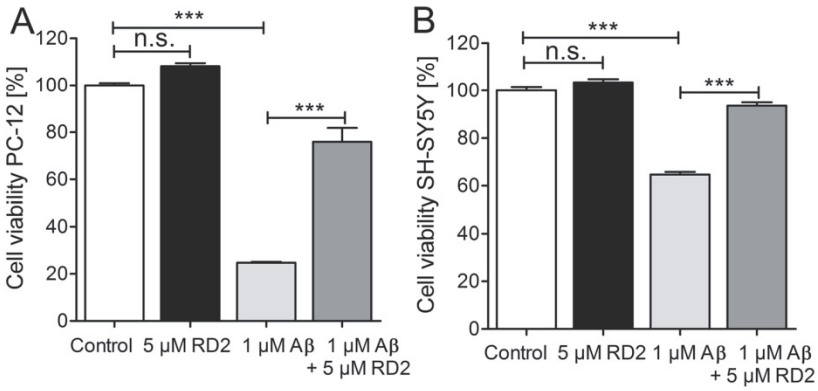

Figure 5. RD2 reduced the negative impact of Aβ(1-42) on cell viability in PC-12 and SH-SY5Y cells. Cell viability was assessed by MTT after incubation of PC-12 (**A**) or SH-SY5Y (**B**) cells with 1 µM Aβ(1-42) (light grey) or 1 µM Aβ(1-42) co-incubated with 5 µM RD2 (grey), respectively. Data confirms the efficacy of RD2 to significantly increase the cell viability after co-incubation with Aβ(1-42) on both cell lines compared to Aβ(1-42) alone. Data is represented as mean ± SD, one-way ANOVA with Bonferroni post hoc analysis, ***$p \leq 0.001$.

Bonferroni post hoc analysis: $p \leq 0.001$). In order to demonstrate that RD2 alone did not influence cell viability, 5 µM RD2 were incubated with both cells lines, which did not result in any change of cell viability compared to buffer control (one-way ANOVA: n.s., $p = 0.4$, Fig. 5A and B).

Treatment with RD2 improved cognition without showing any influence on activity or anxiety. Implantation of Alzet osmotic minipumps filled with RD2 solution or saline (placebo) into APP/PS1 mice neither changed any obvious physiological parameters (e.g. growth as measured by body weight (placebo: 25.7 ± 0.9 g vs RD2: 26.8 ± 0.8 g) or general health, i.e. look of fur, posture, and motor activity) in the implanted mice, nor caused any noticeable discomfort. None of the mice developed any health or motor problems.

After three weeks of placebo or RD2 treatment of APP/PS1 mice, both groups were tested in the open field and zero maze tests. As demonstrated in Fig. 6, there were no significant differences in activity or anxiety levels between the two groups of mice (Fig. 6A; total distance moved in the open field: 2143 ± 217 cm vs 2121 ± 163 cm, respectively, both two-way ANOVA with Bonferroni post hoc analysis, $p = 1$). Speeds in the open field was 8.9 ± 0.9 cm/s vs 8.8 ± 0.7 cm/s, respectively, while in the zero maze the average speed of movement was 5.0 ± 0.6 vs 4.8 ± 0.4 cm/s, respectively (Fig. 6A and B). In the following week, the mice were tested in the Morris water maze. There was no difference in the swimming speed between the groups of mice (placebo: 19.0 ± 1 cm/s and RD2: 18.8 ± 1 cm/s). RD2 treated mice did significantly improve their performance during the week of training

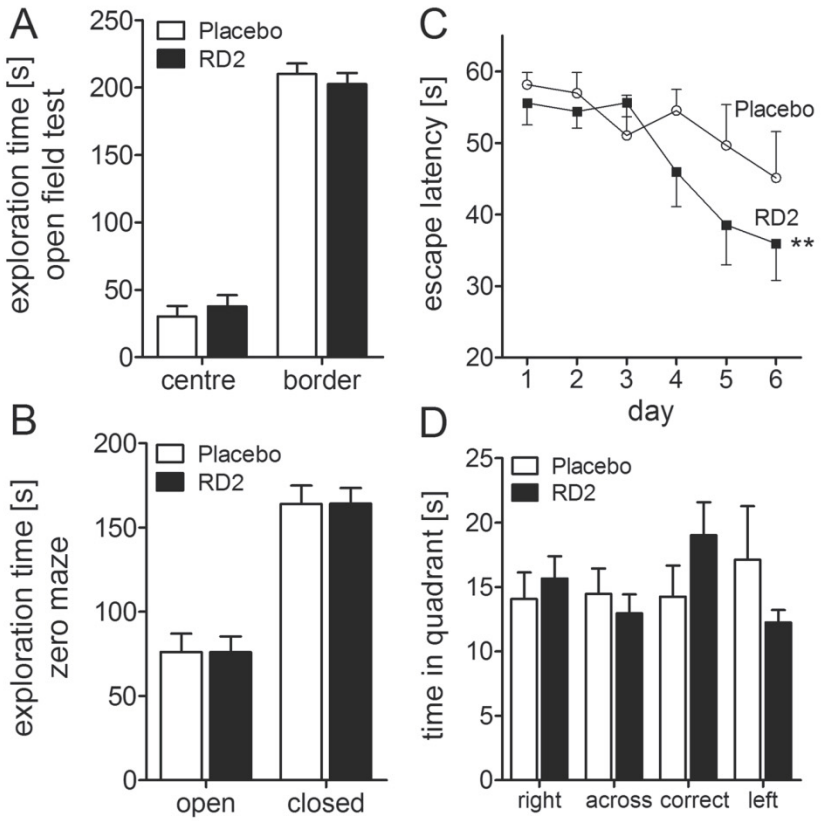

Figure 6. Effects of RD2 on cognition and evaluation of activity and anxiety. Four graphs showing the behaviour of placebo and RD2 treated mice. Assessment of the open field test (**A**) and zero maze (**B**) exhibits no difference of activity or anxiety of RD2 and placebo treated mice. Performance in the water maze showed a significantly improved cognition of RD2 treated mice in contrast to the performance of placebo treated mice (**C**). The RD2 treated group showed a preference for the correct quadrant in the probe trial which followed the last training trial (**D**). Data is represented as mean ± SEM, Friedman Repeated Measures ANOVA on Ranks, (**C**) $^{**}p = 0.003$.

in the Morris water maze compared to the placebo treated mice (escape latency, Friedman RM ANOVA, RD2 treated mice $p = 0.003$, Dunn's post hoc analysis $p \leq 0.05$, placebo treated mice $p = 0.13$, Fig. 6C). Furthermore, the RD2 group showed a preference for the correct quadrant in the probe trial, which followed the last training trial (Fig. 6D). After completion of the behavioural testing, the animals were sacrificed and the brains were removed for further analysis.

The Aβ load was measured in the dorsal hippocampus and parietal cortex by immunohistochemical staining for human Aβ(4-10) (W0-2 antibody). Treatment with RD2 did not reveal any reduction of the Aβ plaque load in the hippocampus or in the cortex compared to the placebo treated mice (% area covered, Fig. 7A–F). Furthermore, analysis of the sections that were stained for activated astrocytes (GFAP) or microglia (Iba-1) revealed that the magnitude of inflammation surrounding Aβ deposits did not differ between the two treatment groups of mice. Neither did RD2 treatment significantly reduce the amount of plaque related microglial inflammation (Iba-1; average density 40.5 ± 2.0 vs 40.7 ± 1.5, respectively; Fig. 7G–I) compared to the placebo treated mice. Nor did treatment with RD2 significantly change the amount of plaque-related activated astrocytes (GFAP; average density 34.6 ± 1.4 vs 36.7 ± 1.7, Fig. 7J–L) compared to the placebo treated mice within the hippocampus. Double staining for microglia and astrocytes confirmed that in the surroundings of all labelled plaques both glial cell types were activated.

The biochemical analysis by ELISA measurements demonstrated that Aβ(x-40) levels did not differ significantly between RD2 and placebo treated mice (insoluble Aβ(x-40): 142.5 ± 3.9 pg/g vs 148.1 ± 3.0 pg/g; soluble Aβ(x-40): 38.9 ± 5.2 pg/g vs 47.8 ± 7.4 pg/g, respectively, Fig. 8A). However, a significant decrease of insoluble Aβ(x-42) levels was detected in the hippocampus of RD2 treated mice in contrast to the placebo treated mice (insoluble Aβ(x-42): 168.8 ± 19.2 pg/g vs 219.4 ± 15.3 pg/g; soluble Aβ(x-42): 15.5 ± 2.6 pg/g vs 23.5 ± 5.1 pg/g respectively, two-way ANOVA, $p = 0.027$ with Bonferroni post hoc analysis, $p = 0.048$, Fig. 8B). Furthermore,

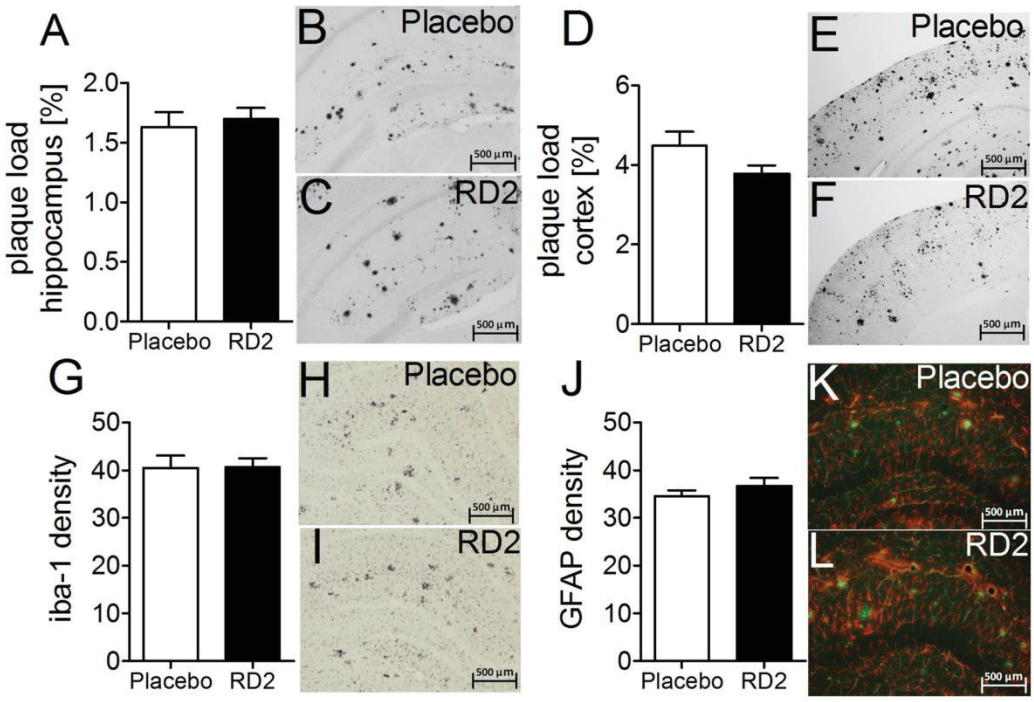

Figure 7. Histopathological analysis of AD pathology in hippocampus revealed no change after intraperitoneal treatment with RD2. Aβ load measured in hippocampus and parietal cortex (**A**–**F**), microglia (**G**–**I**) and activated astrocytes (**J**,**K**) were analysed after the behavioural tests. Data indicates that there is no change in AD typical pathology after 28 days of intraperitoneal treatment with RD2 compared to the pathology of placebo treated mice. Data is represented as mean ± SEM.

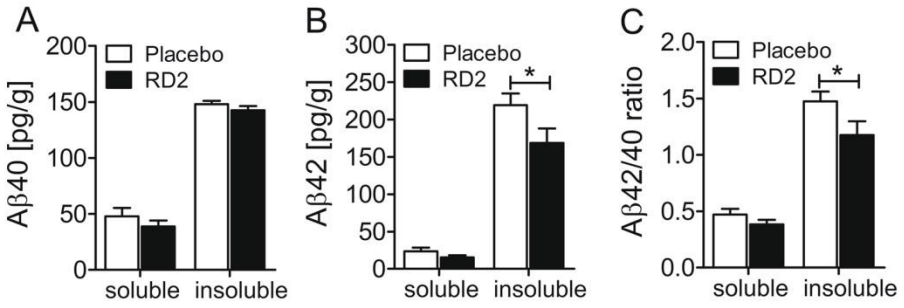

Figure 8. Treatment with RD2 significantly reduced the level of insoluble Aβ(x-42). Levels of Aβ(x-40) (**A**) and Aβ(x-42) (**B**) were analysed in soluble and insoluble fractions of hippocampus by ELISA. Treatment with RD2 exhibited a significant decrease of insoluble Aβ(x-42) level in the hippocampus and significantly lowered the Aβ42/40 ratio (**C**). Data is represented as mean ± SEM, two-way ANOVA with Bonferroni post hoc analysis, (**B**) *p = 0.027, (**C**) *p = 0.026.

treatment with RD2 lowered significantly the ratio of insoluble Aβ42/40 (insoluble Aβ42/40: RD2 1.2 ± 0.1 vs placebo 1.5 ± 0.1; soluble Aβ42/40: RD2 0.4 ± 0.1 vs placebo 0.5 ± 0.1, respectively: two-way ANOVA, p = 0.026 with Bonferroni post hoc analysis, p = 0.047, Fig. 8C).

Discussion

Finding a curative and disease modifying treatment for AD is one of the major challenges of the 21st century. Despite the fact of increasing prevalence of AD, current treatment options are only symptomatic[39], a situation that is considered inacceptable. Today, soluble Aβ oligomers are postulated to be the disease causing

agent and consequently, their elimination is a promising target for therapy. Within the last years, we developed D-enantiomeric peptides, solely consisting of D-enantiomeric amino acid residues, for stabilisation of Aβ monomers in an aggregation incompetent conformation, leading to the specific and direct elimination of Aβ oligomers[23,26].

Here, we characterised our all-D-enantiomeric amino acid residue compound RD2. RD2 is a derivative of the lead compound D3, which was characterised before[24,27,40]. Based on steady state analysis, both compounds, D3 and RD2, showed similar binding affinities to Aβ(1-42) monomers with an equilibrium dissociation constant in the micromolar range, which was shown previously and validated within this study[41]. However, the potential of RD2 to eliminate Aβ oligomers is significantly increased in comparison to D3. Moreover, RD2 eliminates Aβ(1-42) oligomers in a dose-dependent manner with an IC_{50} of 8.4 µM. Additionally, RD2 significantly reduced the cytotoxic potential of Aβ(1-42), shown by the enhanced cell viability in PC-12 and SHSY-5Y cells after co-incubation of Aβ(1-42) with RD2 and inhibited the Aβ(1-42) fibril formation with an IC_{50} of 7.7 µM. This is in very good agreement with the results of the QIAD assay. In accordance with the Aβ oligomer eliminating properties of RD2, RD2 also inhibited the seeding potential of Aβ aggregates.

Investigation of the *in vivo* efficacy of RD2 was carried out in an intraperitoneal treatment study with APP/PS1 transgenic mice. Thereby we could prove our hypothesis that RD2 showed a similar or increased efficacy compared to D3. Short term treatment with RD2 improved cognitive performance significantly after three weeks compared to the placebo control group. Treatment with RD2 did not lead to a significant reduction in the amount of Aβ deposits in the hippocampus. As it is expected that there is an equilibrium between soluble and plaque Aβ, longer treatment periods could have possibly led to a significant reduction of Aβ pathology. Furthermore, analysis of the microglia and astrocytes did not show significant reduction in activated microglia and astrocytes in RD2 treated mice compared to the placebo treated mice. Consequently, improved cognitive performance was not related to a decrease in plaque pathology. Since RD2 significantly reduced the amount of Aβ oligomers *in vitro*, a more likely explanation is that RD2 decreases synaptic toxicity and pathology by reducing the amount of Aβ oligomers *in vivo*, even without significantly changing the Aβ plaque load.

RD2 significantly reduced levels of insoluble Aβ(x-42) in the hippocampus, but did not show any significant reduction of Aβ(x-40) levels. This ultimately led to a decrease of the Aβ42/Aβ40 ratio, without affecting total Aβ levels. What that actually means remains to be elucidated. We hypothesize that the Aβ oligomer eliminating activity of RD2 is based on its binding to Aβ monomers and their stabilisation in an aggregation-incompetent conformation, thereby shifting the equilibrium between monomeric and oligomeric Aβ away from Aβ oligomers, ultimately leading to the elimination of Aβ oligomers. It certainly increases the need to further investigate the underlying mechanism of RD2 based on the improvement of cognitive performance. Irrespective of that, these observations strengthen the potential role of RD2 as a disease-modifying agent for AD treatment. Besides that, the outcome of this study supports the finding that there is not a necessarily dependence between plaque pathology and cognition. Compared with other drugs targeting Aβ oligomers (e.g. antibodies) our compound RD2 does not only interact with Aβ oligomers but directly destroys them without relying on the contribution of components of the immune system. Future treatment studies with RD2 in other transgenic AD mouse models will further elucidate the compound's mechanism of action and its future potential.

Conclusion

Summarised, the identified derivative of the lead compound D3, named RD2, was significantly more efficient in elimination of Aβ oligomers than D3. RD2 improved cognitive performance of APP/PS1 mice already after a short, three weeks, treatment and reduced insoluble Aβ(x-42) levels in the brain without a negative impact on activity or anxiety. Based on this, RD2 is a promising compound to be further developed as a drug candidate for therapy of AD.

References

1. Hirtz, D. *et al.* How common are the "common" neurologic disorders? *Neurology* **68**, 326–337, https://doi.org/10.1212/01.wnl.0000252807.38124.a3 (2007).
2. Montine, T. J. *et al.* National Institute on Aging-Alzheimer's Association guidelines for the neuropathologic assessment of Alzheimer's disease: a practical approach. *Acta neuropathologica* **123**, 1–11, https://doi.org/10.1007/s00401-011-0910-3 (2012).
3. Ballard, C. *et al.* Alzheimer's disease. *Lancet* **377**, 1019–1031, https://doi.org/10.1016/S0140-6736(10)61349-9 (2011).
4. O'Brien, R. J. & Wong, P. C. Amyloid precursor protein processing and Alzheimer's disease. *Annual review of neuroscience* **34**, 185–204, https://doi.org/10.1146/annurev-neuro-061010-113613 (2011).
5. Selkoe, D. J. & Hardy, J. The amyloid hypothesis of Alzheimer's disease at 25 years. *EMBO molecular medicine* **8**, 595–608, https://doi.org/10.15252/emmm.201606210 (2016).
6. Bertram, L. & Tanzi, R. E. Alzheimer's disease: one disorder, too many genes? *Human molecular genetics* **13**(Spec No 1), R135–141, https://doi.org/10.1093/hmg/ddh077 (2004).
7. Bertram, L., Lill, C. M. & Tanzi, R. E. The genetics of Alzheimer disease: back to the future. *Neuron* **68**, 270–281, https://doi.org/10.1016/j.neuron.2010.10.013 (2010).
8. Van Broeck, B., Van Broeckhoven, C. & Kumar-Singh, S. Current insights into molecular mechanisms of Alzheimer disease and their implications for therapeutic approaches. *Neurodegenerative Diseases.* **4**, 349–365 (2007).
9. Pauwels, K. *et al.* Structural basis for increased toxicity of pathologicalabeta42: abeta40 ratios in Alzheimer disease. *The Journal of biological chemistry* **287**, 5650–5660, https://doi.org/10.1074/jbc.M111.264473 (2012).
10. Rovelet-Lecrux, A. *et al.* APP locus duplication causes autosomal dominant early-onset Alzheimer disease with cerebral amyloid angiopathy. *Nature genetics* **38**, 24–26, https://doi.org/10.1038/ng1718 (2006).
11. Sleegers, K. *et al.* APP duplication is sufficient to cause early onset Alzheimer's dementia with cerebral amyloid angiopathy. *Brain: a journal of neurology* **129**, 2977–2983, https://doi.org/10.1093/brain/awl203 (2006).
12. Jonsson, T. *et al.* A mutation in APP protects against Alzheimer's disease and age-related cognitive decline. *Nature* **488**, 96–99, https://doi.org/10.1038/nature11283 (2012).
13. Braak, H. & Braak, E. Neuropathological stageing of Alzheimer-related changes. *Acta neuropathologica* **82**, 239–259 (1991).

14. Braak, H. & Braak, E. Staging of Alzheimer's disease-related neurofibrillary changes. *Neurobiology of aging* **16**, 271–278; discussion 278–284 (1995).
15. Hardy, J. A. 'anatomical cascade hypothesis' for Alzheimer's disease. *Trends in Neurosciences* **15**, 200–201 (1992).
16. Crews, L. & Masliah, E. Molecular mechanisms of neurodegeneration in Alzheimer's disease. *Human molecular genetics* **19**, R12–20, https://doi.org/10.1093/hmg/ddq160 (2010).
17. Larson, M. E. & Lesne, S. E. Soluble Abeta oligomer production and toxicity. *Journal of neurochemistry* **120**(Suppl 1), 125–139, https://doi.org/10.1111/j.1471-4159.2011.07478.x (2012).
18. Ferreira, S. T., Lourenco, M. V., Oliveira, M. M. & De Felice, F. G. Soluble amyloid-beta oligomers as synaptotoxins leading to cognitive impairment in Alzheimer's disease. *Frontiers in cellular neuroscience* **9**, 191, https://doi.org/10.3389/fncel.2015.00191 (2015).
19. Ferreira, S. T. & Klein, W. L. The Abeta oligomer hypothesis for synapse failure and memory loss in Alzheimer's disease. *Neurobiology of learning and memory* **96**, 529–543, https://doi.org/10.1016/j.nlm.2011.08.003 (2011).
20. Wilcox, K. C., Lacor, P. N., Pitt, J. & Klein, W. L. Abeta oligomer-induced synapse degeneration in Alzheimer's disease. *Cellular and molecular neurobiology* **31**, 939–948, https://doi.org/10.1007/s10571-011-9691-4 (2011).
21. Schumacher, T. N. *et al.* Identification of D-peptide ligands through mirror-image phage display. *Science* **271**, 1854–1857 (1996).
22. Wiesehan, K. *et al.* Selection of D-amino-acid peptides that bind to Alzheimer's disease amyloid peptide abeta1-42 by mirror image phage display. *Chembiochem: a European journal of chemical biology* **4**, 748–753, https://doi.org/10.1002/cbic.200300631 (2003).
23. Brener, O. *et al.* QIAD assay for quantitating a compound's efficacy in elimination of toxic Abeta oligomers. *Scientific reports* **5**, 13222, https://doi.org/10.1038/srep13222 (2015).
24. van Groen, T. *et al.* Reduction of Alzheimer's disease amyloid plaque load in transgenic mice by D3, A D-enantiomeric peptide identified by mirror image phage display. *ChemMedChem* **3**, 1848–1852, https://doi.org/10.1002/cmdc.200800273 (2008).
25. van Groen, T., Kadish, I., Wiesehan, K., Funke, S. A. & Willbold, D. *In vitro* and *in vivo* staining characteristics of small, fluorescent, Abeta42-binding D-enantiomeric peptides in transgenic AD mouse models. *ChemMedChem* **4**, 276–282, https://doi.org/10.1002/cmdc.200800289 (2009).
26. Funke, S. A. *et al.* Oral Treatment with the d-Enantiomeric Peptide D3 Improves the Pathology and Behavior of Alzheimer's Disease Transgenic Mice. *ACS chemical neuroscience* **1**, 639–648, https://doi.org/10.1021/cn100057j (2010).
27. van Groen, T., Kadish, I., Funke, A. S., Bartnik, D. & Willbold, D. Treatment with Aβ42 Binding d-Amino Acid Peptides Reduce Amyloid Deposition and Inflammation in APP/PS1 Double Transgenic Mice. *Advances in Protein Chemistry and Structural Biology* **88**, 133–152 (2012).
28. van Groen, T., Kadish, I., Funke, S. A., Bartnik, D. & Willbold, D. Treatment with D3 removes amyloid deposits, reduces inflammation, and improves cognition in aged AbetaPP/PS1 double transgenic mice. *Journal of Alzheimer's disease: JAD* **34**, 609–620, https://doi.org/10.3233/JAD-121792 (2013).
29. Klein, A. N. *et al.* Optimization of the All-D Peptide D3 for Abeta Oligomer Elimination. *PloS one* **11**, e0153035, https://doi.org/10.1371/journal.pone.0153035 (2016).
30. Ziehm, T. *et al.* Increase of Positive Net Charge and Conformational Rigidity Enhances the Efficacy of d-Enantiomeric Peptides Designed to Eliminate Cytotoxic Abeta Species. *ACS chemical neuroscience*, https://doi.org/10.1021/acschemneuro.6b00047 (2016).
31. Klein, A. N. *et al.* Optimization of D-peptides for Abeta monomer binding specificity enhances their potential to eliminate toxic Abeta oligomers. *ACS chemical neuroscience*, https://doi.org/10.1021/acschemneuro.7b00045 (2017).
32. Jiang, N. *et al.* Preclinical Pharmacokinetic Studies of the Tritium Labelled D-Enantiomeric Peptide D3 Developed for the Treatment of Alzheimer s Disease. *PloS one* **10**, e0128553, https://doi.org/10.1371/journal.pone.0128553 (2015).
33. Leithold, L. H. *et al.* Pharmacokinetic Properties of a Novel D-Peptide Developed to be Therapeutically Active Against Toxic beta-Amyloid Oligomers. *Pharmaceutical research* **33**, 328–336, https://doi.org/10.1007/s11095-015-1791-2 (2016).
34. Frenzel, D. *et al.* Immobilization of homogeneous monomeric, oligomeric and fibrillar Abeta species for reliable SPR measurements. *PloS one* **9**, e89490, https://doi.org/10.1371/journal.pone.0089490 (2014).
35. Biedler, J. L., Roffler-Tarlov, S., Schachner, M. & Freedman, L. S. Multiple neurotransmitter synthesis by human neuroblastoma cell lines and clones. *Cancer research* **38**, 3751–3757 (1978).
36. Jankowsky, J. L. *et al.* Co-expression of multiple transgenes in mouse CNS: a comparison of strategies. *Biomolecular engineering* **17**, 157–165 (2001).
37. van Groen, T., Kiliaan, A. J. & Kadish, I. Deposition of mouse amyloid beta in human APP/PS1 double and single AD model transgenic mice. *Neurobiology of disease* **23**, 653–662, https://doi.org/10.1016/j.nbd.2006.05.010 (2006).
38. Clark, R. A., Shoaib, M., Hewitt, K. N., Stanford, S. C. & Bate, S. T. A comparison of *InVivo*Stat with other statistical software packages for analysis of data generated from animal experiments. *Journal of psychopharmacology* **26**, 1136–1142, https://doi.org/10.1177/0269881111420313 (2012).
39. Briggs, R., Kennelly, S. P. & O'Neill, D. Drug treatments in Alzheimer's disease. *Clinical Medicine* **16**, 247–253 (2016).
40. Funke, A. S. *et al.* Oral treatment with the d-enantiomeric peptide D3 improves the pathology and behavior of Alzheimer's Disease transgenic mice. *ACS chemical neuroscience* **1**, 639–648, https://doi.org/10.1021/cn100057j (2010).
41. Olubiyi, O. O. *et al.* Amyloid aggregation inhibitory mechanism of arginine-rich D-peptides. *Current medicinal chemistry* **21**, 1448–1457 (2014).

Acknowledgements

Financial support of D.W. was provided by "Portfolio Technology and Medicine", the Helmholtz-Validierungsfonds of the Impuls and Vernetzungs-Fonds der Helmholtzgemeinschaft. D.W. was supported by the "Portfolio Drug Research" of the Impuls and Vernetzungs-Fonds der Helmholtzgemeinschaft. T.V.G. was partially supported by P30 NS47466.

Author Contributions

D.W., T.v.G., and I.K. designed and planned the study. SPR and ThT experiments were performed by T.Z. O.B. and L.G. designed the QIAD assay, O.B. and L.N.-S. performed the QIAD assays. M.T. conducted the MTT tests and A.E. the seeding assay. The *in vivo* study and all associated experiments were performed by T.V.G. and I.K. Statistical analysis was largely done by S.S. T.V.G., S.S. and D.W. wrote the manuscript, whereas all other authors (E.S., D.J., A.W., J.K.) reviewed and contributed to the manuscript.

Additional Information

Competing Interests: The authors declare that they have no competing interests.

Publisher's note: Springer Nature remains neutral with regard to jurisdictional claims in published maps and institutional affiliations.

3.6 Comparison of blood-brain barrier penetration efficiencies between linear and cyclic all-D-enantiomeric peptides developed for the treatment of Alzheimer's disease

Autoren:	**Schartmann E**, Schemmert S, Ziehm T, Leithold LHE, Jiang N, Tusche M, Jon Shah N, Langen KJ, Kutzsche J, Willbold D, Willuweit A
Journal:	European Journal of Pharmaceutical Sciences
	veröffentlicht am 07.12.2017
DOI:	10.1016/j.ejps.2017.12.005
Impact Factor:	3,756 (2016)
Beitrag:	Planung aller Experimente
	Durchführung aller pharmakokinetischer Experimente
	Durchführung der Tests zur proteolytischen Stabilität
	Durchführung der Plasmaproteinbindungs-Experimente
	Auswertung und grafische Darstellung aller Experimente
	Berechnung aller pharmakokinetischer Parameter und der Blut-Hirn-Schranken-Durchlässigkeits-Parameter
	Schreiben des Manuskripts

European Journal of Pharmaceutical Sciences 114 (2018) 93–102

Contents lists available at ScienceDirect

European Journal of Pharmaceutical Sciences

journal homepage: www.elsevier.com/locate/ejps

Comparison of blood-brain barrier penetration efficiencies between linear and cyclic all-D-enantiomeric peptides developed for the treatment of Alzheimer's disease

Elena Schartmann[a], Sarah Schemmert[a], Tamar Ziehm[a], Leonie H.E. Leithold[a], Nan Jiang[a], Markus Tusche[a], N. Joni Shah[b,c,d], Karl-Josef Langen[b,e], Janine Kutzsche[a], Dieter Willbold[a,f,*], Antje Willuweit[b,**]

[a] Institute of Complex Systems, Structural Biochemistry (ICS-6), Forschungszentrum Jülich GmbH, 52425 Jülich, Germany
[b] Institute of Neuroscience and Medicine, Medical Imaging Physics (INM-4), Forschungszentrum Jülich GmbH, 52425 Jülich, Germany
[c] Department of Neurology, Faculty of Medicine, JARA, RWTH Aachen University, 52074 Aachen, Germany
[d] Department of Electrical and Computer Systems Engineering and Monash Biomedical Imaging, School of Psychological Sciences, Monash University, Melbourne, Victoria, Australia
[e] Department of Nuclear Medicine, Universitätsklinikum der RWTH Aachen, 52074 Aachen, Germany
[f] Institut für Physikalische Biologie, Heinrich-Heine-Universität Düsseldorf, 40225 Düsseldorf, Germany

ABSTRACT

Alzheimer's disease (AD), until now, is an incurable progressive neurodegenerative disease. To target toxic amyloid β oligomers in AD patients' brains and to convert them into non-toxic aggregation-incompetent species, we designed peptides consisting solely of D-enantiomeric amino acid residues. The original lead compound was named D3 and several D3 derivatives were designed to enhance beneficial properties. Here, we compare four D-peptides concerning their efficiencies to pass the blood-brain barrier (BBB). We demonstrate that the D-peptides' concentrations in murine brain directly correlate with concentrations in cerebrospinal fluid. The cyclic D-enantiomeric peptide cRD2D3 is characterized by the highest efficiency to pass the BBB. For in total three cyclic peptides we show that administration of cyclic peptides resulted in up to tenfold higher peak concentrations in brain as compared to their linear equivalents which have partially been characterized before (Jiang et al., 2015; Leithold et al., 2016a). These results suggest that cyclic peptides pass the murine BBB more efficiently than their linear equivalents. cRD2D3's proteolytic stability, oral bioavailability, long duration of action and its favorable brain/plasma ratio reveal that it may become a suitable drug for long-term AD-treatment from a pharmacokinetic point of view.

1. Introduction

More than 20 million people worldwide are currently affected by Alzheimer's disease (AD). There is clear unmet medical need to find a curative treatment for this progressive neurodegenerative disease.

Major hallmarks of AD are neurodegeneration, extracellular deposits or plaques of amyloid β (Aβ), and intracellular deposits of hyperphosphorylated tau protein. Aβ is formed constantly throughout our lifetime and is able to form soluble Aβ oligomers and insoluble Aβ fibrils that make up the plaques (Thal et al., 2006). Currently, oligomers are thought to be the most neurotoxic Aβ species (Haass and Selkoe, 2007). Both, Aβ and tau, and their formation and degradation are prominent targets in AD drug development (Anand et al., 2014).

We focused on the identification and development of substances that specifically and directly eliminate toxic Aβ oligomers. Previously, we described the properties of the compound D3 (Table 1), which is a peptide consisting of 12 D-enantiomeric amino acid residues and has been identified by mirror image phage display against Aβ monomers (Funke and Willbold, 2009; Schumacher et al., 1996; Wiesehan et al., 2003; Wiesehan et al., 2008; Wiesehan and Willbold, 2003). The lead compound D3 stabilizes Aβ monomers in an aggregation-incompetent conformation thus shifting the equilibrium between Aβ oligomers and monomers towards monomers. D3 was shown to eliminate Aβ *in vitro*, improved cognition and lowered Aβ plaque load in transgenic AD

* Correspondence to: D. Willbold, Institute of Complex Systems, Structural Biochemistry (ICS-6), Forschungszentrum Jülich GmbH, 52425 Jülich, Germany.
** Corresponding author.
E-mail addresses: d.willbold@fz-juelich.de (D. Willbold), a.willuweit@fz-juelich.de (A. Willuweit).

https://doi.org/10.1016/j.ejps.2017.12.005
Received 10 July 2017; Received in revised form 25 October 2017; Accepted 6 December 2017
Available online 07 December 2017

Table 1
Peptides' sequences and configurations.

Peptide	Amino acid residue sequence	Amino acid residue configuration
(^{3}H-)cRD2D3	ptlhthnrrrrrrprtrlhthrnr head-to-tail cyclized	All-D-enantiomeric
(^{3}H-)RD2D3	ptlhthnrrrrrrprtrlhthrnr-NH_2	All-D-enantiomeric
(^{3}H-)cD3D3	rprtrlhthrnrrprtrlhthrnr head-to-tail cyclized	All-D-enantiomeric
(^{3}H-)D3D3	rprtrlhthrnrrprtrlhthrnr-NH_2	All-D-enantiomeric
(^{3}H-)cD3r	rprtrlhthrnrr head-to-tail cyclized	All-D-enantiomeric
(^{3}H-)D3	rprtrlhthrnr-NH_2	All-D-enantiomeric
(^{3}H-)L-D3	RPRTRLHTHRNR-NH_2	All-L-enantiomeric
(^{3}H-)RD2	ptlhthnrrrrr-NH_2	All-D-enantiomeric

mouse models, and revealed promising *in vivo* properties, *e.g.* beneficial pharmacokinetic characteristics (Bartnik et al., 2010; Brener et al., 2015; Funke et al., 2010; Jiang et al., 2016; Jiang et al., 2015; Liu et al., 2010; Olubiyi et al., 2014; Olubiyi and Strodel, 2012; van Groen et al., 2012; van Groen et al., 2013; van Groen et al., 2009; van Groen et al., 2008). Derivatives of D3 with rearranged amino acid residue sequences (*e.g.* RD2, Table 1) have been developed to increase Aβ affinity and inhibition of Aβ aggregation *in vitro* (Klein et al., 2016; Kutzsche et al., 2017; Olubiyi et al., 2014). Also, linear tandem 24-mer peptides in head-to-tail arrangement (*e.g.* RD2D3, D3D3; Table 1) have been designed, pharmacokinetically investigated, and successfully tested *in vitro* as well as *in vivo* in an AD mouse model in which they improved symptoms of AD pathology (Brener et al., 2015; Leithold et al., 2016a). Another approach to increase the peptides' Aβ binding affinities and their efficiencies to eliminate toxic Aβ oligomers was head-to-tail cyclization of D3 (*e.g.* cD3r, Table 1). cD3r was shown to be more active *in vitro* and *in vivo* as compared to D3 and other non-cyclized D3 derivatives (Ziehm et al., 2016).

Here, we compared four D3 derivatives concerning their efficiencies to cross the blood-brain barrier (BBB) after intraperitoneal (i.p.) administration to C57BL/6N mice and investigated correlations between peptide concentrations in murine brain, plasma, and cerebrospinal fluid (CSF). The peptide with the highest efficiency to cross the murine BBB, cRD2D3, was pharmacokinetically further characterized, especially regarding its oral bioavailability. Finally, we investigated whether head-to-tail cyclization generally increases a peptide's efficiency to cross the murine BBB.

2. Materials and methods

2.1. Peptides

^{3}H-cRD2D3, ^{3}H-RD2D3, ^{3}H-RD2, ^{3}H-cD3r, ^{3}H-cD3D3, ^{3}H-L-D3, and ^{3}H-D3 were produced by Quotient Bioresearch (Radiochemicals) Ltd. (United Kingdom) with 1 mCi/mL and purity > 95% (Table 1). Non-^{3}H-labelled peptides were delivered by peptides & elephants GmbH (Germany). Recombinant $A\beta_{1-42}$ was obtained from Isoloid GmbH (Germany).

2.2. Animals

For *ex vivo* tests for proteolytic stability, plasma, and organ homogenates from brain, liver, and kidney were taken from a male C57BL/6N wildtype mouse (15.5 weeks). cRD2D3's pharmacokinetic profile was investigated in male C57Bl/6N mice aged 12–13 weeks, weighing about 26 g in average. These mice were ordered at Charles River (Germany) and housed at least one week under standard housing conditions (12/12 h light-dark cycle, approximately 22 °C room temperature and 54% humidity; water and food available *ad libitum*) in the animal facility of the Forschungszentrum Jülich GmbH before the experiments were carried out. All animal experiments were approved by the Animal Protection Committee of the local government (LANUV, North-Rhine-Westphalia, Germany, Az.84-02.04.2011.A356) according to the German Protection of Animals Act.

2.3. Comparison of four peptides concerning their BBB-passage efficiency

Here, we compared four D3 derivatives concerning their efficiencies to cross the murine BBB after i.p. administration to C57BL/6N mice. We investigated the linear 12-mer peptide RD2, the cyclic 13-mer peptide cD3r as well as two cyclic 24-mer tandem peptides, cRD2D3 and cD3D3. All peptides had previously shown promising *in vitro* results. Their sequences are shown in Table 1.

2.3.1. Concentration-time profiles for peptide selection

To determine the concentration-time profiles of cRD2D3, RD2, cD3r, and cD3D3 after i.p. administration (30, 60, 240, 1440 min) in murine brain, plasma, and CSF, mixed solutions of non-labelled and ^{3}H-labelled peptides were prepared. The administered solutions contained 3 mg/mL of the respective peptide including small amounts of ^{3}H-labelled peptides (1.86 µg/mL ^{3}H-cRD2D3, 0.65 µg/mL ^{3}H-RD2, 0.64 µg/mL ^{3}H-cD3r, or 1.52 µg/mL ^{3}H-cD3D3). Doses were administered by body weight with 10 mg/kg. Three to five mice were investigated per time point whereby for two time points (RD2: 240 min, cD3r: 1440 min), CSF could only be taken from two mice.

Approximately 10 min before each sampling time point, the respective animal was anesthetized with i.p. ketamine/medetomidine anesthesia. Once the mouse was deeply narcotized, the *cisterna magna* was laid free and punctuated to extract about 5 µL CSF with a small capillary as described before (Liu et al., 2012). Afterwards, blood was taken by heart puncture. Heparinized blood was centrifuged (3000*g*, 5 min, 4 °C) to get plasma, which was 1:1 diluted with PBS (phosphate-buffered saline). The right brain hemisphere was extracted, weighed, and homogenized in 500 µL PBS (Precellys Ceramic Kit 1.4 mm, Precellys 24, Bertin technologies SAS, France). 100 µL diluted plasma or brain homogenate (in triplicate each), or 5 µL CSF (single determination) were mixed with 10 mL scintillation cocktail (Ultima Gold XR, PerkinElmer, USA) and incubated overnight (100 rpm, room temperature). Quantitative measurements were carried out in a liquid scintillation counter (LSC) (Packard Tri-Carb 2100TR Liquid Scintillation Analyzer, PerkinElmer, USA). LSC results (dpm/sample) were converted into mg/mL or % injected dose (%ID)/mL for plasma and for CSF, or in mg/g or %ID/g for brain as described before (Jiang et al., 2015). Total peptide concentrations in the samples were back-calculated from the measured ^{3}H-labelled peptides' radioactivity.

The determined peptide concentrations were plotted over time to allow for comparison of all peptides' uptakes into brain, plasma, and CSF. Concentrations at 0 min were set to be 0%ID/mL or 0%ID/g. To make differences more obvious, the areas under the concentration-time curves from the first to the last measured time point (AUC_{last}) and the maximum concentrations (C_{max}) were determined by Phoenix WinNonlin (Non-Compartmental Analysis and PK/PD Modeling and Simulation, Certara).

2.3.2. Correlation of peptides' brain, CSF, and plasma concentrations

Additionally, peptide concentrations in brain, CSF, and plasma were assessed in relation to each other: brain/CSF, brain/plasma, and CSF/plasma ratios were computed and plotted over time.

2.4. Further characterization of the peptide with the highest efficiency to cross the BBB: cRD2D3

2.4.1. Proteolytic stability

Proteolytic stability was investigated by thin layer chromatography (TLC) after incubation of a ^{3}H-cRD2D3 (cyclic D-peptide, 11.76 µM) or ^{3}H-L-D3 (linear L-peptide, 9.71 µM) solution in murine plasma, brain-, liver-, and kidney-homogenate as well as in human liver microsomes

(Sigma-Aldrich, Germany) as described before (Jiang et al., 2015; Leithold et al., 2016b). ^{3}H-L-D3 served as control for enzyme functionality. In brief, ^{3}H-peptide solutions were mixed 1:3 with murine plasma, organ-homogenates, or human liver microsomes solution and incubated for 0, 4, and 24 h at 37 °C on a shaker with 300 rpm. After the respective incubation time, the enzymes in the different solutions were denatured by adding 2 µL mobile phase (10 mL 28% ammonia/34 mL pyridine/39 mL *n*-butanol/26 mL double distilled H_2O) to each 5 µL incubated solution. 2 µL of the denatured solutions were spotted on ProteoChrom HPTLC Silica gel 60 F_{254s} plates (Merck, Germany) and put into a TLC chamber with mobile phase until the solvent front reached about 5 cm. After drying, the TLC plate was developed on a Fuji Imaging Plate BAS-TR2025 20 × 25 cm (FUJIFILM, Japan) for 72 h and analyzed with a BAS reader with AIDA software (Raytest GmbH, Germany) similar to the tests for ^{3}H-RD2D3 described before (Leithold et al., 2016b).

2.4.2. Plasma protein binding

cRD2D3's plasma protein binding (PPB) to human serum albumin (HSA) and to α1-acid glycoprotein (AGP) was analyzed according to the manufacturer's protocol of TRANSIL^{XL} HSA and AGP binding kits (Sovicell GmbH, Germany). To cover a larger range of HSA and AGP concentrations, the bead concentrations in the kits were modified. For detection, a mixture of ^{3}H-cRD2D3 and non-labelled cRD2D3 (final concentration of 4.8 µM) was added to different HSA (7.4 µM to 420 µM, 9 different concentrations) or AGP concentrations (0.04 µM to 30 µM, 18 different concentrations). The amount of unbound cRD2D3 (in %) was determined using the LSC. The *Kd* as well as the free drug fraction (f_u) in human plasma were calculated as described before (Leithold et al., 2016b). The calculation is based on a cRD2D3 blood concentration of 0.29 µM, which was measured in the blood 4 h after single oral administration (10 mg/kg).

2.4.3. Pharmacokinetic profiles

To determine cRD2D3's concentration-time profiles after i.p., intravenous (i.v.) and oral (p.o.) administration in murine plasma, brain, liver, and kidney, again a mixed solution of non-labelled and ^{3}H-labelled cRD2D3 was prepared. For i.p. and p.o. administration the solution contained 3 mg/mL cRD2D3 (including 1.86 µg/mL ^{3}H-cRD2D3). For i.v. administration the solution contained 1 mg/mL (including 0.62 µg/mL ^{3}H-cRD2D3). Doses were administered per body weight (i.p. and p.o. 10 mg/kg, i.v. 3.3 mg/kg). Approximately 2 min before each organ harvesting time point, the respective animal was anesthetized with isofluran (cp-pharma, Germany) inhalation anesthesia. Organs were harvested as follows: i.p.: 10, 20, 30*, 60, 120, 180, 240*, 360, 840, 1080, 1440*, 2880, 5760 min; time points marked with * were taken from Section 2.3.1 for animal health and safety considerations; i.v.: 5, 10, 15, 30, 60, 240, 360, 840, 1080, 1440, 2880, 5760 min; p.o.: 10, 30, 60, 120, 180, 240, 360, 840, 1080, 1440, 2880, 5760 min; three mice for each time point except of one (5760 min, i.v., only two mice). Blood was taken by heart puncture. The following steps and calculations were carried out as described above (Section 2.3.1). CSF was not taken but instead about 200 mg of the liver and the right kidney were extracted and investigated similar to the right brain hemisphere. All samples were quantified in triplicate by LSC measurements. Total cRD2D3 concentrations in the samples were back-calculated from the measured ^{3}H-cRD2D3 radioactivity.

2.4.4. Pharmacokinetic parameters

To determine cRD2D3's pharmacokinetic parameters for plasma and brain, concentration-time profiles were analyzed. 0 min plasma and brain concentrations for i.p. and p.o. administration as well as 0 min brain concentrations for i.v. administration were set to be 0 mg/mL or mg/g while 0 min plasma concentrations for i.v. administration were linearly back-extrapolated based on the first two measured time points (5 min, 10 min). Non-compartmental data analysis was performed in combination of different programs as described before (Leithold et al., 2016a): the AUC_{last}, the area under the first moment curve from the first to the last measured data pair ($AUMC_{last}$), the mean residence time (MRT), and the terminal elimination rate constant (λ_z, nonlinear regression of the last three (i.p., i.v.) to five (p.o.) measured concentrations) were calculated using Phoenix WinNonlin. Further pharmacokinetic parameters were calculated with the help of the formulas listed in Table 2.

Table 2
Formulas for calculation of pharmacokinetic parameters and BBB values.

		Unit	Formula
Pharmacokinetic parameter			
$t_{1/2}$	Terminal half-life	h	$t_{1/2} = \ln(2)/\lambda_z$
D	Dose	mg/kg	
$F_{AUC_{last}}$	Bioavailability	%	$F_{AUC_{0-last}} = \frac{AUC_{last_{e.v.}} * D_{i.v.}}{AUC_{last_{i.v.}} * D_{e.v.}}$
CL	Terminal plasma clearance	mL/(min * kg)	$CL = \lambda_z * V_{last}$
BBB value			
logBB	Blood-brain equilibrium distribution	–	$\log BB = \log (AUC_{last,br}/AUC_{last,pl})$
K_{in}	Unidirectional influx rate constant	mL/(g * min)	$\frac{C_b(t)}{C_p(t)} = K_{in} * \frac{AUC_p(t)}{C_p(t)} + V_i$
V_i	Initial distribution volume	mL/g	
PS	Permeability surface-area product	mL/(g * min)	$PS = (-CBF) * \ln(1 - K_{in}/CBF)$
CBF	(Murine) cerebral blood flow	mL/(g * min)	1.07 (Muir et al., 2008)

Additionally, we determined some universally used BBB values to allow for direct comparison with other peptides (Van Dorpe et al., 2012): the blood-brain equilibrium distribution (logBB), the universal influx rate constant (K_{in}), the initial distribution volume in brain (V_i), and the permeability surface-area product (PS). The BBB values were determined based on the i.v. concentration-time profile values and pharmacokinetic parameters with formulas listed in Table 2. K_{in} and V_i were graphically determined by plotting the brain concentration to plasma concentration ratio at certain time points (C_b (t)/C_p (t) [mL/g]) on the y-axis against the exposure time (AUC_p (t)/C_p (t) [min]) on the x-axis. For both peptides, the linear range was between 0 and 240 min (R^2 (cRD2D3): 0.9216, R^2 (RD2D3): 0.9995). For calculation of the PS, the murine cerebral blood flow (CBF) was assumed to be 1.07 mL/(g * min) (Muir et al., 2008).

3. Results

3.1. Comparison of four peptides concerning their BBB-passage efficiencies

3.1.1. Concentration-time profiles for peptide selection

We compared four peptides regarding their efficiencies to enter the brain. cRD2D3's, RD2's, cD3D3's, and cD3r's concentration-time profiles in brain, plasma, and CSF after i.p. administration are shown in Fig. 1. The highest AUC_{last} as well as C_{max} in the brain was observed for cRD2D3, followed by RD2, cD3D3, and cD3r. Peptide concentrations in CSF revealed the same order as in the brain. All investigated peptides showed plasma concentration-time courses in the same range whereby initial concentrations (0.5 h after administration) were highest for the single peptides RD2 and cD3r. In plasma, C_{max} was highest for RD2 followed by cD3r, cRD2D3, and cD3D3.

3.1.2. Correlation of peptides' brain, CSF, and plasma concentrations

We further investigated whether peptides' concentrations in brain, plasma, and CSF correlated by calculating brain/plasma, CSF/plasma,

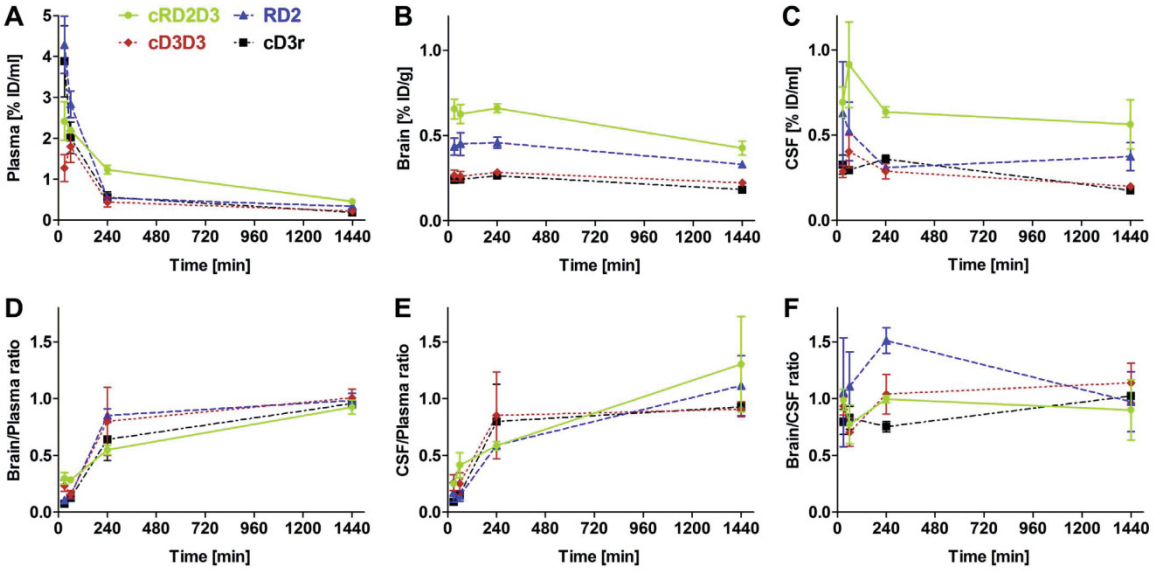

Fig. 1. Concentration-time profiles of four peptides and their ratios in murine plasma, CSF, and brain.
Mixtures of non-labelled and ^{3}H-labelled cRD2D3 (*green line, diamonds*), RD2 (*blue dashed line, triangles*), cD3D3 (*red dashed line, diamonds*), and cD3r (*black dashed line, squares*) were administered i.p. (10 mg/kg) to wildtype mice. ^{3}H-peptides' concentrations (triplicate) in plasma (A), brain (B), and CSF (C) were measured with liquid scintillation counting. Total peptide concentrations were calculated as % of the injected dose per g or mL (% ID/g for the brain; % ID/mL for plasma and CSF) and plotted over time.
Brain concentrations in % ID/g, CSF, and plasma concentrations in % ID/mL for each peptide were assessed in relation to each other. The brain/plasma (D), CSF/plasma (E), and brain/CSF (F) ratios were plotted over time to investigate correlation. (For interpretation of the references to color in this figure legend, the reader is referred to the web version of this article.)

and brain/CSF ratios (Fig. 1). Here, we showed a strong and direct correlation between all peptides' brain and CSF concentrations as the brain/CSF ratios were approx. 1 already 0.5 h after administration. In the following time course, some fluctuations were detected (4 h: ratios between 0.8 and 1.5). However, all peptides' brain/CSF ratios returned to approx. 1 24 h after administration. Brain/plasma as well as the CSF/plasma ratios time-dependently increased from low values shortly after administration (1 h: ratios between 0.1 and 0.4) to values of about 1 at 24 h after administration.

After evaluation of the concentration-time profiles (Fig. 1) cRD2D3 was selected as most promising of those four D-enantiomeric AD drug candidates regarding its efficiency to enter the brain and was subsequently characterized in more detail.

3.2. Further characterization of the peptide with the highest efficiency to cross the BBB: cRD2D3

3.2.1. Proteolytic stability

The proteolytic stability of the D-enantiomeric peptide cRD2D3 was investigated *ex vivo* in brain, liver, and kidney homogenates, in plasma, and in human liver microsomes and autoradiographically visualized *via* TLC. The TLC profile of ^{3}H-L-D3, the L-enantiomeric control peptide for enzyme activity, showed additional bands (black arrows) after incubation in brain, liver, and kidney homogenates, in plasma and human liver microsomes indicating proteolytic digestion (Fig. 2). In contrast, the TLC profile of ^{3}H-cRD2D3 did not show any additional bands even after 24 h of incubation suggesting proteolytic stability of the D-peptide.

3.2.2. Plasma protein binding

In order to estimate the plasma protein binding of cRD2D3 and thus, the unbound fraction (f_u), we investigated the dissociation constants of cRD2D3 to the two most abundant proteins in human plasma, HSA and AGP. Our results showed higher affinity of cRD2D3 to AGP (*Kd*: 1.2 μM, f_u: 6%) than to HSA (*Kd*: 33 μM, f_u: 5%) (Fig. 3). The overall predicted f_u in plasma considering binding to both investigated plasma proteins was 2.8%.

3.2.3. Pharmacokinetic profiles

Since we have shown that cRD2D3 efficiently passes the BBB, we generated a full pharmacokinetic profile of this peptide including brain, plasma, liver, and kidney concentration-time profiles and compared three different administration routes: i.p., i.v., and p.o. In general, these profiles showed the highest cRD2D3 concentrations in liver and kidney (metabolization and excretion) followed by plasma (distribution) and brain (site of action) (Fig. 4). This was especially pronounced for i.v. and i.p. administration, whereas the concentrations after oral administration were in a comparable range in all organs. The maximum concentration relative to the dose (C_{max}/D) after i.v. administration was detected immediately after the administration while the C_{max}/D for i.p. administration was detected 10 min after administration. From about 6 h after administration until 2 days after administration, the plasma concentration-time courses were very similar for all administration routes. On day 3 and 4 after administration, plasma concentrations following i.v. administration declined faster than those after i.p. and p.o. administration, finally leading to shorter terminal half-life ($t_{1/2}$) values after i.v. administration (Section 3.2.4).

The administration routes which are followed by initial high plasma concentration peaks, i.v. and i.p., were linked to much higher cRD2D3 concentrations in liver and kidney from the beginning to the last measured time point. In contrast, cRD2D3's concentration-time course in the brain was independent from the administration route (Fig. 4). These findings suggest that uptake and deposition of cRD2D3 in liver and kidney are concentration dependent whereas cRD2D3's uptake into the brain, which is of particular importance for an AD drug candidate, underlies a saturable mechanism.

3.2.4. Pharmacokinetic parameters

Despite the small initial concentration peaks after i.v. and i.p.

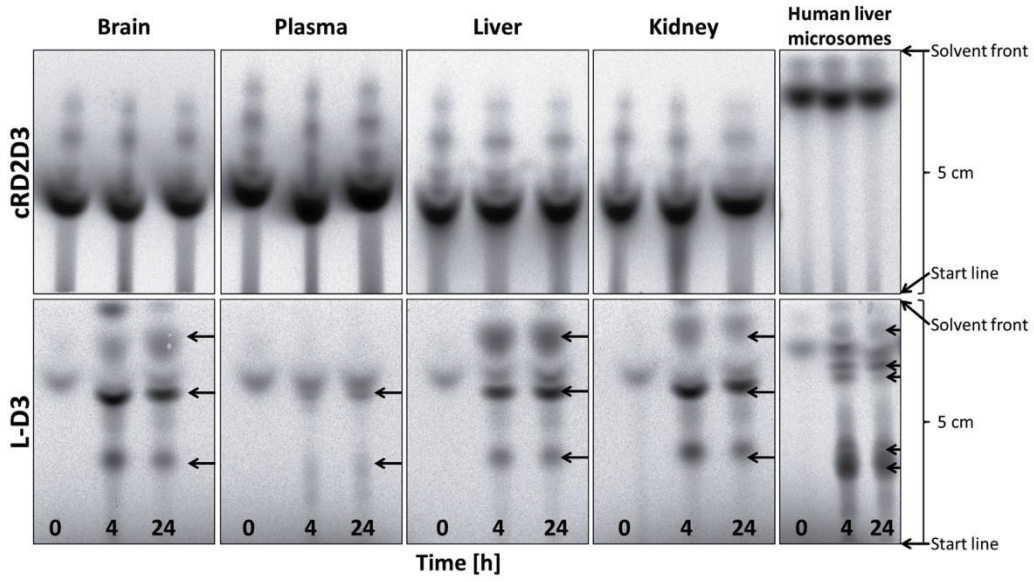

Fig. 2. Proteolytic stability.
^{3}H-cRD2D3's and ^{3}H-L-D3's (control) proteolytic stability after incubation in murine organ homogenates and plasma as well as in human liver microsomes was investigated. Samples and potential metabolites were separated *via* thin layer chromatography and bands were detected by autoradiography. Arrows highlight ^{3}H-L-D3 metabolites. As ^{3}H-cRD2D3 did not show any additional bands after incubation in the respective solutions, no metabolites were detected and cRD2D3 was considered proteolytically stable.

administration in plasma, drug exposure over time relative to the dose (AUC_{last}/D) was similar for all administration routes (approx. 0.6 (min ∗ mg/mL)/(mg/kg)). This is also why bioavailabilities (F) for i.p. and p.o. administration were calculated to be about 100%. The mean residence time (MRT) increased from i.v. (29 h) over i.p. (34 h) to p.o. (39 h) administration. Terminal clearance (CL) was slightly lower for i.p. and p.o. than for i.v. administration while calculated $t_{1/2}$ values following i.p. and p.o. administration (58 h) were considerably longer than following i.v. administration (29 h) (Table 3). In the brain, values for C_{max}/D ranged between 0.23 and 0.28 (µg/g)/(mg/kg), and for AUC_{last}/D between 0.53 and 0.61 (min ∗ mg/mL)/(mg/kg) indicating that both values were independent from the administration route (Table 3). Brain/plasma ratios for all administration routes increased from low ratios (i.p. 0.32, p.o. 0.57, and i.v. 0.14) early after administration to ratios around 1 which remained from 4 h after administration until the last measured time point (Fig. 5). Notably, the brain/plasma ratio after p.o. administration was higher than 1 already 1 h after administration, which was due to the lack of any plasma concentration peak after p.o. administration.

3.3. Impact of cyclization on a peptide's efficiency to cross the blood-brain barrier

We hypothesized that cyclization has a noteworthy influence on the peptide's pharmacokinetic parameters, especially raising its efficiency to pass the BBB, which is considered to be favorable for AD drugs. To proof this hypothesis, we compared cRD2D3 data to data of its linear equivalent RD2D3, which had been generated by Leithold, Jiang et al. before, using exactly the same experimental setup (Jiang et al., 2015; Leithold et al., 2016a) (Table 4). Comparing brain AUC_{0-2880}/D as well as brain concentrations (1 h after administration) of both, cyclic and linear, D-peptides after i.p. and i.v. administration, we could substantiate our hypothesis. cRD2D3's AUC_{0-2880}/D in the brain was 3.8 (i.p.) and 6.6 (i.v.) times higher than RD2D3's. One hour after administration, cRD2D3's brain concentrations were 5.9 (i.p.) and 7.1 (i.v.) times higher than RD2D3's (Table 4).

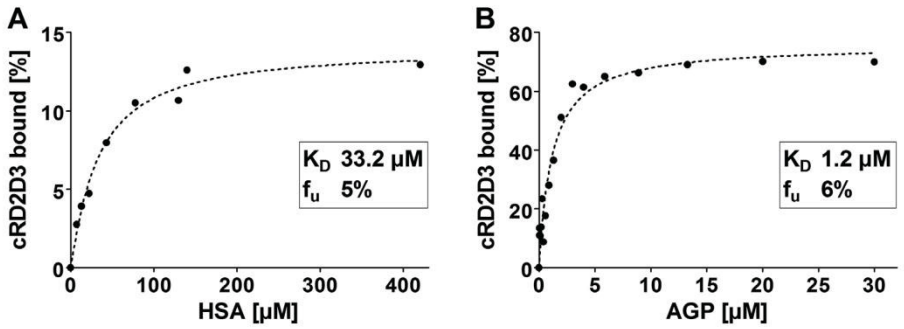

Fig. 3. Plasma protein binding to human serum albumin (HSA) and α1-acid glycoprotein (AGP).
Plasma protein binding (PPB) of a mixture of ^{3}H-cRD2D3 and cRD2D3 to HSA (A) and AGP (B) was investigated. The cRD2D3 amount (%) bound to HSA or AGP after incubation was plotted against the respective plasma protein concentration. The dissociation constants (*K*d) and fractions unbound (f_u) were determined. PPB was stronger to AGP than to HSA.

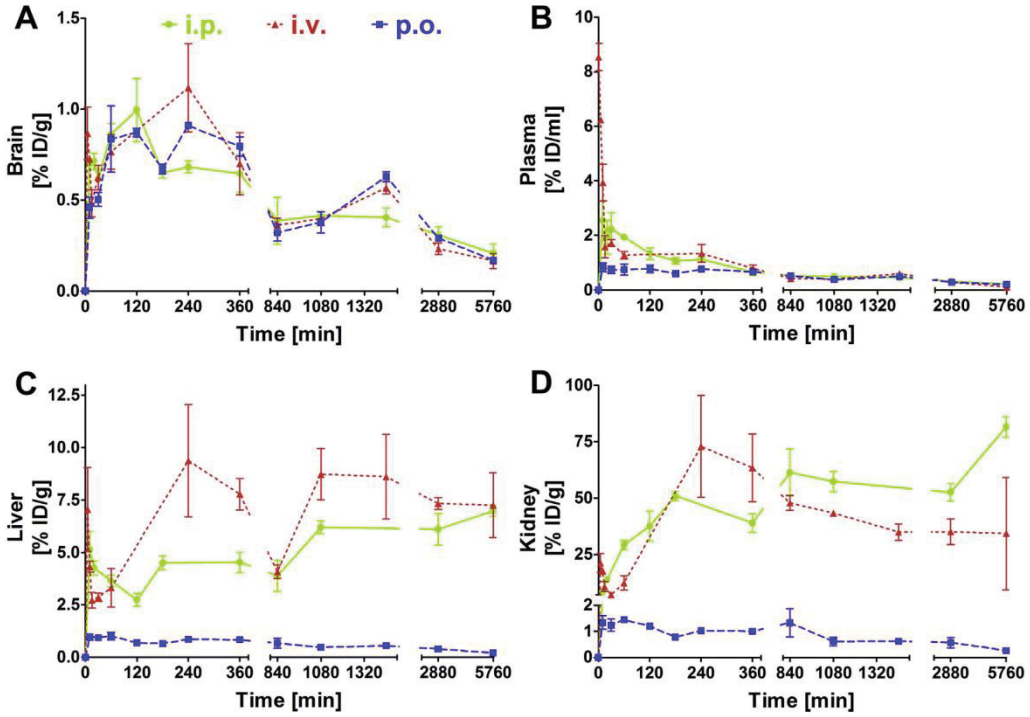

Fig. 4. Pharmacokinetic profiles of cRD2D3.
Mixtures of non-labelled and ^{3}H-labelled cRD2D3 were administered to wildtype mice: i.p. (10 mg/kg; *green line, diamonds*), i.v. (3.3 mg/kg; *red dashed line, triangles*), and p.o. (10 mg/kg; *blue dashed line, squares*). ^{3}H-cRD2D3 concentrations (triplicate) in brain (A), plasma (B), liver (C), and kidney (D) were measured with liquid scintillation counting. Total peptide concentrations were calculated as % of the injected dose per g or mL (% ID/g for brain, liver, and kidney; % ID/mL for plasma) and plotted over time. (For interpretation of the references to color in this figure legend, the reader is referred to the web version of this article.)

Table 3
Pharmacokinetic parameters for cRD2D3 in murine plasma and brain.

Parameter	Unit	i.v.	i.p.	p.o.
Plasma				
C_{max}/D	(µg/mL)/(mg/kg)	1.64	0.69	0.24
AUC_{last}/D	(min ∗ mg/mL)/(mg/kg)	0.60	0.65	0.59
MRT	h	29	34	38
λ_z	1/min	0.0004	0.0002	0.0002
$t_{1/2}$	h	29	58	58
F (AUC_{last})	%	100[b]	108[a]	98
CL	mL/(min ∗ kg)	1.5	1.1	1.2
Brain				
C_{max}/D	(µg/g)/(mg/kg)	0.23	0.28	0.25
AUC_{last}/D	(min ∗ mg/g)/(mg/kg)	0.53	0.56	0.61

See list of abbreviations for explanation of pharmacokinetic parameters.
[a] Interindividual fluctuations lead to a mathematical bioavailability of 108%.
[b] By definition.

Next, we verified that higher cRD2D3 concentrations in brain resulted from cRD2D3's more efficient BBB permeation and not from higher cRD2D3 concentrations in plasma by comparing the amounts of cRD2D3 and RD2D3 found in plasma ($AUC_{0–2880}$/D, plasma concentrations 1 h after administration). Thereby, we showed that uptake into plasma (after i.p. administration), and clearance out of plasma (after i.p., and i.v. administration) did not notably differ between cRD2D3 and RD2D3: cRD2D3's $AUC_{0–2880}$/D in plasma was only 2.4 (i.p.) or 4.5 (i.v.) times higher than RD2D3's while plasma concentrations were nearly equal for cRD2D3 and RD2D3 1 h after administration (Table 4). Furthermore, the brain/plasma ratio based on the $AUC_{0–2880}$/D was determined. For cRD2D3, the ratio was 1.62 (i.p.) or 1.37 (i.v.) times higher than for RD2D3 (Table 4) leading to the conclusion that brain uptake across the BBB was more efficient for the cyclic peptide and independent from its uptake into plasma.

The BBB values determined for cRD2D3 and RD2D3 (RD2D3 values based on data which had been generated by Leithold, Jiang et al. before using exactly the same experimental setup (Jiang et al., 2015; Leithold et al., 2016a)) were listed in Table 4 to allow for direct comparison of the cyclic peptide and its linear equivalent. While the logBB value represents the blood-brain equilibrium distribution, the K_{in} describes the kinetics of the BBB permeability. Directly linked to determination of the K_{in} is the V_i describing the investigated peptides' fictional distribution volume in the brain shortly after administration. Here, we determined a nearly threefold higher logBB value for cRD2D3 than for RD2D3. K_{in} was nearly seven times higher for cRD2D3 than for RD2D3, and V_i was nearly four times higher for the cyclic than for the linear D-peptide. Finally, the permeability surface-area product (PS), representing uptake clearance from blood to brain, was determined. As PS values were, due to the estimated CBF of 1.07 mL/(g ∗ min) (Muir et al., 2008), nearly the same values as the K_{in} values, the relative proportion between cRD2D3 and RD2D3 was the same as for K_{in}.

To investigate whether increased BBB penetration is a general property of cyclic peptides, we compared cD3D3 and cD3r with their linear equivalents D3D3 (Leithold et al., 2016a) and D3 (Jiang et al., 2015) after i.p. administration. Here, we could show once more that all brain concentrations of the cyclic peptides were considerably higher than those of their linear equivalents while plasma concentrations were in the same range (Fig. 6). Taking the brain/plasma ratios based on the $AUC_{0–1440}$ into account we found factors between the cyclic and the

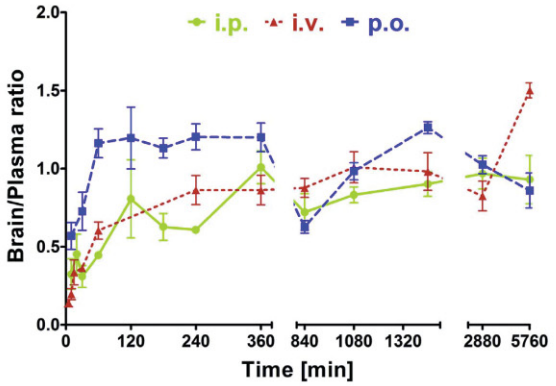

Fig. 5. Brain/Plasma ratios for different cRD2D3 administration routes.
Ratios of cRD2D3 brain concentrations divided by cRD2D3 plasma concentrations were plotted over time after administration to wildtype mice: i.p. (*green line, diamonds*), i.v. (*red dashed line, triangles*) and p.o. (*blue dashed line, squares*). Concentrations in brain and plasma equalized fastest after p.o. administration as the brain/plasma ratio was about 1 already 60 min after administration. (For interpretation of the references to color in this figure legend, the reader is referred to the web version of this article.)

Table 4
Pharmacokinetic parameters and BBB values for cRD2D3 and RD2D3* (Leithold et al., 2016a) in murine brain and plasma.

Parameter	Unit	i.v.		i.p.	
		cRD2D3	RD2D3*	cRD2D3	RD2D3*
Brain					
AUC_{0-2880}/D	(min * mg/g)/(mg/kg)	0.37	0.06	0.35	0.09
$C_{60\ min}/D$	(µg/g)/(mg/kg)	0.17	0.02	0.23	0.04
Plasma					
AUC_{0-2880}/D	(min * mg/mL)/(mg/kg)	0.45	0.10	0.43	0.18
$C_{60\ min}/D$	(µg/mL)/(mg/kg)	0.29	0.28	0.52	0.47
$t_{1/2}$	h	29	0.85	58	2.29
BBB values					
AUC_{0-2880}/D (brain)/ AUC_{0-2880}/D (plasma)	–	0.82	0.60	0.81	0.50
logBB	–	− 0.086	− 0.222	na	na
K_{in}	mL/(g * min)	0.002	0.0003	na	na
V_{in}	mL/g	0.1955	0.0512	na	na
PS	mL/(g * min)	0.002	0.0003	na	na

linear peptides' ratios of 1.46 for the comparison between cD3r and D3, and 3.67 for the comparison between cD3D3 and D3D3.

4. Discussion

Initially, we compared four D-enantiomeric peptides concerning their efficiencies to cross the BBB. For AD drugs, passing the BBB is particularly important as the brain is the potential site of action. Considering brain, plasma, and CSF concentration-time profiles of the investigated D-peptides after i.p. administration, cRD2D3 overall achieved the highest brain and CSF concentrations (Fig. 1). Its plasma concentration-time profile was in the same range as the other peptides' profiles. These findings suggested that cRD2D3 was similarly taken up into plasma after i.p. administration but revealed an extraordinarily high drug exposure in the brain. This was not expected before since permeability for the BBB was thought to be dependent on the peptide lengths (Leithold et al., 2016a). cRD2D3 consists of twice as many amino acid residues as RD2 and cD3r and includes the same number of amino acid residues as cD3D3 (Table 1). Remarkably, comparison of brain concentrations of the linear 12-mer peptide RD2 and the cyclic 13-mer peptide cD3r disclosed that the linear peptide yielded higher brain concentrations than the cyclic one although they do consist of the same amino acid residues (except of one additional arginine in cD3r), only arranged in different sequences (Table 1). Obviously, the amino acid residue sequence of RD2 had more beneficial influence on BBB permeability than the sequence of D3 in combination with cyclization. Summarizing, cRD2D3 combined both beneficial BBB permeation properties, cyclization and the RD2 sequence, and is thus the D-peptide with the highest brain levels. As we were interested whether peptide concentrations in brain and CSF correlate, we investigated the peptides' brain/plasma, CSF/plasma, and brain/CSF ratios (Fig. 1). Brain/plasma and CSF/plasma ratios increased from values around 0.1 and 0.4 shortly after administration to values around 1 at 24 h after administration. This suggested that it took some time until the equilibrium between plasma and brain as well as plasma and CSF was reached. In contrast, there was no gradient to overcome between brain and CSF concentrations as the brain/CSF ratio was about 1 already at the first measured time point. Although a clear distinction of D-peptide penetration into CSF, across the blood-CSF barrier in the choroid plexus, and D-peptide penetration into the brain parenchyma, across the BBB, has to be made (Pardridge, 2016), correlation of D-peptide concentrations in brain parenchyma with those in CSF is reasonable. Of course, D-peptides' transport across the BBB cannot directly be reflected by their CSF concentrations as permeation of substances from CSF into the brain parenchyma is restricted by slow diffusion. Remarkably, the CSF/plasma ratio of IgG and other therapeutic antibodies is in the range of 0.2% (Pardridge, 2016) whereas the D-peptides investigated in this study reached CSF/plasma as well as brain/plasma ratios higher than 50% already 4 h after administration. Additionally, the D-peptides' brain/CSF ratios were about 100% (ratios varied between 75 and 150%) from the first (30 min) to the last (1440 min) measured time point. Summarizing, these findings speak for direct BBB permeation of the D-peptides from plasma into the brain; instead of initial blood-CSF barrier (choroid plexus) permeation from plasma into the CSF, which would then be followed by slow diffusion from CSF into the brain.

The methodology applied here does not allow for differentiation between the amount of D-peptide in brain parenchyma compared to the amount of D-peptide in and on brain capillaries. However, Jiang et al. have previously shown that the fluorescently labelled D-enantiomeric D3 (Table 3), the lead compound after which the peptides examined in this study were designed, did not bind to capillaries in the brain (Jiang et al., 2016). Furthermore, as animals were sacrificed by heart puncture, only little blood was left in the brain after finalization. Thus, we considered the residual volume of blood in the brain and bound to brain vessels as negligible.

Besides other advantages, we designed D-peptides targeting Aβ oligomers because of their high proteolytic stability. Here, we proved that cRD2D3 can be considered proteolytically stable as no additional band appeared in the TLC profile after incubation in plasma, organ homogenates, or human liver microsomes within 24 h of incubation. Of note, cRD2D3 already showed multiple bands at time point 0 h (negative control) most likely due to peptide binding to different ingredients of the respective organ homogenate or plasma solution, resulting in different retention times in the TLC. To show that degrading enzymes in the respective solutions were proteolytically active, an L-enantiomeric control peptide was also incubated and, as expected, additional bands in its TLC patterns were observed already after 4 h incubation indicating formation of metabolites. No metabolites were observed after cRD2D3 incubation. Thus, the measured ^{3}H-cRD2D3 radioactivity was anticipated to correctly reflect the total cRD2D3 concentration in the following pharmacokinetic experiments as described for other D-peptides before, where this methodology was evaluated in further detail (Jiang et al., 2015; Leithold et al., 2016a; Leithold et al., 2016b). All

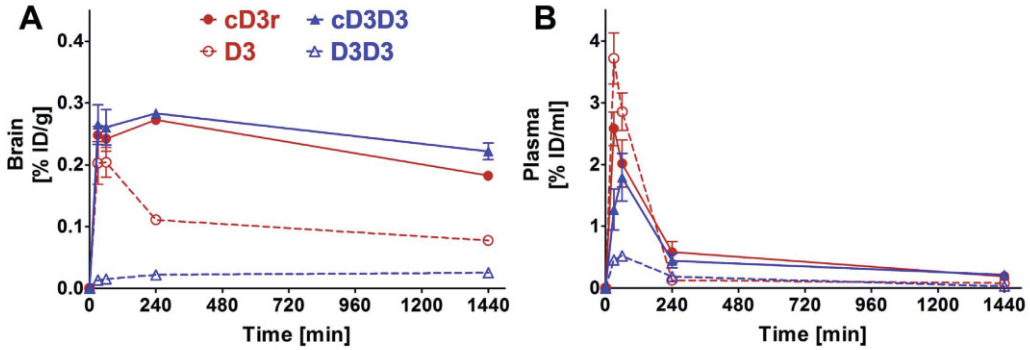

Fig. 6. Comparison of cyclic and linear peptides' brain and plasma concentration-time profiles.
Mixtures of non-labelled and ^{3}H-labelled of two cyclic D-enantiomeric peptides (cD3r: *red line, filled circles*; cD3D3: *blue line, filled triangles*) and their linear equivalents (D3: *red dashed line, open circles*; D3D3: *blue dashed line, open triangles*) were i.p. (10 mg/kg) administered to wildtype mice. ^{3}H-peptides' concentrations (triplicate) in brain (A) and plasma (B) were measured with liquid scintillation counting. Total peptide concentrations were calculated as % of the injected dose per g or mL (% ID/g for brain; % ID/mL for plasma) and plotted over time. Values for D3 were derived from Jiang et al. (Jiang et al., 2015) and values for D3D3 were derived from Leithold et al. (Leithold et al., 2016a). (For interpretation of the references to color in this figure legend, the reader is referred to the web version of this article.)

peptides were tritium-labelled in position 4 and 5 of a D-leucine amino acid residue (4,5-^{3}H-D-Leu) by tritium gassing of a precursor peptide which included 4,5-dehydro-D-leucine. As the tritium-label position is in an alkyl group, the labels were considered to be biologically stable. Any significant fraction of metabolites formed from cRD2D3 would have led to additional radioactive bands in the autoradiography of the TLC plate. In addition, recently Elfgen et al. conducted stability experiments with the lead compound D3 (Table 3), where they could show that the peptide was stable after different incubation periods in different media simulating the oral administration route (*e.g.* plasma, and human liver microsomes) using reversed phase HPLC analytics (Elfgen et al., 2017).

The stronger a drug binds to plasma proteins, the smaller is the amount of the drug freely circulating in plasma (f_u). High plasma protein binding might result in lower concentrations at the site of action but can also be advantageous because plasma proteins can work as drug releasing depot. This depot function can lead to consistent drug distribution in plasma over time. Thus, the risk of adverse side effects is lowered while longer MRTs are achieved (Gillette, 1973; Lambrinidis et al., 2015). In the most favorable case, once daily drug administration becomes possible for therapeutic regimens, which in turn is known to lead to the highest possible compliance (Eisen et al., 1990). We investigated binding to HSA which tends to bind acidic and neutral drugs rather than basic ones and to AGP which tends to bind alkaline drugs. These two proteins represent about 55% (HSA) and 1–3% (AGP) of all human plasma proteins (Lambrinidis et al., 2015). For cRD2D3, we expected stronger binding to AGP due to the high amount of basic arginines in its amino acid sequence (Table 1). This assumption was verified (*K*d AGP: 1.2 μM; *K*d HSA: 33 μM). Here, we calculated a total f_u of 2.8% considering influence of HSA and AGP. As > 97% of the administered drug is bound to plasma proteins, the above mentioned advantages might play a role for cRD2D3.

Having a closer look at cRD2D3's concentration-time profiles in the drug metabolization and excretion organs (liver and kidney) revealed a huge difference depending on the respective administration route (Fig. 4). The discrepancy might be explained by the initial high (i.v. and i.p.) or low (p.o.) plasma concentrations following drug administration. The more cRD2D3 was taken up directly after administration, the higher were the concentrations in liver and kidney hours after administration. This suggests that cRD2D3 may be enriched in these organs after i.v. and i.p. administration and is only slowly excreted from there. Compared to other previously examined D-peptides, the calculated CL values were quite similar within all administration routes (cRD2D3: i.v. 1.5, i.p. 1.1, p.o. 1.2 mL/(min ∗ kg); RD2D3 (Leithold et al., 2016a): i.v. 10.2, i.p. 5.4 mL/(min ∗ kg)). Nevertheless, the slightly different CL values as well as differences in λ_z and $t_{1/2}$ between intravenous and extravascular administration routes might be explained due to retarded distribution processes after extravascular administrations. As AD-treatment mainly targets elderly people and needs to be long-term, oral administration is the preferable administration route. In our experiments, low concentrations in liver and kidney were observed after oral administration. This is beneficial as strong accumulation can be a hindrance for adequate therapeutic dosing in long-term treatment. Furthermore, drugs with high oral bioavailability and long $t_{1/2}$ are of enormous benefit for long-term treatment. Thus, it additionally is of advantage that cRD2D3 is characterized by a much longer $t_{1/2}$ in plasma in contrast to its linear equivalent (Table 4). Of note, drugs with long $t_{1/2}$ are considered to be "forgiving drugs" and at the same time usually allow therapeutic regimens with once daily administration being beneficial for compliance (Eisen et al., 1990; Urquhart, 1996). Another beneficial property of cRD2D3 is a brain/plasma ratio higher than 1 already one hour after oral administration suggesting rapid uptake into the brain (Fig. 5).

In order to allow for BBB value comparison of the D-peptides examined in this study to other peptides listed in "Brainpeps: the blood-brain barrier peptide database", we determined different parameters (Table 4) (Van Dorpe et al., 2012): For cRD2D3, we calculated a nearly three times higher logBB value than for RD2D3 leading to the conclusion that the cyclic peptide enters the brain from plasma nearly three times more efficiently than the linear peptide. Nevertheless, one has to keep in mind that the logBB value depends on binding to plasma and brain tissue as well as on active transport. Graphic determination of K_{in} resulted in a nearly sevenfold higher K_{in} for cRD2D3 than for RD2D3 indicating that cRD2D3 crosses the BBB faster than RD2D3. As the calculated PS values did not notably differ from the previously determined K_{in} values, a higher uptake clearance from blood to brain for cRD2D3 than for RD2D3 is assumed. Comparison of the values determined for cRD2D3 with values of Dermorphin, a potent natural opioid consisting of five amino acid residues including one D-enantiomeric amino acid residue listed in "Brainpeps", revealed that they are in a similar range. K_{in} values determined for Dermorphin lie between 0.0002 and 0.0022 mL/(g ∗ min) while Dermorphin's V_i values were determined to be between 0.0162 and 0.0215 mL/g (Stalmans et al., 2015; Van Dorpe et al., 2010). As Dermorphin has even been suggested to be used as positive control in BBB permeability experiments (Van Dorpe et al., 2012), these results additionally underline cRD2D3's efficient BBB permeability.

As comparison of three cyclic peptides and their linear equivalents

with special attention to cRD2D3 and RD2D3 clearly indicated that cyclization has a positive impact on peptides' efficiencies to cross the BBB, it was of interest how this increased efficiency could be explained. Interestingly, brain concentrations were independent from any plasma concentration peak, which most likely suggests a saturable BBB passage mechanism. This was already reported in detail for the lead compound D3 by Jiang et al. (Jiang et al., 2016) and for the D3 derivative RD2 (Leithold et al., 2016b). D3 and RD2 have arginine-rich motifs (ARMs) and were suggested to be transported across membranes, and ultimately across the BBB, with a human deficiency virus type 1 (HIV-1) transactivator of transcription (Tat) like BBB transport mechanism (Futaki et al., 2003; Vives et al., 1997). As cRD2D3 is a cyclized version of the head-to-tail combination RD2D3, similarities in its pharmacokinetic behavior can be anticipated. However, the assumption for the underlying mechanism is also true for linear RD2D3, although the cyclic version is even more efficiently transported. We set up three hypotheses, which are partly connected to the HIV-1 Tat hypothesis, trying to explain this circumstance. According to our first hypothesis, cRD2D3 exposes the ARM with its numerous guanidinium groups more efficiently than the linear RD2D3, enabling passive transduction to a higher extent. According to the second hypothesis, cyclization downsizes the hydrodynamic radius of cRD2D3 and thus further simplifies passive transduction. Passive membrane permeability has been shown before for cyclic peptides (*e.g.* cyclosporine A) (Ahlbach et al., 2015). According to the third hypothesis, there might be a difference in cRD2D3's and RD2D3's brain efflux vulnerabilities by *e.g.* ATP binding cassette (ABC) transporters, and the Low Density Lipoprotein Receptor-related Protein 1 (LRP1) which might be more efficient for the linear RD2D3 than for the cyclic cRD2D3. Both, ABC transporters as well as LRP1 are responsible for the outward transport of peptides, *e.g.* Aβ, across the BBB from the brain back into the blood (Pahnke et al., 2014; Storck et al., 2016). As the N- and C-termini of cyclic peptides are modified, ABC transporters as well as LRP1 might not directly be able to identify the cyclic peptide, thus its transport out of the brain is decreased. Summarized, peptides' cyclization resulted in increased efficiencies to pass the murine BBB while the peptides' uptake from peritoneum into plasma, for example, was far less affected due to cyclization.

5. Conclusion

The hereby presented results suggest that concentrations of the investigated Aβ oligomer-targeting D-enantiomeric peptides in murine brain and CSF directly correlate. Furthermore, the head-to-tail cyclized D-peptide cRD2D3 was determined, out of four optimized D3 derivatives, to be the one with the highest efficiency to pass the murine BBB. Direct comparison of three cyclic D-peptides to their linear equivalents revealed an increase in the peptides' efficiencies to pass the murine BBB due to cyclization. Further experiments showed that cRD2D3 is characterized by high proteolytic stability and oral bioavailability, long duration of action and a favorable brain/plasma ratio proposing that it is a suitable drug for long-term AD-treatment from a pharmacokinetic perspective.

Abbreviations

ABC	ATP binding cassette
AD	Alzheimer's disease
ARM	arginine rich motif
AUC_p (t)	area under the curve in plasma from the first measured time point to time point t
AUC_{last}	area under the curve from the first to the last measured data pair
$AUMC_{last}$	area under the first moment curve from the first to the last measured data pair
Aβ	amyloid β
BBB	blood-brain barrier
CBF	(murine) cerebral blood flow
C_b (t)	D-peptide concentration in brain at time t
CL	clearance
C_{max}	maximum concentration
C_p (t)	D-peptide concentration in plasma at time t
CSF	cerebrospinal fluid
D	administered dose
e.v.	extravascular
f_u	free drug fraction; fraction unbound
F	bioavailability
i.p.	intraperitoneal
i.v.	intravascular
HIV-1	human deficiency virus type 1
ICS-6	Institute of Complex Systems, Structural Biochemistry
INM-4	Institute of Neuroscience and Medicine
Kd	dissociation constant
K_{in}	unidirectional influx rate constant
logBB	blood-brain equilibrium distribution
LRP1	Low Density Lipoprotein Receptor-related Protein 1
LSC	liquid scintillation counter
MRT	mean residence time
p.o.	oral
PBS	phosphate buffered saline
PPB	plasma protein binding
PS	permeability surface-area product
$t_{1/2}$	terminal half-life
Tat	transactivator of transcription
TLC	thin layer chromatography
V_i	initial distribution volume
λ_z	terminal elimination rate constant

Author contributions

A.W. and D.W. designed the overall study. D.W., A.W., J.K. and E.S. designed the experiments. E.S. and M.T. carried out preliminary experiments that were important for the final study design. E.S. and S.S. planned and carried out all pharmacokinetic experiments. E.S. calculated the pharmacokinetic parameters and implemented the proteolytic stability tests with support from L.H.E.L. and N.J. E.S. performed the plasma protein binding tests and evaluated the results with support from T.Z. E.S., A.W., J.K. and D.W. wrote the manuscript. All other authors contributed to writing.

Competing financial interest

The authors declare no competing financial interests.

Acknowledgement

D.W. and K.J.L. were supported by grants from the "Portfolio Technology and Medicine", and D.W. was additionally supported by the "Portfolio Drug Research" and the Helmholtz-Validierungsfonds of the "Impuls und Vernetzungs-Fonds der Helmholtzgemeinschaft". The study was supported by the TT-Fonds of the Technology Transfer Department of the Forschungszentrum Jülich.

References

Ahlbach, C.L., Lexa, K.W., Bockus, A.T., Chen, V., Crews, P., Jacobson, M.P., Lokey, R.S., 2015. Beyond cyclosporine A: conformation-dependent passive membrane permeabilities of cyclic peptide natural products. Future Med. Chem. 7, 2121–2130.

Anand, R., Gill, K.D., Mahdi, A.A., 2014. Therapeutics of Alzheimer's disease: past, present and future. Neuropharmacology 76 (Pt A), 27–50.

Bartnik, D., Funke, S.A., Andrei-Selmer, L.-C., Bacher, M., Dodel, R., Willbold, D., 2010. Differently selected D-enantiomeric peptides act on different Aβ species. Rejuvenation Res. 13, 202–205.

Brener, O., Dunkelmann, T., Gremer, L., van Groen, T., Mirecka, E.A., Kadish, I., Willuweit, A., Kutzsche, J., Jurgens, D., Rudolph, S., Tusche, M., Bongen, P., Pietruszka, J., Oesterhelt, F., Langen, K.J., Demuth, H.U., Janssen, A., Hoyer, W., Funke, S.A., Nagel-Steger, L., Willbold, D., 2015. QIAD assay for quantitating a compound's efficacy in elimination of toxic Abeta oligomers. Sci. Rep. 5, 13222.
Eisen, S.A., Miller, D.K., Woodward, R.S., Spitznagel, E., Przybeck, T.R., 1990. The effect of prescribed daily dose frequency on patient medication compliance. Arch. Intern. Med. 150, 1881–1884.
Elfgen, A., Santiago-Schubel, B., Gremer, L., Kutzsche, J., Willbold, D., 2017. Surprisingly high stability of the Abeta oligomer eliminating all-d-enantiomeric peptide D3 in media simulating the route of orally administered drugs. Eur. J. Pharm. Sci. 107, 203–207.
Funke, S.A., Willbold, D., 2009. Mirror image phage display—a method to generate D-peptide ligands for use in diagnostic or therapeutical applications. Mol. BioSyst. 5, 783–786.
Funke, S.A., van Groen, T., Kadish, I., Bartnik, D., Nagel-Steger, L., Brener, O., Sehl, T., Batra-Safferling, R., Moriscot, C., Schoehn, G., Horn, A.H., Muller-Schiffmann, A., Korth, C., Sticht, H., Willbold, D., 2010. Oral treatment with the D-enantiomeric peptide D3 improves the pathology and behavior of Alzheimer's disease transgenic mice. ACS Chem. Neurosci. 1, 639–648.
Futaki, S., Goto, S., Sugiura, Y., 2003. Membrane permeability commonly shared among arginine-rich peptides. J. Mol. Recognit. 16, 260–264.
Gillette, J.R., 1973. Overview of drug-protein binding. Ann. N. Y. Acad. Sci. 226, 6–17.
Haass, C., Selkoe, D.J., 2007. Soluble protein oligomers in neurodegeneration: lessons from the Alzheimer's amyloid beta-peptide. Nat. Rev. Mol. Cell Biol. 8, 101–112.
Jiang, N., Leithold, L.H., Post, J., Ziehm, T., Mauler, J., Gremer, L., Cremer, M., Schartmann, E., Shah, N.J., Kutzsche, J., Langen, K.J., Breitkreutz, J., Willbold, D., Willuweit, A., 2015. Preclinical pharmacokinetic studies of the tritium labelled D-enantiomeric peptide D3 developed for the treatment of Alzheimer's disease. PLoS One 10, e0128553.
Jiang, N., Frenzel, D., Schartmann, E., van Groen, T., Kadish, I., Shah, N.J., Langen, K.J., Willbold, D., Willuweit, A., 2016. Blood-brain barrier penetration of an Abeta-targeted, arginine-rich, D-enantiomeric peptide. Biochim. Biophys. Acta 1858, 2717–2724.
Klein, A.N., Ziehm, T., Tusche, M., Buitenhuis, J., Bartnik, D., Boeddrich, A., Wiglenda, T., Wanker, E., Funke, S.A., Brener, O., Gremer, L., Kutzsche, J., Willbold, D., 2016. Optimization of the all-D peptide D3 for Abeta oligomer elimination. PLoS One 11, e0153035.
Kutzsche, J., Schemmert, S., Tusche, M., Neddens, J., Rabl, R., Jurgens, D., Brener, O., Willuweit, A., Hutter-Paier, B., Willbold, D., 2017. Large-scale oral treatment study with the four most promising D3-derivatives for the treatment of Alzheimer's disease. Molecules (Basel, Switzerland) 22.
Lambrinidis, G., Vallianatou, T., Tsantili-Kakoulidou, A., 2015. In vitro, in silico and integrated strategies for the estimation of plasma protein binding. A review. Adv. Drug Deliv. Rev. 86, 27–45.
Leithold, L.H., Jiang, N., Post, J., Niemietz, N., Schartmann, E., Ziehm, T., Kutzsche, J., Shah, N.J., Breitkreutz, J., Langen, K.J., Willuweit, A., Willbold, D., 2016a. Pharmacokinetic properties of tandem d-peptides designed for treatment of Alzheimer's disease. Eur. J. Pharm. Sci. 89, 31–38.
Leithold, L.H., Jiang, N., Post, J., Ziehm, T., Schartmann, E., Kutzsche, J., Shah, N.J., Breitkreutz, J., Langen, K.J., Willuweit, A., Willbold, D., 2016b. Pharmacokinetic properties of a novel D-peptide developed to be therapeutically active against toxic beta-amyloid oligomers. Pharm. Res. 33, 328–336.
Liu, H., Funke, S.A., Willbold, D., 2010. Transport of Alzheimer disease amyloid-beta-binding D-amino acid peptides across an in vitro blood-brain barrier model. Rejuvenation Res. 13, 210–213.
Liu, H.N., Tjostheim, S., Dasilva, K., Taylor, D., Zhao, B., Rakhit, R., Brown, M., Chakrabartty, A., McLaurin, J., Robertson, J., 2012. Targeting of monomer/misfolded SOD1 as a therapeutic strategy for amyotrophic lateral sclerosis. J. Neurosci. 32, 8791–8799.
Muir, E.R., Shen, Q., Duong, T.Q., 2008. Cerebral blood flow MRI in mice using the cardiac-spin-labeling technique. Magn. Reson. Med. 60, 744–748.
Olubiyi, O.O., Strodel, B., 2012. Structures of the amyloid beta-peptides Abeta1-40 and Abeta1-42 as influenced by pH and a D-peptide. J. Phys. Chem. B 116, 3280–3291.
Olubiyi, O.O., Frenzel, D., Bartnik, D., Gluck, J.M., Brener, O., Nagel-Steger, L., Funke, S.A., Willbold, D., Strodel, B., 2014. Amyloid aggregation inhibitory mechanism of arginine-rich D-peptides. Curr. Med. Chem. 21, 1448–1457.
Pahnke, J., Langer, O., Krohn, M., 2014. Alzheimer's and ABC transporters—new opportunities for diagnostics and treatment. Neurobiol. Dis. 72 (Pt A), 54–60.
Pardridge, W.M., 2016. CSF, blood-brain barrier, and brain drug delivery. Expert Opin. Drug Deliv. 13, 963–975.
Schumacher, T.N.M., Mayr, L.M., Minor, D.L., Milhollen, M.A., Burgess, M.W., Kim, P.S., 1996. Identification of D-peptide ligands through mirror-image phage display. Science 271, 1854–1857.
Stalmans, S., Bracke, N., Wynendaele, E., Gevaert, B., Peremans, K., Burvenich, C., Polis, I., De Spiegeleer, B., 2015. Cell-penetrating peptides selectively cross the blood-brain barrier in vivo. PLoS One 10, e0139652.
Storck, S.E., Meister, S., Nahrath, J., Meissner, J.N., Schubert, N., Di Spiezio, A., Baches, S., Vandenbroucke, R.E., Bouter, Y., Prikulis, I., Korth, C., Weggen, S., Heimann, A., Schwaninger, M., Bayer, T.A., Pietrzik, C.U., 2016. Endothelial LRP1 transports amyloid-beta(1-42) across the blood-brain barrier. J. Clin. Invest. 126, 123–136.
Thal, D.R., Capetillo-Zarate, E., Del Tredici, K., Braak, H., 2006. The development of amyloid beta protein deposits in the aged brain. Sci. Aging Knowl. Environ. 2006 (6), re1–9.
Urquhart, J., 1996. Patient non-compliance with drug regimens: measurement, clinical correlates, economic impact. Eur. Heart J. 17 (Suppl. A), 8–15.
Van Dorpe, S., Adriaens, A., Polis, I., Peremans, K., Van Bocxlaer, J., De Spiegeleer, B., 2010. Analytical characterization and comparison of the blood-brain barrier permeability of eight opioid peptides. Peptides 31, 1390–1399.
Van Dorpe, S., Bronselaer, A., Nielandt, J., Stalmans, S., Wynendaele, E., Audenaert, K., Van De Wiele, C., Burvenich, C., Peremans, K., Hsuchou, H., De Tre, G., De Spiegeleer, B., 2012. Brainpeps: the blood-brain barrier peptide database. Brain Struct. Funct. 217, 687–718.
van Groen, T., Wiesehan, K., Funke, S.A., Kadish, I., Nagel-Steger, L., Willbold, D., 2008. Reduction of Alzheimer's disease amyloid plaque load in transgenic mice by D3, a D-enantiomeric peptide identified by mirror image phage display. ChemMedChem 3, 1848–1852.
van Groen, T., Kadish, I., Wiesehan, K., Funke, S.A., Willbold, D., 2009. In vitro and in vivo staining characteristics of small, fluorescent, Abeta42-binding D-enantiomeric peptides in transgenic AD mouse models. ChemMedChem 4, 276–282.
van Groen, T., Kadish, I., Funke, A., Bartnik, D., Willbold, D., 2012. Treatment with Abeta42 binding D-amino acid peptides reduce amyloid deposition and inflammation in APP/PS1 double transgenic mice. Adv. Protein Chem. Struct. Biol. 88, 133–152.
van Groen, T., Kadish, I., Funke, S.A., Bartnik, D., Willbold, D., 2013. Treatment with D3 removes amyloid deposits, reduces inflammation, and improves cognition in aged AbetaPP/PS1 double transgenic mice. J. Alzheimers Dis. 34, 609–620.
Vives, E., Brodin, P., Lebleu, B., 1997. A truncated HIV-1 Tat protein basic domain rapidly translocates through the plasma membrane and accumulates in the cell nucleus. J. Biol. Chem. 272, 16010–16017.
Wiesehan, K., Willbold, D., 2003. Mirror-image phage display: aiming at the mirror. Chembiochem 4, 811–815.
Wiesehan, K., Buder, K., Linke, R.P., Patt, S., Stoldt, M., Unger, E., Schmitt, B., Bucci, E., Willbold, D., 2003. Selection of D-amino-acid peptides that bind to Alzheimer's disease amyloid peptide abeta1-42 by mirror image phage display. Chembiochem 4, 748–753.
Wiesehan, K., Stohr, J., Nagel-Steger, L., van Groen, T., Riesner, D., Willbold, D., 2008. Inhibition of cytotoxicity and amyloid fibril formation by a D-amino acid peptide that specifically binds to Alzheimer's disease amyloid peptide. Protein Eng. Des. Sel. 21, 241–246.
Ziehm, T., Brener, O., van Groen, T., Kadish, I., Frenzel, D., Tusche, M., Kutzsche, J., Reiss, K., Gremer, L., Nagel-Steger, L., Willbold, D., 2016. Increase of positive net charge and conformational rigidity enhances the efficacy of D-enantiomeric peptides designed to eliminate cytotoxic Abeta species. ACS Chem. Neurosci. 7, 1088–1096.

3.7 Development and validation of an UHPLC-ESI-QTOF-MS method for quantification of the highly hydrophilic amyloid-β oligomer eliminating all-D-enantiomeric peptide RD2 in mouse plasma

Autoren:	Hupert M, Elfgen A, **Schartmann E**, Schemmert S, Buscher B, Kutzsche J, Willbold D, Santiago-Schübel B
Journal:	Journal of Chromatography B
	veröffentlicht am 15.01.2018
DOI:	10.1016/j.jchromb.2017.12.009
Impact Factor:	2,603 (2016)
Beitrag:	RD2-Behandlung der Mäuse
	Plasma-Entnahme der behandelten Mäuse
	Beteiligung beim Schreiben und Prüfen des Manuskripts

Journal of Chromatography B 1073 (2018) 123–129

Contents lists available at ScienceDirect

Journal of Chromatography B

journal homepage: www.elsevier.com/locate/jchromb

Development and validation of an UHPLC-ESI-QTOF-MS method for quantification of the highly hydrophilic amyloid-β oligomer eliminating all-D-enantiomeric peptide RD2 in mouse plasma

Michelle Hupert[a,1], Anne Elfgen[b,1], Elena Schartmann[b], Sarah Schemmert[b], Brigitte Buscher[c], Janine Kutzsche[b], Dieter Willbold[b,d,*], Beatrix Santiago-Schübel[a,*]

[a] Forschungszentrum Jülich GmbH, Central Institute for Engineering, Analytics (ZEA-3), Jülich, Germany
[b] Forschungszentrum Jülich GmbH, Institute of Complex Systems, Structural Biochemistry (ICS-6), Jülich, Germany
[c] Triskelion B.V., Zeist, The Netherlands
[d] Institut für Physikalische Biologie, Heinrich-Heine-Universität Düsseldorf, Düsseldorf, Germany

ARTICLE INFO

Keywords:
UHPLC-ESI-QTOF-MS
Mouse plasma
D-peptide
Amyloid-β peptide
Therapeutic compound
Alzheimer's disease

ABSTRACT

During preclinical drug development, a method for quantification of unlabeled compounds in blood plasma samples from treatment or pharmacokinetic studies in mice is required. In the current work, a rapid, specific, sensitive and validated liquid chromatography mass-spectrometric UHPLC-ESI-QTOF-MS method was developed for the quantification of the therapeutic compound RD2 in mouse plasma. RD2 is an all-D-enantiomeric peptide developed for the treatment of Alzheimer's disease, a progressive neurodegenerative disease finally leading to dementia. Due to RD2's highly hydrophilic properties, the sample preparation and the chromatographic separation and quantification were very challenging. The chromatographic separation of RD2 and its internal standard were accomplished on an Acquity UPLC BEH C18 column (2.1 × 100 mm, 1.7 µm particle size) within 6.5 min at 50 °C with a flow rate of 0.5 mL/min. Mobile phases consisted of water and acetonitrile with 1% formic acid and 0.025% heptafluorobutyric acid, respectively. Ions were generated by electrospray ionization (ESI) in the positive mode and the peptide was quantified by QTOF-MS. The developed extraction method for RD2 from mouse plasma revealed complete recovery. The linearity of the calibration curve was in the range of 5.3 ng/mL to 265 ng/mL ($r^2 > 0.999$) with a lower limit of detection (LLOD) of 2.65 ng/mL and a lower limit of quantification (LLOQ) of 5.3 ng/mL. The intra-day and inter-day accuracy and precision of RD2 in plasma ranged from −0.54% to 2.21% and from 1.97% to 8.18%, respectively. Moreover, no matrix effects were observed and RD2 remained stable in extracted mouse plasma at different conditions. Using this validated bioanalytical method, plasma samples of unlabeled RD2 or placebo treated mice were analyzed. The herein developed UHPLC-ESI-QTOF-MS method is a suitable tool for the quantitative analysis of unlabeled RD2 in plasma samples of treated mice.

1. Introduction

RD2 is an all-D-enantiomeric peptide specifically and directly targeting amyloid β peptide (Aβ) oligomers, which play a major role in the pathogenesis of Alzheimer's disease (AD), a progressive neurodegenerative disease leading to loss of memory [1]. The neuropathological cause for the development of AD is the aggregation of monomeric Aβ into Aβ oligomers and fibrils followed by the deposition of characteristic senile plaques accompanied by neuronal degeneration [2,3]. However, not the insoluble senile plaques but the soluble Aβ oligomers are currently widely believed to be the most toxic species triggering AD pathology [4–6]. The compound RD2 consists of 12 D-enantiomeric amino acid residues and has an amidated C-terminus (sequence: ptlhthnrrrrr-NH_2). It is the rationally rearranged sequence of the lead compound D3, which was previously selected by mirror image phage display against monomeric Aβ [7]. The rearrangement resulted in enhanced Aβ oligomer elimination [8,9]. *In vitro* assays also revealed that RD2 inhibits Aβ fibril formation efficiently [9]. In studies with AD transgenic mice, RD2 reduced the AD pathology in the mice's brains and showed improvement of cognition [9]. A pharmacokinetic study with the radiolabeled compound (^{3}H-RD2) revealed that RD2 has a high oral bioavailability, long blood circulation and an efficient blood brain

* Corresponding authors.
[1] These authors contributed equally to this work.

https://doi.org/10.1016/j.jchromb.2017.12.009
Received 22 September 2017; Received in revised form 30 November 2017; Accepted 6 December 2017
Available online 08 December 2017
1570-0232/

barrier permeability [10]. In these studies, it could be shown via thin layer chromatography with auto-radiographic detection that ^{3}H-RD2 remains stable after incubation in different body fluids and tissues. However, it is desirable to monitor RD2 levels also without any radioactive label in order to follow for example long-term treatment studies. Thus, as a first step, a suitable extraction method for the highly hydrophilic, arginine-rich RD2 from blood plasma followed by a rapid, sensitive and validated method for quantitative analysis of unlabeled RD2 via LC–MS has been developed for pharmacokinetic or treatment studies in this work. All validation parameters were carried out on the Guideline on bioanalytical method validation of the European Medicines Agency [11]. Using the validated method, plasma samples of RD2 or placebo treated mice were then analyzed as proof of concept.

2. Material and methods

2.1. Chemicals and reagents

UPLC-grade acetonitrile (ACN) was purchased from VWR (Langenfeld, Germany), UPLC-grade water from Merck (Darmstadt, Germany), heptafluorobutyric acid (HFBA) in LC-grade from Sigma Aldrich (Taufkirchen, Germany), formic acid (FA) in UPLC–MS grade from Biosolve (Valkenswaard, Netherlands) and trichloroacetic acid (TCA) from Sigma-Aldrich (Taufkirchen, Germany). Low binding Eppendorf tubes (Eppendorf, Hamburg, Germany) and auto-sampler vials (Agilent, Santa Clara, USA) were used because of the sticky characteristic of the peptides. Blank pooled blood plasma from healthy CD-1 mice (Innovative Grade US Origin Mouse Plasma – CD-1) was purchased from Dunn Labortechnik GmbH (Asbach, Germany). K3-EDTA served as anti-coagulator.

2.2. Peptides

The all-D-enantiomeric peptide RD2 consists of 12 amino acid residues each in D-configuration and has an amidated C-terminus (ptlhthnrrrrr-NH_2). RD2 has a monoisotopic mass of 1597.914 Da. The peptide was purchased from CBL Patras (Patras, Greece). The RD2 concentration was corrected for purity (92.3%), water content (3.7%), residual trifluoroacetic acid (TFA) (0.15%) and acetate content (25.5%). The internal standard (ISTD) has the same sequence as RD2 but with a substitution of leucine against valine at position three. It has a monoisotopic mass of 1583.898 Da. The ISTD was purchased from Peptides & Elephants GmbH (Potsdam, Germany) with a purity of 99.8%.

2.3. Stock solutions, calibration curve and quality control (QC) samples preparation

Calibration stock solutions of RD2 and ISTD were separately prepared in a water/ACN/FA (85/15/0.1%) mixture at a final concentration of 1.0 mg/mL, respectively. Dilution of 1:100 of the stock solutions in the same water/ACN/FA mixture resulted in the working solutions (10 µg/mL). Appropriate volumes of RD2 working solutions were diluted in blank mouse plasma samples to prepare the calibration standards and the QC standards. For the calibration curve, 5.30, 13.25, 26.5, 53, 132.5 and 265 ng/mL RD2 was prepared dissolving an appropriate volume of RD2 working solution. 33 ng/mL ISTD was added to correct the loss of analytes during sample preparation. For the extraction of RD2 and the ISTD, 3% TCA were added while vortexing the solution for 10 s. Precipitated proteins were removed by centrifugation at 14,000 *g* for 5 min at 4 °C. The supernatants containing the peptides were transferred to a low binding autosampler vial and stored at −20 °C. Blank plasma samples were prepared using water instead of RD2 working solution and ISTD. In addition, low quality control (LQC, 21.2 ng/mL), medium quality control (MQC, 106 ng/mL) and high quality control (HQC, 212 ng/mL) samples were prepared in the same manner. Furthermore, a quality control sample in water/ACN/FA (50 ng/mL) was prepared (QC-P) to check the performance of the method and the instrument before every series of measurements. The coefficient of determination (r^2) was used to evaluate the linearity of the calibration curve. The calibration standards were always prepared in triplicate and each extract was analyzed three times.

2.4. Chromatographic and mass spectrometry conditions

An Agilent UHPLC-ESI-QTOF-MS system was used for separation of RD2 from the ISTD and the remaining plasma components. The UHPLC (Agilent 1290 Infinity series) system consisted of a binary pump system, an autosampler, a thermostatted column compartment and a 6250 accurate-mass QTOF-MS with an electrospray ionization (ESI) interface with a resolution of 20,000. Chromatographic separation was performed on an Acquity UPLC BEH C18 column (2.1 × 100 mm, 1.7 µm particle size; Waters, Milford, USA). Column temperature was kept at 50 °C. Flow rate was 500 µL/min. The mobile phase consisted of solvent A, which was 0.025% HFBA and 1% FA in water, and solvent B, which was 0.025% HFBA and 1% FA in ACN. Sample injection volume was 20 µL. At the beginning of the run was an isocratic step of 5% B (0–2 min) followed by an increase to 22% B within 0.1 min, which was held for 0.5 min. The gradient increased from 22% to 25% B (2.6–6.5 min) in which RD2 eluted separately from the ISTD and other extracted plasma products from the column. Afterwards, the gradient increased rapidly within 0.7 min to 95% B and was held for cleaning with 95% B for 2 min. The gradient returned to 5% B within 0.1 min and equilibrated the system until 11 min. Detection was performed with the QTOF mass detector in the ESI positive ionization mode. The nebulizer pressure was set to 20 psi and the drying gas flow was set to 11 L/min. A fragmentation voltage of 215 V, a skimmer voltage of 68 V and an octopole voltage of 750 V were used. The mass range was set to *m/z* 500–600 and data acquisition rate was two spectra. Source temperature was set to 300 °C. MassHunter software LC–MS Data Acquisition B.05.01 (Agilent Technologies, Santa Clara, USA) was used to control the instrument and data acquisition. To correct the loss of analytes during sample preparation, quantification of RD2 was carried out with the ISTD. The first isotope of the three times loaded species RD2 ($(M+H^+)^{3+} = 533.649$) and ISTD ($(M+H^+)^{3+} = 528.977$) ± 8 ppm was extracted using the MassHunter software Quantitative Analysis for QTOF B.05.02 (Agilent Technologies, Santa Clara, USA). The correct isotopic ratio of RD2 and ISTD was a requirement for the identification and quantification of RD2. The advantage of this quantification method, which relies on the correct monoisotopic mass/isotopic ratio of RD2 compared to the quantification using a multiple reaction monitoring (MRM) mode, is the identification of possible metabolites of RD2 with only small modification, e.g., deamidation. We know from other studies that deamidation of RD2 sometimes occurs. In the case of deamidation of RD2, the isotope distribution ratio will be shifted to the second isotope. With an MRM method, this modification would not be detectable.

2.5. Method validation

All validation parameters were carried out on the Guideline on bioanalytical method validation of the European Medicines Agency [11].

2.5.1. Selectivity

For investigation of the method selectivity, six different blank mouse plasma matrix samples were exposed to the same extraction procedures as described before. The samples were tested for any interference peaks at retention time of RD2 or ISTD matching the chromatogram with RD2 and the ISTD spiked plasma. The assay is assured to be selective if the peak responses of tested samples were limited to ≤ 20% of the peak response of LLOQ and ≤ 5% of the ISTD.

2.5.2. Linearity, sensitivity and carry-over

Linearity and sensitivity of the suggested procedure were assessed on the basis of three individually prepared calibration curves. The calibration samples were freshly prepared and extracted with the described method. Statistical least square method was applied for the analysis of the resulting data. The % deviation for each calibrator should be ≤ 15% and for the LLOQ ≤ 20%. At least 75% of the calibration standards must fulfill this criterion. LLOQ and LLOD were calculated as a signal/noise ratio of 10 (LLOQ) or 3 (LLOD) comparing measured signals from standards of low concentrations of RD2 with those of blank samples.

Carry-over was assessed by injecting three blank plasma samples after highest calibration standard (265 ng/mL). The area response of blank samples must not exceed 20% of LLOQ and 5% of ISTD.

2.5.3. Accuracy and precision studies

Intra-day accuracy studies were carried out with the LQC, MQC and HQC samples. All samples were measured six times within one day. Additionally inter-day measurements were done in the same way in three successive days. For expression accuracy and precision of the method, the percentages error (% error) and the percentages relative standard deviation (% RSD) were used. The accuracy was determined as follows: % error = [(average measured concentration-expected concentration)/expected concentration] × 100, whereas the precision was determined as follows: % RSD = (standard deviation/average measured concentration) × 100. The acceptance criterion for accuracy was ≤ 15% of the actual values and precision should be ≤ 15%, except for LLOQ (≤ 20%) for both parameters.

2.5.4. Recovery and matrix effect

The extraction recovery was evaluated by comparing the concentrations of the extracted QC samples with the equal concentrations of RD2 spiked to plasma after extraction. Therefore, six lots of plasma were pre-treated and the extracts were spiked with RD2 concentrations corresponding to the QC samples.

The percentage of matrix effect was calculated by comparing the peak area of RD2 or ISTD spiked into blank plasma to the peak area of equal amounts of RD2 or ISTD in water/ACN/FA. The matrix factor (MF) of both RD2 and ISTD was calculated and the ISTD normalized MF was also determined. If MF is = 1, then there is no matrix effect. An MF < 1 means ion suppression and an MF > 1 means ion enhancement effects.

2.5.5. Reproducibility, performance and robustness

The QC-P sample was tested on every measurement day for one month. To show the variation within the days, the peak areas of RD2 were documented in a control chart.

2.5.6. Stability and dilution integrity

For assessing the RD2 stability in plasma matrix, the QC samples were used to perform the stability studies under different conditions. The samples were measured immediately after preparation, after 24 h at room temperature and after 72 h in the autosampler at 15 °C to assess the bench top and autosampler stability. Additionally, RD2 in plasma was measured after two weeks in the freezer (−20 °C). Moreover, the stability of the samples during three freeze-thaw-cycles was examined.

Furthermore, dilution integrity of RD2 samples was evaluated to confirm the integrity of concentrated RD2 samples that need a dilution step. Therefore, a 530 ng/mL RD2 solution was spiked into blank plasma or into water/ACN/FA to attain a concentration of two times of highest calibration standard. Then, the samples were five- or tenfold diluted with blank plasma or water/ACN/FA. Three replicates of each dilution were evaluated and the integrity of the samples was accepted when the deviation laid below 15% of the nominal values.

2.6. Applicability of the validated method for analysis of samples from a preclinical treatment study

2.6.1. Animals

Old male double transgenic APPswe/PS1ΔE9 mice [12] were purchased from The Jackson Laboratory (Sacramento, USA) and bred in-house. Water and food were available *ad libitum*. Housing rooms were maintained on a 12/12 h light–dark cycle (7:00 a.m.–7:00 p.m.) with a temperature of 22 °C and approx. 54% humidity. All animal experiments were performed in accordance with the German Law on the protection of animals and were approved by the local ethics committee (LANUV, North-Rhine-Westphalia, Germany, AZ84-02.04.2011.A359).

2.6.2. Treatment and blood collection

Treatment with RD2 or placebo was performed via intraperitoneal micro-osmotic pumps (type no. 1004) purchased from Alzet Osmotic Pumps (Cupertino, USA). The pumps were primed with 0.9% sodium chloride for 24 h at room temperature before filling with RD2 dissolved in 0.9% sodium chloride (n = 3) or 0.9% sodium chloride without peptide (placebo; n = 3). The pumps were implanted as described before [13]. In brief, for the implantation, the mice were anaesthetized intraperitoneally with 100 mg/kg ketamine (Bela-Pharm, Vechta, Germany) and 5 mg/kg medetomidine (Alfavet, Neumuenster, Germany). The skin and the muscle layer below the skin were cut in the midline and the pump was inserted into the abdominal cavity. Afterwards, the wound was sutured. The mice were treated with 40 mg/kg/day RD2 or placebo for 28 days. Subsequently, the mice were anaesthetized intraperitoneally with 100 mg/kg ketamine and 0.3 mg/kg medetomidine for blood collection via cardiac puncture. About 50 µL of 100 U/mL heparin (BD, Franklin Lakes, NJ, USA) served as anti-coagulator in the syringe.

The blood samples were centrifuged at 3,000 *g* and 4 °C for 10 min to obtain the cell free plasma. The plasma samples were frozen and stored at −20 °C.

2.6.3. Sample preparation and peptide extraction

Three RD2 and three placebo treated mice were analyzed in triplicates. The peptides were extracted from the plasma samples by the method described above. The supernatant containing the peptides RD2 and ISTD were stored at −20 °C. The samples were quantitatively analyzed in triplicate using the described method. If necessary, the samples were diluted in water/ACN/FA.

3. Results and discussion

3.1. Chromatographic separation and mass spectrometry

High resolution instruments have the ability to determine accurate mass and isotopic distribution and therefore enable high selectivity and specificity. In ESI, peptides are charged by excess of positive ions such as NH_4^+. The number of charges of each peptide depends on the experimental conditions but much more on protonable functional groups of the amino acid residues (e.g., amino groups in lysine, arginine and histidine). In addition, peptides show characteristic isotopic patterns depending on the functional groups of their amino acid composition. These two parameters were used for identification and quantification of RD2. RD2, which contains five arginine residues, has a monoisotopic mass of 1597.914 Da and was detected with two to four charges, in which > 95% was in the charge of three with a *m/z* of 533.649 $(M+H^+)^{3+}$ at all concentration levels of the calibration samples. The ISTD with a mass of 1583.898 Da was also detected > 95% via the threefold charged state with a *m/z* of 528.977 $(M+H^+)^{3+}$. As a consequence, the threefold charged state was used for quantification. The accuracy for confirmation of the extracted masses of RD2 and ISTD was within ± 8 ppm mass error showing high mass accuracy for the components' identification. The experimentally obtained isotopic pattern

was in close agreement with the theoretical isotopic pattern of RD2 and ISTD. Several parameters of mass spectrometry were optimized to obtain the highest stabilized mass response.

In addition, chromatographic conditions were adjusted. RD2 is very polar and hence difficult to chromatograph without ion pairing. We tried different additives, such as formic acid and TFA in different concentrations, but finally the combination of 1% formic acid and 0.025% HFBA improved the chromatography significantly. A run time of 7 min was capable for a good separation of ISTD (retention time: 3.5 min) and RD2 (retention time: 3.7 min) (Fig. 1).

3.2. Method validation

3.2.1. Selectivity

The developed method is specific as no interference from components of the extracted mouse plasma matrix was observed at the retention time of ISTD or RD2. ISTD and RD2 were well separated under the optimized chromatographic conditions with retention times at 3.5 min and 3.7 min, respectively (Fig. 1A).

3.2.2. Linearity, sensitivity and carry-over

The suggested method was sensitive and reliable for quantifying RD2 in mouse plasma. The linear regression analysis for the results was carried out using the least square method. The calibration curve showed linearity of RD2 concentrations between 5.3 ng/mL and 265 ng/mL with a correlation coefficient (r^2) > 0.999 in mouse plasma. The calibration curve of RD2 in plasma has a regression equation of $y = 1.01\,x–0.14$. The precision (RSD) of each concentration point did not exceed 7% and varied between 0.44% and 6.13%. Accuracy ranged from −4.34% to 4.79% (Table 1). The high r^2 value was indicative for the good linearity and the values of standard deviation were indicative for the significant validity of the calibration points.

Table 1
Back-calculated RD2 concentration of the calibration standards in mouse plasma.

Nominal concentration [ng/mL]	Mean [ng/mL]	Standard deviation [ng/mL]	Precision [%]	Accuracy [%]
5.30	5.07	0.18	3.60	−4.34
13.25	13.24	0.81	6.10	−0.08
26.5	27.77	0.72	2.59	4.79
53	53.22	3.26	6.13	0.42
132.5	132.72	0.58	0.44	0.55
265	269.10	16.36	6.08	1.55

No carry-over effect for RD2 or ISTD was observed in three blank plasma samples measured directly after the highest calibration standard. The peak area of blank mouse plasma revealed less than 4% of the peak area of the lowest RD2 calibration standard and less than 5% of the ISTD peak area.

The analytical measurement range started with 5.3 ng/mL as the lower limit of quantification (LLOQ). The calibration standard at 2.65 ng/mL was still detectable but was not in the linear range for quantification any more. Therefore, the lower limit of detection (LLOD) was set to 2.65 ng/mL.

3.2.3. Accuracy and precision studies

The developed method was confirmed to be reproducible using intra- and inter-day precision and accuracy of the QC samples. For expressing precision and accuracy, % RSD and % error were used. The

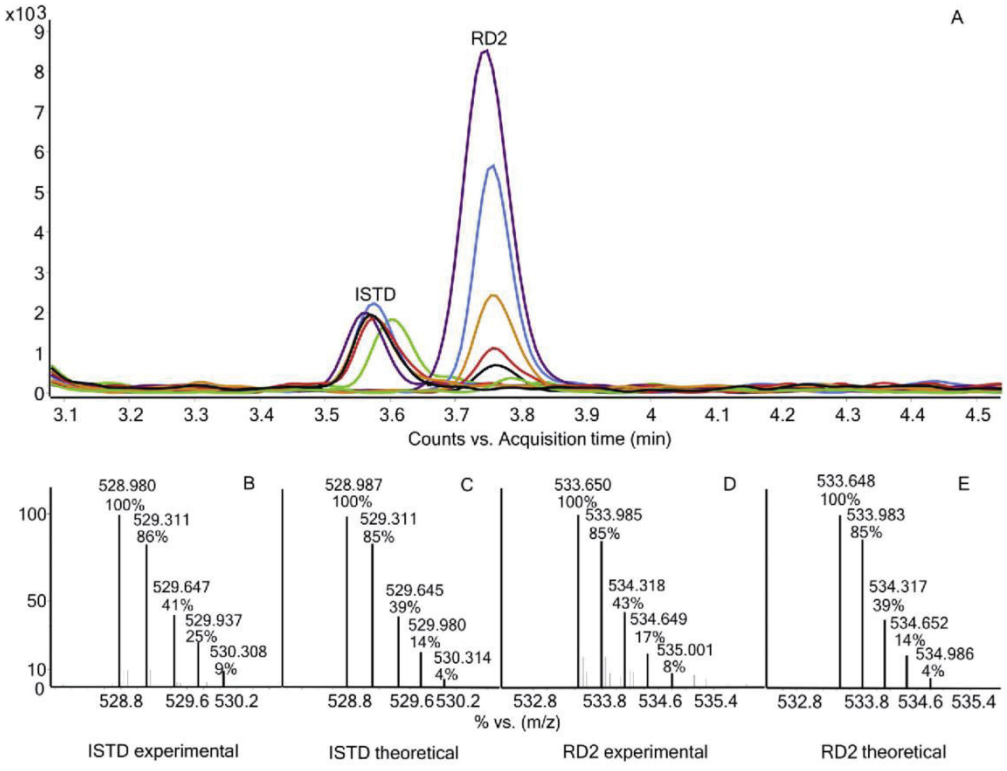

Fig. 1. Chromatographic separation and isotopic ratios of RD2 and the internal standard (ISTD). Extracted ion chromatogram (EIC) of RD2 (5.3–265 ng/mL) and ISTD (33 ng/mL) (A). Experimental (B, D) and theoretical (C, E) isotopic intensity distribution of the 3^+ charge peptide ion cluster of RD2 (D, E) and ISTD (B, C).

Table 2
Intra-day and inter-day precision and accuracy values of RD2 in mouse plasma.

	LQC [21.2 ng/mL]		MQC [106 ng/mL]		HQC [212 ng/mL]	
	Intra-day	Inter-day	Intra-day	Inter-day	Intra-day	Inter-day
Mean [ng/mL]	21.2	21.1	106.2	108.3	211.4	211.6
Standard deviation [ng/mL]	1.74	1.41	5.95	4.02	4.17	5.73
Precision [%]	8.18	6.69	5.60	3.71	1.97	2.71
Accuracy [%]	−0.24	−0.54	0.22	2.21	−0.29	−0.18

Table 3
Extraction recovery of QC samples of RD2 in mouse plasma (n = 6).

	RD2 extracted from mouse plasma			RD2 spiked to blank mouse plasma extract		
Nominal concentration [ng/mL]	21.2	106.0	212	21.2	106.0	212
Mean [ng/mL]	21.2	106.2	211.3	22.5	112.6	210.7
Recovery [%]	99.8	100.2	99.7	106.2	105.8	99.4
Standard deviation [ng/mL]	1.74	5.95	4.17	2.54	6.21	4.05
Precision [%]	8.18	5.60	1.97	11.24	5.52	1.92
Accuracy [%]	−0.24	2.83	−0.29	6.18	5.75	−0.61

values laid in the suitable range following the Guideline on bioanalytical method validation of the European Medicines Agency (2011) (Table 2).

3.2.4. Extraction recovery and matrix effect

Sample preparation for LC–MS of peptides is a critical step since peptides can undergo undesired phenomena such as adsorption to surfaces, degradation, variable recoveries or loss during transferring or drying steps. To minimize these issues, the use of a fast, simple technique such as protein precipitation with an organic solvent is preferred. To optimize the extraction of RD2 out of plasma, we used several organic solvents (ACN, methanol) and acids (HCOOH, TCA) in different ratios (varying concentrations). Finally, the extraction with 3% TCA showed best recoveries. In addition, the use of Low binding Eppendorf vials was indispensable because of the sticky character of the RD2 peptide.

Table 3 summarizes the extraction recoveries of the QC samples of RD2 in mouse plasma. The extraction recovery of RD2 was determined comparing the calculated concentration of RD2 extracted from plasma and extracted plasma spiked with corresponding amounts of RD2. The extraction efficiency was determined for the three QC samples with 99.8% (LQC), 100.2% (MQC) and 99.7% (HQC), respectively. Theoretically, the recovery rate cannot be above 100%. Due to the precision of the measurement, which was determined to be 7.1% (see 3.2.5), however, the calculations can ultimately lead to recovery rates slightly above 100%.

Table 5
Determination of RD2 in mouse plasma of intraperitoneally treated mice.

Mouse	RD2 treated			Placebo treated
	1	2	3	4–6
Mean [ng/mL]	1157.6	1554.3	1804.6	< LLOD
Standard deviation [ng/mL]	57.31	53.30	50.01	
Precision [%]	4.95	3.43	2.77	

For evaluation of the matrix effect, the peak area of RD2 or ISTD spiked into blank plasma was compared to the peak area of equal amounts of RD2 or ISTD in water/ACN/FA. The peak areas of RD2 and ISTD in water/ACN/FA and plasma samples showed that plasma has a maximal influence of 9% on the ionization of RD2 and 7% on the ionization of ISTD. The ISTD normalized MF values were 1.03 (LQC), 0.95

Table 4
RD2 stability and dilution integrity of RD2 in mouse plasma (n = 6).

	Nominal concentration [ng/mL]	Mean [ng/mL]	Recovery [%]	Precision [%]	Accuracy [%]
After extraction, 0 min	21.2	21.6	101.9	2.8	1.9
	106.0	107.7	101.5	3.6	1.5
	212.0	217.8	102.7	5.0	2.7
Room temp., after 24 h	21.2	21.4	100.9	8.3	0.9
	106.0	109.3	103.1	3.7	3.1
	212	211.0	99.5	2.8	−0.5
−20 °C, after 2 weeks	21.2	20.3	95.7	6.7	−4.2
	106.0	110.5	104.2	9.1	4.2
	212	202.1	95.3	1.7	−4.7
15 °C, 72 h	21.2	19.2	90.7	4.9	−9.3
	106.0	107.1	101.0	2.1	1.0
	212	210.7	99.4	2.0	−0.6
Three freeze-thaw-cycles	21.2	20.7	97.6	8.9	−2.4
	106.0	110.1	103.9	3.5	3.9
	212	210.4	99.3	2.5	−0.7
Dilution integrity	106.0 in plasma	114.8	108.3	4.0	8.3
	53.0 in plasma	55.4	104.6	4.6	4.6
	106.0 in water/ACN/FA	114.0	107.6	4.6	7.6
	53.0 in water/ACN/FA	55.1	104.0	3.9	4.0

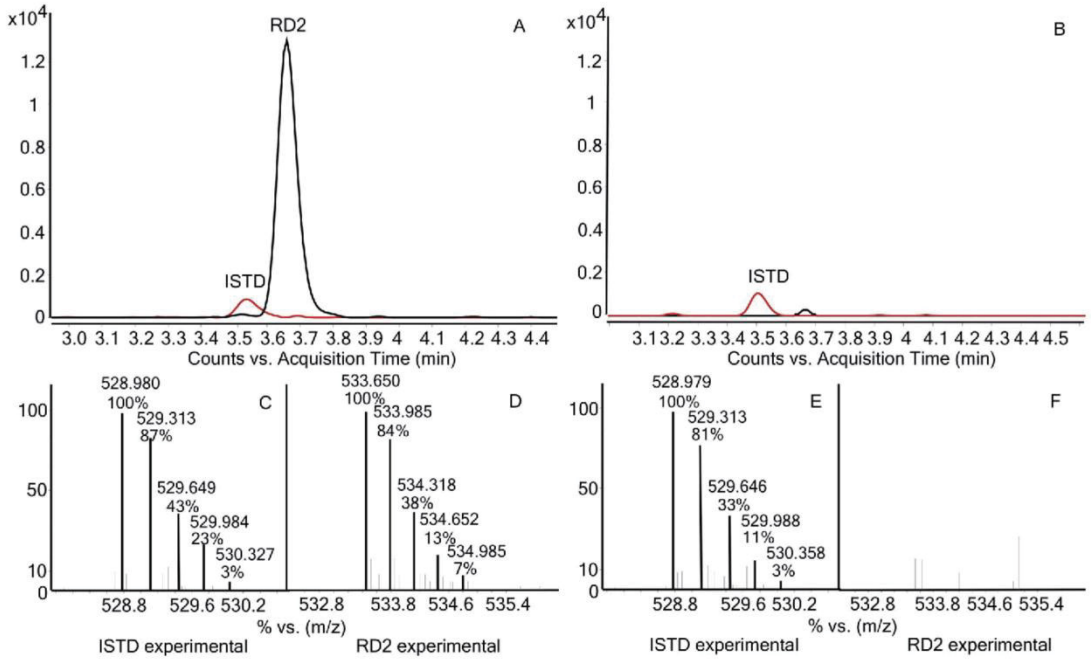

Fig. 2. Extracted ion chromatogram (EIC) of RD2 (black) and ISTD (red) of samples from RD2 treated mouse 2 (A) and placebo treated mouse 6 (B). Experimental distribution of the 3+ charged peptide ion cluster of ISTD (C, E) and RD2 (D, F). (For interpretation of the references to colour in this figure legend, the reader is referred to the web version of this article.)

(MQC) and 1.01 (HQC) respectively. This confirms matrix independency of this assay due to co-eluting matrix components.

3.2.5. Reproducibility, performance and robustness

The system is reproducible and robust. This was demonstrated by determination of the mean area of the QC-P standard over one month, which showed a precision of 7.1%.

3.2.6. Stability and dilution integrity

QC samples of RD2 were used to perform the stability studies under different conditions. The results of the stability studies are shown in Table 4. No loss of RD2 was observed during the storage at the tested conditions.

For evaluation of dilution integrity of RD2 samples, the mean recovery % and the precision % for the 1/5 and 1/10 dilution samples in plasma and in water/ACN/FA were determined. The recovery was within 104% and 108% and the precision was < 4.6%.

3.3. Applicability of the validated method for analysis of samples from a preclinical treatment study

To determine the applicability of the method for future treatment or pharmacokinetic studies, we analyzed plasma samples from mice after intraperitoneal treatment with 40 mg/kg/day unlabeled RD2 or with placebo (Table 5). Every mouse plasma sample was extracted in triplicate. The samples from the RD2 treated mice yielded ISTD and RD2 well separated with retention times at 3.5 and 3.7 min, respectively (Fig. 2A). The correct isotopic ratios of ISTD and RD2 were detected (Fig. 2C, D, E). In addition, no interferences from components of the extracted mouse plasma matrix were observed at the retention time of RD2 in placebo treated mice (Fig. 2F) substantiating the selectivity of the method.

Plasma of RD2 treated mice revealed an RD2 concentration of 1157.6, 1554.3 and 1804.6 ng/mL with a precision of 4.95%, 3.34% and 2.77%, respectively. As expected, RD2 has not been found in placebo treated mice (Table 5). From these results, we can conclude that the validated analytical method is reliable and suitable for the quantification of RD2 in plasma of treated mice.

4. Conclusion

Here, we describe the development and evaluation of a rapid UHPLC-ESI-QTOF-MS method for quantification of the highly hydrophilic, arginine-rich all-D-enantiomeric peptide RD2 in mouse plasma. The applied method showed a linearity range for RD2 spiked in plasma between 5.3 and 265 ng/mL with an LLOD of 2.65 ng/mL. The analysis was performed within 6.5 min with low solvent consumption. Quantifying several RD2 samples within one day as well as spread over various days demonstrated the accuracy, precision and reproducibility of the procedure. The developed method was successfully applied for the quantification of RD2 in intraperitoneally treated mice. These results provide a meaningful basis to evaluate preclinical or clinical applications of RD2.

Declaration of interest

The authors declare no competing financial or personal interests.

Acknowledgements

This work was funded by the Portfolio Technology and Medicine, the Portfolio Drug Research and the "Helmholtz-Validierungsfond" of the "Impuls- und Vernetzungsfond der Helmholtzgemeinschaft" and by the Technology Transfer Department of the Forschungszentrum Jülich.

References

[1] Alzheimer's Association, Alzheimer's disease facts and figures, Alzheimer's Dementia 12 (2016) (2016).

[2] J.A. Hardy, G.A. Higgins, Alzheimer's disease: the amyloid cascade hypothesis, Science 256 (1992) 184–185.
[3] D.J. Selkoe, J. Hardy, The amyloid hypothesis of Alzheimer's disease at 25 years, EMBO Mol. Med. 8 (2016) 595–608.
[4] S.T. Ferreira, W.L. Klein, The Abeta oligomer hypothesis for synapse failure and memory loss in Alzheimer's disease, Neurobiol. Learn. Mem. 96 (2011) 529–543.
[5] M.E. Larson, S.E. Lesne, Soluble Abeta oligomer production and toxicity, J. Neurochem. 120 (Suppl. 1) (2012) 125–139.
[6] I. Benilova, E. Karran, B. De Strooper, The toxic Abeta oligomer and Alzheimer's disease: an emperor in need of clothes, Nat. Neurosci. 15 (2012) 349–357.
[7] S.A. Funke, D. Willbold, Mirror image phage display–a method to generate D-peptide ligands for use in diagnostic or therapeutical applications, Mol. Biosyst. 5 (2009) 783–786.
[8] O.O. Olubiyi, D. Frenzel, D. Bartnik, J.M. Glück, O. Brener, L. Nagel-Steger, S.A. Funke, D. Willbold, B. Strodel, Amyloid aggregation inhibitory mechanism of arginine-rich D-peptides, Curr. Med. Chem. 21 (2014) 1448–1457.
[9] T. van Groen, S. Schemmert, O. Brener, L. Gremer, T. Ziehm, M. Tusche, L. Nagel-Steger, I. Kadish, E. Schartmann, A. Elfgen, D. Jürgens, A. Willuweit, J. Kutzsche, D. Willbold, The Aβ oligomer eliminating D-enantiomeric peptide RD2 improves cognition without changing plaque pathology, Sci. Rep. 7 (2017) 16275, http://dx.doi.org/10.1038/s41598-017-16565-1.
[10] L.H. Leithold, N. Jiang, J. Post, T. Ziehm, E. Schartmann, J. Kutzsche, N.J. Shah, J. Breitkreutz, K.J. Langen, A. Willuweit, D. Willbold, Pharmacokinetic properties of a novel D-peptide developed to be therapeutically active against toxic beta-amyloid oligomers, Pharm. Res. 33 (2016) 328–336.
[11] European Medicines Agency, Guideline on Validation of Bioanalytical Methods, Committee for Medicinal Products for Human Use, London, 2011.
[12] J.L. Jankowsky, H.H. Slunt, T. Ratovitski, N.A. Jenkins, N.G. Copeland, D.R. Borchelt, Co-expression of multiple transgenes in mouse CNS a comparison of strategies, Biomol. Eng. 17 (2001) 157–165.
[13] Alzet Osmotic Pumps, Intraperitoneal Implantation: Alzet Surgical Instuction Sheet, Alzet Osmotic Pumps, 2017.

3.8 Aβ oligomer elimination restores cognition in transgenic Alzheimer's mice with full-blown pathology

Autoren:	Schemmert S, **Schartmann E**, Zafiu C, Kass B, Hartwig S, Lehr S, Bannach O, Langen KJ, Shah NJ, Kutzsche J, Willuweit A, Willbold D
Journal:	European Molecular Biology Organization (EMBO) Reports
	eingereicht am 23.03.2018
Impact Factor:	8,568 (2016)
Beitrag:	Planung der Therapiestudie gemeinsam mit Sarah Schemmert
	Unterstützung bei der Behandlung der Mäuse
	Unterstützung bei der Durchführung der Verhaltenstests
	Beteiligung an der Durchführung der immunhistochemischen Analyse der Gehirne und des Plasmas der behandelten Mäuse
	Unterstützung beim Schreiben und Prüfen des Manuskripts

1 **Title Page**

2 **Aβ oligomer elimination restores cognition in transgenic Alzheimer's mice with full-**
3 **blown pathology**

4 Sarah Schemmert[1], Elena Schartmann[1], Christian Zafiu[1], Bettina Kass[1], Sonja Hartwig[2,3], Stefan Lehr[2,3], Oliver
5 Bannach[1], Karl-Josef Langen[4,5], Nadim Joni Shah[4,6], Janine Kutzsche[1], Antje Willuweit[4*], Dieter Willbold[1,7]*

6 Affiliations

7 [1]*Institute of Complex Systems, Structural Biochemistry (ICS-6), Forschungszentrum Jülich, Jülich, Germany*

8 [2]*Institute of Clinical Biochemistry and Pathobiochemistry, German Diabetes Center at the Heinrich Heine*
9 *University Düsseldorf, Leibniz Centre for Diabetes Research, Düsseldorf, Germany*

10 [3]*German Center for Diabetes Research (DZD), Partner Düsseldorf, Germany*

11 [4]*Institute of Neuroscience and Medicine, Medical Imaging Physics (INM-4), Forschungszentrum Jülich, Jülich,*
12 *Germany*

13 [5]*Clinic for Nuclear Medicine, RWTH Aachen University, Aachen, Germany*

14 [6]*Department of Neurology, Faculty of Medicine, JARA, RWTH Aachen University, Aachen, Germany*

15 [7]*Institut für Physikalische Biologie, Heinrich-Heine-Universität Düsseldorf, Düsseldorf, Germany*

16 *Correspondence to:

17 **Dieter Willbold**

18 Forschungszentrum Jülich, Institute of Complex Systems, Structural Biochemistry (ICS-6)
19 52425 Jülich
20 Germany
21 E-mail: d.willbold@fz-juelich.de
22 Phone: +49-2461-612100
23 Fax: +49-2461-612023

24 **Antje Willuweit**

25 Forschungszentrum Jülich, Institute of Neuroscience and Medicine (INM-4)
26 52425 Jülich
27 Germany
28 E-mail: a.willuweit@fz-juelich.de
29 Phone: +49-2461-6196358
30 Fax: +49-2461-612302

Running title: Aβ oligomer elimination restores cognition

Abstract

Oligomers of the amyloid β protein (Aβ) are suspected to be responsible for the development and progression of Alzheimer's disease. Thus, development of compounds that are able to eliminate already formed, toxic Aβ oligomers is very desirable. Here, we describe the *in vivo* efficacy of the compound RD2, which was developed to directly and specifically eliminate toxic Aβ oligomers. In a truly therapeutic, rather than preventive study, oral treatment with RD2 was able to reverse the cognitive deficits and to significantly reduce Aβ pathology in old-aged transgenic AD mice with full-blown pathology and behavioral deficits. For the first time, we demonstrate *in vivo* target engagement of RD2, in particular by showing a significant reduction of Aβ oligomers in the brains of RD2-treated compared to placebo-treated mice. The correlation of Aβ elimination *in vivo* and the reversal of cognitive deficits in old-aged transgenic mice are in support of Aβ oligomers being relevant not only for disease development and progression, but also for Aβ oligomers as a promising target for the causal treatment of Alzheimer's disease.

Keywords

Alzheimer's disease therapy, amyloid β oligomer elimination, transgenic mice, D-enantiomeric peptides, target engagement;

Introduction

The most common form of dementia worldwide is Alzheimer's disease (AD), a progressive and incurable neurodegenerative disease (Ferreira & Klein, 2011; Haass & Selkoe, 2007; Selkoe & Hardy, 2016). Presently available treatments with acetylcholinesterase inhibitors and an NMDA receptor antagonist are only able to treat some symptoms and hold the risk of unpleasant side effects (Jakob-Roetne & Jacobsen, 2009). Thus, there is an urgent need for the development of new therapeutic strategies for the causal treatment of AD (Karran et al, 2011).

The pathological hallmarks of AD are neurofibrillary tangles, consisting of hyperphosphorylated tau protein, progressive neurodegeneration and the accumulation of toxic amyloid β (Aβ) species (Karran et al, 2011; Selkoe & Hardy, 2016). The central dogma for the development of AD is the so called amyloid cascade hypothesis (Hardy, 1992; Hardy & Selkoe, 2002). It states that an imbalance between the production and clearance of Aβ in the brain of affected people is responsible for neurodegeneration and finally dementia. Monomeric Aβ, a cleavage product of the proteolytic processing of the amyloid protein precursor (APP) by a β- and a γ-secretase, aggregates into Aβ oligomers and finally into amyloid fibrils, which are found in AD plaques and were supposed to be the cause of cognitive deficits (Blennow et al, 2006). Nowadays, more and more evidence exists that instead of Aβ monomers or fibrils, small and diffusible Aβ oligomers may be the main cause for the development and progression of cognitive decline in AD (Ferreira et al, 2015; Selkoe & Hardy, 2016). Therefore, their elimination is highly desirable for therapy development and some attempts have been made in the past (Kumar et al, 2015; Rosenblum, 2014). So far, no treatment strategy based on prevention of Aβ oligomer formation with small molecule inhibitors against β- and γ-secretases has successfully completed clinical phase III. Many developments have been discontinued because of missing therapeutic benefit and side effects. In addition, therapeutic antibodies directed against monomeric or fibrillary Aβ, or both, showed so far no therapeutic efficiency in clinical phase III trials either, but suffer very often from dangerous side effects called amyloid-related imaging abnormalities (ARIA), which seems to be a consequence of an antibody-related activation of the immune system. Recent passive immunization approaches try to target Aβ oligomers more specifically by using stabilized oligomers of various size or conformation as antigens. Still, their efficacy needs to be demonstrated in clinical trials (Liu et al, 2016).

We propose a treatment strategy directed towards the specific and direct elimination of toxic Aβ oligomers, irrespective of their size and conformation, via their direct disruption without the need to rely on the immune system for their destruction. This is achieved by binding of our drug candidate to monomeric Aβ, stabilizing it in an aggregation-incompetent state, and thereby shifting the chemical equilibrium away from toxic Aβ oligomers (Cavini et al, 2018). Using this approach not only prevention of oligomer formation but also disruption of already formed Aβ oligomers is possible. Successful proof of this mode of action has been achieved for the orally available compound D3 and its derivatives *in vitro* by demonstrating removal of preformed, toxic Aβ oligomers (Brener et al, 2015). D3 has been identified by mirror image phage display and is a peptide that consists solely of D-enantiomeric amino acid residues. *In vivo* D3 has been shown to improve pathology and cognition after administration via different routes including oral application (Brener et al, 2015; Funke et al, 2010; van Groen et al, 2013;

van Groen et al, 2009; van Groen, 2012; van Groen et al, 2008). Additionally, pharmacokinetic studies have demonstrated the proteolytic stability and bioavailability of D3 (Elfgen et al, 2017; Jiang et al, 2015). The compound investigated in this study, RD2, is a derivative of D3 with a rationally repositioned amino acid sequence to enhance the Aβ oligomer elimination efficiency. Previously, we were able to demonstrate that RD2 has a higher efficacy to eliminate toxic Aβ oligomers *in vitro* by use of the Aβ-QIAD (quantitative determination of interference with Aβ aggregate size distribution) assay (Brener et al, 2015; van Groen et al, 2017). This assay is based on the fractionation of $Aβ_{(1-42)}$-assemblies (Aβ monomers, oligomers, protofibrills, larger aggregates) according to their sizes (after a predefined incubation time) by density gradient ultracentrifugation (DGC). Using this assay, it is possible to quantitatively determine the potency of a compound to reduce preformed toxic Aβ oligomers *in vitro*. According to Brener et al., the toxicity of oligomeric Aβ species is reduced after co-incubation with Aβ oligomer eliminating compounds (Brener et al, 2015). Besides oligomer removal several tests illustrate the *in vitro* efficacy of RD2 to reduce $Aβ_{(1-42)}$ fibril formation, the catalytic effect of preformed seeds on $Aβ_{(1-42)}$ aggregation and to reduce the $Aβ_{(1-42)}$ mediated cell toxicity (van Groen et al, 2017). Already in two preclinical proof of concept studies, RD2 demonstrated its efficacy by improving cognition in two different transgenic AD mouse models (Kutzsche et al, 2017; van Groen et al, 2017).

In the present study, we set out to support the suggested mode of action by demonstrating *in vivo* target engagement, which would be the reduction of the Aβ oligomer concentrations in brains of RD2-treated mice as compared to placebo-treated mice. This, however, requires an appropriate detection and quantitation method for Aβ oligomers. One of the major challenges of those attempts is to clearly distinguish between monomeric and oligomeric/aggregated Aβ species. To adequately meet this need, some attempts have been made, mostly based on ELISA techniques (Savage et al, 2014; Wang et al, 2017). One of the techniques that have been developed to quantify Aβ oligomers, is the sFIDA (surface-based fluorescence intensity distribution analysis) assay. The sFIDA assay uses a sandwich-ELISA biochemical setup using anti-Aβ-antibodies to capture all Aβ species to a glass surface, and fluorescence-labelled anti-Aβ-antibodies as probes that recognize the same, or overlapping Aβ-epitopes as the capture does, in order to avoid any contribution of Aβ monomers to the measurement. In contrast to conventional ELISAs, however, the readout is obtained by taking fluorescence micrographs from the glass surface by total internal reflection (TIRF) microscopy, which then yields single particle sensitivity. The absolute Aβ oligomer concentrations are then calculated on the basis of a suitable calibration standard (Herrmann et al, 2017a; Herrmann et al, 2017b; Hulsemann et al, 2016; Kravchenko et al, 2017; Kuhbach et al, 2016; Wang-Dietrich et al, 2013).

Besides demonstration of *in vivo* target engagement, the aim of the current study was to proof the proposed mode of action, i.e. the elimination of already formed Aβ oligomers, *in vivo* in a real therapeutic, rather than preventive setting. Therefore, we challenged the efficacy of the drug candidate RD2 by using it for the oral treatment of old-aged APP/PS1 transgenic AD mice that have developed full-blown pathology and severe cognition impairments and behavior deficits before treatment start.

Material and Methods

Ethical approval

All animal experiments were performed in accordance with the German Law on the protection of animals (TierSchG §§ 7–9) and were approved by a local ethics committee (LANUV, North-Rhine-Westphalia, Germany, reference number: 84-02.04.2011.A359).

Animals

In the present study, the double transgenic APPswe/PS1ΔE9 (APP/PS1) AD mouse model was used. The model was introduced by Jankowsky et al. in 2004 (Jankowsky et al, 2004) and its pathology and behavioral deficits are well characterized. At 6 months of age, the mice develop Aβ deposits, gliosis and cognitive deficits, especially detectable in the Morris water maze (MWM). The pathology and cognitive deficits progressively intensify with age (Garcia-Alloza et al, 2006; Jankowsky et al, 2004; Janus et al, 2015; Kamphuis et al, 2012). APP/PS1 mice were ordered by the Jackson Laboratory (Jackson Laboratory, USA) and bred in-house in a controlled environment on a light/dark cycle (12/12 h), with 54% humidity and a temperature of 22 °C. Food and water were available *ad libitum*.

Aged male APP/PS1 mice (n = 21) and their non-transgenic littermates (n = 11) were tested in the present study (average age at treatment initiation: 18 months +/- 3 weeks). During the study all mice were housed single caged.

Peptide

RD2 was purchased from CBL Patras (CBL Patras, Greece) and its amino acid residue sequence is as follows: H-ptlhthnrrrrr-NH_2.

Treatment

Mice were treated orally, every day, for 12 weeks with either RD2 (n = 11) or placebo (drinking water) (n = 10) both formulated in tailor-made jellies composed of gelatin (30% sucrose, 10% sucralose, 18.75% instant gelatin) (Dr. Oetker, Bielefeld, Germany). The mice ate each single jelly completely and voluntarily. Every week, the RD2 amount in the jellies was adjusted to the average body weights of the mice to achieve a daily dose as close as possible to 200 mg/kg. During the last weeks of treatment, for example, each jelly for the RD2 treatment group contained 6.7 mg RD2.

Behavioral assessments

In all experiments conducted the behavioral performance of RD2- and placebo-treated mice was compared to those of non-transgenic littermates, which were left untreated and assured for the quality of the behavioral assessments.

Nesting behavior and marble burying. To assess species-typical behavior, nesting behavior and marble burying were performed. Both protocols were adopted from Deacon (Deacon, 2006a; Deacon, 2006b). In short, for nesting behavior mice were placed in a new cage with a fresh nestlet (Sniff, Germany) 1 h before the dark phase of the animal house. The next morning, the built nests were

161 scored according to Deacon's scores from 0 to 5, whereby 0 represents no nest and 5 represents a
162 perfect nest (Deacon, 2006a). For marble burying, mice were placed in a new cage with 5 cm deep
163 wood chip bedding on which 12 glass marbles (diameter: 1.6 cm, weight: 5.3 g) were laid down in a
164 predefined order. After 30 min, the number of marbles buried was counted.

165 *Open field test*. The open field test is an experimental arrangement for the quantitative representation
166 of the explorative and anxiety behavior of animals (Archer, 1973). After 30 min of habituation to the
167 experiment's room, mice were placed in a square-shaped arena (45 cm x 45 cm x 45 cm). The arena
168 was imaginarily divided into two zones: center and border zone (center: 19 cm x 19 cm, border: space
169 around the center zone). Mice were allowed to observe the arena for 30 min. They were recorded with
170 a camera driven tracking system, Ethovision 11 (Noldus, Wageningen, The Netherlands). For
171 analysis, the first 25 min of the record were subdivided into five time slots (1: 0-5 min, 2: 5-10 min, 3:
172 10-15 min, 4: 15-20 min, 5: 20-25 min). The duration of stay in the center and the border zone was
173 evaluated concerning explorative and anxiety behavior in total and separately for each time slot.

174 *Morris water maze*. The Morris water maze (MWM) is a spatial learning test to investigate cognitive
175 impairments. The apparatus used consists of a circular white pool (120 cm in diameter and 60 cm in
176 height), filled with water (24 ± 1°C) to a depth of 30 cm. The water is rendered opaque by addition of a
177 non-toxic white pigment. The pool is imaginarily subdivided into four quadrants: north-east (NE, target
178 quadrant with an invisible round platform 1 cm below the surface), south-east (SE), south-west (SW)
179 and north-west (NW). The protocol was modified after Morris et al., 1982 (Morris et al, 1982). During
180 the training, the mice swam four 60 s trials daily starting from different quadrants on five consecutive
181 days. If they did not find the hidden but fixed platform within the 60 s of a trial, they were set on the
182 platform for 10 s to orient themselves before they were returned to their cages. Between each trial, the
183 mice had a recovery period of 60 s under a heating lamp to avoid a decrease in body temperature. On
184 the sixth day, the probe trial was performed in which the mice had to swim in the pool for 60 s without
185 a platform. During the trials, the mice were tracked with Ethovision 11 (Noldus, Wageningen, The
186 Netherlands). The following parameters were analyzed for the training days: escape latency to
187 platform (s), covered distance (cm), swimming speed (cm/s), and the duration in the platform quadrant
188 (s). The duration in the platform quadrant was analyzed for the probe trial, too.

189 Plasma and tissue collection

190 Mice were anesthetized with 100 mg/kg ketamine (bela-pharm, Vechta, Germany) and 0.3 mg/kg
191 medetomidine (Dormilan, alfavet, Neumünster, Germany) intraperitoneally before the final collection of
192 blood samples by terminal cardiac puncture. Brains were removed, divided into the two hemispheres
193 and snap frozen in -80 °C isopentane. The left hemispheres were used for immunohistochemistry
194 (IHC); the right hemispheres were used for biochemical analysis.

195 Immunohistochemistry and biochemical analysis

196 *Immunohistochemistry*. IHC was performed on 20 µm sagittal frozen brain sections. In brief, room
197 tempered sections were fixed in 4% paraformaldehyde (10 min, room temperature). For antigen
198 retrieval, sections were incubated in 70% formic acid (5 min, room temperature). Elimination of

endogenous peroxidases was performed with 3% H_2O_2 in methanol (15 min, room temperature). In between, the sections were washed 3 times for 5 min in 1% Triton in TBS (TBST). Sections were incubated with the primary antibody over night at 4 °C in a humid chamber (6E10: 1:2500, Bio Legend, San Diego, USA; GFAP: 1:1000, DAKO, Agilent Technologies, Santa Clara, USA; CD11b: 1:2500, Abcam, Cambridge, United Kingdom) in TBST with 1% bovine serum albumin (BSA), followed by incubation with a biotinylated secondary anti-mouse or anti-rabbit antibody (both 1:1000 in TBST + 1% BSA, Sigma-Aldrich, Darmstadt, Germany). Staining was visualized with the use of 3,3'-Diaminobenzidine (DAB) enhanced with saturated nickel ammonium sulphate solution. Sections were mounted with DPX Mountant (Sigma-Aldrich, Darmstadt, Germany) after washing in an ascending alcohol series.

To avoid differences in staining intensity and light exposure which might affect measurements, all slides were stained in one batch and acquired in one microscopy session. Sections were visualized with the use of a Zeiss SteREO Lumar V12 microscope and the according software (Zeiss AxioVision 6.4 RE) or a Leica LMD6000 microscope and the according software (LAS 4.0 software). Quantification was performed with ImageJ (National Institute of Health, Bethesda, USA). The plaque count of RD2- (n = 11) and placebo-treated (n = 8) mice was analyzed in cerebrum (8-10 slides/mouse), cortex (5-6 slides/mouse) and hippocampus (8-10 slides/mouse). Astrogliosis of RD2- (n = 8) and placebo-treated (n = 7) mice was analyzed in cortex (6 slides/mouse with 6 equally distributed pictures per slide) and hippocampus (6 slides/mouse). The activated microglia of RD2- (n = 9) and placebo-treated (n = 9) mice were analyzed in cortex (7 slides/mouse) and hippocampus (7 slides/mouse).

Aβ ELISA. For generation of three fractions (Tris-, diethanolamine (DEA)-, and formic acid (FA) fraction) the right hemispheres of RD2- (n = 10) and placebo-treated (n = 8) mice were used. To obtain the Tris-fraction, hemispheres were homogenized 2 x 20 s at 6500 rpm (Precellys® 24, Bertin Instruments, Montigny-le-Bretonneux, France) with Tris buffer (pH 8.3, 20 mM Tris, 250 mM NaCl, protease and phosphatase inhibitors (both Roche, Basel, Switzerland)). Afterwards, the homogenized samples were sonicated (5 min) and centrifuged (30 min, 175.000 x g, 4 °C). Supernatant was taken as the Tris-soluble fraction. DEA-fractions were gained after dissolving the pellet in 2% DEA, incubation (1 h on ice), and centrifugation (30 min, 175.000 x g, 4 °C). Supernatant was taken as the DEA fraction. The pellet was dissolved in 70% FA, incubated (1 h on ice), and centrifuged (30 min, 175.000 x g, 4 °C). Supernatant was taken as the FA-fraction. All fractions were snap frozen in liquid nitrogen and stored at -80 °C until further analysis.

Aβ x–40 and Aβ x–42 ELISAs were purchased from BioLegend (BioLegend, San Diego, United States) and performed according to the manufacturer's protocol with the three brain homogenate fractions described above. All samples were measured as duplicates.

Surface-based fluorescence intensity distribution analysis (sFIDA) assay

sFIDA assays were performed in 384 flat-bottom square well microplates (Sensoplate Plus, Greiner Bio-One GmbH, Frickenhausen, Germany) with a glass bottom of 170 µm thickness. The glass bottom

of the microplate was silanized with APTES (99 %; (3-Aminopropyltriethoxysilane; Sigma-Aldrich, Germany) by vapor deposition. For this procedure, a microplate was placed in a desiccator above a solution of 5% APTES in Toluene (99% Sigma-Aldrich, Germany) in an Argon atmosphere for 1 h before removing the APTES solution and drying for 2 h in a vacuum. To the wells, 2 mM succinimidyl carbonate-poly-(ethylene glycol)–carboxymethyl (MW 3400, Laysan Bio, Arab, USA) in dd H_2O was added, incubated for 4 h, and washed three times after incubation. This procedure covalently links PEG to APTES and presents carboxylic acids to the surface, which are activated by 200 mM N-(3-dimethylaminopropyl)-N′-ethylcarbodiimide hydrochloride (98%; Sigma-Aldrich, Germany), and 50 mM N-hydroxysuccinimide (98%; Sigma-Aldrich, Germany), and incubated for 30 min. After washing three times with dd H_2O, 10 µg/ml of Nab228 monoclonal antibody (Sigma-Aldrich, St. Louis, USA) in PBS was added to the wells and incubated for 1 h. After washing for three times with TBS + 0.1%Tween20 (TBST) and TBS each of the wells was blocked with Smartblock solution (Candor Bioscience, Germany) over night. The next day, samples and standards were added to the plate an incubated for 1 h. All samples were diluted tenfold in TBS. $A\beta_{(1-42)}$-SiNaPs (silica nanoparticles) with a diameter of 20 nm and approx. 30 epitopes ($A\beta_{(1-42)}$), synthesized and analyzed by methods described previously (Hulsemann et al, 2016), served as a calibration standard for Aβ oligomers. After washing the excessive sample away with TBS three times, 1.25 µg/ml mAb IC16 (epitope $A\beta_{1-8}$) (Hellmert et al, 2015), labelled with CF-633 dye, (Sigma-Aldrich, Germany) and 1.25 µg/ml Nab228 (epitope $A\beta_{1-11}$) labelled with CF-488 dye (both: Sigma-Aldrich, Germany), that were ultracentrifuged (100.000 g, 1 h, 4 °C) before adding to the wells, were incubated for 1 h. After incubation, the excessive detection antibodies were washed away three times with TBS and the plate was sealed with a plastic foil and transferred to a Leica multi-color TIRF (total internal reflection fluorescence) system (AM TIRF MC, Leica Microsystems, Wetzlar, Germany). The TIRF system operated with an automated stage and a 100 x oil immersion objective (1.47 oil CORR TIRF Leica). Images were recorded consecutively with Ex/Em = 633/705 nm and 488/525 nm with 500 ms exposure time and a gain of 800 for both color channels at a penetration depth of 200 nm. The microscope took 5 x 5 images per well in each channel, which corresponds to ca. 3% of the well surface. Each images consisted of 1000 x 1000 pixels with a lateral resolution of 116 nm (pixel to pixel) and an intensity resolution of 14 bit (grey scale).

Image analysis was performed using sFIDAta, a custom made software. After removing “out of focus” images (ca. 5%) cutoff values were calculated for each channel based on the blank. The software then applied the cutoff values to the sample results and counted pixels that were in both channels and at the same position higher than the cutoff. The number of these co-localized pixels was the sFIDA readout. Using the $A\beta_{(1-42)}$-SiNaP standards, the sFIDA readout was converted to oligomer concentration. All samples were measured in triplicate.

For all sFIDA experiments, with the expectation the one performed with the three fractions also used for ELISA, 150 µl of brain homogenate was centrifuged at 1200 g for 10 min. 100 µl supernatant of each homogenate was loaded on the top of a density gradient consisting of 5 to 50% (w/v) iodixanol (OptiPrep, Axis-Shield, Norway). After centrifugation (3 h, 259.000 x g, at 4 °C) (Optima TL-100, Beckman Coulter, USA), 14 fractions (140 µl each), were removed from top to bottom of the tubes. 10 µl of each fraction was diluted in 90 µl TBS before being applied to the sFIDA microplates.

Clinical Chemistry

Tests for the quantitative determination of lactate dehydrogenase (LDH), aspartate aminotransferase (AST), alanine aminotransferase (ALT) and alkaline phosphatase (AP) were performed with plasma samples from RD2- or placebo-treated mice, or their non-transgenic littermates using Roche automated clinical chemistry analyzers (cobas 8000 modular analyzer series, Roche, Basel, Switzerland) according to the manufacturer's protocol.

Cytokine assay

Plasma samples from RD2- or placebo-treated mice, or their non-transgenic littermates were tested for interleukin 1 alpha (IL-1α), interleukin 10 (IL-10), interleukin 12p40 (IL-12p40), interleukin 13 (IL-13), interleukin 17 (IL-17), granulocyte-colony stimulating factor (G-CSF), interferon gamma (IFN-γ), monocyte chemoattractant protein-1 (MCP-1), macrophage inflammatory proteins alpha and beta (MIP-1α and MIP-1β), regulated on activation, normal T-cell expressed and secreted (RANTES), and tumor necrosis factor alpha (TNF-α) (Bio-Plex Pro Mouse Cytokine 23-plex Assay, Bio-Rad, California, USA). The assay was performed following the manufacturer's protocol. Samples that were out of the detection limit were excluded from analysis.

Statistical analysis

All statistical calculations were performed using GraphPad Prism 5 (GraphPad Software, Inc., La Jolla, USA) or SigmaPlot Version 11 (Systat Software, Germany). All data are represented as mean ± SEM. Gaussian distribution of all data was tested in the D'Agostino & Pearson omnibus normality test. Normally distributed data was analyzed in the one-way analysis of variance (ANOVA) with Tukey post hoc analysis (nesting behavior, probe trial MWM) or unpaired one-tailed t-test (6E10 staining). Data, which were not normally distributed, was tested with Kruskal-Wallis test with Dunn's Multiple Comparison Test (marble burying, open field test, cytokine assay, IHC, clinical chemistry). MWM was analyzed with the use of InVivoStat 2.5 (InVivoStat by Simon Bate and Robin Clarke, United Kingdom) (Clark et al, 2012) with the Repeated Measures (RM) Parametric Analysis and SigmaPlot. The escape latency to the platform was considered as not normally distributed and therefore analyzed by Friedman Repeated Measures ANOVA on Ranks. Distance moved and the percentage duration in the platform quadrant were analyzed by a repeated measures two-way ANOVA. As the fractions generated from each brain homogenate (Tris-, DEA- and FA-fraction, or DGC fractions 1 to 14) were considered to be related, results from ELISA and sFIDA measurements were analyzed with a two-way RM ANOVA. p-values smaller than 0.05 were considered to indicate significant statistical differences in the tests.

Results

RD2 treatment resulted in improved cognition and behavior of treated mice, indistinguishable from non-transgenic mice

In the present study, three groups of mice were tested. Two groups consisted of 18 months old transgenic APP/PS1 mice. In the first group, eleven mice were orally treated with RD2. Oral treatment was carried out by giving daily one jelly containing roughly 200 mg/kg of RD2 (treatment group). In the second group, ten APP/PS1 mice were daily given a jelly without RD2 (placebo group, ten mice). The third group, consisting of eleven non-transgenic littermates, was left untreated (wild-type group) and assured for the quality of the behavioral assessments. At the end of the twelve-week treatment period, different behavioral experiments were conducted to evaluate the treatment effect. Thereafter, different immunohistochemical and biochemical experiments were performed to investigate the treatment effect on Aβ pathology, inflammation, and possible side effects.

To assess the potential consequences of long-term oral treatment with RD2 over twelve weeks on species-typical behavior and to investigate possible adverse side effects caused by the treatment, nesting behavior and marble burying, as basic behavioral tests, were performed with RD2- in comparison to placebo-treated APP/PS1 mice and their non-transgenic littermates (Fig. 1 a, b). Neither nesting behavior nor marble burying revealed any significant differences between the three groups (Fig. 1 a, b; nesting behavior score (mean ± SEM): ntg 3.3 ± 0.5, placebo 2.1 ± 0.3, RD2 2.3 ± 0.5, one-way ANOVA $F_{(2,31)} = 2.21$, n.s. $p = 0.13$; marble burying (mean ± SEM): ntg 6.6 ± 0.5, placebo 8.4 ± 0.8, RD2 7.8 ± 0.6, one-way ANOVA, $F_{(2,31)} = 1.91$, n.s. $p = 0.17$). Afterwards, an open field test was performed to assay general differences in exploratory and anxiety related behavior of treated mice and their non-transgenic littermates. Analysis of the open field test did not reveal significant differences in the analyzed parameters between RD2-treated mice and non-transgenic littermates, but did between RD2- and placebo-treated mice. This indicates that phenotypic impairments of the transgenic mice were reversed by RD2 treatment (Fig. 1 c; two-way ANOVA, $F_{(2,58)} = 0$, Tukey post hoc analysis: ntg vs. placebo n.s. $p = 0.14$, ntg vs. RD2 n.s. $p = 0.75$, placebo vs. RD2. $p = 0.03$). In detail, RD2-treated mice stayed significantly longer in the center zone than placebo-treated mice (Fig. 1 d), while the time spent in border and center zone did not significantly differ between RD2-treated mice and their non-transgenic littermates (Fig. 1 d). This suggests decreased anxiety related behavior of RD2- compared to the placebo-treated mice, again leading to reversal of the behavior of RD2-treated mice to the level of the non-transgenic littermates. Also, there was a difference in the exploratory behavior during the course of the test. RD2-treated mice and non-transgenic littermates explored the center zone significantly longer than placebo-treated mice. Thus, RD2-treated mice and non-transgenic littermates showed the typical habituation effect to the new and so far unexplored arena, while this habituation effect was not present in placebo-treated transgenic mice (Fig. 1 c; two-way RM ANOVA, $F_{(2,116)} = 4.12$, $p = 0.03$, Tukey post hoc analysis time slot 5: ntg vs. placebo $p = 0.01$, ntg vs. RD2 n.s. $p = 0.76$, placebo vs. RD2 $p = 0.001$). The presence of the habituation effect, or its absence, became especially prominent during the second half of the test, suggesting that RD2

348 treatment led to the reversal of the transgenic mouse phenotype towards the phenotype of the non-
349 transgenic littermates.

350 The Morris water maze (MWM) was conducted for the assessment of cognitive impairment, especially
351 for deficits in cognitive abilities, and in spatial learning and memory. During the five days training
352 phase of the MWM, placebo-treated transgenic mice showed impaired performance without an
353 apparent learning effect over time. In contrast, RD2-treated mice showed a significant learning effect
354 over time in the training phase of the MWM, with their performance being indistinguishable from
355 non-transgenic littermates (Fig. 1 e; Friedman repeated measure (RM) ANOVA on Ranks, RD2-
356 treated mice $p < 0.001$, non-transgenic littermates $p = 0.008$, placebo-treated mice n.s. $p = 0.1$).
357 Moreover, RD2-treated mice spent significantly more time in the target quadrant than the placebo-
358 treated mice. Also here, RD2-treated transgenic mice were indistinguishable from non-transgenic
359 littermates (Fig. 1 f; two-way RM ANOVA, $F_{(2,116)} = 4.39$, $p = 0.02$, Tukey post hoc analysis day 5, ntg
360 vs. placebo $p < 0.001$, ntg vs. RD2 n.s. $p = 0.3$, placebo vs. RD2 n.s. $p = 0.006$). Memory retrieval
361 during the probe trial on day six did not reveal significant differences in performance between RD2-
362 treated and placebo-treated mice, but did reveal differences between non-transgenic littermates and
363 placebo-treated mice. The placebo-treated mice spent significantly less time in the quadrant, where
364 the platform was located, than the non-transgenic littermates. This emphasizes the cognitive
365 impairment of the placebo-treated transgenic mice (Fig. 1 g; one-way ANOVA $F_{(2,31)} = 6.77$, $p = 0.004$,
366 Tukey post hoc analysis, non-transgenic littermates vs. placebo $p = 0.003$, non-transgenic littermates
367 vs. RD2 n.s. $p = 0.06$, placebo vs. RD2 n.s. $p = 0.4$).

368 Treatment with RD2 led to significant decrease of Aβ plaque load

369 Staining of brain tissue sections against human Aβ (6E10), activated astrocytes (GFAP), and activated
370 microglia (CD11b) was accomplished to investigate the effects of long-term oral RD2 treatment on Aβ
371 pathology and gliosis of the APP/PS1 transgenic mouse model (Garcia-Alloza et al, 2006; Kamphuis
372 et al, 2012). Fig. 2 a-c shows the results of 6E10, GFAP, and CD11b staining with subsequent
373 quantification of different brain areas (cerebrum, cortex, hippocampus). Overall, the data suggest that
374 RD2 treatment led to reduction of Aβ plaque load (Fig. 2 a). This became significant only for the Aβ
375 plaque load in the cortex (unpaired one-tailed Student's t-test, $p = 0.02$). There was no significance for
376 the Aβ plaque load reduction of the whole cerebrum or the hippocampus (unpaired one-tailed
377 Student's t-test, cerebrum n.s. $p = 0.2$, hippocampus n.s. $p = 0.1$). We observed a tendency for
378 reduction of gliosis after RD2 treatment that was close to being significant in the cortex of RD2-treated
379 mice (Fig. 2 b; GFAP staining: unpaired one-tailed Student's t-test, cortex n.s. $p = 0.064$, hippocampus
380 n.s. $p = 0.3$) (Fig 2 c; CD11b staining: unpaired one-tailed Student's t-test, cortex n.s. $p = 0.051$,
381 hippocampus n.s. $p = 0.28$).

382 Biochemical quantitation of Aβ(x–40) and Aβ(x–42) was accomplished with three fractions (Tris-
383 soluble-, DEA-soluble- and formic acid (FA)-fraction) prepared from brain homogenates of RD2-
384 treated and placebo-treated mice (Fig. 2 d-g). There were no significant differences for the contents of
385 Aβ(x–40) in any of the fractions from RD2-treated mice compared to placebo-treated mice (Fig. 2 d;
386 two-way RM ANOVA treatment, $F_{(1,32)} = 0.87$ n.s., $p = 0.365$; fractions, $F_{(2,32)} = 69.19$, $p < 0.001$;

interaction, $F_{(2,32)}$ = 0.85, n.s., p = 0.44; Tukey post hoc analysis RD2 vs. placebo, Tris-fraction n.s. p = 0.99, DEA-fraction n.s. p = 0.97, FA-fraction n.s. p = 0.12). RD2-treated mice showed a significant increase of Aβ(x–42) in the FA-fraction (Fig. 2 e; two-way RM ANOVA treatment, $F_{(1,32)}$ = 2.32 n.s., p = 0.15; fractions, $F_{(2,32)}$ = 155.58, p < 0.001; interaction, $F_{(2,32)}$ = 2.61, n.s., p = 0.089; Tukey post hoc analysis RD2 vs. placebo, Tris-fraction n.s. p = 0.94, DEA-fraction n.s. p = 0.98, FA-fraction p = 0.009). The Aβ42/40 ratio was nearly 1 in all samples, except for the Tris-fraction of placebo-treated mice that differed significantly from the Tris-fraction of RD2-treated mice (Fig. 2 f; two-way RM ANOVA treatment, $F_{(1,32)}$ = 0.026 n.s., p = 0.88; fractions, $F_{(2,32)}$ = 1.26 n.s., p = 0.3; interaction, $F_{(2,32)}$ = 3.85, n.s., p = 0.032; Tukey post hoc analysis RD2 vs. placebo, Tris-fraction p = 0.03, DEA-fraction n.s. p = 0.64, FA-fraction n.s. p = 0.146). Analysis of Aβ oligomer concentration within the Tris-, DEA-, and FA-fraction was conducted using the surface-based fluorescence intensity distribution analysis (sFIDA) assay. Results displayed a significant increase in Aβ oligomers within the DEA-fraction of RD2-treated mice compared to placebo-treated mice (Fig. 2 g; two-way RM ANOVA treatment, $F_{(1,16)}$ = 1.48 n.s., p = 0.24; fractions, $F_{(1,16)}$ = 5.68, p = 0.03; interaction, $F_{(2,32)}$ = 1.66, n.s., p = 0.22; Tukey post hoc analysis RD2 vs. placebo, Tris-fraction n.s. p = 0.73, DEA-fraction n.s. p = 0.04). The sFIDA assay is highly specific and sensitive to aggregated Aβ species and completely insensitive to monomers. All protein assemblies from the FA-solubilized pellet can be expected to be fully denatured and dissolved. Indeed, the FA-fractions yielded Aβ oligomer concentrations close to zero.

Measurement of Aβ oligomer concentrations by the sFIDA assay revealed significant reduction of Aβ oligomers in RD2 treated mice

RD2 was designed to directly and specifically eliminate Aβ oligomers. To develop a suitable method to investigate target engagement *in vivo*, an assay was developed that is able to quantitate Aβ oligomers in body liquids (e.g. cerebrospinal fluid, plasma). The assay, called sFIDA, is insensitive to Aβ monomers and achieves single particle sensitivity (Herrmann et al, 2017b; Hulsemann et al, 2016; Kuhbach et al, 2016). In the present study, we developed this technique further in order to measure Aβ oligomers in organ homogenates. Therefore, we fractionated full brain homogenates of RD2- and placebo-treated mice by density gradient centrifugation (DGC) according to particle sizes and applied each of the 14 obtained fractions to the sFIDA assay. The sFIDA assay combines the specificity of immunological assays with the sensitivity of high-resolution fluorescence microscopy, which allows a lower limit of detection, down to the single aggregate level. The selectivity for aggregated species is realized by using anti-Aβ antibodies for capturing and probing that recognize overlapping epitopes located at the N-terminus of Aβ subunits (Hellmert et al, 2015; Wang-Dietrich et al, 2013). To test for successful target engagement due to RD2 treatment, we compared DGC-fractionated brain homogenates of RD2- and placebo-treated mice. The result is shown in Figure 3 and revealed a significant decrease of Aβ oligomer levels of RD2- compared to placebo-treated mice especially in fraction 10 (Fig. 3 e; two-way RM ANOVA treatment, $F_{(1,91)}$ = 0.69 n.s., p = 0.44; fractions, $F_{(13,91)}$ = 7.3, p < 0.001; interaction, $F_{(13,91)}$ = 0.96, n.s., p = 0.49; Tukey post hoc analysis RD2 vs. placebo, Tukey post hoc analysis fraction 10 p = 0.003, fraction 1 to 9 an 11 to 14: n.s.).

426 Treatment with RD2 did not affect plasma-levels of different cytokines

427 The plasma cytokine levels of RD2- and placebo-treated mice, and their non-transgenic littermates
428 were determined using the Bio-Plex Pro Mouse Cytokine 23-plex assay (Table 1). Some values were
429 below the limit of detection (LoD) and were therefore excluded from evaluation. The only significant
430 difference found between RD2- and placebo-treated mice was the IL-1α level (Table 1, Kruskal-Wallis
431 one-way ANOVA on Ranks $p = 0.04$, ntg vs. placebo n.s., ntg vs. RD2 n.s., placebo vs. RD2 $p < 0.05$).
432 There was no significant difference between RD2-treated mice and non-transgenic littermates.
433 Additionally, a significant reduction in MIP-1α in placebo-treated mice compared to non-transgenic
434 littermates, but not between RD2- and placebo-treated mice, was observed (Table 1, Kruskal-Wallis
435 one-way ANOVA on Ranks $p = 0.008$, ntg vs. placebo $p < 0.05$, ntg vs. RD2 n.s., placebo vs. RD2
436 n.s.).

437 Adverse drug reactions have not been observed after long-term oral treatment with RD2

438 To test for any adverse or even toxic side effects of the RD2 treatment, four plasma parameters were
439 analyzed: lactate dehydrogenase (LDH), aspartate aminotransferase (AST), alanine aminotransferase
440 (ALT), and alkaline phosphatase (AP). These parameters are also analyzed in clinical routine to give
441 indications about possible drug mediated liver or heart targeted toxicity. The results did not reveal any
442 changes in these parameters (Fig. 4 a-d). Additionally, RD2 treatment did not result in significant gain
443 or loss of body weight (before vs. after treatment, mean ± SEM: RD2: 34.4 g ± 1.0 g vs. 33.5 g ± 0.9 g,
444 placebo: 34.3 g ± 0.9 g vs. 34.2 g ± 0.7 g, non-transgenic littermates 36.4 g ± 1.1 g vs. 34.1 g ± 0.8 g)
445 or a change in the general physiological or behavioral condition of the mice.

Discussion

In the present study, we examined the drug candidate RD2 for true therapeutic rather than only preventive efficacy in old-aged transgenic APP/PS1 mice. RD2 has previously proven to specifically eliminate toxic Aβ oligomers using the Aβ-QIAD assay, and to reduce formation of $A\beta_{(1\text{-}42)}$ fibrils and their seeding potential *in vitro (van Groen et al, 2017)*. *In vivo* it could be shown that RD2 has very favorable pharmacokinetic properties (Leithold et al, 2016). Additionally, intraperitoneal administration of RD2 over four weeks led to significant cognitive improvement in young APP/PS1 mice that displayed little Aβ pathology at the beginning of the treatment. This study could clearly demonstrate that RD2 is able to block progression of the disease. During a second study using the APP Swedish London mouse model it was possible to prove that also oral treatment with RD2 leads to a significant improvement of cognition and memory. Here, we decided to challenge the efficiency of RD2 by orally treating old-aged APP/PS1 mice with full-blown pathology over twelve weeks. This may closer mimic the patients´ situation at moderate and farer progressed disease stages, at least in respect to plaque pathology and cognitive deficits.

As a result of the treatment, we were able to demonstrate the curative *in vivo* efficacy of RD2. It is very well documented that APP/PS1 mice develop cognitive deficits by 7 months of age, which are clearly pronounced at the age of 18 months (Savonenko et al, 2005; Volianskis et al, 2010; Zhang et al, 2011). Because the cognitive abilities of RD2-treated mice were significantly improved over the placebo-treated mice and were indistinguishable from non-transgenic littermates, we conclude that RD2 treatment led to an overall reversal of the cognitive impairments of the transgenic mice. This is supported by the observations made in the open field test, where RD2-treated mice behaved indistinguishable from non-transgenic littermates.

RD2 treatment over 12 weeks decreased Aβ plaque load, which became significant in the cortex. We had not observed such a significant reduction in Aβ plaque load in previous RD2 treatment studies which had shorter treatment durations and used lower RD2 doses, but nevertheless yielded significant improvement in cognition (Kutzsche et al, 2017; van Groen et al, 2017). We conclude that cognitive improvement is not dependent on Aβ plaque load reduction. This is in line with the well-known fact that plaque load does not correlate with cognitive decline in humans (Aizenstein et al, 2008). The observation that cognitive improvement is achieved with shorter treatment duration and lower doses of RD2 before any reduction of plaque load becomes significant, might have implications for future clinical study designs. Therefore, one may carefully consider whether plaque load should be a primary efficacy endpoint in clinical studies for treatment of AD. As we had not observed significant plaque load reductions in the previously reported RD2 treatment studies with shorter treatment duration and lower doses, we were not surprised that there had not been a significant reduction in activated astrocytes and microglia in those studies. The significant reduction in cortex plaque load in the present study, subsequently also led to decreased gliosis, although not to a significant extent. Due to the manifested phenotype of the utilized mouse model, it is likely that the chronic inflammation could not be fully reversed during the course of the experiment and that an even longer treatment period would have been necessary to act significantly on cerebral inflammation.

485 RD2 was designed to specifically and directly eliminate toxic Aβ oligomers. Such target engagement
486 has already been shown *in vitro* using the QIAD assay (van Groen et al, 2017), where RD2 had very
487 significantly reduced the most toxic Aβ oligomers in DGC fractions 4 to 6, resembling particle sizes of
488 about 100 kDa (Brener et al, 2015). To develop an experiment that allows the investigation of target
489 engagement *in vivo*, we decided to use brain homogenates without enrichment steps for human Aβ,
490 as this could potentially lead to destruction of native Aβ oligomers and also to the formation of artificial
491 Aβ aggregates formed during Aβ precipitation steps. Because the brain homogenates contain not only
492 Aβ, but also all other brain derived components, we used the ultra-sensitive and specific sFIDA assay
493 (Herrmann et al, 2017b; Hulsemann et al, 2016; Kravchenko et al, 2017; Kuhbach et al, 2016) for
494 quantification of Aβ oligomers in the DGC-fractionated brain homogenates *ex vivo*. The most
495 significant reduction of Aβ containing particles by RD2 treatment was observed in fraction 10, which
496 corresponds to particles with a molecular weight of larger than 400 kDa (Brener et al, 2015). We
497 speculate that the elevated molecular weight of those *ex vivo* obtained particles as compared to the *in*
498 *vitro* generated Aβ oligomers of the Aβ-QIAD (Brener et al, 2015) was due to other proteins, besides
499 Aβ, that can be expected to be attached to Aβ oligomers. To the best of our knowledge, this is the first
500 time that a reduction of Aβ oligomers has been shown *in vivo* and confirms the proposed mechanism
501 of action for RD2 to be valid also in the functional brain.

502 Based on the results of additional assays probing for species typical behavior like marble burying and
503 nesting behavior (Deacon, 2006a; Deacon, 2006b; Filali & Lalonde, 2009; Torres-Lista & Gimenez-
504 Llort, 2013), we conclude that RD2 treatment did not cause any adverse side effects affecting
505 behavior. Moreover, the lack of significant changes in plasma-concentrations of enzymes like AST,
506 ALT, LDH, and AP between RD2- and placebo-treated mice as well as their non-transgenic littermates
507 further supports the absence of any adverse side effects. Otherwise, changes in plasma-
508 concentrations of these enzymes would have given indications about liver or heart targeted toxicity
509 (Ozer et al, 2008). This is particularly important, because relatively high doses of RD2 were
510 administered daily over twelve weeks.

511 In contrast to active and passive immunization against Aβ species, the postulated mechanism of
512 action of RD2 does not require components of the immune system. Therefore, one would not expect a
513 significant activation of the immune system, which would be indicated, for example, by significant
514 changes of plasma inflammation markers. Indeed, determination of various inflammation markers did
515 not yield any signs of immune system activation upon RD2 treatment. The necessity to rely on the
516 immune system might lead to a negative activation of e.g. T-cells, in the worst case resulting in
517 adverse side effects (e.g. microhemorrhages or meningoencephalitis) (Anand et al, 2014). Those
518 adverse side effects were visible occasionally during the clinical testing's of the first generation of Aβ
519 immunization, e.g. Bapineuzumab and Solanezumab (Carlson et al, 2016; Kerchner & Boxer, 2010). A
520 further advantage of RD2 in comparison to anti-Aβ-antibodies is the oral availability. Pharmacokinetic
521 profiles of RD2 and its lead compound D3 revealed high oral bioavailabilities (Jiang et al, 2015;
522 Leithold et al, 2016). Oral administration is the most attractive application method in humans and
523 usually leads to highest possible compliance.

Conclusion

Here, we describe the effects of a truly curative oral long-term treatment of old-aged APP/PS1 mice with full-blown pathology. We were able to demonstrate that RD2 reversed the cognitive and behavioral deficits in these old transgenic mice to the levels of non-transgenic littermates. Moreover, we demonstrated *in vivo* target engagement of RD2 on oligomeric Aβ species.

Even though the mice were treated with a relatively high dose this was tolerated very well, as no obvious adverse drug effects were observed. This strengthens the hypothesis that the observed improvement of cognition was due to the direct and specific reduction of oligomers, further supporting Aβ oligomer elimination as a successful therapeutic strategy against Alzheimer´s disease.

533 **Acknowledgements**

534 We thank Dr Carsten Korth for providing us the IC16 antibody. Moreover, we thank Dominik Honold
535 for excellent technical support.

536 **Author contributions**

537 S.S., A.W., J.K. and D.W. planned and designed the study. Most parts of the experiments were
538 performed by S.S. and E.S., with technical support. Data analysis was performed by S.S.. Cytokine
539 assay was conducted by S.H. and S.L.. DGC was conducted and analyzed by B.K.. The sFIDA assay
540 design, performance, analysis and interpretation were done by C.Z., O.B. and D.W.. S.S., A.W. and
541 D.W. wrote the manuscript and E.S., C.Z., B.K. S.H., S.L., J.K., N.J.S., and K-J.L. contributed to the
542 manuscript.

543 **Funding**

544 D.W. was supported by the "Portfolio Technology and Medicine" and the Helmholtz-Validierungsfonds
545 of the Impuls and Vernetzungs-Fonds der Helmholtzgemeinschaft. D.W. and K.-J.L. were supported
546 by the "Portfolio Drug Research" of the Impuls and Vernetzungs-Fonds der Helmholtzgemeinschaft

547 **Conflict of Interest**

548 The authors declare that they have no conflict of interest.

549 **References**

550 Aizenstein HJ, Nebes RD, Saxton JA, Price JC, Mathis CA, Tsopelas ND, Ziolko SK, James JA, Snitz
551 BE, Houck PR et al (2008) Frequent amyloid deposition without significant cognitive impairment
552 among the elderly. Archives of neurology 65: 1509-1517

553 Anand R, Gill KD, Mahdi AA (2014) Therapeutics of Alzheimer's disease: Past, present and future.
554 Neuropharmacology 76 Pt A: 27-50

555 Archer J (1973) Tests for emotionality in rats and mice: a review. Animal behaviour 21: 205-235

556 Blennow K, de Leon MJ, Zetterberg H (2006) Alzheimer's disease. Lancet 368: 387-403

557 Brener O, Dunkelmann T, Gremer L, van Groen T, Mirecka EA, Kadish I, Willuweit A, Kutzsche J,
558 Jurgens D, Rudolph S et al (2015) QIAD assay for quantitating a compound's efficacy in elimination of
559 toxic Abeta oligomers. Scientific reports 5: 13222

560 Carlson C, Siemers E, Hake A, Case M, Hayduk R, Suhy J, Oh J, Barakos J (2016) Amyloid-related
561 imaging abnormalities from trials of solanezumab for Alzheimer's disease. Alzheimer's & dementia 2:
562 75-85

563 Cavini IA, Munte CE, Beck Erlach M, van Groen T, Kadish I, Zhang T, Ziehm T, Nagel-Steger L,
564 Kutzsche J, Kremer W et al (2018) Inhibition of Amyloid A[small beta] Aggregation by High Pressures
565 or Specific D-Enantiomeric Peptides. Chemical Communications

566 Clark RA, Shoaib M, Hewitt KN, Stanford SC, Bate ST (2012) A comparison of InVivoStat with other
567 statistical software packages for analysis of data generated from animal experiments. Journal of
568 psychopharmacology 26: 1136-1142

569 Deacon RM (2006a) Assessing nest building in mice. Nat Protoc 1: 1117-1119

570 Deacon RM (2006b) Digging and marble burying in mice: simple methods for in vivo identification of
571 biological impacts. Nature protocols 1: 122-124

572 Elfgen A, Santiago-Schubel B, Gremer L, Kutzsche J, Willbold D (2017) Surprisingly high stability of
573 the Abeta oligomer eliminating all-d-enantiomeric peptide D3 in media simulating the route of orally
574 administered drugs. European journal of pharmaceutical sciences : official journal of the European
575 Federation for Pharmaceutical Sciences 107: 203-207

576 Ferreira ST, Klein WL (2011) The Abeta oligomer hypothesis for synapse failure and memory loss in
577 Alzheimer's disease. Neurobiology of learning and memory 96: 529-543

578 Ferreira ST, Lourenco MV, Oliveira MM, De Felice FG (2015) Soluble amyloid-beta oligomers as
579 synaptotoxins leading to cognitive impairment in Alzheimer's disease. Frontiers in cellular
580 neuroscience 9: 191

581 Filali M, Lalonde R (2009) Age-related cognitive decline and nesting behavior in an APPswe/PS1
582 bigenic model of Alzheimer's disease. Brain research 1292: 93-99

583 Funke SA, van Groen T, Kadish I, Bartnik D, Nagel-Steger L, Brener O, Sehl T, Batra-Safferling R,
584 Moriscot C, Schoehn G et al (2010) Oral treatment with the d-enantiomeric peptide D3 improves the
585 pathology and behavior of Alzheimer's Disease transgenic mice. ACS chemical neuroscience 1: 639-
586 648

587 Garcia-Alloza M, Robbins EM, Zhang-Nunes SX, Purcell SM, Betensky RA, Raju S, Prada C,
588 Greenberg SM, Bacskai BJ, Frosch MP (2006) Characterization of amyloid deposition in the
589 APPswe/PS1dE9 mouse model of Alzheimer disease. Neurobiology of disease 24: 516-524

590 Haass C, Selkoe DJ (2007) Soluble protein oligomers in neurodegeneration: lessons from the
591 Alzheimer's amyloid beta-peptide. Nature reviews Molecular cell biology 8: 101-112

592 Hardy J (1992) An 'anatomical cascade hypothesis' for Alzheimer's disease. . Trends in
593 Neurosciences 15: 200-201

Hardy J, Selkoe DJ (2002) The amyloid hypothesis of Alzheimer's disease: progress and problems on the road to therapeutics. Science 297: 353-356

Hellmert M, Muller-Schiffmann A, Peters MS, Korth C, Schrader T (2015) Hybridization of an Abeta-specific antibody fragment with aminopyrazole-based beta-sheet ligands displays striking enhancement of target affinity. Organic & biomolecular chemistry 13: 2974-2979

Herrmann Y, Bujnicki T, Zafiu C, Kulawik A, Kuhbach K, Peters L, Fabig J, Willbold J, Bannach O, Willbold D (2017a) Nanoparticle standards for immuno-based quantitation of alpha-synuclein oligomers in diagnostics of Parkinson's disease and other synucleinopathies. Clinica chimica acta; international journal of clinical chemistry 466: 152-159

Herrmann Y, Kulawik A, Kuhbach K, Hulsemann M, Peters L, Bujnicki T, Kravchenko K, Linnartz C, Willbold J, Zafiu C et al (2017b) sFIDA automation yields sub-femtomolar limit of detection for Abeta aggregates in body fluids. Clinical biochemistry 50: 244-247

Hulsemann M, Zafiu C, Kuhbach K, Luhmann N, Herrmann Y, Peters L, Linnartz C, Willbold J, Kravchenko K, Kulawik A et al (2016) Biofunctionalized Silica Nanoparticles: Standards in Amyloid-beta Oligomer-Based Diagnosis of Alzheimer's Disease. J Alzheimers Dis 54: 79-88

Jakob-Roetne R, Jacobsen H (2009) Alzheimer's disease: from pathology to therapeutic approaches. Angewandte Chemie (International ed in English) 48: 3030-3059

Jankowsky JL, Fadale DJ, Anderson J, Xu GM, Gonzales V, Jenkins NA, Copeland NG, Lee MK, Younkin LH, Wagner SL et al (2004) Mutant presenilins specifically elevate the levels of the 42 residue beta-amyloid peptide in vivo: evidence for augmentation of a 42-specific gamma secretase. Human molecular genetics 13: 159-170

Janus C, Flores AY, Xu G, Borchelt DR (2015) Behavioral abnormalities in APPSwe/PS1dE9 mouse model of AD-like pathology: comparative analysis across multiple behavioral domains. Neurobiology of aging 36: 2519-2532

Jiang N, Leithold LH, Post J, Ziehm T, Mauler J, Gremer L, Cremer M, Schartmann E, Shah NJ, Kutzsche J et al (2015) Preclinical Pharmacokinetic Studies of the Tritium Labelled D-Enantiomeric Peptide D3 Developed for the Treatment of Alzheimer s Disease. PloS one 10: e0128553

Kamphuis W, Mamber C, Moeton M, Kooijman L, Sluijs JA, Jansen AH, Verveer M, de Groot LR, Smith VD, Rangarajan S et al (2012) GFAP isoforms in adult mouse brain with a focus on neurogenic astrocytes and reactive astrogliosis in mouse models of Alzheimer disease. PloS one 7: e42823

Karran E, Mercken M, De Strooper B (2011) The amyloid cascade hypothesis for Alzheimer's disease: an appraisal for the development of therapeutics. Nature reviews Drug discovery 10: 698-712

Kerchner GA, Boxer AL (2010) Bapineuzumab. Expert opinion on biological therapy 10: 1121-1130

Kravchenko K, Kulawik A, Hulsemann M, Kuhbach K, Zafiu C, Herrmann Y, Linnartz C, Peters L, Bujnicki T, Willbold J et al (2017) Analysis of anticoagulants for blood-based quantitation of amyloid beta oligomers in the sFIDA assay. Biological chemistry 398: 465-475

Kuhbach K, Hulsemann M, Herrmann Y, Kravchenko K, Kulawik A, Linnartz C, Peters L, Wang K, Willbold J, Willbold D et al (2016) Application of an Amyloid Beta Oligomer Standard in the sFIDA Assay. Frontiers in neuroscience 10: 8

Kumar A, Singh A, Ekavali (2015) A review on Alzheimer's disease pathophysiology and its management: an update. Pharmacological reports : PR 67: 195-203

Kutzsche J, Schemmert S, Tusche M, Neddens J, Rabl R, Jurgens D, Brener O, Willuweit A, Hutter-Paier B, Willbold D (2017) Large-Scale Oral Treatment Study with the Four Most Promising D3-Derivatives for the Treatment of Alzheimer's Disease. Molecules (Basel, Switzerland) 22

Leithold LH, Jiang N, Post J, Ziehm T, Schartmann E, Kutzsche J, Shah NJ, Breitkreutz J, Langen KJ, Willuweit A et al (2016) Pharmacokinetic Properties of a Novel D-Peptide Developed to be Therapeutically Active Against Toxic beta-Amyloid Oligomers. Pharmaceutical research 33: 328-336

641 Liu J, Yang B, Ke J, Li W, Suen WC (2016) Antibody-Based Drugs and Approaches Against Amyloid-
642 beta Species for Alzheimer's Disease Immunotherapy. Drugs & aging 33: 685-697

643 Morris RG, Garrud P, Rawlins JN, O'Keefe J (1982) Place navigation impaired in rats with
644 hippocampal lesions. Nature 297: 681-683

645 Ozer J, Ratner M, Shaw M, Bailey W, Schomaker S (2008) The current state of serum biomarkers of
646 hepatotoxicity. Toxicology 245: 194-205

647 Rosenblum WI (2014) Why Alzheimer trials fail: removing soluble oligomeric beta amyloid is essential,
648 inconsistent, and difficult. Neurobiology of aging 35: 969-974

649 Savage MJ, Kalinina J, Wolfe A, Tugusheva K, Korn R, Cash-Mason T, Maxwell JW, Hatcher NG,
650 Haugabook SJ, Wu G et al (2014) A sensitive abeta oligomer assay discriminates Alzheimer's and
651 aged control cerebrospinal fluid. J Neurosci 34: 2884-2897

652 Savonenko A, Xu GM, Melnikova T, Morton JL, Gonzales V, Wong MP, Price DL, Tang F, Markowska
653 AL, Borchelt DR (2005) Episodic-like memory deficits in the APPswe/PS1dE9 mouse model of
654 Alzheimer's disease: relationships to beta-amyloid deposition and neurotransmitter abnormalities.
655 Neurobiology of disease 18: 602-617

656 Selkoe DJ, Hardy J (2016) The amyloid hypothesis of Alzheimer's disease at 25 years. EMBO
657 molecular medicine 8: 595-608

658 Torres-Lista V, Gimenez-Llort L (2013) Impairment of nesting behaviour in 3xTg-AD mice. Behavioural
659 brain research 247: 153-157

660 van Groen T, Kadish I, Funke SA, Bartnik D, Willbold D (2013) Treatment with D3 removes amyloid
661 deposits, reduces inflammation, and improves cognition in aged AbetaPP/PS1 double transgenic
662 mice. Journal of Alzheimer's disease : JAD 34: 609-620

663 van Groen T, Kadish I, Wiesehan K, Funke SA, Willbold D (2009) In vitro and in vivo staining
664 characteristics of small, fluorescent, Abeta42-binding D-enantiomeric peptides in transgenic AD
665 mouse models. ChemMedChem 4: 276-282

666 van Groen T, Kadish, I., Funke, A. S., Bartnik, D., Willbold, D. (2012) Treatment with Aβ42 Binding d-
667 Amino Acid Peptides Reduce Amyloid Deposition and Inflammation in APP/PS1 Double Transgenic
668 Mice. Advances in Protein Chemistry and Structural Biology 88: 133-152

669 van Groen T, Schemmert S, Brener O, Gremer L, Ziehm T, Tusche M, Nagel-Steger L, Kadish I,
670 Schartmann E, Elfgen A et al (2017) The Abeta oligomer eliminating D-enantiomeric peptide RD2
671 improves cognition without changing plaque pathology. Scientific reports 7: 16275

672 van Groen T, Wiesehan K, Funke SA, Kadish I, Nagel-Steger L, Willbold D (2008) Reduction of
673 Alzheimer's disease amyloid plaque load in transgenic mice by D3, A D-enantiomeric peptide
674 identified by mirror image phage display. ChemMedChem 3: 1848-1852

675 Volianskis A, Kostner R, Molgaard M, Hass S, Jensen MS (2010) Episodic memory deficits are not
676 related to altered glutamatergic synaptic transmission and plasticity in the CA1 hippocampus of the
677 APPswe/PS1deltaE9-deleted transgenic mice model of ss-amyloidosis. Neurobiology of aging 31:
678 1173-1187

679 Wang-Dietrich L, Funke SA, Kuhbach K, Wang K, Besmehn A, Willbold S, Cinar Y, Bannach O,
680 Birkmann E, Willbold D (2013) The amyloid-beta oligomer count in cerebrospinal fluid is a biomarker
681 for Alzheimer's disease. Journal of Alzheimer's disease : JAD 34: 985-994

682 Wang MJ, Yi S, Han JY, Park SY, Jang JW, Chun IK, Kim SE, Lee BS, Kim GJ, Yu JS et al (2017)
683 Oligomeric forms of amyloid-beta protein in plasma as a potential blood-based biomarker for
684 Alzheimer's disease. Alzheimer's research & therapy 9: 98

685 Zhang W, Hao J, Liu R, Zhang Z, Lei G, Su C, Miao J, Li Z (2011) Soluble Abeta levels correlate with
686 cognitive deficits in the 12-month-old APPswe/PS1dE9 mouse model of Alzheimer's disease.
687 Behavioural brain research 222: 342-350

688 **Tables**

[pg/ml]	ntg	Placebo	RD2	Statistic
IL-1α	23.54 ± 4.89	24.42 ± 2.16*	15.1 ± 2.18*	Placebo vs. ntg n.s. RD2 vs. Placebo p < 0.05 RD2 vs. ntg n.s.
IL-10	22.17 ± 5.76	39.44 ± 18.52	26.89 ± 6.78	n.s.
IL-12 (p40)	191.7 ± 19.39	187.0 ± 24.30	208.9 ± 18.22	n.s.
IL-13	147.9 ± 26.83	106.8 ± 32.31	176.2 ± 44.57	n.s.
IL-17	2.25 ± 0.42	5.03 ± 1.53	5.85 ± 1.80	n.s.
G-CSF	187.6 ± 61.63	116.2 ± 29.08	118.2 ± 19.14	n.s.
IFN-γ	16.67 ± 3.46	11.09 ± 2.19	18.38 ± 4.89	n.s.
MCP-1	131.2 ± 19.31	156.4 ± 26.47	146.0 ± 27.46	n.s.
MIP-1α	31.97 ± 3.31*	14.75 ± 2.23*	28.03 ± 6.02	Placebo vs. ntg p < 0.05 RD2 vs. Placebo n.s. RD2 vs. ntg n.s.
MIP-1β	19.72 ± 3.99	22.23 ± 4.15	30.27 ± 6.93	n.s.
RANTES	27.15 ± 10.4	16.55 ± 4.32	25.88 ± 9.57	n.s.
TNF-α	64.12 ± 7.32	87.89 ± 14.02	106.6 ± 28.51	n.s.

689 **Table 1: Cytokine assay of non-transgenic littermates, RD2- and placebo-treated mice.** For the evaluation of
690 a potential change in the amount of different cytokines, a Bio-Plex Pro Mouse Cytokine 23-plex Assay was
691 performed with heparinized plasma samples of non-transgenic littermates (ntg), RD2- and placebo-treated mice.
692 Data revealed a significant reduction in IL-1α due to RD2 treatment in comparison to placebo treatment.
693 Furthermore, significantly decreased concentrations of MIP-1α were detected in placebo-treated mice compared
694 to ntg, but no differences between RD2-treated mice and ntg were observed. Cytokine concentrations are given
695 as pg/ml. Data is represented as mean ± SEM, * < 0.05.

Figures

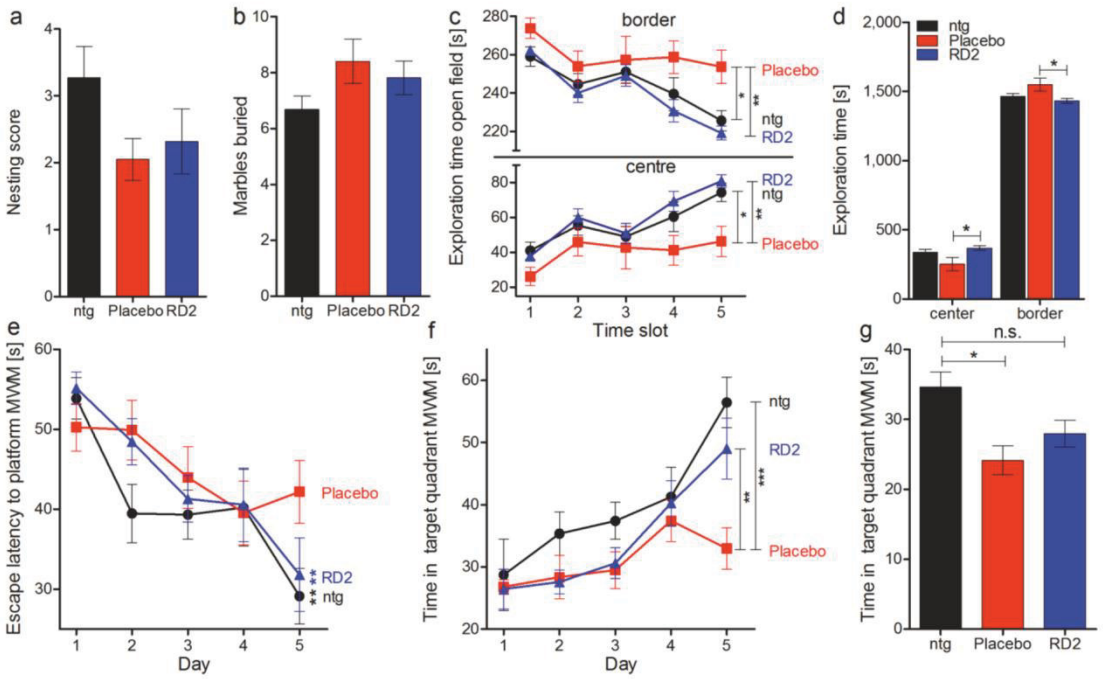

Fig. 1: RD2 treatment of old-aged APP/PS1 mice resulted in significantly improved cognitive performance. Nesting behavior (a) and marble burying (b) were examined to investigate species-typical behavior. Neither RD2 nor placebo treatment had a significant influence on the nesting behavior, nor on the marble burying results compared to non-transgenic littermates (ntg). An open field test was performed to analyze and compare the exploratory and anxiety related behavior of RD2- and placebo-treated mice, as well as their ntg (c, d). Mice were allowed to explore the arena, divided into border and center zone, for 25 min. Exploration of the center and border zone is represented as 5 different time slots (c). In contrast to placebo-treated mice, RD2-treated mice and ntg exhibited a habituation effect to the arena that significantly differs from the performance of placebo-treated mice (c). Analysis of overall exploration revealed a significant difference in the exploratory and anxiety related behavior between RD2- and placebo-treated mice but not between RD2-treated mice and ntg, indicating that RD2 treatment reversed the phenotype of the transgenic mice (d). Additionally, a Morris water maze (MWM) was conducted in which mice were trained for 5 days to find a hidden platform (e-f). Escape latencies to the platform of RD2-treated mice were significantly lower compared to placebo-treated mice indicating improved learning, similar to ntg (e). In addition, RD2 treated-mice and ntg spent significantly more time in the platform quadrant compared to placebo-treated mice on the last training day (f). Analysis of the probe trial revealed a significant difference between ntg and placebo-treated mice, but not between ntg and RD2-treated mice, respectively (g). Each behavioral performance of RD2-treated mice was similar to those of ntg, suggesting a reversed phenotype. Data is represented as mean ± SEM, RD2 n = 11, placebo n = 10, ntg n = 11.

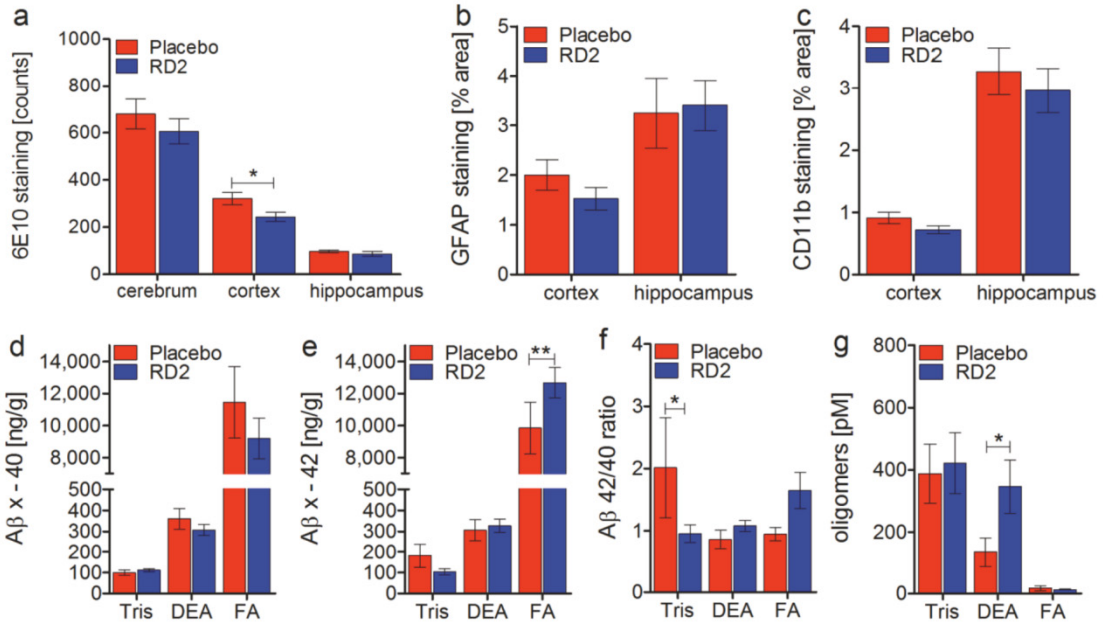

Fig. 2: Effects of RD2 treatment on Aβ pathology, gliosis, and Aβ oligomers in the brains of APP/PS1 mice. Investigations of a potential reduction in either Aβ plaque load or astrogliosis after RD2-treatment were performed using immunohistochemical analysis. Plaque count was analyzed by 6E10 staining in different areas of the brain (cerebrum, cortex, and hippocampus). Compared to placebo-treated mice, RD2-treated mice showed a decreased number of Aβ deposits in all analyzed regions being significant in the cortex (a). Activated astrocytes were quantified after GFAP staining (b) and activated microglia were quantified after CD11b staining (c). Results exhibited no significant difference in gliosis between RD2- and placebo-treated mice. Levels of Aβ x–40 (d) and Aβ x–42 (e) in the Tris-soluble (Tris), DEA-soluble (DEA) and formic acid fractions (FA) of brain homogenates of RD2- and placebo-treated mice were analyzed by ELISA, resulting in a significant increase of Aβ(x-42) in the FA-fraction of RD2-treatded mice. Concentrations were presented in ng (Aβ(x–40) or Aβ(x–42))/g (brain). Aβ 42/40 ratio is shown in (f) and yielded a significantly higher ratio in the Tris fraction of placebo-treated mice. Aβ oligomer concentrations were analyzed in the above-mentioned fractions by sFIDA assay, resulting in a significant increase in Aβ oligomers within the DEA-fraction of RD2- compared to placebo-treated mice (g). Data is represented as mean ± SEM. All: * $p > 0.05$.

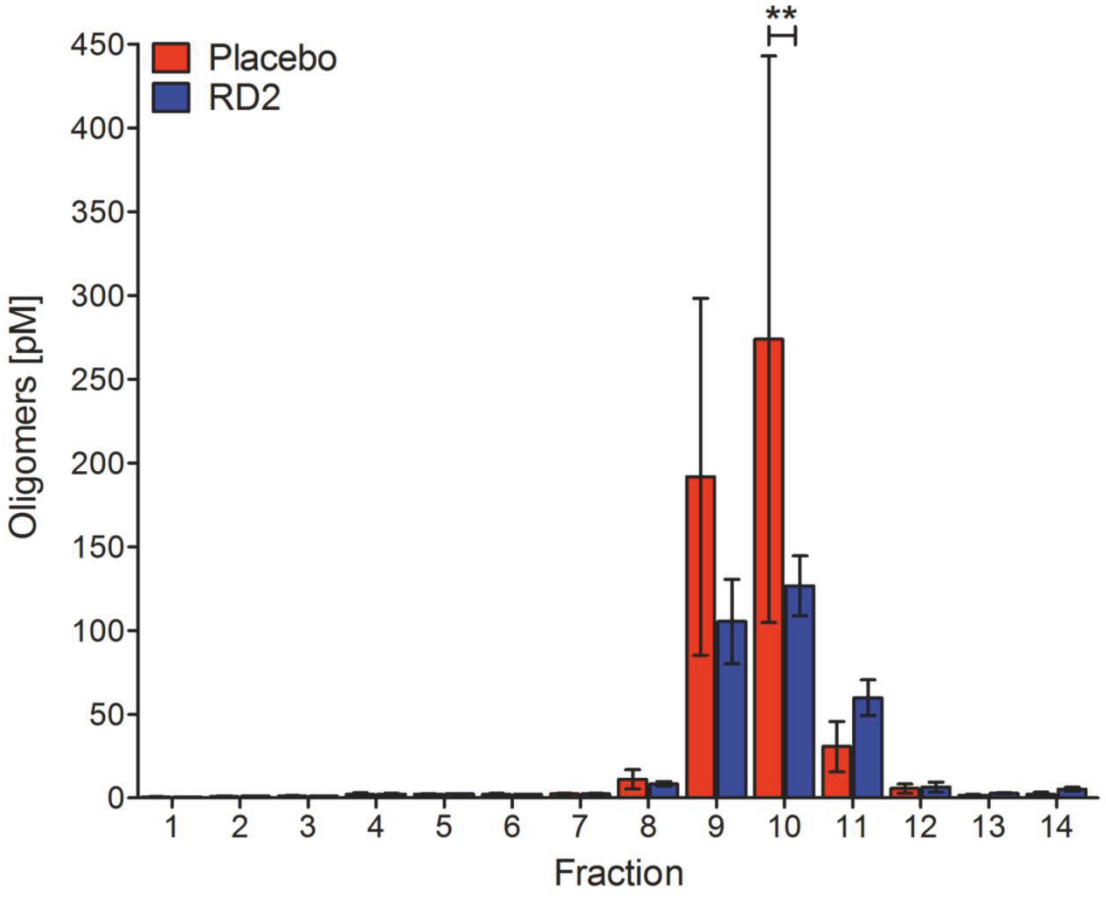

731

732 **Fig. 3: Treatment with RD2 significantly reduced oligomeric Aβ species.** Oligomeric Aβ levels in the fractions
733 of density gradient ultra-centrifuged brain homogenates of RD2- and placebo treated APP/PS1 mice were
734 analyzed by the aggregate specific and highly sensitive sFIDA assay. Results revealed a significant decrease in
735 oligomeric Aβ species in fraction 10 of RD2- compared to placebo-treated mice. sFIDA read-out was converted to
736 Aβ oligomer concentrations after calibration with $A\beta_{1\text{-}42}$-SiNaP (internal standard calibration) (silica nanoparticles).
737 Data is represented as mean ± SEM.. Placebo n = 4, RD2 n = 5. **p < 0.01.

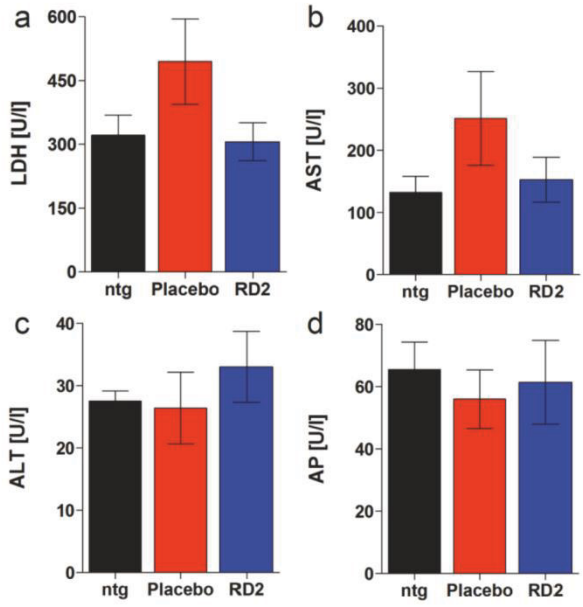

Fig. 4: Effects of long-term RD2 treatment on different plasma enzymes. Examination of lactate dehydrogenase (LDH) (a), aspartate aminotransferase (AST) (b), alanine aminotransferase (ALT) (c), and alkaline phosphatases (AP) (d). These plasma enzymes, usually analyzed to investigate whether a treatment with a new medication induces e.g. liver intoxication, indicated no toxic adverse side effects due to long-term RD2 treatment. No significant differences were detected between non-transgenic littermates (ntg), RD2- or placebo-treated APP/PS1 mice. This is particularly important based on the high administered concentration (200 mg/kg daily). Data is represented as mean ± SEM. Kruskal-Wallis one-way ANOVA on Ranks, (a): n.s. $p = 0.33$; One-way ANOVA, (b): $F_{(2,13)} = 1.42$ n.s. $p = 0.28$, (c): $F_{(2,13)} = 0.5$ n.s. $p = 0.62$, (d): $F_{(2,13)} = 0.18$ n.s. $p = 0.84$. ntg n = 4, Placebo n = 5, RD2 n = 5.

3.9 *In vitro* potency and preclinical pharmacokinetic comparison of all-D-enantiomeric peptides developed for the treatment of Alzheimer's disease

Autoren: **Schartmann E**, Schemmert S, Niemietz N, Honold D, Ziehm T, Tusche M, Elfgen A, Gering I, Brener O, Shah NJ, Langen KJ, Kutzsche J, Willbold D, Willuweit A

Journal: Journal of Alzheimer's Disease

eingereicht am 15.02.2018

Impact Factor: 3,731 (2017)

Beitrag: Planung aller Experimente

Durchführung der *in vitro*-Tests zur Aβ-Interaktion (ThT, QIAD)

Durchführung aller pharmakokinetischer Experimente

Durchführung der Plasmaproteinbindungs-Experimente

Auswertung und grafische Darstellung aller Experimente

Berechnung aller pharmakokinetischer Parameter und der Blut-Hirn-Schranken-Durchlässigkeits-Parameter

Schreiben des Manuskripts

In vitro potency and preclinical pharmacokinetic comparison of all-D-enantiomeric peptides developed for the treatment of Alzheimer's disease

Elena Schartmann[1], Sarah Schemmert[1], Nicole Niemietz[2], Dominik Honold[1], Tamar Ziehm[1], Markus Tusche[1], Anne Elfgen[1], Ian Gering[1], Oleksandr Brener[1,3], Nadim Joni Shah[2,4], Karl-Josef Langen[2,5], Janine Kutzsche[1], Dieter Willbold[1,3,*], Antje Willuweit[2,*]

[1]*Institute of Complex Systems, Structural Biochemistry (ICS-6), Forschungszentrum Jülich GmbH, 52425 Jülich, Germany*

[2]*Institute of Neuroscience and Medicine, Medical Imaging Physics (INM-4), Forschungszentrum Jülich GmbH, 52425 Jülich, Germany*

[3]*Institut für Physikalische Biologie, Heinrich-Heine-Universität Düsseldorf, 40225 Düsseldorf, Germany*

[4]*Department of Neurology, Faculty of Medicine, JARA, RWTH Aachen University, 52074 Aachen, Germany*

[5]*Department of Nuclear Medicine, Universitätsklinikum der RWTH Aachen, 52074 Aachen, Germany*

Pharmacokinetics of D-enantiomeric peptides

*Correspondence to:

A. Willuweit, Institute of Neuroscience and Medicine, Medical Imaging Physics (INM-4), Forschungszentrum Jülich GmbH, 52425 Jülich, Germany

E-Mail: a.willuweit@fz-juelich.de

Phone: 0049 - 2461 - 6196358

D. Willbold, Institute of Complex Systems, Structural Biochemistry (ICS-6), Forschungszentrum Jülich GmbH, 52425 Jülich, Germany

E-mail: d.willbold@fz-juelich.de

Phone: 0049 - 2461 - 612100

Abstract

Diffusible amyloid-β (Aβ) oligomers are currently presumed to be the most cytotoxic Aβ assembly and held responsible to trigger the pathogenesis of Alzheimer's disease (AD). Thus, Aβ oligomers are a prominent target in AD drug development. Previously, we reported on our solely D-enantiomeric peptide D3 and its derivatives as AD drug candidates. Here, we compare one of the most promising D3 derivatives, ANK6, with its tandem version (tANK6), and its head-to-tail cyclized isoform (cANK6r). *In vitro* tests investigating the D-peptides' potencies to inhibit Aβ aggregation, eliminate Aβ oligomers, and reduce Aβ-induced cytotoxicity revealed that all three D-peptides efficiently target Aβ. Subsequent preclinical pharmacokinetic studies of the three all-D-peptides in wildtype mice showed promising blood-brain barrier permeability with cANK6r yielding the highest levels in brain. The peptides' potencies to lower Aβ toxicity and their remarkable brain/plasma ratios make them promising AD drug candidates.

Keywords

Alzheimer's disease, amyloid-β, D-enantiomeric peptides, pharmacokinetic profile

Introduction

Neurodegenerative diseases caused by the aggregation of misfolded proteins are about to become a threatening risk for our aging society and health care systems. Alzheimer's disease (AD) is one of the most intensively researched progressive neurodegenerative diseases. More than 20 million people worldwide are currently affected by AD and no curative therapy has been developed in the last 110 years since Alois Alzheimer described the disease. This circumstance manifests the extensive medical need for development of a disease modifying or even a curative treatment of AD.

AD is characterized by three major hallmarks: extracellular deposits or plaques consisting of amyloid-β protein (Aβ), intracellular deposits consisting of hyperphosphorylated tau protein, and neurodegeneration. Aβ is natively generated throughout lifetime and able to aggregate, thus forming lower molecular weight soluble Aβ oligomers or insoluble Aβ fibrils that make up the plaques [1]. Since about one decade, researchers entitle soluble oligomers to be the most neurotoxic Aβ species [2]. Both, Aβ and tau, with their formation, aggregation and degradation are prominent targets in AD drug development [3, 4].

In our lab, we identified and developed compounds that specifically and directly eliminate toxic Aβ oligomers. Previously, we described the properties of our lead compound D3 (**Table 1**). D3 consists of twelve D-enantiomeric amino acid residues and has been identified by mirror image phage display [5-9]. It stabilized Aβ monomers in an aggregation-incompetent conformation thus shifting the equilibrium between Aβ monomers and oligomers away from oligomers towards monomers. D3 eliminated Aβ oligomers *in vitro*, improved cognition and lowered Aβ plaque load in transgenic AD mouse models, and revealed promising *in vivo* properties, e.g. extraordinary high proteolytic stability and beneficial pharmacokinetic characteristics [10-22]. In an optimization approach, D3's amino acid residue sequence was systematically replaced by natural and unnatural amino acid residues, using peptide microarrays, and screened for their affinity and specificity to monomeric Aβ. The most

promising seven peptides (ANK1-ANK7) were selected and further investigated *in vitro* awarding ANK6 the most promising properties [23]. Another optimization strategy to increase the peptides' efficiency to eliminate toxic Aβ oligomers as well as to increase pharmacokinetic availability was the head-to-tail cyclization of D3 and various derivatives [24, 25]. Additionally, linear tandem 24-mer D3-derivatives in head-to-tail arrangement were designed, pharmacokinetically investigated [26], and successfully tested *in vitro* as well as *in vivo* to reduce symptoms of AD pathology, even more efficiently than the corresponding 12-mer peptides [19, 26, 27].

Here, we further investigated and characterized the most promising microarray-derived derivative ANK6 and compared it to two ANK6-variants, the head-to-tail linear tandem ANK6 (tANK6) and the head-to-tail cyclic ANK6 with an additional arginine (cANK6r) to maintain the total net charge, thus combining different peptide optimization tools. We conducted *in vitro* experiments that exhibit the D-peptides' impacts on $A\beta_{1-42}$ aggregation (Aβ aggregation assay), on Aβ oligomer elimination (QIAD assay), and on $A\beta_{1-42}$-induced cytotoxicity (cell viability assay). In another pre-*in vivo* test, the D-peptides' plasma protein binding affinities were determined. Thereby, we explored whether ANK6 and its two variants are efficient and non-toxic Aβ-targeting AD drug candidates. Afterwards, pharmacokinetic studies with intravenous (i.v.) and oral (p.o.) D-peptide administration to C57BL/6N mice were carried out to evaluate the D-peptides' eligibility for implementation in further treatment studies. Within the pharmacokinetic studies, special attention was paid to the D-peptides' uptake into the brain and their blood-brain barrier (BBB) permeability.

Materials and Methods

Peptides

Non-labelled peptides ANK6, tANK6, and cANK6r peptides were synthesized by peptides & elephants GmbH (Germany). Radio-labelled ^{3}H-ANK6, ^{3}H-tANK6, and ^{3}H-cANK6r

were produced by Cambridge Research Biochemicals (United Kingdom) with 1 mCi/mL. The peptides' sequences are shown in Table 1. Recombinant $A\beta_{1-42}$ was obtained from Isoloid GmbH (Germany). Synthetic $A\beta_{1-42}$ was obtained from Bachem AG (Switzerland).

D-peptides' *in vitro* potencies

Aβ aggregation assay

ANK6's, tANK6's, cANK6r's, and D3's potency to inhibit $A\beta_{1-42}$ aggregation was examined using Thioflavin T (ThT). For this purpose, a buffer solution composed of 20 mM sodium phosphate buffer (pH 7.4) including 50 mM sodium chloride, and 5 µM ThT was prepared. Afterwards, ANK6, tANK6, cANK6r, or D3 were diluted in this solution, respectively, to final peptide concentrations between 0.3125 and 80 µM (ANK6 and tANK6: 0.3125, 0.625, 1.25, 2.5, 5, 10, 20 µM; cANK6r: 1.25, 2.5, 5, 10, 20, 40, 80 µM; D3: 1.17, 2.34, 4.7, 9.4, 18.8, 37.5, 75 µM). The buffer solution only served as negative control (blank). Lyophilized $A\beta_{1-42}$ was dissolved in the respective peptide solution to a final concentration of 10 µM. D-peptide solutions with the highest concentration of the respective D-peptide containing all components, except of $A\beta_{1-42}$, served as negative controls. $A\beta_{1-42}$ solved in buffer solution without D-peptide served as positive control. 100 µL of each solution were transferred into the wells (triplicates) of 96 well microplates (PS, black, non-binding from Greiner Bio-One, Germany) and fluorescence signals (excitation λ 440 nm, emission λ 490 nm) were measured in a Polarstar Optima plate reader (BMG, Germany) at 37 °C every 20 min for 70 h. Afterwards, the respective blank curves were subtracted from each aggregation curve to exclude background fluorescence. The inhibition potency of each D-peptide's concentration was calculated by normalizing the final fibril mass to the positive control, which shows maximal Aβ aggregation and therefore maximal fluorescence signals (0% Aβ aggregation inhibition). The half maximal inhibitory concentration (IC_{50} value) was determined by plotting the percent inhibition against the respective D-peptides'

concentrations. Datasets were fitted by nonlinear regression (one site – specific binding with Hill slope, GraphPad Prism 5).

Cell viability assay

ANK6's, tANK6's, and cANK6r's ability to neutralize the toxicity of oligomeric $A\beta_{1-42}$ was investigated with 3-(4,5-Dimethylthiazol-2-yl)-2,5-diphenyltetrazoliumbromid (MTT). In this experiment, we used rat phaeochromocytoma cells (PC12 cells, Leibniz Institute DSMZ, Germany) cultivated in DMEM supplemented with 10 % fetal calf serum, 5 % horse serum and 1 % penicillin-streptomycin at 37 °C, 5 % CO_2 and 95 % humidity. The cells (10,000 cells/well) were incubated on collagen coated 96 well plates (Gibco, Life Technologies, # A11428-03) for growth in adherent cell culture (24 h, 37 °C). Oligomeric Aβ was generated by incubating monomeric $A\beta_{1-42}$ in sodium phosphate buffer (10 mM Na_2HPO_4/NaH_2PO_4, pH 7.4) at 21 °C and 600 rpm agitation for 4.5 h. The cell viability was investigated after the incubation with buffer only (positive control, set to 100 % cell viability), Triton X-100 (0.125 %, cytotoxic agent, negative control), $A\beta_{1-42}$ alone (1 µM), ANK6, tANK6, or cANK6r alone (15 µM each), as well as $A\beta_{1-42}$ (1 µM) in the presence of ANK6, tANK6, or cANK6r (each D-peptide in 7 different concentrations varying between 0.008 and 15 µM, in quintuplicates) (overnight, 37 °C) using the Cell Proliferation Kit I (MTT) according to the manufacturer's protocol (Roche, Switzerland). Absorbance readout was detected with a Polarstar Optima plate reader (BMG, Germany) at 570 and 660 nm. The relative cell viability [%] was calculated by normalizing the absorbance readout to the positive control (PC12 cells incubated with buffer). The IC_{50} value was determined by plotting the relative cell viability [%] against the respective D-peptides' concentrations. Datasets were fitted by nonlinear regression (logistic fit; OriginPro 9.0G).

Quantitative determination of interference with Aβ aggregate size distribution

As soluble Aβ oligomers are currently expected to be the most neurotoxic Aβ species causing AD, ANK6's, tANK6's, and cANK6r's $A\beta_{1-42}$ oligomer elimination potency was

investigated by the quantitative determination of interference with Aβ aggregate size distribution (QIAD) similar as described before [19]. In short, lyophilized $A\beta_{1-42}$ was dissolved in sodium phosphate buffer to a final concentration of 80 µM and incubated for 2.5 h (21 °C, 600 rpm) to achieve an Aβ aggregate distribution including monomers, oligomers and higher molecular aggregates. Then, sodium phosphate buffer (control), 20 µM ANK6, 20 µM tANK6, or 20 µM cANK6r were added and incubated for further 40 min (21 °C, 600 rpm). Afterwards, the samples were loaded on top of a density gradient (5 to 50% (w/v) iodixanol, OptiPrep, Axis-Shield, Norway) and ultra-centrifuged for 3 h (4 °C, 259.000 × g, Optima TL-100, Beckman Coulter, USA). In the following, 14 fractions (140 µL each) were taken from top to bottom, whereby the top fractions (1-2) contained Aβ monomers, the middle fractions (4-6) contained the Aβ oligomers of special interest, and the bottom fractions (11-14) contained high molecular weight co-precipitates. The left-over was diluted in 60 µL 6 M guanidine hydrochloride (fraction 15). Finally, the $A\beta_{1-42}$ concentrations in all fractions were determined via analytical RP-HPLC (reversed phase-high performance liquid chromatography) and UV absorbance detection at 214 nm.

Statistical calculation

Statistical analyses were performed using GraphPad Prism 5 (GraphPad Software, Inc., USA) and SigmaPlot Version 11 (Systat Software, Germany). Gaussian distribution was analyzed by use of a normal probability plot (SigmaPlot or InVivoStat by Simon Bate and Robin Clark, United Kingdom) [28]. Data is represented as mean ± SEM, $p > 0.05$ was considered to be not significant. Data was analyzed by one-way ANOVA with Bonferroni post hoc analysis.

Preclinical pharmacokinetic characterization

Plasma protein binding

ANK6's, tANK6's, and cANK6r's plasma protein binding (PPB) to human serum albumin (HSA) and α1-acid glycoprotein (AGP) was analyzed according to the manufacturer's

protocol of TRANSIL^{XL} HSA and AGP binding kits (Sovicell GmbH, Germany). To cover a larger range of HSA and AGP concentrations, the bead concentrations in the kit were modified. For detection, a mixture of ^{3}H-labelled and non-labelled ANK6, tANK6, and cANK6r (final concentrations of 5 µM) was added to different concentrations of HSA (7.4 µM to 420 µM, 10-12 different concentrations) or AGP beads (0.04 µM to 3 µM, 9-12 different concentrations). The amount of unbound ANK6, tANK6, and cANK6r (in %) to HSA or AGP, respectively, was determined by liquid scintillation counter (LSC) measurements. The dissociation constants (K_D) as well as the free drug fractions (f_u) in human plasma were calculated as described before [29]. Calculations were based on peptide concentrations detected in the blood 4 h after single oral administration of 10 mg/kg: 0.01 µM ANK6, 0.01 µM tANK6, and 0.01 µM cANK6r.

Animals

The pharmacokinetic profiles were investigated in 180 male C57Bl/6N mice aged 13-14 weeks, weighing about 27.4 g in average. Mice were ordered at Charles River (Germany) and housed at least one week under standard housing conditions (12/12 h light-dark cycle, approximately 22 °C room temperature and 54% humidity; water and food available *ad libitum*) in the animal facility of the Forschungszentrum Jülich GmbH before the experiments were carried out. All animal experiments were approved by the Animal Protection Committee of the local government according to the German Protection of Animals Act (LANUV, North-Rhine-Westphalia, Germany, Az.84-02.04.2017.A029).

Pharmacokinetic concentration-time profiles

To determine the concentration-time profiles of ANK6, tANK6, and cANK6r in murine brain, plasma, liver, kidney, and cerebrospinal fluid (CSF) after i.v. and p.o. administration, mixed solutions of non-labelled and ^{3}H-labelled peptides were prepared. The administered solutions contained 1 mg/mL (i.v.) or 3 mg/mL (p.o.) of the respective D-peptide including small amounts of ^{3}H-labelled peptides (0.54 µg/mL ^{3}H-ANK6, 1.79 µg/mL ^{3}H-tANK6, or 0.98 µg/mL

^{3}H-cANK6r). Doses were administered by body weight: i.v. 3.3 mg/kg, ANK6 & tANK6 p.o. 10 mg/kg, cANK6r p.o. 15 mg/kg. Three male C57Bl/6N mice aged 13-14 weeks were investigated per time point whereby individual outliers were excluded from further evaluation. Organs were harvested as follows: i.v. 5, 10, 30, 60, 120, 240, 360, 1080, 1440 min; p.o.: 10, 20, 30, 60, 120, 240, 360, 1080, 1440 min.

Animals whose CSF was not extracted were anesthetized with isoflurane (cp-pharma, Germany) inhalation approximately 2 min before each organ harvesting time point. Afterwards, blood was taken by cardiac puncture and the heparinized blood was centrifuged (3000 g, 5 min, 4 °C) to get plasma. The plasma in the supernatant was separated and 1:1 diluted with PBS. The right brain hemisphere, 200 mg of the big liver lobe, and the right kidney were removed, weighed, and homogenized in 500 µL PBS (Precellys Ceramic Kit 1.4 mm, Precellys 24, Bertin technologies SAS, France). 100 µL of the diluted plasma, the homogenized brain, liver, or kidney (in triplicates), or 1-5 µL (exactly determined) of the extracted CSF (extraction procedure see below, single determination) were mixed with 10 mL scintillation cocktail (Ultima Gold XR, PerkinElmer, USA). The mixture was incubated overnight (100 rpm, room temperature).

Animals whose CSF was extracted (organ harvesting time points: 60 min, 240 min, 1440 min) were i.p. anesthetized with ketamine/medetomidine approximately 20 min before each sampling time point. When the mouse was in deep narcosis, the *cisterna magna* was laid free and punctuated with a small capillary to extract about 5 µL of CSF as described before [30]. Afterwards, cardiac puncture, organ extractions, and sample preparations were performed as described above.

Quantification of the amount of ^{3}H-labelled D-peptides was performed with a LSC and the results (dpm/sample) were converted into mg/mL or % injected dose (%ID)/mL for plasma and for CSF, or in mg/g or %ID/g for brain as described before [29]. Total peptide concentrations in the samples were back-calculated from the measured ^{3}H-labelled peptides' radioactivity as described before [20, 25, 26, 29].

The determined peptide concentrations were plotted over time to allow for comparison of all peptides' uptake into brain, plasma, liver, kidney, and CSF. Concentrations at 0 min were set to 0 %ID/mL or 0 %ID/g except for plasma concentrations after i.v. administration. There, concentrations were linearly back-extrapolated based on the first two measured time points (5 min, 10 min).

Pharmacokinetic parameters

To calculate ANK6's, tANK6's, and cANK6r's pharmacokinetic parameters for plasma and brain, concentration-time profiles were analyzed. Non-compartmental data analysis was performed with Phoenix WinNonlin (Pharsight, a Certara Company; USA) to calculate the area under the curve from the first to the last measured data pair (AUC_{last}), the mean residence time (MRT), and the terminal elimination rate constant (λ_z, nonlinear regression of the last four to five measured concentrations). Further pharmacokinetic parameters were calculated with the help of the formulas listed in Table 2.

To allow for direct comparison with other peptides, four universally applied BBB parameters were determined [31]: the blood-brain equilibrium distribution (logBB), the universal influx rate constant (K_{in}), the initial distribution volume in brain (V_i), and the permeability surface-area product (PS). Based on data of the concentration-time profiles and pharmacokinetic parameters after i.v. administration, the BBB parameters were calculated with the help of the formulas listed in Table 2. Graphical determination of K_{in} and V_i was conducted by plotting the brain concentration to plasma concentration ratio at certain time points (C_b (t)/C_p (t) [mL/g]) on the y-axis against the exposure time (AUC_p (t)/C_p (t) [min]) on the x-axis. The linear range for K_{in} and V_i determination was between 0 and 240 min for ANK6 and cANK6r (R^2: 0.9970, 0.9996) and between 0 and 1440 min for tANK6 (R^2: 0.9758). PS was calculated on the basis of a murine cerebral blood flow (CBF) of 1.07 mL/(g*min) [32].

Results

D-peptides' *in vitro* potencies

The Aβ aggregation assay was performed to compare ANK6's, tANK6's, cANK6r's, with D3's potency to inhibit the formation of ThT-positive $A\beta_{1-42}$ fibrils. In Figure 1, the Aβ aggregation inhibition [%], relative to $A\beta_{1-42}$ aggregation without peptide, was plotted against different ANK6, tANK6, cANK6, or D3 concentrations (0.3125-80 µM). The data fits resulted in the following IC_{50} values: 3.6 µM ANK6, 2.1 µM tANK6, 3.7 µM cANK6r, 7.2 µM D3. Equimolar concentrations of ANK6 relative to $A\beta_{1-42}$ as well as of tANK6 relative to $A\beta_{1-42}$ reduced the aggregation amplitude by more than 97%, while cANK6r and D3 needed about 8-fold molar excess relative to $A\beta_{1-42}$ to reduce the aggregation amplitude by more than 95%.

To find out whether ANK6, tANK6, and cANK6r lowered the cytotoxic effect of $A\beta_{1-42}$ on the cell viability of PC12 cells, MTT assays were performed with various D-peptide concentrations (Figure 2). In a 1:5 ratio of Aβ:D-peptide, ANK6, tANK6, or cANK6r could hold up the cell viability to 65.3%, 75.5%, or 58% as compared to the cell viability in buffer. Previously published data revealed that D3 could hold up cell viability to about 60% in the same Aβ:D-peptide ratio [23]. For each evaluated D-peptide, we observed a significant reduction of the Aβ-induced cytotoxicity from 15 down to 5 respectively 1 µM D-peptide (ANK6: one-way ANOVA $F_{(7,39)} = 77.088$ Bonferroni post hoc analysis 1:15, 1:10, 1:5, 1:1 (Aβ:ANK6) all $p \leq 0.001$; tANK6: one-way ANOVA $F_{(7,39)} = 203.781$, Bonferroni post hoc analysis 1:15, 1:10, 1:5 (Aβ:tANK6) all $p \leq 0.001$; cANK6r: one-way ANOVA $F_{(7,39)} = 179.813$, Bonferroni post hoc analysis 1:15, 1:10, 1:5 (Aβ:cANK6r) all $p \leq 0.001$).

The D-peptides alone did not show negative influence on the cell viability. By plotting the cell viability [%] against the different ANK6, tANK6, or cANK6 concentrations, the following IC_{50} values were determined: 11 µM ANK6, 4.4 µM tANK6, 14 µM cANK6r (Figure 2).

To investigate the D-peptides' impact on Aβ oligomer elimination, a quantitative determination of interference with Aβ aggregate size distribution (QIAD) assay was

performed as described in the methods section. The results showed that ANK6, tANK6, and cANK6r significantly lowered the Aβ oligomer concentrations in fractions 4 to 6 which contain oligomeric Aβ [19] (fraction 4 one-way ANOVA $F_{(3,11)} = 176.336$, $Aβ_{1-42}$ vs. ANK6, tANK6, or cANK6r $p \leq 0.001$, fraction 5 one-way ANOVA $F_{(3,11)} = 54.555$, $Aβ_{1-42}$ vs. ANK6, tANK6, or cANK6r $p \leq 0.001$, fraction 6 one-way ANOVA $F_{(3,11)} = 356.147$, $Aβ_{1-42}$ vs. ANK6, tANK6, or cANK6r $p \leq 0.001$) (Figure 3). While cANK6r only slightly lowered Aβ concentrations in fractions 1 and 2 that contain Aβ monomers, linear ANK6 and tANK6 reduced the Aβ monomer concentrations much stronger. As a consequence, fractions 11 and 12, which contain amorphous high molecular weight Aβ co-precipitates with the respective compound, showed higher Aβ content after incubation with ANK6 and tANK6 as compared to cANK6r.

Preclinical pharmacokinetic characterization

Preclinical pharmacokinetic investigations were performed with ANK6, tANK6, and cANK6r *in vitro* and *in vivo*. First, affinity to the two most recurrent human plasma proteins, HSA and AGP, were determined in order to estimate the D-peptides' plasma protein binding (PPB) and the resulting fractions unbound (f_u) in plasma after oral administration. Results revealed about 2000 times higher affinities of all three D-peptides to AGP (K_D: ANK6 0.29 µM, tANK6 0.06 µM, cANK6r 0.28 µM) as compared to HSA (K_D: ANK6 not analyzable, tANK6 137.7 µM, cANK6r 598.6 µM) (Figure 4). The obtained affinities to HSA and AGP were used for prediction of the D-peptides' overall f_u in plasma (1.43% ANK6, 0.29% tANK6, 1.36% cANK6r).

Since we have shown that ANK6, tANK6, and cANK6r inhibit $Aβ_{1-42}$ aggregation, eliminate toxic Aβ oligomers, and lower $Aβ_{1-42}$-induced cytotoxicity, we conducted pharmacokinetic studies of these peptides via two different administration routes, intravenous (i.v.) and oral (p.o.). Concentration-time profiles of brain, plasma, liver, and kidney are presented in Figure 5 A, B, E, F while the condensed CSF concentration-time profiles for four time points are shown in Figure 5 D. The highest D-peptide concentrations relative to the injected dose per gram organ or milliliter plasma (%ID/g, %ID/mL) were detected in liver and kidney (organs of

metabolization and elimination) followed by plasma (distribution), CSF, and the brain (site of action). As i.v. administration was followed by high initial plasma concentration peaks, the amount of D-peptides detected in liver and kidney from the first to the last measured time point (AUC [min*%ID/g]) was much higher as compared to amounts detected after oral administration. From 6 h until 24 h after administration, plasma levels were in the same range independent from the administration route (0.005 to 0.02 %ID/mL). Brain levels were substantially higher after i.v. administration as compared to oral administration of the respective D-peptides at all investigated time points. Thus, higher initial plasma levels led to higher brain levels, but interestingly also for the time points when plasma levels had already equalized (>6 h). An exception from these differences for the respective administration routes, i.e. i.v. levels > p.o. levels, was observed in CSF. Here, D-peptide levels were, contrary to expectations, higher after oral administration than after i.v. administration. Extraordinary high CSF levels were observed for ANK6 about 60 min after both types of administration. 4 h after administration, CSF levels of ANK6 were again in the same range as those of tANK6 and cANK6r. Of note, the brain/plasma ratios were about one or even higher already 4 h after administration (Figure 5 C). 24 h after administration, the ratios were between 1.17 (cANK6r, p.o.) and 6.89 (tANK6, i.v.).

The maximum concentrations relative to the injected dose (C_{max}, %ID/mL) in plasma increased from tANK6 (i.v. 0.40, p.o. 0.02) over ANK6 (i.v. 3.17, p.o. 0.02) to cANK6r (i.v. 3.29, p.o. 0.05) while in the brain, the C_{max} value (%ID/g) was dependent on the administration route. After i.v. administration, C_{max} increased from tANK6 (0.06) over ANK6 (0.07) to cANK6r (0.12). After oral administration, C_{max} increased from ANK6 (0.01) to tANK6 (0.02) and cANK6r (0.02).

The pharmacokinetic parameters in plasma and brain are summarized in Table 3. In plasma, compound exposure over time relative to the dose ($AUC_{\%ID,\ 0\text{-}1440}$, min*%ID/mL) after i.v. administration was highest for the cyclic 13-mer cANK6r (i.v. 181) followed by the linear 12-mer ANK6 (91.7) and finally by the linear 24-mer tANK6 (26.1). After oral administration,

$AUC_{\%ID,\ 0\text{-}1440}$ was still highest for cANK6r (17.9) but tANK6 (12.9) and ANK6 (10.8) changed the order whereby differences between the three D-peptides' $AUC_{\%ID,\ 0\text{-}1440}$ were smaller after oral administration. These findings were also reflected in the terminal half-lives ($t_{1/2}$) which were determined to be longer after oral (22-31 h) than after i.v. (15-18 h) administration. Consistently, terminal clearance (CL, mL/(min*kg)) was lowest for cANK6r (i.v. 18.4), followed by ANK6 (i.v. 32.0), and tANK6 (i.v. 88.9). Oral bioavailability (F) was calculated to be 9.9% for cANK6r, 11.8% for ANK6, and 49.4% for tANK6. Interestingly, the mean residence time (MRT) had the same order within the three D-peptides (tANK6 > ANK6 > cANK6r) for both administration routes. Overall, the MRT values were higher after oral administration (9-11 h) than after i.v. administration (2-7 h).

In the brain, $AUC_{\%ID,\ 0\text{-}1440}$ (min*%ID/g) after i.v. administration for cANK6r (85.6) was higher than for tANK6 (56.6), and for ANK6 (35.8). In contrast to the plasma values after oral administration, tANK6 (22.5) showed the highest $AUC_{\%ID,\ 0\text{-}1440}$ followed by cANK6r (19.1) and ANK6 (11.0) in the brain. MRT in the brain was similar for all three D-peptides (11-14 h) independent from the respective administration route.

Calculated values of four commonly used BBB parameters, determined to allow for global comparison of any peptides' efficiencies to cross the BBB, are listed in Table 4. The logBB value describes the blood-brain equilibrium distribution: negative logBB values result from lower AUCs in the brain than in plasma, whereas positive logBB values result from higher AUCs in the brain than in plasma. K_{in} describes the BBB permeability kinetics while V_i describes a peptides' fictional (initial) distribution volume in the brain. The PS represents the uptake clearance from blood to brain. In this study, logBB values of ANK6 and cANK6r were below zero while tANK6's logBB value was greater than zero. Regarding the graphically determined K_{in} and V_i values, ANK6 and cANK6r were in the same range while the values of tANK6 were increased by around factor 10. As PS was determined in consideration of a presumed CBF of 1.07 mL/(g*min) [32], values of all three D-peptides were the same as for K_{in}.

Discussion

The approach of Aβ oligomer elimination by D-peptides clearly differs as compared to e.g. antibodies directed against Aβ, or β- or γ-secretase inhibitors that already failed in several clinical trials. As opposed to passive immunization, the D-peptides' therapeutic efficacy is independent from the individual immune system, and they are able to destroy already existing Aβ oligomers, a property which makes them superior to secretase inhibitors. The most obvious reason why numerous Aβ antibodies have failed in clinical trials is most likely that they had been either directed against Aβ fibrils or monomers, which are the wrong targets, or do bind to all forms of Aβ assemblies. In contrast, the results published so far for the Aβ oligomer targeting antibody Aducanumab are very promising and do underline the reasonability of the therapeutic approach of our Aβ oligomer eliminating D-peptides [33]. Consequently, the D-peptides could already show very promising results of therapeutic *in vivo* studies in various transgenic AD mouse models [10, 12, 15, 17, 19, 27, 34, 35].

In this study, we focused on optimizing ANK6 regarding its potency to eliminate toxic Aβ oligomers as well as its pharmacokinetic *in vivo* characteristics by designing two derivatives. To increase the D-peptide's binding avidity to Aβ, so-called tandem peptides were developed and investigated before [19, 26]. They usually are head-to-tail juxtapositions of two 12-mer D-peptides resulting in a linear 24-residue D-peptide. Thus, tANK6 was included in this study to find out whether a tandem version indeed showed enhanced Aβ-targeting potency as compared to single ANK6. Another optimization approach, which aimed to increase blood-brain barrier permeation, revealed the 13-mer cANK6r. Previously, it had been shown that cyclic isoforms of several D3-derivatives reached remarkably higher brain levels after administration to wild type mice as compared to the corresponding linear peptides [25]. Consequently, we included cANK6r in this study to find out whether cyclization had an impact on ANK6's *in vitro* potency and whether cyclization, here, also led to higher brain levels in comparison to the originally selected linear peptide although it contains six amino acid residue substitutions as compared to D3.

The comparison of *in vitro* properties of ANK6, tANK6, and cANK6r included different experimental approaches, namely Aβ aggregation, cell viability, and QIAD assays. Thereby we could validate our assumption that tANK6 has an enhanced potency as it most efficiently inhibited the $A\beta_{1-42}$ fibril formation with a resulting IC_{50} of 2.1 µM as compared to ANK6 (3.6 µM), cANK6r (3.7 µM), and D3 (7.2 µM). Additionally, one could observe that only tANK6 and ANK6 did completely inhibit $A\beta_{1-42}$ fibril formation by two-fold molar excess with regard to Aβ whereas cANK6r and D3 needed about eight-fold molar excess. Cell viability assays, which were conducted to investigate the D-peptides' efficiencies to reduce Aβ-induced cytotoxicity in PC12 cells, showed a similar trend: tANK6 was most efficient with an IC_{50} value of 4.4 µM followed by ANK6 (11 µM) and cANK6r (14 µM). PC12 cells were used for this experiment because they had originally been established by Greene and Tischler for "neurobiological and neurochemical studies" [36] and are nowadays a commonly used cell line in AD research [37, 38]. Additionally, the MTT test with PC12 cells belongs to our standard test battery for newly developed D-peptides to allow for comparison with data generated previously [10, 27]. The most meaningful *in vitro* assay QIAD awarded all three investigated D-peptides very promising oligomer eliminating characteristics as they drastically eliminated Aβ oligomers (>96% oligomer reduction in fractions 4-6). Previously published data for D3, generated in this test with exactly the same setting, show that D3 could, in the same molar ratio of Aβ:D-peptide as used in this study, reduce the Aβ oligomers by 51% [34]. Because we have developed the ANK compounds for their ability to stabilize Aβ monomers in an aggregation-incompetent conformation, one would expect to see an increase of the Aβ content in the monomer containing fractions (1 and 2), however in presence of the high µM concentrations of Aβ and compound, it is well imaginable that instead the observed high molecular weight co-precipitates were observed. In any case all three compounds were able to eliminate the Aβ oligomers and converted them into non-toxic co-precipitates as was already shown previously for the lead compound D3 [12, 24] and another D3 derivative, RD2 [34].

In the following, PPB experiments were conducted to predict the D-peptides' affinities to the most abundant human plasma proteins, HSA and AGP. If a drug strongly binds to plasma proteins, it is possible that the drug is in the organism but is not able to leave the circulation to the site of action. For AD drugs, this could mean that the drug circulates in plasma, but does not reach the brain, at least not to a very high proportion. Conversely, one can make use of PPB to a certain extent as there is always a dynamic equilibrium between drug bound and freely circulating in plasma (f_u). Thus, plasma proteins can work as kind of drug releasing depots leading to consistent drug distribution in plasma over time. This can lower the risk of adverse side effects and at the same time lead to longer MRTs [39, 40]. Slow drug release from the plasma proteins might even also allow for once daily drug administration, which is followed by the best patients' compliance [41].

ANK6, tANK6, as well as cANK6r bound to AGP (K_D between 0.06 and 0.29 µM) much stronger than to HSA (K_D of 138 µM and higher). This had been expected before as all three D-peptides have a positive net charge and AGP is known to more strongly bind positively charged molecules as compared to HSA, which is known to bind rather acidic or neutral molecules [40]. This had been observed previously for D3 in a similar manner. Jiang et al. determined a K_D of 1.8 µM for D3 to AGP while the K_D of D3 to AGP was above the detection limit of the used kit (>1.4 mM) [20]. The unbound fractions (f_u) of the three D-peptides regarding PPB to HSA and AGP were determined to be in the same range (0.29-1.43%). Results again confirmed the assumption that tANK6 (f_u 0.29%) bound strongest to AGP because it consists of twice as many basic amino acid residues as compared to ANK6 and cANK6r.

Summarizing the *in vitro* studies, cANK6r's slight inferiorities after the Aβ aggregation inhibition and cell viability tests, possibly caused by structural hindrances due to cyclization, could be balanced by cANK6r's very beneficial QIAD outcome in eliminating Aβ oligomers while not strongly affecting Aβ monomer levels. Nevertheless, tANK6 showed very promising results in all conducted *in vitro* tests especially supporting the hypothesis that our tandem

peptides do possess enhanced Aβ-targeting efficacy *in vitro*. As compared to the lead structure D3, the ANK peptides investigated in this study do show the same or, especially in the most important *in vitro* QIAD assay, even more promising results in these Aβ interaction assays. This is why we consider these D-peptides, especially tANK6 and cANK6r, very promising Aβ-targeting D-peptides which are supposed to be therapeutically active even if they reach lower brain levels than D3. One example for the importance of high efficacy, as determined *in vitro*, is the tandem D-peptide D3D3, which has demonstrated already higher efficacy than D3 *in vivo*, despite lower brain penetrance [19].

After extensive *in vitro* investigation of the three D-peptides, they were pharmacokinetically investigated in further detail. For these studies, a mixture of ^{3}H-labelled and non-labelled D-peptide was administered to C57Bl/6N wild type mice. On the one hand, we used C57Bl/6N mice as it is the gold standard to conduct pharmacokinetic experiments with new compounds in young, healthy wild type organisms, especially in rodents [42, 43]. On the other hand, we used exactly these mice at this age in order to allow for direct comparison to our results of D3 and other D3-derivatives that had been determined before using exactly the same experimental method [20, 26, 29]. As D-peptides had been proven to be extraordinary stable against proteolytic degradation and metabolites can therefore be neglected, the detected amount of ^{3}H-labelled D-peptide in the murine samples (brain, plasma, liver, and kidney) was anticipated to correctly reflect the total D-peptide concentration. This has been described and evaluated several times before [20, 25, 26, 29]. As each D-peptide's ^{3}H-label was located in a leucine alkyl group (4,5-^{3}H-D-Leu), the labels were also considered to be biologically stable [25]. Further underlining the D-peptides' stabilities, Elfgen et al. confirmed this by incubation in several media simulating the oral administration route with HPLC analyses [22]. Thus, the amount of ^{3}H-labelled D-peptide quantified in LSC measurements was used for back-calculation of the total D-peptide concentration in the respective samples and pharmacokinetic parameters were calculated subsequently.

Apparently, the pharmacokinetic profiles of liver and kidney revealed huge differences after i.v. and oral administration. The fact that i.v. administration was followed by far higher D-peptide levels in the organs responsible for metabolization and excretion could be explained by the initially higher plasma levels. After the rapid initial rise, liver and kidney levels remained quite constant throughout the observation time of 24 h. Thus, one could surmise that the D-peptides were not immediately excreted but that they accumulated in liver and kidney for some time. Although the administered dose was three times higher for oral than for i.v. administration, only relatively small amounts of the D-peptides were taken up via the gastrointestinal tract. Direct comparison to data of D3 (generated by Jiang et al. using exactly the same experimental setup before [20]), revealed that plasma levels of ANK6, tANK6, and cANK6r were considerably lower especially in plasma after oral administration. Regarding the brain, the AUCs of D3 after oral administration were 7.2 (tANK6), 7.7 (cANK6r), and 13.4 (ANK6) times higher as compared to the respective D-peptides. Thus, the notable differences in plasma and consequently also in brain levels between D3, and ANK6 and its derivative most likely derived from the different amino acid residue compositions. This assumption is substantiated by the fact that brain and plasma levels of other D3-derivatives, composed of the same amino acid residues as D3, were rather in comparable ranges to those of D3 than to those of ANK6 and its derivatives [20, 25, 26]. These pharmacokinetic findings might also partially explain why the intraperitoneal treatment study (4 weeks) with ANK6, conducted by Klein et al., only showed “a non-significant tendency for improving memory performance of tg-APPSwDI mice” [23]. Despite the fact that ANK6 and its derivatives do reach lower brain levels as compared to their lead compound D3, we still consider tANK6 and cANK6r very promising drug candidates for future therapeutic studies because of their superior Aβ interaction *in vitro* efficiencies.

Probably, huge parts of orally administered ANK6, tANK6, and cANK6r in this pharmacokinetic study were immediately excreted. Interestingly, plasma levels after i.v. and oral administration were in the same range about 6 h after administration while brain levels of

the i.v. administered D-peptides, especially those of cANK6r and tANK6, remained higher than those of the orally administered D-peptides. These findings suggested that the D-peptides' outward transport across the BBB, back into plasma, was not as fast as plasma clearance. A reason for that might have been that the D-peptides bound to structures in the murine brain or that the outward transport was limited. Either way is beneficial for an AD drug candidate as the brain is supposed to be its site of action. In this context, the cyclic peptide (cANK6r) revealed higher brain levels than its linear equivalent (ANK6) or the tandem D-peptide (tANK6) after i.v. administration, again substantiating the previously set up hypothesis that cyclization results in more efficient BBB permeation [25]. Finally regarding the C_{max} values in plasma as well as in brain for both administration routes, cANK6r always revealed the highest values suggesting and confirming high stability and enhanced abilities to cross membranes.

Regarding pharmacokinetic parameters in plasma disclosed a bigger difference within the $AUC_{\%ID,\ 0\text{-}1440}$ values after i.v. than after oral administration, most likely due to different uptake and accumulation characteristics in liver and kidney. These characteristics had more impact after i.v. administration, as plasma levels were initially higher. After oral administration, when most of the administered D-peptides had already been eliminated due to the first-pass effect, the impact of liver and kidney over time was smaller. The unexpected result that tANK6 revealed the highest oral bioavailability might be relativized by consideration that tANK6 had a relatively low plasma $AUC_{\%ID,\ 0\text{-}1440}$ after i.v. administration in contrast to the two other peptides. Thus, tANK6's oral bioavailability was higher than those of ANK6 and cANK6r despite the fact that their plasma $AUC_{\%ID,\ 0\text{-}1440}$ after oral administration were in a similar range. Conversely, cANK6r's unexpected low bioavailability was explained by the same approach. Regarding $t_{1/2}$, a therapeutic regimen with once daily dosing would be applicable as the values varied between 15 and 31 h. During a therapeutic study, the steady state levels would be attained after 3 to 6.5 days as a general rule states that the steady state is reached after five $t_{1/2}$ periods [44]. As $t_{1/2}$ for ANK6 was determined to be shorter than for tANK6 and

cANK6r, the two derivatives could be awarded being more favorable regarding $t_{1/2}$. Comparison of i.v. and oral administration generally pointed out longer $t_{1/2}$ after oral administration. These findings were in accordance with the general opinion that long-term AD-treatment in elderly people would be done best orally, not least because of the small impact on the patients' daily living.

To allow for comparability to other peptides listed in "Brainpeps: the blood-brain barrier peptide database", four characterizing BBB values were determined (Table 4) [31]. tANK6's logBB value (positive sign) reflected that the peptide's drug exposure over time was greater in the brain than in plasma whereas for ANK6 and cANK6r (negative signs) it was the other way around. Thus, tANK6r seemed to have entered the brain from plasma most efficiently. However, one may not neglect that logBB values depend on binding to plasma and brain tissue as well as on active transport. K_{in} and V_i had been graphically determined with regard to investigate the velocity of the three D-peptides' BBB passage. Remarkably, both values were tenfold greater for tANK6 than for ANK6, and cANK6r underlining that tANK6 crossed the BBB fastest. Uptake clearance from blood to brain was calculated based on K_{in} so that tANK6 here also revealed the highest PS value. To classify ANK6 and its two derivatives, their BBB parameters were compared to those of Dermorphin, a potent natural opioid consisting of seven amino acid residues including one D-enantiomeric amino acid residue. Dermorphin had been suggested as positive control [31]. Dermorphin's K_{in} values were determined to be between 0.0002 and 0.0022 mL/(g*min) while its V_i values were determined to be between 0.0162 and 0.0215 mL/g [45, 46]. By all means, especially tANK6's, but also ANK6's and cANK6r's, BBB parameters were in the same scale as Dermorphin's awarding the three D-peptides a very efficient BBB permeability.

Summarized, ANK6 and its two derivatives, tANK6 and cANK6r, showed very beneficial Aβ-targeting *in vitro* efficacies. Analyzing the results, it became obvious that both newly developed ANK6-derivatives, tANK6 and cANK6r, had superior Aβ interacting properties as compared to ANK6. As shown already for ANK6's predecessor peptide D3, i.v. administration

led to accumulation in liver and kidney, whereas p.o. administration did not [20]. Oral bioavailabilities were with about 10 % for ANK6 and cANK6r and 50 % for tANK6 very high when compared with typical oral bioavailabilities of L-enantiomeric peptides. cANK6r showed the highest drug exposure over time in the brain. All three investigated compounds revealed very high BBB penetration as indicated by typically determined BBB values (**Table 4**).

Acknowledgement

D.W. and K.J.L. were supported by grants from the "Portfolio Technology and Medicine", and D.W. was additionally supported by the "Portfolio Drug Research" and the Helmholtz-Validierungsfonds of the "Impuls und Vernetzungs-Fonds der Helmholtzgemeinschaft". The study was supported by the TT-Fonds of the Technology Transfer Department of the Forschungszentrum Jülich.

Conflict of interest

The authors have no conflict of interest to report.

Author's information

Corresponding authors

Dr. Antje Willuweit (a.willuweit@fz-juelich.de)

Prof. Dr. Dieter Willbold (d.willbold@fz-juelich.de)

Author contributions

A.W. and D.W. designed the overall study. D.W., A.W., J.K., E.S., and S.S. designed the experiments. E.S., M.T., and T.Z. carried out and evaluated the *in vitro* experiments on the

570 D-peptides' interaction with Aβ. O.B. carried out HPLC measurements for the QIAD assay. E.S. performed the plasma protein binding tests and evaluated the results with support from T.Z.. E.S. and S.S. planned and carried out all pharmacokinetic experiments with the help of N.N., and D.H.. E.S. determined the pharmacokinetic parameters and the blood-brain barrier values. A.E. and I.G. carried out preliminary experiments that were important for the final study design. E.S., A.W., J.K., N.J.S., K.J.L., and D.W. wrote the manuscript. All other authors contributed to writing.

References

[1] Thal DR, Capetillo-Zarate E, Del Tredici K, Braak H (2006) The development of amyloid beta protein deposits in the aged brain. *Sci Aging Knowledge Environ* **2006**, re1.

[2] Haass C, Selkoe DJ (2007) Soluble protein oligomers in neurodegeneration: lessons from the Alzheimer's amyloid beta-peptide. *Nat Rev Mol Cell Biol* **8**, 101-112.

[3] Anand R, Gill KD, Mahdi AA (2014) Therapeutics of Alzheimer's disease: Past, present and future. *Neuropharmacology* **76 Pt A**, 27-50.

[4] Gremer L, Scholzel D, Schenk C, Reinartz E, Labahn J, Ravelli RBG, Tusche M, Lopez-Iglesias C, Hoyer W, Heise H, Willbold D, Schroder GF (2017) Fibril structure of amyloid-beta(1-42) by cryo-electron microscopy. *Science* **358**, 116-119.

[5] Schumacher TNM, Mayr LM, Minor DL, Milhollen MA, Burgess MW, Kim PS (1996) Identification of D-peptide ligands through mirror-image phage display. *Science* **271**, 1854-1857.

[6] Wiesehan K, Willbold D (2003) Mirror-image phage display: aiming at the mirror. *Chembiochem* **4**, 811-815.

[7] Wiesehan K, Buder K, Linke RP, Patt S, Stoldt M, Unger E, Schmitt B, Bucci E, Willbold D (2003) Selection of D-amino-acid peptides that bind to Alzheimer's disease amyloid peptide abeta1-42 by mirror image phage display. *Chembiochem* **4**, 748-753.

[8] Wiesehan K, Stohr J, Nagel-Steger L, van Groen T, Riesner D, Willbold D (2008) Inhibition of cytotoxicity and amyloid fibril formation by a D-amino acid peptide that specifically binds to Alzheimer's disease amyloid peptide. *Protein Eng Des Sel* **21**, 241-246.

[9] Funke SA, Willbold D (2009) Mirror image phage display--a method to generate D-peptide ligands for use in diagnostic or therapeutical applications. *Mol Biosyst* **5**, 783-786.

[10] van Groen T, Wiesehan K, Funke SA, Kadish I, Nagel-Steger L, Willbold D (2008) Reduction of Alzheimer's disease amyloid plaque load in transgenic mice by D3, A D-enantiomeric peptide identified by mirror image phage display. *ChemMedChem* **3**, 1848-1852.

[11] van Groen T, Kadish I, Wiesehan K, Funke SA, Willbold D (2009) In vitro and in vivo staining characteristics of small, fluorescent, Abeta42-binding D-enantiomeric peptides in transgenic AD mouse models. *ChemMedChem* **4**, 276-282.

[12] Funke SA, van Groen T, Kadish I, Bartnik D, Nagel-Steger L, Brener O, Sehl T, Batra-Safferling R, Moriscot C, Schoehn G, Horn AH, Muller-Schiffmann A, Korth C, Sticht H, Willbold D (2010) Oral treatment with the d-enantiomeric peptide D3 improves the pathology and behavior of Alzheimer's Disease transgenic mice. *ACS Chem Neurosci* **1**, 639-648.

[13] Bartnik D, Funke SA, Andrei-Selmer L-C, Bacher M, Dodel R, Willbold D (2010) Diffenrently Selected D-Enantiomeric Peptides Act on Different Aβ Species. *Rejuvenation Res.* **13**, 202-205.

[14] Liu H, Funke SA, Willbold D (2010) Transport of Alzheimer disease amyloid-beta-binding D-amino acid peptides across an in vitro blood-brain barrier model. *Rejuvenation Res* **13**, 210-213.

[15] van Groen T, Kadish I, Funke A, Bartnik D, Willbold D (2012) Treatment with Abeta42 binding D-amino acid peptides reduce amyloid deposition and inflammation in APP/PS1 double transgenic mice. *Adv Protein Chem Struct Biol* **88**, 133-152.

[16] Olubiyi OO, Strodel B (2012) Structures of the amyloid beta-peptides Abeta1-40 and Abeta1-42 as influenced by pH and a D-peptide. *J Phys Chem B* **116**, 3280-3291.

[17] van Groen T, Kadish I, Funke SA, Bartnik D, Willbold D (2013) Treatment with D3 removes amyloid deposits, reduces inflammation, and improves cognition in aged AbetaPP/PS1 double transgenic mice. *J Alzheimers Dis* **34**, 609-620.

[18] Olubiyi OO, Frenzel D, Bartnik D, Gluck JM, Brener O, Nagel-Steger L, Funke SA, Willbold D, Strodel B (2014) Amyloid Aggregation Inhibitory Mechanism of Arginine-rich D-peptides. *Current Medicinal Chemistry* **21**, 1448-1457.

[19] Brener O, Dunkelmann T, Gremer L, van Groen T, Mirecka EA, Kadish I, Willuweit A, Kutzsche J, Jurgens D, Rudolph S, Tusche M, Bongen P, Pietruszka J, Oesterhelt F, Langen KJ, Demuth HU, Janssen A, Hoyer W, Funke SA, Nagel-Steger L, Willbold D (2015) QIAD assay for quantitating a compound's efficacy in elimination of toxic Abeta oligomers. *Sci Rep* **5**, 13222.

[20] Jiang N, Leithold LH, Post J, Ziehm T, Mauler J, Gremer L, Cremer M, Schartmann E, Shah NJ, Kutzsche J, Langen KJ, Breitkreutz J, Willbold D, Willuweit A (2015) Preclinical

Pharmacokinetic Studies of the Tritium Labelled D-Enantiomeric Peptide D3 Developed for the Treatment of Alzheimer s Disease. *PLoS One* **10**, e0128553.

[21] Jiang N, Frenzel D, Schartmann E, van Groen T, Kadish I, Shah NJ, Langen KJ, Willbold D, Willuweit A (2016) Blood-brain barrier penetration of an Abeta-targeted, arginine-rich, d-enantiomeric peptide. *Biochim Biophys Acta* **1858**, 2717-2724.

[22] Elfgen A, Santiago-Schubel B, Gremer L, Kutzsche J, Willbold D (2017) Surprisingly high stability of the Abeta oligomer eliminating all-d-enantiomeric peptide D3 in media simulating the route of orally administered drugs. *Eur J Pharm Sci* **107**, 203-207.

[23] Klein AN, Ziehm T, van Groen T, Kadish I, Elfgen A, Tusche M, Thomaier M, Reiss K, Brener O, Gremer L, Kutzsche J, Willbold D (2017) Optimization of D-peptides for Aβ monomer binding specificity enhances their potential to eliminate toxic Aβ oligomers. *ACS Chem Neurosci*.

[24] Ziehm T, Brener O, van Groen T, Kadish I, Frenzel D, Tusche M, Kutzsche J, Reiss K, Gremer L, Nagel-Steger L, Willbold D (2016) Increase of Positive Net Charge and Conformational Rigidity Enhances the Efficacy of d-Enantiomeric Peptides Designed to Eliminate Cytotoxic Abeta Species. *ACS Chem Neurosci* **7**, 1088-1096.

[25] Schartmann E, Schemmert S, Ziehm T, Leithold LHE, Jiang N, Tusche M, Joni Shah N, Langen KJ, Kutzsche J, Willbold D, Willuweit A (2017) Comparison of blood-brain barrier penetration efficiencies between linear and cyclic all-d-enantiomeric peptides developed for the treatment of Alzheimer's disease. *Eur J Pharm Sci* **114**, 93-102.

[26] Leithold LH, Jiang N, Post J, Niemietz N, Schartmann E, Ziehm T, Kutzsche J, Shah NJ, Breitkreutz J, Langen KJ, Willuweit A, Willbold D (2016) Pharmacokinetic properties of tandem d-peptides designed for treatment of Alzheimer's disease. *Eur J Pharm Sci* **89**, 31-38.

[27] Dunkelmann T, Teichmann K, Ziehm T, Schemmert S, Frenzel D, Tusche M, Dammers C, Jürgens D, Langen K-J, Demuth H-U, Shah NJ, Kutzsche J, Willuweit A, Willbold D (2017) Aβ oligomer eliminating compounds interfere successfully with pEAβ (3–42) induced motor neurodegenerative phenotype in transgenic mice. *Neuropeptides*.

[28] Clark RA, Shoaib M, Hewitt KN, Stanford SC, Bate ST (2012) A comparison of InVivoStat with other statistical software packages for analysis of data generated from animal experiments. *J Psychopharmacol* **26**, 1136-1142.

[29] Leithold LH, Jiang N, Post J, Ziehm T, Schartmann E, Kutzsche J, Shah NJ, Breitkreutz J, Langen KJ, Willuweit A, Willbold D (2016) Pharmacokinetic Properties of a Novel D-Peptide Developed to be Therapeutically Active Against Toxic beta-Amyloid Oligomers. *Pharm Res* **33**, 328-336.

[30] Liu HN, Tjostheim S, Dasilva K, Taylor D, Zhao B, Rakhit R, Brown M, Chakrabartty A, McLaurin J, Robertson J (2012) Targeting of monomer/misfolded SOD1 as a therapeutic strategy for amyotrophic lateral sclerosis. *J Neurosci* **32**, 8791-8799.

[31] Van Dorpe S, Bronselaer A, Nielandt J, Stalmans S, Wynendaele E, Audenaert K, Van De Wiele C, Burvenich C, Peremans K, Hsuchou H, De Tre G, De Spiegeleer B (2012) Brainpeps: the blood-brain barrier peptide database. *Brain Struct Funct* **217**, 687-718.

[32] Muir ER, Shen Q, Duong TQ (2008) Cerebral blood flow MRI in mice using the cardiac-spin-labeling technique. *Magn Reson Med* **60**, 744-748.

[33] Sevigny J, Chiao P, Bussiere T, Weinreb PH, Williams L, Maier M, Dunstan R, Salloway S, Chen T, Ling Y, O'Gorman J, Qian F, Arastu M, Li M, Chollate S, Brennan MS, Quintero-Monzon O, Scannevin RH, Arnold HM, Engber T, Rhodes K, Ferrero J, Hang Y, Mikulskis A, Grimm J, Hock C, Nitsch RM, Sandrock A (2016) The antibody aducanumab reduces Abeta plaques in Alzheimer's disease. *Nature* **537**, 50-56.

[34] van Groen T, Schemmert S, Brener O, Gremer L, Ziehm T, Tusche M, Nagel-Steger L, Kadish I, Schartmann E, Elfgen A, Jurgens D, Willuweit A, Kutzsche J, Willbold D (2017) The Abeta oligomer eliminating D-enantiomeric peptide RD2 improves cognition without changing plaque pathology. *Sci Rep* **7**, 16275.

[35] Kutzsche J, Schemmert S, Tusche M, Neddens J, Rabl R, Jurgens D, Brener O, Willuweit A, Hutter-Paier B, Willbold D (2017) Large-Scale Oral Treatment Study with the Four Most Promising D3-Derivatives for the Treatment of Alzheimer's Disease. *Molecules* **22**.

[36] Greene LA, Tischler AS (1976) Establishment of a noradrenergic clonal line of rat adrenal pheochromocytoma cells which respond to nerve growth factor. *Proc Natl Acad Sci U S A* **73**, 2424-2428.

[37] Dong H, Mao S, Wei J, Liu B, Zhang Z, Zhang Q, Yan M (2012) Tanshinone IIA protects PC12 cells from β-amyloid25–35-induced apoptosis via PI3K/Akt signaling pathway. *Molecular Biology Reports* **39**, 6495-6503.

[38] Zeng Z, Xu J, Zheng W (2017) Artemisinin protects PC12 cells against β-amyloid-induced apoptosis through activation of the ERK1/2 signaling pathway. *Redox Biol* **12**, 625-633.
[39] Gillette JR (1973) Overview of drug-protein binding. *Ann N Y Acad Sci* **226**, 6-17.
[40] Lambrinidis G, Vallianatou T, Tsantili-Kakoulidou A (2015) In vitro, in silico and integrated strategies for the estimation of plasma protein binding. A review. *Adv Drug Deliv Rev* **86**, 27-45.
[41] Eisen SA, Miller DK, Woodward RS, Spitznagel E, Przybeck TR (1990) The effect of prescribed daily dose frequency on patient medication compliance. *Arch Intern Med* **150**, 1881-1884.
[42] Beconi MG, Howland D, Park L, Lyons K, Giuliano J, Dominguez C, Munoz-Sanjuan I, Pacifici R (2012) Pharmacokinetics of memantine in rats and mice. *PLoS Curr* **3**.
[43] Chen C, Ortega F, Alameda L, Ferrer S, Simonsson US (2016) Population pharmacokinetics, optimised design and sample size determination for rifampicin, isoniazid, ethambutol and pyrazinamide in the mouse. *Eur J Pharm Sci* **93**, 319-333.
[44] Zhao W, Jacqz-Aigrain E (2011) Principles of therapeutic drug monitoring. *Handb Exp Pharmacol* **205**, 77-90.
[45] Stalmans S, Bracke N, Wynendaele E, Gevaert B, Peremans K, Burvenich C, Polis I, De Spiegeleer B (2015) Cell-Penetrating Peptides Selectively Cross the Blood-Brain Barrier In Vivo. *PLoS One* **10**, e0139652.
[46] Van Dorpe S, Adriaens A, Polis I, Peremans K, Van Bocxlaer J, De Spiegeleer B (2010) Analytical characterization and comparison of the blood-brain barrier permeability of eight opioid peptides. *Peptides* **31**, 1390-1399.

Tables

Table 1: Peptides' sequences and configurations

peptide	amino acid residue sequence	amino acid residue configuration
D3	rprtrlhthrnr-NH_2	all-D-enantiomeric
ANK6	rkrirlvtkkkr-NH_2	all-D-enantiomeric
tANK6	rkrirlvtkkkrrkrirlvtkkkr-NH_2	all-D-enantiomeric
cANK6r	rkrirlvtkkkrr head-to-tail cyclized	all-D-enantiomeric

720

Table 2: Formulas for calculation of pharmacokinetic parameters and blood-brain barrier values

pharmacokinetic parameter		unit	formula
$t_{1/2}$	terminal half-life	h	$t_{1/2} = \ln(2)/\lambda_z$
D	dose	mg/kg	
$F_{AUC_{\%ID}}$	bioavailability	%	$F_{AUC_{\%ID}} = \frac{AUC_{\%ID_{e.v.}}}{AUC_{\%ID_{i.v.}}}$
CL	terminal plasma clearance	mL/(min*kg)	$CL = \lambda_z * V_{last}$
blood-brain barrier value		**unit**	**formula**
logBB	blood-brain equilibrium distribution	-	$logBB = \log(AUC_{last,br}/AUC_{last,pl})$
K_{in}	unidirectional influx rate constant	mL/(g*min)	$\frac{C_b(t)}{C_p(t)} = K_{in} * \frac{AUC_p(t)}{C_p(t)} + V_i$
V_i	initial distribution volume	mL/g	see formula for K_{in}
PS	permeability surface-area product	mL/(g*min)	$PS = (-CBF)*\ln(1-K_{in}/CBF)$
CBF	(murine) cerebral blood flow	mL/(g*min)	1.07 [32]

Table 3: Pharmacokinetic parameters for ANK6, tANK6, and cANK6r in murine plasma and brain

PLASMA							
D-peptide		**ANK6**	**tANK6**	**cANK6r**	**ANK6**	**tANK6**	**cANK6r**
administration route		**i.v.**	**i.v.**	**i.v.**	**p.o.**	**p.o.**	**p.o.**
parameter	**unit**						
D	mg/kg	3.3	3.3	3.3	10	10	15
C_{max}	%ID/mL	3.17	0.40	3.29	0.02	0.02	0.05
t_{max}	min	0	0	0	120	240	60
$AUC_{\%ID,\ 0\text{-}1440}$	min*%ID/mL	91.7	26.1	181.0	10.8	12.9	17.9
MRT	h	3	7	2	10	11	9
λ_z	1/min	0.00077	0.00063	0.00064	0.00054	0.00038	0.00039
$t_{1/2}$	h	15	18	18	22	31	30
F ($AUC_{\%ID}$)	%	na	na	na	11.8	49.4	9.9
CL	mL/(min*kg)	32.0	88.9	18.4	174.5	113.0	135.5
BRAIN							
D-peptide		**ANK6**	**tANK6**	**cANK6r**	**ANK6**	**tANK6**	**cANK6r**
administration route		**i.v.**	**i.v.**	**i.v.**	**p.o.**	**p.o.**	**p.o.**
parameter	**unit**						
C_{max}	%ID/g	0.07	0.06	0.12	0.01	0.02	0.02
t_{max}	min	5	30	5	60	1080	360
$AUC_{\%ID,\ 0\text{-}1440}$	min*%ID/g	35.8	56.6	85.6	11.0	22.5	19.1

730 **Table 4: Blood-brain barrier values for ANK6, tANK6, and cANK6r after i.v. administration**

Parameter	Unit	ANK6	tANK6	cANK6r
logBB	-	-0.401	0.335	-0.329
K_{in}	mL/(g*min)	0.0003	0.0016	0.0003
V_{im}	mL/g	0.0575	0.5833	0.0396
PS	mL/(g*min)	0.0003	0.0016	0.0003

Figures

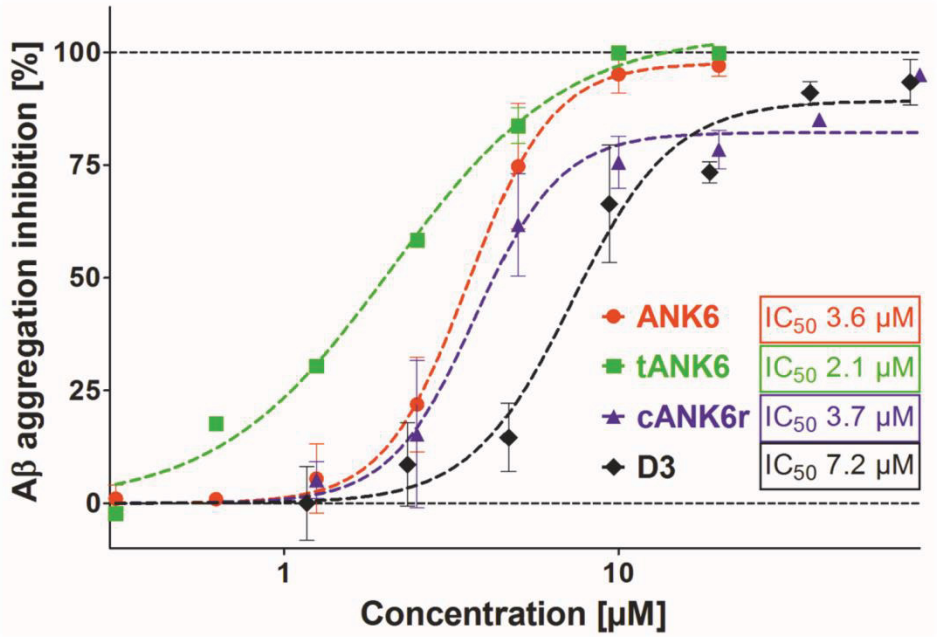

Figure 1: Aβ aggregation assay

To investigate ANK6's (red circles), tANK6's (green squares), cANK6r's (blue triangles), and D3's (black diamonds) potencies to inhibit $A\beta_{1-42}$ monomer aggregation into ThT-positive fibrils, different concentrations of the respective peptides (0.3125-80 µM) were incubated with 10 µM $A\beta_{1-42}$ each. The Aβ aggregation inhibition [%], relative to the fluorescence signal of ThT-positive $A\beta_{1-42}$ fibrils which were formed without any peptide added, was plotted against the respective D-peptides' concentrations. The IC_{50} values were determined by nonlinear regression.

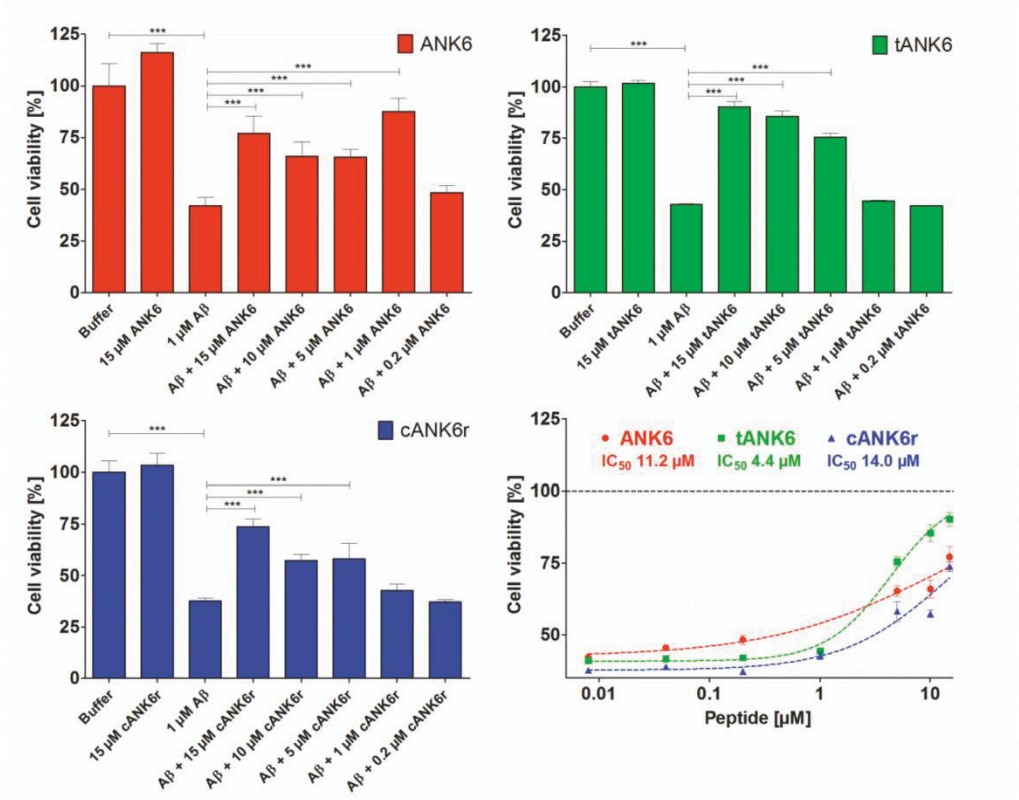

Figure 2: Cell viability assay

To investigate ANK6's (red circles), tANK6's (green squares), and cANK6r's (blue triangles) potencies to reduce the toxicity of $A\beta_{1-42}$, a cell viability assay was performed. After pre-incubation of $A\beta_{1-42}$ monomers to ensure Aβ oligomerization, solutions containing either $A\beta_{1-42}$ alone (1 µM final concentration), or $A\beta_{1-42}$ with different amounts of ANK6, tANK6, and cANK6r (final concentrations between 0.008 and 15 µM) were incubated on PC12 cells overnight. Cell viabilities [%], relative to buffer-treated cells, were plotted against the respective D-peptides' concentrations. Datasets were fitted by nonlinear regression to determine the IC_{50} values. Data is represented as mean ± SEM; one-way ANOVA, ***p ≤ 0.001.

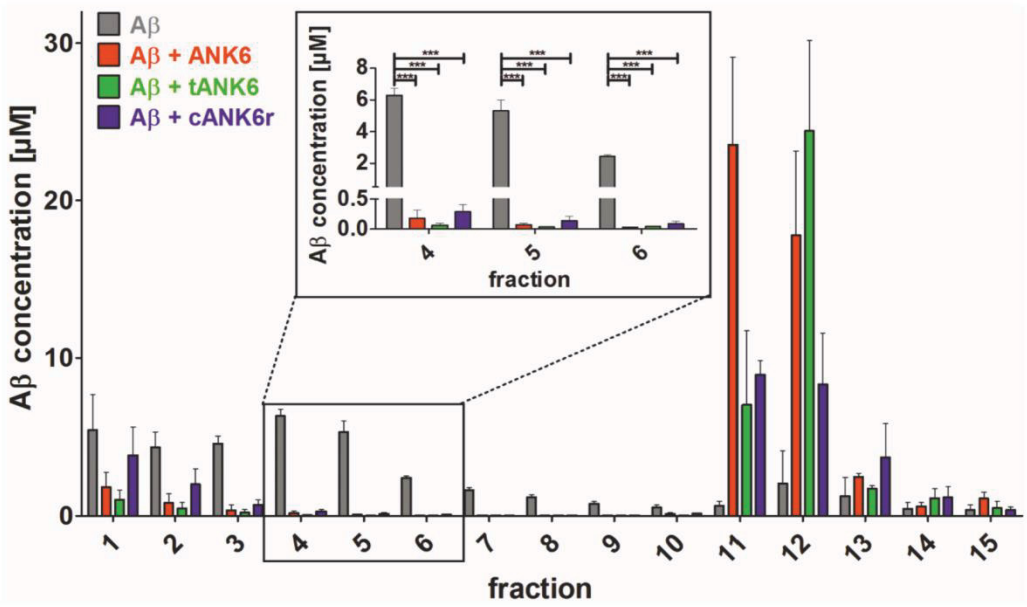

Figure 3: Quantitative determination of interference with Aβ aggregate size distribution (QIAD) assay

To investigate the D-peptides' impact on Aβ oligomer elimination, a quantitative determination of interference with Aβ aggregate size distribution (QIAD) assay was performed. $Aβ_{1-42}$ was pre-incubated to form the natural Aβ aggregate size distribution. Afterwards, sodium phosphate buffer (control, grey bars), ANK6 (red bars), tANK6 (green bars), or cANK6r (blue bars) was added. The samples were separated via density gradient centrifugation into 15 different fractions containing different Aβ particle sizes (fractions 1-2: monomers, 4-6: oligomers, 11-14: high molecular weight co-precipitates). Results revealed that ANK6, tANK6, and cANK6r significantly lowered the Aβ oligomer concentrations in fractions 4 to 6 as compared to the control (Aβ alone). Data is represented as mean ± SEM; one-way ANOVA, ***$p \leq 0.001$.

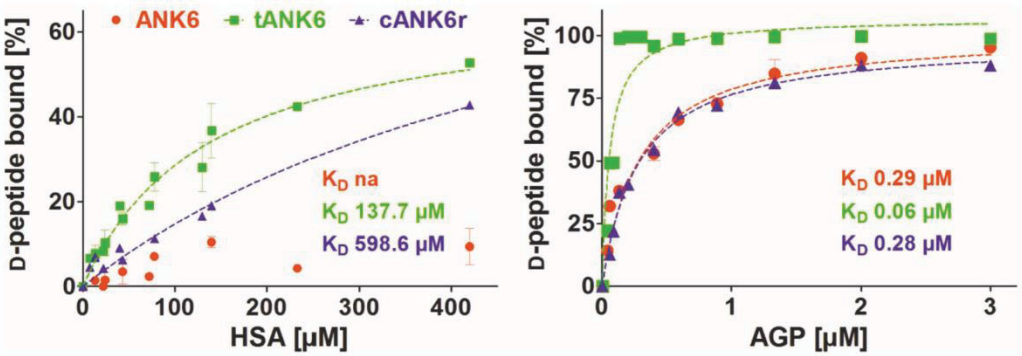

Figure 4: Binding to the plasma proteins HSA and AGP

ANK6's (red circles), tANK6's (green squares), and cANK6r's (blue triangles) binding to the plasma proteins human serum albumin (HSA) and to α1 acid glycoprotein (AGP) was analyzed. The D-peptides were applied at
770 5 µM while HSA and AGP concentrations were adjusted as follows: HSA 7.4 µM to 420 µM, AGP 0.04 µM to 3 µM. The unbound amount of ANK6, tANK6, and cANK6r (in %) to HSA or AGP respectively was plotted against the D-peptides' concentrations. Datasets were fitted by nonlinear regression to determine the K_D.

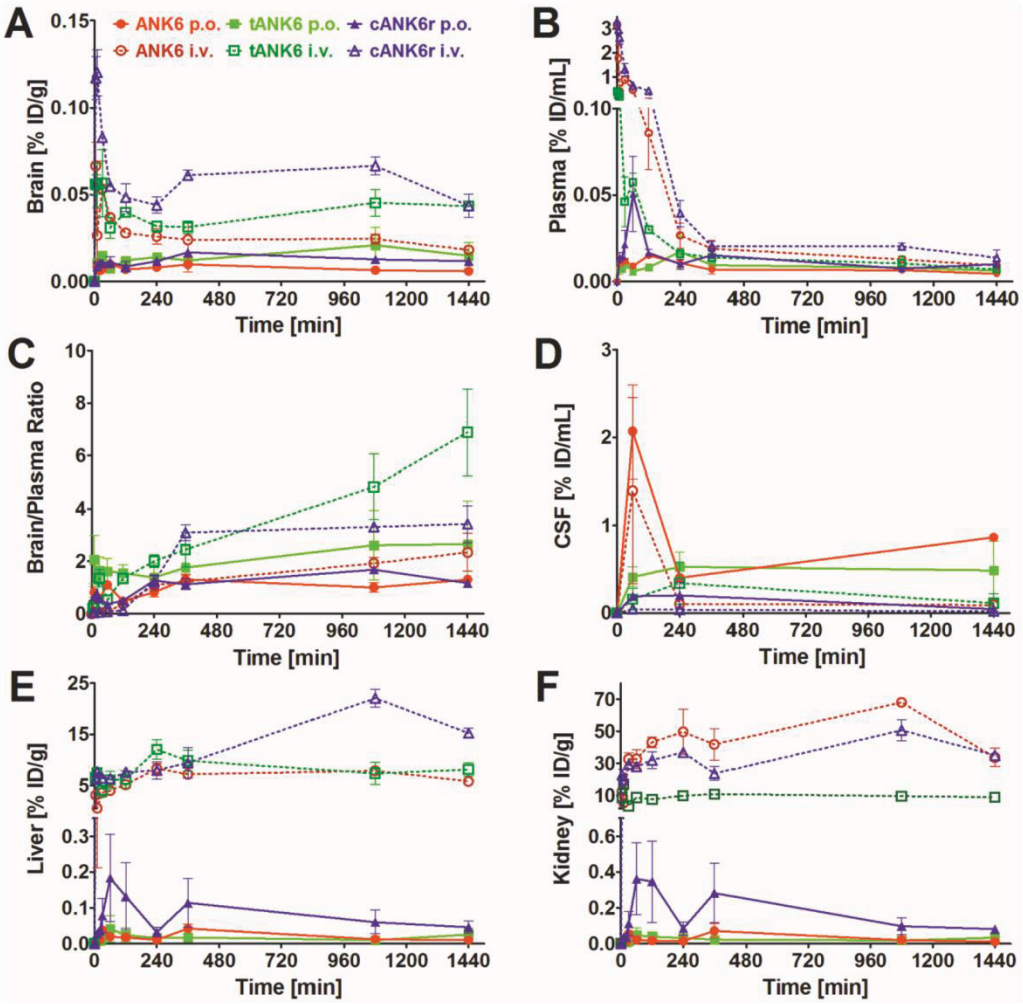

Figure 5: Pharmacokinetic concentration-time profiles of ANK6, tANK6, and cANK6r

Pharmacokinetic concentration-time profiles of ANK6 (red circles), tANK6 (green squares), and cANK6r (blue triangles) were investigated in brain (A), plasma (B), CSF (D), liver (E), and kidney (F) after i.v. (3.3 mg/kg, dotted lines) and p.o. (10 mg/kg ANK6 & tANK6, 15 mg/kg cANK6r, continuous lines) administration to wild type mice (3 mice/time point). The D-peptides were administered as a mixture of ^{3}H-labelled and non-labelled peptide in 0.9% sodium chloride solution. The ^{3}H-peptides' concentrations (triplicate) in the respective organs and plasma were measured with liquid scintillation counting. Total peptide concentrations were calculated as % of the injected dose per g or mL (% ID/g for brain, liver, kidney; % ID/mL for plasma, CSF) and plotted over time. The brain and plasma concentrations were set in relation to each other and plotted against the time as the brain/plasma ratio (C).

Abbreviations

	Aβ	amyloid-β
	AD	Alzheimer's disease
	AGP	α1-acid glycoprotein
790	AUC_{last}	area under the curve from the first to the last measured data pair
	BBB	blood-brain barrier
	C	concentration
	CBF	(murine) cerebral blood flow
	CL	terminal plasma clearance
	CSF	cerebrospinal fluid
	D	administered dose
	F	bioavailability
	f_u	free drug fraction = fraction unbound
	HSA	human serum albumin
800	IC_{50} value	half maximal inhibitory concentration
	ID	injected dose = intravenously or orally administered dose
	i.v.	intravenous
	K_D	dissociation constant
	K_{in}	universal influx rate constant
	logBB	blood-brain equilibrium distribution
	LSC	liquid scintillation counter
	MRT	mean residence time
	MTT	3-(4,5-Dimethylthiazol-2-yl)-2,5-diphenyltetrazoliumbromid
	PC12 cells	rat phaeochromocytoma cells
810	p.o.	oral
	PPB	plasma protein binding
	PS	permeability surface-area product
	QIAD	quantitative determination of interference with Aβ aggregate size distribution
	RP-HPLC	reversed phase-high performance liquid chromatography
	ThT	Thioflavin T
	t	time
	$t_{1/2}$	terminal half-life
	V_i	initial distribution volume in brain
	λ_z	terminal elimination rate constant
820		

4 Zusammenfassung und Schlussfolgerung

In der zunehmend älter werdenden Bevölkerung spielen neurodegenerative Erkrankungen eine immer größer werdende Rolle. Die AD stellt dabei die häufigste Form der Demenz dar und führt, als bisher unheilbare Erkrankung, innerhalb weniger Jahre zum Tod [4, 11]. Sowohl für die Patienten als auch für ihre Angehörigen ist der schnell fortschreitende Verlauf der Erkrankung nach Ausbruch der ersten Symptome, z.B. Gedächtnis- und Persönlichkeitsstörungen, eine sehr große psychische und physische Belastung. Aus diesem Grund sind Forscher weltweit auf der Suche nach einer kurativen Therapie oder sogar Prophylaxe gegen die AD. Zahlreiche Wirkansätze zielen dabei auf zwei pathologische Hauptmerkmale, beides neurotoxische Proteinablagerungen im Gehirn, ab: extrazelluläre Aβ-Ablagerungen und intrazelluläre Tau Protein-Aggregate [2].

Im Arbeitskreis um Professor Willbold wird seit einigen Jahren an der Entwicklung D-enantiomerer Peptide gearbeitet, die besonders toxische Aβ-Oligomere spezifisch und direkt eliminieren [74, 80]. Infolgedessen wird die von den Aβ-Oligomeren ausgehende Neurotoxizität vermindert. Die therapeutische Aktivität der Leitstruktur, D3, konnte bereits in zahlreichen Studien in transgenen Mausmodellen der AD bestätigt werden [95, 96]. Um die pharmakodynamischen und pharmakokinetischen Eigenschaften der D-Peptide zu optimieren, wurden in den vergangenen Jahren und werden fortwährend zahlreiche direkte (gleiche AS-Reste-Zusammensetzung) und indirekte (unterschiedliche AS-Reste-Zusammensetzung) D3-Derivate entwickelt. Die von Willbold et al. selektierten D-Peptide zeichnen sich durch ihre besondere proteolytische Stabilität und ihre sehr gute Verträglichkeit bzw. geringe Immunogenität aus [68]. Als sehr vielversprechender Kandidat gilt derzeit das D3-Derivat RD2 [80]. Die Untersuchung pharmakokinetischer Eigenschaften neuer Wirkstoffe macht bei deren präklinischer Entwicklung einen wichtigen Selektions-Bestandteil aus [113].

4.1 Untersuchung der pharmakokinetischen Eigenschaften sowie der Blut-Hirn-Schranken-Gängigkeit D-enantiomerer Peptide gegen die AD

In der Regel ist eine gute BHS-Gängigkeit für Wirkstoffe, deren Wirkort nicht im ZNS liegt, unvorteilhaft, da diese dort unerwünschte zentralnervöse Wirkungen hervorrufen könnten. Für Wirkstoffe, deren Wirkort im Gehirn ist, z.B. Wirkstoffe zur Therapie der AD, ist eine effiziente BHS-Gängigkeit jedoch von großer Wichtigkeit. Zu Beginn dieser Arbeit wurden D3 und seine direkten Derivat RD2, D3D3 und RD2D3 in Wildtyp-Mäusen auf ihre pharmakokinetischen Eigenschaften nach unterschiedlichen Applikationsarten untersucht. In Voruntersuchungen stellte sich heraus, dass alle vier Peptide proteolytisch stabil waren. Die

nach intravenöser Gabe (3,3 mg/kg Körpergewicht) erreichten c_{max}-Level im Gehirn der Wildtyp-Mäuse waren für die Einzel-Peptide (D3 und RD2) höher als für die Tandem-Peptide (D3D3 und RD2D3). Ein nennenswerter Unterschied zwischen den Einzel- und den Tandem-Peptiden wurde auch in Bezug auf die ermittelten terminalen Halbwertszeiten im Plasma deutlich. Während die Einzel-Peptide Halbwertszeiten im Bereich von ca. 30 bis 60 h aufwiesen, hatten die Tandem-Peptide lediglich Halbwertszeiten zwischen 0,5 und 3 h. Aufgrund der pharmakokinetischen Unterlegenheit der Tandem-Peptide sollte in weiteren Studien im Rahmen dieser Arbeit versucht werden, die pharmakokinetischen Eigenschaften der Tandem-Peptide effizienter zu gestalten. Dabei sollte v.a. die BHS-Gängigkeit der *in vitro* sehr gut Aβ-Oligomer-eliminierenden Tandem-Peptide [74] erhöht werden, um in anschließenden therapeutischen Studien höhere D-Peptid-Level im Gehirn erreichen zu können. Daraufhin wurde in einer Studie getestet, ob eine N- zu C-terminale Zyklisierung der D-Peptide deren BHS-Gängigkeit positiv beeinflussen kann. Der direkte Vergleich dreier linearer D3-Derivate und ihrer zyklischen Äquivalente zeigte, dass die D-Peptid-Zyklisierung deren BHS-Gängigkeit in Wildtyp-Mäusen (i.p. Applikation) deutlich effizienter macht, obwohl sich die Plasmawerte der linearen und zyklischen Äquivalente im Verlauf der Plasmakonzentrations-Zeit-Kurven kaum voneinander unterschieden (Abbildung 6).

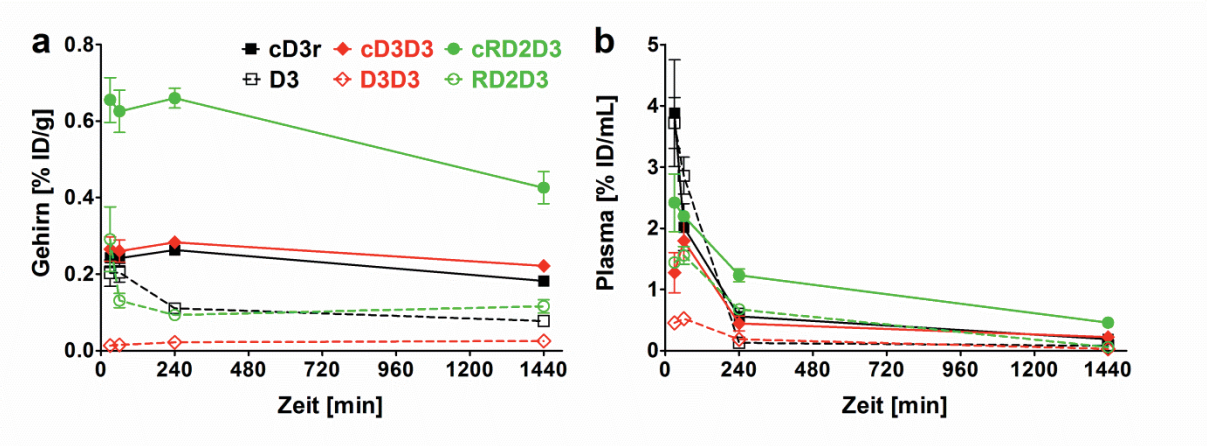

Abbildung 6: Gehirn- & Plasmakonzentrations-Zeit-Kurven zyklischer und linearer D-Peptide nach i.p. Applikation

cD3r (schwarze durchgezogene Linie, gefüllte Quadrate), D3 (schwarze gestrichelte Linie, leere Quadrate), cD3D3 (rote durchgezogene Linie, gefüllte Rauten), D3D3 (rote gestrichelte Linie, leere Rauten), cRD2D3 (grüne durchgezogene Linie, gefüllte Kreise) und RD2D3 cRD2D3 (grüne gestrichelte Linie, leere Kreise) wurden Wildtyp-Mäusen i.p. (10 mg/kg) verabreicht. Der Konzentrations-Verlauf der D-Peptide in Gehirn (a) und Plasma (b) wurde gegen die Zeit aufgetragen. Die Konzentration wurde als prozentualer Anteil der injizierten Dosis pro Gramm Gehirn (% ID/g) oder pro Milliliter Plasma (% ID/mL) angegeben. Die zyklischen D-Peptide (durchgezogene Linien) weisen höhere Konzentrationen im Gehirn auf als ihre linearen Äquivalente (gestrichelte Linien), während die Konzentrationen im Plasma für die zyklischen und die linearen D-Peptid-Paare jeweils ähnlich verlaufen.

Pharmakodynamisch wurde exemplarisch für cD3r bereits gezeigt, dass die mit der Zyklisierung einhergehende Erhöhung der konformativen Starrheit eines D-Peptids seine Affinität zum Zielmolekül, seine Effizienz, zytotoxische Oligomere zu eliminieren sowie seine Fähigkeit, Aβ-induzierte Neurotoxizität zu vermindern, erhöhen kann [89]. Diese pharmakodynamischen Aspekte, in Kombination mit den vorteilhaften pharmakokinetischen Eigenschaften, stellen eine erhöhte *in vivo* Effizienz der zyklischen D-Peptide in Aussicht. Das aus RD2 und D3 zusammengesetzte, zyklische Tandem-D-Peptid, cRD2D3, wurde in einer Studie mit vier D3-Derivaten (drei Zyklische und ein Lineares) als D-Peptid mit der effizientesten BHS-Gängigkeit selektiert (Abbildung 6) und daraufhin intensiver untersucht. Tests zur proteolytischen Stabilität und zur Plasmaproteinbindung sprachen cRD2D3 die gleichen vielversprechenden Eigenschaften wie D3, RD2 und den Tandem-D-Peptiden RD2D3 und D3D3 zu. Die in Wildtyp-Mäusen untersuchten pharmakokinetischen Profile nach i.v., i.p. und oraler Gabe bestätigten cRD2D3, im Gegensatz zu den linearen Tandem-D-Peptiden, eine wünschenswert lange Halbwertszeit (29-58 h). Weiterhin zeigte cRD2D3 eine sehr hohe orale Bioverfügbarkeit (Tabelle 1, Abbildung 8). Sowohl eine lange Halbwertszeit mit großer proteolytischer Stabilität, sprich eine ausreichend lange Wirkungsdauer, als auch eine hohe orale Bioverfügbarkeit sind für Wirkstoffe zur Therapie der AD äußerst vorteilhaft. Da davon auszugehen ist, dass eine AD-Therapie über einen längeren Zeitraum (unter Umständen mehrere Jahre bis Jahrzehnte) stattfinden soll, ist ein Therapieregime mit einer einmal täglichen oralen Wirkstoffeinnahme für den Patienten am komfortabelsten. Therapieregime mit einmal täglicher Wirkstoffeinnahme, die nur bei Wirkstoffen mit einer ausreichend hohen Halbwertszeit angewandt werden können, werden zudem mit einer deutlich höheren Therapietreue (Compliance) verbunden als solche, bei denen die Wirkstoffeinnahme mehrmals täglich durchgeführt werden muss. Eine Übersicht über die Halbwertszeiten und oralen Bioverfügbarkeiten einiger für diese Arbeit relevanter D-Peptide ist in Tabelle 1 zusammengestellt. Während RD2 mit einer enorm langen Halbwertszeit von fast 60 h nach intravenöser Gabe hervorsticht, konnte die Zyklisierung bei cRD2D3 die Halbwertszeit im Vergleich zu der seines linearen Äquivalents RD2D3 um ein Vielfaches verlängern. Weiterhin zeigte cRD2D3 eine herausragende orale Bioverfügbarkeit, wobei auch die der anderen, nach oraler Gabe untersuchten D-Peptide, verglichen mit L-enantiomeren Peptiden, außergewöhnlich hoch war.

Tabelle 1: Pharmakokinetische Parameter nach einmaliger Applikation

D-Peptid	$t_{1/2}$ [h] (i.v.)	F [%] (p.o.)
D3	32	58,3
RD2	59	76,5
D3D3	0,7	na
RD2D3	0,8	na

cRD2D3	29	98,0
ANK6	15	11,8
tANK6	18	49,4
cANK6r	18	9,9

Da die Konzentration eines Wirkstoffs im menschlichen Gehirn i.d.R. nicht direkt bestimmt werden kann, die in der CSF jedoch schon, wird behandelten Patienten häufig CSF entnommen und geschaut, ob der Wirkstoff dort in für eine zu erwartende Wirkung ausreichend hohen Konzentrationen vorliegt. Dabei wird davon ausgegangen, dass die Wirkstoff-Konzentrationen im Gehirn und der CSF direkt miteinander korrelieren. Da dies jedoch nicht immer der Fall ist [114], wurde in dieser Arbeit untersucht, in wie fern die D-Peptid-Konzentrations-Zeit-Verläufe nach Einmalgabe (i.p.) in Gehirn, CSF und Plasma von Wildtyp-Mäusen korrelieren. Dabei verlief das Verhältnis der D-Peptid-Konzentrationen in CSF und Gehirn konstant, was auf ein sich rasch nach der Applikation einstellendes Gleichgewicht zwischen CSF und Gehirn, also eine direkte Korrelation hindeutete (Abbildung 7 a). Die Verhältnisse der D-Peptid-Konzentrationen in Gehirn und Plasma bzw. CSF und Plasma stiegen wiederum von 0 h bis etwa 24 h nach der Applikation konstant an und erreichten erst dann einen vergleichbaren Wert (Abbildung 7 b&c). Aufgrund der schnellen, aber nicht proportional zur Plasmakonzentration ansteigenden, D-Peptid-Aufnahme ins murine Gehirn sowie aufgrund der langanhaltend hohen D-Peptid-Konzentrationen im Gehirn wurde angenommen, dass die D-Peptide direkt (Endozytose-unabhängig) über die BHS ins Gewebe eindringen und dass dieser Prozess sättigbar ist [85, 115]. Die Sättigbarkeit der BHS-Gängigkeit wird, exemplarisch für cRD2D3, deutlich, wenn man beachtet, dass die Konzentrationen im Gehirn nach intravenöser Gabe, also anfänglich extrem hohen Plasmakonzentrationen, in etwa in der gleichen Größenordnung liegen wie nach oraler Gabe, also anfänglich eher niedrigen Plasmakonzentrationen. Erst wenn ein Teil des zirkulierenden D-Peptids im Gehirn angekommen ist und ein Teil aus dem Plasma bereits metabolisiert oder eliminiert wurde, sind die Konzentrationen in Gehirn und Plasma äquivalent und bleiben es dann auch für mehrere Tage (Abbildung 7 d). Weiterhin wird angenommen, dass D3 und seine Derivate die BHS besonders effizient (vom Blut Richtung Gehirn) überwinden können, weil ihre AS-Sequenz zahlreiche Arginine (bei D3 und RD2 sind 5 von 12 AS-Resten Arginine) beinhaltet. Sie haben in ihrer AS-Sequenz ein sog. „arginine rich motif“ (Arginin-reiche Sequenz), das dem des Humanen Immundefizienz-Virus Typ 1 Transkriptions-Transaktivator (HIV-1 Tat)-Protein ähnelt [116, 117]. Aufgrund dieser Ähnlichkeit wird vermutet, dass die D-Peptide durch einen ähnlichen, direkten Transportmechanismus über Membranen und letztlich auch die BHS transportiert werden wie die HIV-1 Tat-Proteine.

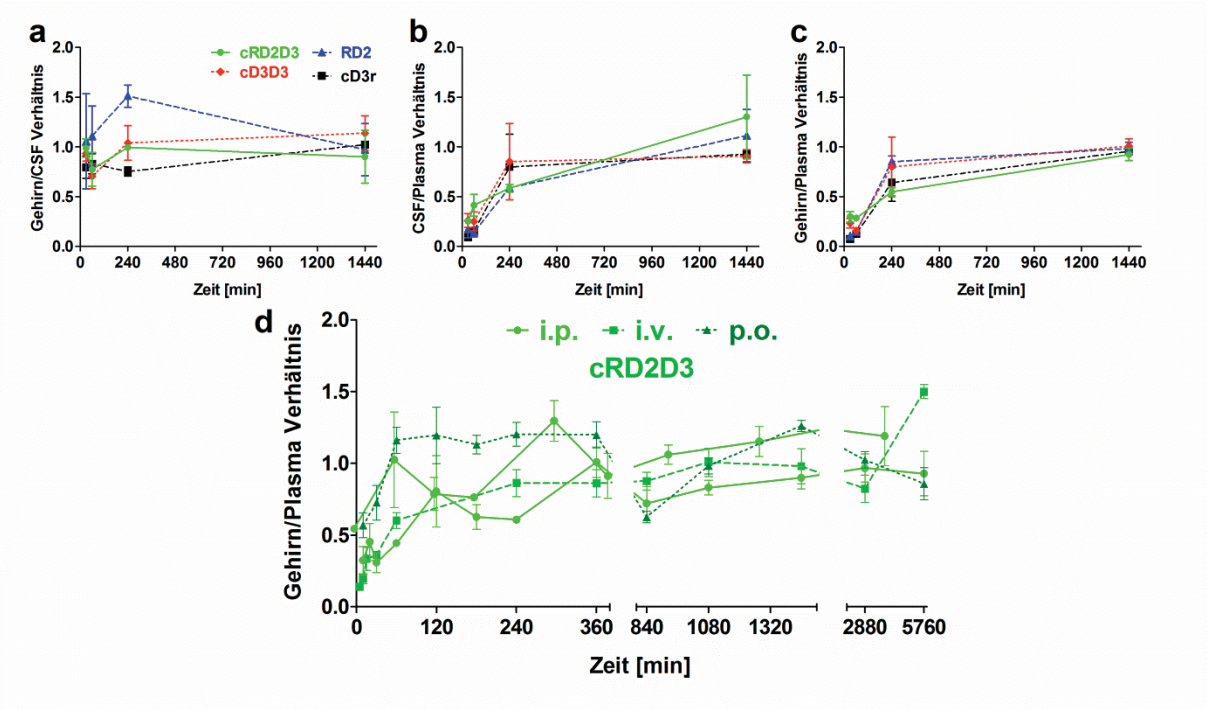

Abbildung 7: Gehirn/CSF-, CSF/Plasma- und Gehirn/Plasma-Verhältnisse

(a-c) cRD2D3 (grüne Linie, Kreise), RD2 (blaue gestrichelte Linie, Dreiecke), cD3D3 (rote gestrichelte Linie, Rauten) und cD3r (schwarze gestrichelte Linie, Quadrate) wurden Wildtyp-Mäusen i.p. (10 mg/kg) verabreicht. Die D-Peptid-Konzentrationen (Dreifachbestimmung) in Plasma, Gehirn und CSF wurden bestimmt und miteinander ins Verhältnis gesetzt. Das Verhältnis von Gehirn/Plasma (a), CSF/Plasma (b) und Gehirn/CSF (c) wurde gegen die Zeit aufgetragen.
(d) Die Gehirn- und Plasmakonzentrationen von cRD2D3 wurden zusätzlich nach i.v. (3,3 mg/kg; mittelgrüne gestrichelte Linie, Quadrate) und p.o. (10 mg/kg; dunkelgrüne gestrichelte Linie, Dreiecke) Applikation untersucht und bis zu 4 Tage nach der einmaligen Applikation miteinander ins Verhältnis gesetzt (d).

Um die BHS-Gängigkeit der entwickelten D-Peptide mit der anderer Peptide, die z.T. bereits als Wirkstoffe für diverse Erkrankungen zugelassen sind, vergleichen zu können, wurden BHS-Durchlässigkeits-Parameter für D3 und einige seiner Derivate bestimmt. Die Vergleichswerte sind in einer internationalen, von der Universität Gent geführten, Datenbank (Brainpeps: www.brainpeps.ugent.be) gelistet [107]. Als Positivkontrolle für gute BHS-Durchlässigkeit wird häufig das Heptapeptid „Dermorphin“ verwendet [118]. In Tabelle 2 sind die BHS-Durchlässigkeits-Parameter D3s und einiger seiner Derivate gelistet. Es wird deutlich, dass cRD2D3 und tANK6 die verhältnismäßig höchsten K_{in}-Werte und vorteilhaftesten logBB-Werte haben. Ein hoher K_{in}-Wert bestätigt den beiden D-Peptiden einen verhältnismäßig schnellen Übergang vom Blut ins Gehirn d.h. sie liegen in der gleichen Größenordnung wie die Positivkontrolle. Je positiver der logBB-Wert eines Peptids ist, desto mehr Peptid gelangt innerhalb von 24 h, relativ zur Plasmakonzentration, ins Gehirn. Die außergewöhnlich guten BHS-Durchlässigkeits-Parameter des tANK6 werden allerdings durch, verglichen mit den anderen D-Peptiden, sehr niedrige initiale Plasmaspiegel nach der

i.v.-Applikation relativiert. Die verhältnismäßig niedrigen initialen tANK6-Plasmakonzentrationen können beispielsweise durch einen hohen First-Pass-Effekt und/oder eine schnelle Elimination entstanden sein. Zusammenfassend zeigte cRD2D3 in diesen Studien herausragende pharmakokinetische Eigenschaften, da es hohe Gehirnspiegel, vorteilhafte BHS-Durchlässigkeits-Parameter, eine lange terminale Halbwertszeit und eine hohe orale Bioverfügbarkeit aufweist. In künftig geplanten Therapiestudien in AD-Mausmodellen mit kognitiven Defiziten soll cRD2D3s *in vivo* Wirksamkeit zur Verbesserung dieser Defizite untersucht werden.

Tabelle 2: Blut-Hirn-Schranken-Durchlässigkeits-Parameter

D-Peptid	K_{in} [mL/(g*min)]	V_i [mL/g]	PS [mL/(g*min)]	logBB (0-24 h)
D3	0,0002	0,0446	0,0002	-0,526
RD2	0,0005	0,0437	0,0005	-0,445
D3D3	0,0003	0,0531	0,0003	-0,396
RD2D3	0,0003	0,0512	0,0003	-0,411
cRD2D3	**0,0020**	**0,1955**	**0,0020**	**-0,105**
ANK6	0,0003	0,0575	0,0003	-0,401
tANK6	**0,0016**	**0,5833**	**0,0016**	**0,335**
cANK6r	0,0003	0,0396	0,0003	-0,329
Dermorphin*	0,0022	0,0215	na	na

* Dermorphin-Werte entnommen aus Brainpeps [108, 119].

4.2 *In vitro* und *in vivo* Vergleich dreier D-enantiomerer Peptide gegen die AD

Die ersten, direkten D3-Derivate bestanden alle aus denselben AS-Resten wie D3, lediglich in unterschiedlichen Anordnungen. Um zu prüfen, ob es jedoch sinnvolle AS-Austausche in der D3-Sequenz gibt, die das Aβ-Oligomer-Eliminierungs-Potenzial weiter erhöhen, wurden die einzelnen D3-AS systematisch jeweils gegen 19 proteinogene bzw. 13 nicht-proteinogene AS-Reste ausgetauscht und, mittels SPR, die Affinität der entstandenen D-Peptide an Aβ-Monomere untersucht [90]. Das vielversprechendste Derivat, das ausschließlich aus proteinogenen AS-Resten besteht (ANK6), wurde daraufhin im Rahmen dieser Arbeit in unterschiedlichen *in vitro* Tests zur Aβ-Interaktion (ThT- und MTT-Test), zum Aβ-Oligomer-Eliminierungspotenzial (QIAD-Assay) und zur Plasmaproteinbindung sowie in pharmakokinetischen *in vivo* Untersuchungen in Wildtyp-Mäusen (Konzentrations-Zeit-Profile, pharmakokinetische und BHS-Durchlässigkeits-Parameter) mit seinem eigenen Tandem-Derivat (tANK6) und seiner zyklisierten Version (cANK6r) verglichen (Tabelle 1, Tabelle 2, Tabelle 3).

Wie erwartet, zeigten alle drei D-Peptide außergewöhnlich gute Ergebnisse in den *in vitro* Tests. Während tANK6 im ThT-Test zur Aβ-Fibrillen-Bildungs-Inhibition und im MTT-Test zur Untersuchung der Verringerung des zytotoxischen Aβ-Einflusses die effizientesten Ergebnisse zeigte, schnitt cANK6r im QIAD-Assay am besten ab. Obwohl cANK6r's Aβ-Oligomer-Eliminierungs-Potenzial in der gleichen Größenordnung lag wie das von ANK6 und tANK6 (Tabelle 3), wurden dem zyklischen Peptid noch bessere Eigenschaften zugesprochen, da es die Aβ-Monomer-Fraktionen (Aβ-Monomere gelten als potentiell neuroprotektiv [33]) weniger stark gesenkt hat als die anderen beiden. Folglich weist es eine noch spezifischere Aβ-Oligomere-Eliminierungs-Spezifität aus als ANK6 und tANK6. Die pharmakokinetischen *in vivo* Untersuchungen in Wildtyp-Mäusen nach i.v. und oraler Applikation zeigten für alle drei D-Peptide verhältnismäßig niedrige Plasma- und Gehirnkonzentrationen im Vergleich zu den D3-Derivaten der ersten Generation (Abbildung 8). Allerdings erreichte das zyklische cANK6r nach i.v. Applikation, wie auch die zyklischen D3-Derivate der ersten Generation, im Gehirn höhere Konzentrationen als die beiden linearen D-Peptide ANK6 und tANK6. Dies bestätigt die Hypothese, dass zyklische D-Peptide effizienter im Gehirn ankommen als ihre linearen Äquivalente, wobei die D-Peptid-AS-Sequenz offenbar eine noch bedeutendere Rolle für die BHS-Gängigkeit spielt. Die relativ hohen Konzentrationen in Leber und Niere sowie die relativ niedrigen Plasmakonzentrationen aller drei D-Peptide könnte darauf hindeuten, dass sie dem enterohepatischen Kreislauf (1.7.1) unterliegen.

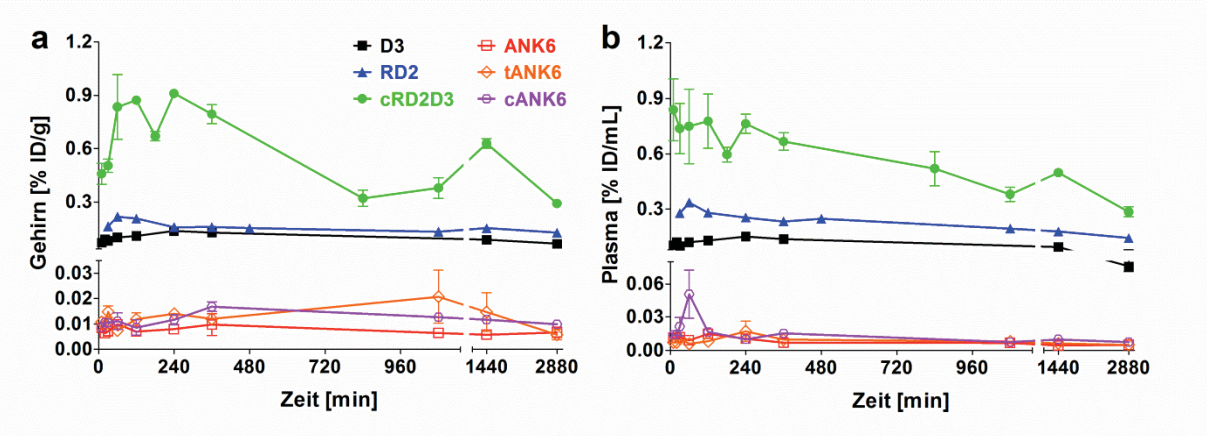

Abbildung 8: Gehirn- & Plasmakonzentrations-Zeit-Kurven verschiedener D3-Derivate nach oraler Applikation

D3 (schwarze Linie, gefüllte Quadrate), RD2 (blaue Linie, gefüllte Dreiecke), cRD2D3 (grüne Linie, gefüllte Kreise), ANK6 (rote Linie, leere Quadrate), tANK6 (orange Linie, leere Rauten) und cANK6r (violette Linie, leere Sechsecke) wurden Wildtyp-Mäusen oral (10 mg/kg) verabreicht. Der Konzentrations-Verlauf der D-Peptide in Gehirn (a) und Plasma (b) wurde gegen die Zeit aufgetragen. Die Konzentration wurde als prozentualer Anteil der injizierten Dosis pro Gramm Gehirn (% ID/g) oder pro Milliliter Plasma (% ID/mL) angegeben. D3 und seine direkten (gleiche Aminosäure-Reste in der Sequenz wie D3) Derivate RD2 und cRD2D3 weisen sowohl im Gehirn als auch

im Plasma deutlich höhere Konzentrationen auf als die indirekten (andere Aminosäure-Reste in der Sequenz als D3) D3-Derivate. Insgesamt weist cRD2D3 nach oraler Gabe die mit Abstand höchsten Konzentrationen in Gehirn und Plasma auf.

Diese Studie zeigte, dass ANK6 und seine beiden Derivate tANK6 und cANK6r zwar in den *in vitro* Tests effizienter sind als D3 und seine Derivate der ersten Generation (Tabelle 3), ihre pharmakokinetischen Eigenschaften jedoch deutlich unvorteilhafter (Tabelle 1), v.a. im Hinblick auf die verhältnismäßig deutlich niedrigen Plasma- und Gehirnkonzentrationen, einzuordnen sind (Abbildung 8). Möglicherweise sind die unterlegenen pharmakokinetischen Eigenschaften z.T. in der bei ANK6 und seinen Derivaten nicht vorhanden HIV-Tat-Sequenz begründet [85, 115]. Diese Ergebnisse in Kombination mit den von Klein et al. beschriebenen Ergebnissen einer Therapiestudie, in der ANK6 keine signifikante Verbesserung der Kognition in einem AD-Mausmodell zeigen konnte [90], machen deutlich, dass eine sehr hohe Aβ-Oligomer-eliminierende *in vitro* Effizienz alleine nicht ausreicht, um einen *in vivo* potenten AD-Wirkstoff zu entwickeln, sondern dass die pharmakokinetischen Eigenschaften ebenfalls eine entscheidende Rolle für die Wirksamkeit spielen. Folglich sollten, trotz des herausragenden Aβ-Oligomer-Eliminierungs-Potenzials der ANK6-Peptide, keine weiteren therapeutischen Studien in transgenen Mäusen eines AD-Mausmodells mit ANK6 und seinen Derivaten durchgeführt werden, bevor deren pharmakokinetische Eigenschaften nicht durch Änderungen der AS-Sequenz, eine geeignete Formulierung o.ä. effizienter gestaltet wurden.

Tabelle 3: Parameter zur D-Peptid-Aβ-Interaktion & Plasmaproteinbindung

	ThT-Test	MTT-Test	QIAD	Plasmaproteinbindung	
D-Peptid	**IC_{50}**	**Zellviabilität (Aβ:Peptid)**	**Aβ-Oligomer-Eliminierung (Aβ:Peptid)**	**K_D (humanes Serumalbumin)**	**K_D (saures α1-Glykoprotein)**
D3	7,2 µM	~60 % (1:5) [90]	50 % (4:1)	≥ 1,4 mM**	1,8 µM
RD2	7,7 µM	76 % (1:5)	71 % (4:1)	≥ 1,4 mM**	2,77 µM
D3D3	nb	~90 % (1:1) [87]	96 % (8:1) [87]	≥ 1,4 mM**	0,03 µM
RD2D3	1,9 µM*	~100 % (1:1) [87]	98 % (8:1) [87]	≥ 1,4 mM**	0,04 µM
cRD2D3	1,8 µM*	82,2 % (1:2,5)*	nb	33,2 µM	1,2 µM
ANK6	3,6 µM	65,3 % (1:5)	98,2 % (4:1)	≥ 1,4 mM**	0,29 µM
tANK6	2,1 µM	75,5 % (1:5)	98,9 % (4:1)	137,7 µM	0,06 µM
cANK6r	3,7 µM	58,2 % (1:5)	96,5 % (4:1)	598,6 µM	0,28 µM

nb = nicht bestimmt * unveröffentlichte Daten.

** Da die D3-Derivate aufgrund ihrer positiven Ladung bei physiologischem pH-Wert lediglich eine geringe Affinität zu humanem Serumalbumin aufweisen, konnte mit dem für die Plasmaproteinbindungs-Bestimmung verwendeten Kit kein K_D ermittelt werden. Das Detektionslimit des Kits lag bei 1,4 mM. Der K_D der mit einem * markierten D3-Derivate liegt folglich darüber.

4.3 Untersuchung der pharmakodynamischen Eignung eines D-enantiomeren Peptids in einem transgenen AD-Mausmodell

Neben pharmakokinetischen Untersuchungen wurde in dieser Arbeit eine orale Darreichungsform für die D-Peptide etabliert, die die minimalinvasive Durchführung einer mehrwöchigen pharmakodynamischen *in vivo* Therapiestudie in einem transgenen AD-Mausmodell ermöglicht. Die häufig verwendete Darreichungsform eines Wirkstoffes in Nagetieren mittels Schlundsonden ist v.a. über einen längeren Therapiezeitraum mit täglicher Applikation stark belastend für die Mäuse. Die hier etablierte orale Darreichungsform ist ein Gummibärchen-artiges „Jelly“ (eine wässrige Lösung mit 30 % Sucrose, 10 % Sucralose und 18,75 % Kaltrührgelatine erwies sich als geeignetste Formulierung), in das entweder Wasser (Placebo) oder eine wässrige D-Peptid-Lösung (Verum), die dem Durchschnittsgewicht der Mäuse und der täglich zu applizierenden Dosis entspricht, hinzugefügt wird. In einer pharmakokinetischen Pilotstudie konnte gezeigt werden, dass der D-Peptid-Wirkstoff in vergleichbaren Mengen im Blut und Gehirn ankommt wie nach Applikation mit der Schlundsonde.

Die „Jellies“ wurden während der Therapiestudie wöchentlich frisch hergestellt, um die D-Peptid-Dosierung an das aktuelle Gewicht der jeweiligen Behandlungsgruppen transgener Mäuse anpassen zu können und um zu gewährleisten, dass die Jellies nicht verderben. Um die tägliche Behandlung der transgenen Mäuse möglichst schonend (gemäß dem 3R-Prinzip bei Tierversuchen: „Replace, Reduce, Refine“) zu gestalten, wurden sie während der mehrwöchigen Therapiephase jeden Vormittag in einen sog. Futterkäfig (leerer Käfig mit einem Wirkstoff- oder Placebo-haltigen „Jelly“) und, nachdem sie das „Jelly“ komplett aufgegessen hatten, zurück in den Haltungskäfig gesetzt.

Die mit dieser Darreichungsform durchgeführte 12-wöchige Therapiestudie (tägliche orale Einmalgabe des Wirkstoffs) in einem transgenen Mausmodell zeigte jeweils eine signifikante Verringerung des AD-Phänotyps der mit dem sehr aussichtsreichen D-Peptid-Wirkstoffkandidaten RD2 behandelten transgenen Mäuse im Vergleich zu den mit Placebo behandelten transgenen Mäusen. Die transgenen Mäuse dieser Studie stammten aus einer internen Zucht des in 1.6.2.2.1 beschriebenen APPswe/PS1dE9-Mausmodells und zeigten aufgrund ihres hohen Alters bereits zu Beginn der Therapie (18 ± 2 Monate) eine vollständig ausgeprägte Pathologie. Sie wurden mit 200 mg RD2/kg Körpergewicht/Tag behandelt. Der „Morris Water Maze“ ist einer der aussagekräftigsten kognitiven Tests, der für transgene AD-Mäuse mit kognitiven Defiziten etabliert wurde [120]. In der pharmakodynamischen Therapiestudie erzielten die mit RD2 behandelten Mäuse signifikant erhöhte kognitive Leistungen als ihre mit Placebo behandelten Geschwistertiere. Kürzlich wurde das Hirnhomogenat der behandelten Mäuse mit einer Kombination zweier oben beschriebener

Testverfahren, QIAD- und sFIDA-Assay (1.6.1, 1.5.2.1), analysiert. Zusammenfassend konnte RD2 in drei AD-Mausmodellen (APP/PS1dE9, TBA2.1 [Schemmert et al. 2018, eingereicht], APP_{SL}) [87]) in drei verschiedenen Laboratorien seine Wirksamkeit unter Beweis stellen und es konnte erstmals *in vivo* nachgewiesen werden, dass die Aβ-Oligomer-Konzentration im Gehirn durch die RD2-Behandlung selektiv gesenkt wurde.

4.4 Ausblick

Nach eingehenden pharmakokinetischen und pharmakodynamischen Studien zeigen einige der von Willbold et al. entwickelten D-Peptide großes Potenzial zur prophylaktischen oder sogar kurativen Therapie der AD.

Das in dieser Arbeit als besonders vorteilhaft charakterisierte D3-Derivat, cRD2D3, soll in naher Zukunft in einer mehrwöchigen, oralen Therapiestudie in einem AD-Mausmodell mit kognitiven Defiziten auf seine pharmakodynamische Eignung untersucht werden. Dabei soll es direkt mit RD2 verglichen werden, dessen therapeutische Aktivität bereits in mehreren oralen Therapiestudien in verschiedenen AD-Mausmodellen bestätigt wurde. Mit diesen Studien soll überprüft werden, ob die gute *in vitro* Effizienz und die vorteilhaften pharmakokinetischen Eigenschaften auch zu einer hohen therapeutischen *in vivo* Effizienz führen.

Um v.a. die orale Bioverfügbarkeit einiger D3-Derivate weiter zu erhöhen, sollen diese künftig mit Substanzen reversibel gekoppelt werden, die die Aufnahme aus dem Gastrointestinaltrakt erhöhen. Nach der Aufnahme sollen diese Substanzen unter physiologischen Bedingungen (z.B. enzymatisch) wieder abgekoppelt werden, sodass das freie D3-Derivat seine Wirkung entfalten kann. So müssten geringere Mengen des Wirkstoffs verabreicht werden, um eine *in vivo* wirksame Konzentration zu erreichen. Infolgedessen sollen die Gefahr potentiell auftretender unerwünschter Arzneimittelwirkungen sowie die Therapiekosten gesenkt werden.

Die AD weist zwei pathologische Hauptmerkmale angesammelter Proteinspezies im Gehirn auf, die Amyloidose und die Tauopathie. Da sich die D-Peptide bei der Amyloidose bewährt haben und auch geeignete pharmakokinetische Eigenschaften aufweisen, soll das Konzept künftig auf die Therapie der Tauopathie ausgeweitet werden. Die D-Peptide sollen dann in entsprechenden AD-Mausmodellen mit einer Tauopathie auf ihre kurative Wirkung untersucht werden.

Auch eine Anwendung der D-Peptide in der AD-(Früh-)Diagnostik ist von großem Interesse. Beispielsweise sollen sie künftig zu PET-Tracern weiterentwickelt werden. Hierzu müssen die D-Peptide radioaktiv markiert werden (z.B. mit ^{18}F oder ^{68}Ga), nach intravenöser

Applikation schnell ins Gehirn gelangen, dort spezifisch an Aβ-Oligomere oder –Plaques bzw. an neurofibrilläre Tau-Bündel binden und anschließend innerhalb einer kurzen Zeit wieder aus dem Gehirn und dem gesamten Organismus ausgeschleust werden.

Gearbeitet wird derzeit außerdem daran, den Wirkmechanismus der D-Peptide auf andere neurodegenerative Erkrankungen auszuweiten, denen ebenfalls Akkumulationen fehlgefalteter Proteine im Gehirn zugrunde liegen. Zu diesen Erkrankungen zählen z.B. Morbus Parkinson, die Amyotrophe Lateralsklerose und Chorea Huntington.

IX. Referenzen

[1] Alzheimer A (1907) Über eine eigenartige Erkrankung der Hirnrinde. *Allgemeine Zeitschrift fur Psychiatrie und Psychisch-gerichtliche Medizin* **64**, 146-148.

[2] Bloom GS (2014) Amyloid-beta and tau: the trigger and bullet in Alzheimer disease pathogenesis. *JAMA Neurol* **71**, 505-508.

[3] Mandelkow EM, Mandelkow E (1998) Tau in Alzheimer's disease. *Trends Cell Biol* **8**, 425-427.

[4] Blennow K, de Leon MJ, Zetterberg H (2006) Alzheimer's disease. *Lancet* **368**, 387-403.

[5] Prince M, Comas-Herrera A, Knapp M, Guercht M, Karagiannidou M (2016) in *Alzheimer's Disease International*.

[6] Brookmeyer R, Johnson E, Ziegler-Graham K, Arrighi HM (2007) Forecasting the global burden of Alzheimer's disease. *Alzheimers Dement* **3**, 186-191.

[7] Gaugler J, James B, Johnson T, Weuve J (2017) 2017 Alzheimer's Disease Facts and Figures. *Alzheimer's & Dementia* **13**, 325-373.

[8] Alom Poveda J, Baquero M, Gonzalez-Adalid Guerreiro M (2013) [Clinical stages of patients with Alzheimer disease treated in specialist clinics in Spain. The EACE study]. *Neurologia* **28**, 477-487.

[9] Albert MS, DeKosky ST, Dickson D, Dubois B, Feldman HH, Fox NC, Gamst A, Holtzman DM, Jagust WJ, Petersen RC, Snyder PJ, Carrillo MC, Thies B, Phelps CH (2011) The diagnosis of mild cognitive impairment due to Alzheimer's disease: recommendations from the National Institute on Aging-Alzheimer's Association workgroups on diagnostic guidelines for Alzheimer's disease. *Alzheimers Dement* **7**, 270-279.

[10] Sperling RA, Aisen PS, Beckett LA, Bennett DA, Craft S, Fagan AM, Iwatsubo T, Jack CR, Jr., Kaye J, Montine TJ, Park DC, Reiman EM, Rowe CC, Siemers E, Stern Y, Yaffe K, Carrillo MC, Thies B, Morrison-Bogorad M, Wagster MV, Phelps CH (2011) Toward defining the preclinical stages of Alzheimer's disease: recommendations from the National Institute on Aging-Alzheimer's Association workgroups on diagnostic guidelines for Alzheimer's disease. *Alzheimers Dement* **7**, 280-292.

[11] James BD, Leurgans SE, Hebert LE, Scherr PA, Yaffe K, Bennett DA (2014) Contribution of Alzheimer disease to mortality in the United States. *Neurology* **82**, 1045-1050.

[12] Lista S, O'Bryant SE, Blennow K, Dubois B, Hugon J, Zetterberg H, Hampel H (2015) Biomarkers in Sporadic and Familial Alzheimer's Disease. *J Alzheimers Dis* **47**, 291-317.

[13] Gorelick PB (2004) Risk factors for vascular dementia and Alzheimer disease. *Stroke* **35**, 2620-2622.

[14] Casserly I, Topol E (2004) Convergence of atherosclerosis and Alzheimer's disease: inflammation, cholesterol, and misfolded proteins. *Lancet* **363**, 1139-1146.

[15] Selkoe DJ (2013) SnapShot: pathobiology of Alzheimer's disease. *Cell* **154**, 468-468 e461.

[16] Corder EH, Saunders AM, Strittmatter WJ, Schmechel DE, Gaskell PC, Small GW, Roses AD, Haines JL, Pericak-Vance MA (1993) Gene dose of apolipoprotein E type 4 allele and the risk of Alzheimer's disease in late onset families. *Science* **261**, 921-923.

[17] Castellano JM, Kim J, Stewart FR, Jiang H, DeMattos RB, Patterson BW, Fagan AM, Morris JC, Mawuenyega KG, Cruchaga C, Goate AM, Bales KR, Paul SM, Bateman RJ, Holtzman DM (2011) Human apoE isoforms differentially regulate brain amyloid-beta peptide clearance. *Sci Transl Med* **3**, 89ra57.

[18] Banci L, Bertini I, Boca M, Girotto S, Martinelli M, Valentine JS, Vieru M (2008) SOD1 and amyotrophic lateral sclerosis: mutations and oligomerization. *PLoS One* **3**, e1677.

[19] Piaceri I, Nacmias B, Sorbi S (2013) Genetics of familial and sporadic Alzheimer's disease. *Front Biosci (Elite Ed)* **5**, 167-177.

[20] Potter R, Patterson BW, Elbert DL, Ovod V, Kasten T, Sigurdson W, Mawuenyega K, Blazey T, Goate A, Chott R, Yarasheski KE, Holtzman DM, Morris JC, Benzinger TL, Bateman RJ (2013) Increased in vivo amyloid-beta42 production, exchange, and loss in presenilin mutation carriers. *Sci Transl Med* **5**, 189ra177.

[21] St George-Hyslop PH (2000) Genetic factors in the genesis of Alzheimer's disease. *Ann N Y Acad Sci* **924**, 1-7.

[22] Shah A, Royston MC (1997) Donezepil for dementia_Shah_1997_.pdf>. *Journal of the royal society of medicine* **90**, 531-532.

[23] Bartsch T, Falkai P (2014) *Gedächtnisstörungen: Diagnostik und Rehabilitation*, Springer Berlin Heidelberg.

[24] Estler CJ, Schmidt H (2007) *Pharmakologie und Toxikologie: für Studium und Praxis ; mit 281 Tabellen*, Schattauer.

[25] Owen RT (2016) Memantine and donepezil: a fixed drug combination for the treatment of moderate to severe Alzheimer's dementia. *Drugs Today (Barc)* **52**, 239-248.

[26] Ali TB, Schleret TR, Reilly BM, Chen WY, Abagyan R (2015) Adverse Effects of Cholinesterase Inhibitors in Dementia, According to the Pharmacovigilance Databases of the United-States and Canada. *PLoS One* **10**, e0144337.
[27] Canter RG, Penney J, Tsai LH (2016) The road to restoring neural circuits for the treatment of Alzheimer's disease. *Nature* **539**, 187-196.
[28] Hardy JA, Higgins GA (1992) Alzheimer's disease: the amyloid cascade hypothesis. *Science* **256**, 184-185.
[29] Dammers C, Reiss K, Gremer L, Lecher J, Ziehm T, Stoldt M, Schwarten M, Willbold D (2017) Pyroglutamate-Modified Amyloid-beta(3-42) Shows alpha-Helical Intermediates before Amyloid Formation. *Biophys J* **112**, 1621-1633.
[30] Wang-Dietrich L, Funke SA, Kuhbach K, Wang K, Besmehn A, Willbold S, Cinar Y, Bannach O, Birkmann E, Willbold D (2013) The amyloid-beta oligomer count in cerebrospinal fluid is a biomarker for Alzheimer's disease. *J Alzheimers Dis* **34**, 985-994.
[31] O'Brien RJ, Wong PC (2011) Amyloid precursor protein processing and Alzheimer's disease. *Annu Rev Neurosci* **34**, 185-204.
[32] Walsh DM, Klyubin I, Fadeeva JV, Rowan MJ, Selkoe DJ (2002) Amyloid-beta oligomers: their production, toxicity and therapeutic inhibition. *Biochemical Society Transactions* **30**, 552-557.
[33] Giuffrida ML, Caraci F, Pignataro B, Cataldo S, De Bona P, Bruno V, Molinaro G, Pappalardo G, Messina A, Palmigiano A, Garozzo D, Nicoletti F, Rizzarelli E, Copani A (2009) Beta-amyloid monomers are neuroprotective. *J Neurosci* **29**, 10582-10587.
[34] Nag S, Sarkar B, Bandyopadhyay A, Sahoo B, Sreenivasan VK, Kombrabail M, Muralidharan C, Maiti S (2011) Nature of the amyloid-beta monomer and the monomer-oligomer equilibrium. *J Biol Chem* **286**, 13827-13833.
[35] Wolff M, Zhang-Haagen B, Decker C, Barz B, Schneider M, Biehl R, Radulescu A, Strodel B, Willbold D, Nagel-Steger L (2017) Abeta42 pentamers/hexamers are the smallest detectable oligomers in solution. *Sci Rep* **7**, 2493.
[36] Haass C, Selkoe DJ (2007) Soluble protein oligomers in neurodegeneration: lessons from the Alzheimer's amyloid beta-peptide. *Nat Rev Mol Cell Biol* **8**, 101-112.
[37] Gremer L, Scholzel D, Schenk C, Reinartz E, Labahn J, Ravelli RBG, Tusche M, Lopez-Iglesias C, Hoyer W, Heise H, Willbold D, Schroder GF (2017) Fibril structure of amyloid-beta(1-42) by cryo-electron microscopy. *Science* **358**, 116-119.
[38] Sultana R, Perluigi M, Allan Butterfield D (2013) Lipid peroxidation triggers neurodegeneration: a redox proteomics view into the Alzheimer disease brain. *Free Radic Biol Med* **62**, 157-169.
[39] LaFerla FM, Glabe C, Green K, Blurton-Jones M, Oddo S, Parachikowa A, Whalley K, Nicholson C, Lee K (2008) Aβ and Tau in Alzheimer's disease. *Nature Reviews Neuroscience*, poster.
[40] Malito E, Hulse RE, Tang WJ (2008) Amyloid beta-degrading cryptidases: insulin degrading enzyme, presequence peptidase, and neprilysin. *Cell Mol Life Sci* **65**, 2574-2585.
[41] Pacheco-Quinto J, Herdt A, Eckman CB, Eckman EA (2013) Endothelin-converting enzymes and related metalloproteases in Alzheimer's disease. *J Alzheimers Dis* **33 Suppl 1**, S101-110.
[42] Gong Y, Lippa CF (2010) Review: disruption of the postsynaptic density in Alzheimer's disease and other neurodegenerative dementias. *Am J Alzheimers Dis Other Demen* **25**, 547-555.
[43] Kumar-Singh S (2008) Cerebral amyloid angiopathy: pathogenetic mechanisms and link to dense amyloid plaques. *Genes Brain Behav* **7 Suppl 1**, 67-82.
[44] Zempel H, Mandelkow E (2014) Lost after translation: missorting of Tau protein and consequences for Alzheimer disease. *Trends Neurosci* **37**, 721-732.
[45] Selkoe DJ, Hardy J (2016) The amyloid hypothesis of Alzheimer's disease at 25 years. *EMBO Mol Med* **8**, 595-608.
[46] Lewis J, Dickson DW, Lin WL, Chisholm L, Corral A, Jones G, Yen SH, Sahara N, Skipper L, Yager D, Eckman C, Hardy J, Hutton M, McGowan E (2001) Enhanced neurofibrillary degeneration in transgenic mice expressing mutant tau and APP. *Science* **293**, 1487-1491.
[47] Jonsson T, Atwal JK, Steinberg S, Snaedal J, Jonsson PV, Bjornsson S, Stefansson H, Sulem P, Gudbjartsson D, Maloney J, Hoyte K, Gustafson A, Liu Y, Lu Y, Bhangale T, Graham RR, Huttenlocher J, Bjornsdottir G, Andreassen OA, Jonsson EG, Palotie A, Behrens TW, Magnusson OT, Kong A, Thorsteinsdottir U, Watts RJ, Stefansson K (2012) A mutation in APP protects against Alzheimer's disease and age-related cognitive decline. *Nature* **488**, 96-99.
[48] Doody RS, Thomas RG, Farlow M, Iwatsubo T, Vellas B, Joffe S, Kieburtz K, Raman R, Sun X, Aisen PS, Siemers E, Liu-Seifert H, Mohs R, Alzheimer's Disease Cooperative Study

Steering C, Solanezumab Study G (2014) Phase 3 trials of solanezumab for mild-to-moderate Alzheimer's disease. *N Engl J Med* **370**, 311-321.

[49] Braak H, Braak E (1991) Neuropathological stageing of Alheimer-related changes. *Acta Neuropathologica* **82**, 239-259.

[50] Jack CR, Jr., Knopman DS, Jagust WJ, Shaw LM, Aisen PS, Weiner MW, Petersen RC, Trojanowski JQ (2010) Hypothetical model of dynamic biomarkers of the Alzheimer's pathological cascade. *Lancet Neurol* **9**, 119-128.

[51] Schaffer C, Sarad N, DeCrumpe A, Goswami D, Herrmann S, Morales J, Patel P, Osborne J (2015) Biomarkers in the Diagnosis and Prognosis of Alzheimer's Disease. *J Lab Autom* **20**, 589-600.

[52] Sevigny J, Chiao P, Bussiere T, Weinreb PH, Williams L, Maier M, Dunstan R, Salloway S, Chen T, Ling Y, O'Gorman J, Qian F, Arastu M, Li M, Chollate S, Brennan MS, Quintero-Monzon O, Scannevin RH, Arnold HM, Engber T, Rhodes K, Ferrero J, Hang Y, Mikulskis A, Grimm J, Hock C, Nitsch RM, Sandrock A (2016) The antibody aducanumab reduces Abeta plaques in Alzheimer's disease. *Nature* **537**, 50-56.

[53] Fuller JP, Stavenhagen JB, Christensen S, Kartberg F, Glennie MJ, Teeling JL (2015) Comparing the efficacy and neuroinflammatory potential of three anti-abeta antibodies. *Acta Neuropathol* **130**, 699-711.

[54] Farlow MR, Andreasen N, Riviere ME, Vostiar I, Vitaliti A, Sovago J, Caputo A, Winblad B, Graf A (2015) Long-term treatment with active Abeta immunotherapy with CAD106 in mild Alzheimer's disease. *Alzheimers Res Ther* **7**, 23.

[55] Yan R (2016) Stepping closer to treating Alzheimer's disease patients with BACE1 inhibitor drugs. *Transl Neurodegener* **5**, 13.

[56] Vassar R (2014) BACE1 inhibitor drugs in clinical trials for Alzheimer's disease. *Alzheimers Res Ther* **6**.

[57] Panza F, Solfrizzi V, Seripa D, Imbimbo BP, Lozupone M, Santamato A, Zecca C, Barulli MR, Bellomo A, Pilotto A, Daniele A, Greco A, Logroscino G (2016) Tau-Centric Targets and Drugs in Clinical Development for the Treatment of Alzheimer's Disease. *Biomed Res Int* **2016**, 3245935.

[58] Kontsekova E, Zilka N, Kovacech B, Novak P, Novak M (2014) First-in-man tau vaccine targeting structural determinants essential for pathological tau-tau interaction reduces tau oligomerisation and neurofibrillary degeneration in an Alzheimer's disease model. *Alzheimers Res Ther* **6**, 44.

[59] Novak P, Schmidt R, Kontsekova E, Zilka N, Kovacech B, Skrabana R, Vince-Kazmerova Z, Katina S, Fialova L, Prcina M, Parrak V, Dal-Bianco P, Brunner M, Staffen W, Rainer M, Ondrus M, Ropele S, Smisek M, Sivak R, Winblad B, Novak M (2017) Safety and immunogenicity of the tau vaccine AADvac1 in patients with Alzheimer's disease: a randomised, double-blind, placebo-controlled, phase 1 trial. *Lancet Neurol* **16**, 123-134.

[60] DeVos SL, Miller RL, Schoch KM, Holmes BB, Kebodeaux CS, Wegener AJ, Chen G, Shen T, Tran H, Nichols B, Zanardi TA, Kordasiewicz HB, Swayze EE, Bennett CF, Diamond MI, Miller TM (2017) Tau reduction prevents neuronal loss and reverses pathological tau deposition and seeding in mice with tauopathy. *Sci Transl Med* **9**.

[61] Sanchez PE, Zhu L, Verret L, Vossel KA, Orr AG, Cirrito JR, Devidze N, Ho K, Yu GQ, Palop JJ, Mucke L (2012) Levetiracetam suppresses neuronal network dysfunction and reverses synaptic and cognitive deficits in an Alzheimer's disease model. *Proc Natl Acad Sci U S A* **109**, E2895-2903.

[62] Nygaard HB, Wagner AF, Bowen GS, Good SP, MacAvoy MG, Strittmatter KA, Kaufman AC, Rosenberg BJ, Sekine-Konno T, Varma P, Chen K, Koleske AJ, Reiman EM, Strittmatter SM, van Dyck CH (2015) A phase Ib multiple ascending dose study of the safety, tolerability, and central nervous system availability of AZD0530 (saracatinib) in Alzheimer's disease. *Alzheimers Res Ther* **7**, 35.

[63] Freiherr J, Hallschmid M, Frey WH, 2nd, Brunner YF, Chapman CD, Holscher C, Craft S, De Felice FG, Benedict C (2013) Intranasal insulin as a treatment for Alzheimer's disease: a review of basic research and clinical evidence. *CNS Drugs* **27**, 505-514.

[64] Cummings J, Scheltens P, McKeith I, Blesa R, Harrison JE, Bertolucci PH, Rockwood K, Wilkinson D, Wijker W, Bennett DA, Shah RC (2017) Effect Size Analyses of Souvenaid in Patients with Alzheimer's Disease. *J Alzheimers Dis* **55**, 1131-1139.

[65] Coelho FG, Vital TM, Stein AM, Arantes FJ, Rueda AV, Camarini R, Teodorov E, Santos-Galduroz RF (2014) Acute aerobic exercise increases brain-derived neurotrophic factor levels in elderly with Alzheimer's disease. *J Alzheimers Dis* **39**, 401-408.

[66] Schumacher TNM, Mayr LM, Minor DL, Milhollen MA, Burgess MW, Kim PS (1996) Identification of D-peptide ligands through mirror-image phage display. *Science* **271**, 1854-1857.

[67] Wiesehan K, Willbold D (2003) Mirror-image phage display: aiming at the mirror. *Chembiochem* **4**, 811-815.

[68] Wiesehan K, Buder K, Linke RP, Patt S, Stoldt M, Unger E, Schmitt B, Bucci E, Willbold D (2003) Selection of D-amino-acid peptides that bind to Alzheimer's disease amyloid peptide abeta1-42 by mirror image phage display. *Chembiochem* **4**, 748-753.

[69] Wiesehan K, Stohr J, Nagel-Steger L, van Groen T, Riesner D, Willbold D (2008) Inhibition of cytotoxicity and amyloid fibril formation by a D-amino acid peptide that specifically binds to Alzheimer's disease amyloid peptide. *Protein Eng Des Sel* **21**, 241-246.

[70] Funke SA, Willbold D (2009) Mirror image phage display--a method to generate D-peptide ligands for use in diagnostic or therapeutical applications. *Mol Biosyst* **5**, 783-786.

[71] van Groen T, Wiesehan K, Funke SA, Kadish I, Nagel-Steger L, Willbold D (2008) Reduction of Alzheimer's disease amyloid plaque load in transgenic mice by D3, A D-enantiomeric peptide identified by mirror image phage display. *ChemMedChem* **3**, 1848-1852.

[72] van Groen T, Kadish I, Wiesehan K, Funke SA, Willbold D (2009) In vitro and in vivo staining characteristics of small, fluorescent, Abeta42-binding D-enantiomeric peptides in transgenic AD mouse models. *ChemMedChem* **4**, 276-282.

[73] Olubiyi OO, Strodel B (2012) Structures of the amyloid beta-peptides Abeta1-40 and Abeta1-42 as influenced by pH and a D-peptide. *J Phys Chem B* **116**, 3280-3291.

[74] Brener O, Dunkelmann T, Gremer L, van Groen T, Mirecka EA, Kadish I, Willuweit A, Kutzsche J, Jurgens D, Rudolph S, Tusche M, Bongen P, Pietruszka J, Oesterhelt F, Langen KJ, Demuth HU, Janssen A, Hoyer W, Funke SA, Nagel-Steger L, Willbold D (2015) QIAD assay for quantitating a compound's efficacy in elimination of toxic Abeta oligomers. *Sci Rep* **5**, 13222.

[75] Funke SA, van Groen T, Kadish I, Bartnik D, Nagel-Steger L, Brener O, Sehl T, Batra-Safferling R, Moriscot C, Schoehn G, Horn AH, Muller-Schiffmann A, Korth C, Sticht H, Willbold D (2010) Oral treatment with the d-enantiomeric peptide D3 improves the pathology and behavior of Alzheimer's Disease transgenic mice. *ACS Chem Neurosci* **1**, 639-648.

[76] Bartnik D, Funke SA, Andrei-Selmer L-C, Bacher M, Dodel R, Willbold D (2010) Diffenrently Selected D-Enantiomeric Peptides Act on Different Aβ Species. *Rejuvenation Res.* **13**, 202-205.

[77] Frenzel D, Gluck JM, Brener O, Oesterhelt F, Nagel-Steger L, Willbold D (2014) Immobilization of homogeneous monomeric, oligomeric and fibrillar Abeta species for reliable SPR measurements. *PLoS One* **9**, e89490.

[78] Olubiyi OO, Frenzel D, Bartnik D, Gluck JM, Brener O, Nagel-Steger L, Funke SA, Willbold D, Strodel B (2014) Amyloid Aggregation Inhibitory Mechanism of Arginine-rich D-peptides. *Current Medicinal Chemistry* **21**, 1448-1457.

[79] Funke SA, Liu H, Sehl T, Bartnik D, Brener O, Nagel-Steger L, Wiesehan K, Willbold D (2012) Identification and characterization of an abeta oligomer precipitating peptide that may be useful to explore gene therapeutic approaches to Alzheimer disease. *Rejuvenation Res* **15**, 144-147.

[80] van Groen T, Schemmert S, Brener O, Gremer L, Ziehm T, Tusche M, Nagel-Steger L, Kadish I, Schartmann E, Elfgen A, Jurgens D, Willuweit A, Kutzsche J, Willbold D (2017) The Abeta oligomer eliminating D-enantiomeric peptide RD2 improves cognition without changing plaque pathology. *Sci Rep* **7**, 16275.

[81] Elfgen A, Santiago-Schubel B, Gremer L, Kutzsche J, Willbold D (2017) Surprisingly high stability of the Abeta oligomer eliminating all-d-enantiomeric peptide D3 in media simulating the route of orally administered drugs. *Eur J Pharm Sci* **107**, 203-207.

[82] Jiang N, Leithold LH, Post J, Ziehm T, Mauler J, Gremer L, Cremer M, Schartmann E, Shah NJ, Kutzsche J, Langen KJ, Breitkreutz J, Willbold D, Willuweit A (2015) Preclinical Pharmacokinetic Studies of the Tritium Labelled D-Enantiomeric Peptide D3 Developed for the Treatment of Alzheimer s Disease. *PLoS One* **10**, e0128553.

[83] Leithold LH, Jiang N, Post J, Ziehm T, Schartmann E, Kutzsche J, Shah NJ, Breitkreutz J, Langen KJ, Willuweit A, Willbold D (2016) Pharmacokinetic Properties of a Novel D-Peptide Developed to be Therapeutically Active Against Toxic beta-Amyloid Oligomers. *Pharm Res* **33**, 328-336.

[84] Leithold LH, Jiang N, Post J, Niemietz N, Schartmann E, Ziehm T, Kutzsche J, Shah NJ, Breitkreutz J, Langen KJ, Willuweit A, Willbold D (2016) Pharmacokinetic properties of tandem d-peptides designed for treatment of Alzheimer's disease. *Eur J Pharm Sci* **89**, 31-38.

[85] Schartmann E, Schemmert S, Ziehm T, Leithold LHE, Jiang N, Tusche M, Joni Shah N, Langen KJ, Kutzsche J, Willbold D, Willuweit A (2017) Comparison of blood-brain barrier penetration efficiencies between linear and cyclic all-d-enantiomeric peptides developed for the treatment of Alzheimer's disease. *Eur J Pharm Sci* **114**, 93-102.

[86] Hupert M, Elfgen A, Schartmann E, Schemmert S, Buscher B, Kutzsche J, Willbold D, Santiago-Schubel B (2017) Development and validation of an UHPLC-ESI-QTOF-MS method for quantification of the highly hydrophilic amyloid-beta oligomer eliminating all-D-enantiomeric peptide RD2 in mouse plasma. *J Chromatogr B Analyt Technol Biomed Life Sci* **1073**, 123-129.

[87] Kutzsche J, Schemmert S, Tusche M, Neddens J, Rabl R, Jurgens D, Brener O, Willuweit A, Hutter-Paier B, Willbold D (2017) Large-Scale Oral Treatment Study with the Four Most Promising D3-Derivatives for the Treatment of Alzheimer's Disease. *Molecules* **22**.

[88] Dunkelmann T, Teichmann K, Ziehm T, Schemmert S, Frenzel D, Tusche M, Dammers C, Jürgens D, Langen K-J, Demuth H-U, Shah NJ, Kutzsche J, Willuweit A, Willbold D (2017) Aβ oligomer eliminating compounds interfere successfully with pEAβ (3–42) induced motor neurodegenerative phenotype in transgenic mice. *Neuropeptides*.

[89] Ziehm T, Brener O, van Groen T, Kadish I, Frenzel D, Tusche M, Kutzsche J, Reiss K, Gremer L, Nagel-Steger L, Willbold D (2016) Increase of Positive Net Charge and Conformational Rigidity Enhances the Efficacy of d-Enantiomeric Peptides Designed to Eliminate Cytotoxic Abeta Species. *ACS Chem Neurosci* **7**, 1088-1096.

[90] Klein AN, Ziehm T, van Groen T, Kadish I, Elfgen A, Tusche M, Thomaier M, Reiss K, Brener O, Gremer L, Kutzsche J, Willbold D (2017) Optimization of D-peptides for Aβ monomer binding specificity enhances their potential to eliminate toxic Aβ oligomers. *ACS Chem Neurosci*.

[91] Benkert O, Hautzinger M, Graf-Morgenstern M (2012) Pharmakokinetik, Pharmakodynamik und Interaktionen In *Psychopharmakologischer Leitfaden für Psychologen und Psychotherapeuten* Springer-Verlag Berlin Heidelberg, pp. 11-20.

[92] Jankowsky JL, Fadale DJ, Anderson J, Xu GM, Gonzales V, Jenkins NA, Copeland NG, Lee MK, Younkin LH, Wagner SL, Younkin SG, Borchelt DR (2004) Mutant presenilins specifically elevate the levels of the 42 residue beta-amyloid peptide in vivo: evidence for augmentation of a 42-specific gamma secretase. *Hum Mol Genet* **13**, 159-170.

[93] Kamphuis W, Mamber C, Moeton M, Kooijman L, Sluijs JA, Jansen AH, Verveer M, de Groot LR, Smith VD, Rangarajan S, Rodriguez JJ, Orre M, Hol EM (2012) GFAP isoforms in adult mouse brain with a focus on neurogenic astrocytes and reactive astrogliosis in mouse models of Alzheimer disease. *PLoS One* **7**, e42823.

[94] Jackson RJ, Rudinskiy N, Herrmann AG, Croft S, Kim JM, Petrova V, Ramos-Rodriguez JJ, Pitstick R, Wegmann S, Garcia-Alloza M, Carlson GA, Hyman BT, Spires-Jones TL (2016) Human tau increases amyloid beta plaque size but not amyloid beta-mediated synapse loss in a novel mouse model of Alzheimer's disease. *Eur J Neurosci* **44**, 3056-3066.

[95] van Groen T, Kadish I, Funke A, Bartnik D, Willbold D (2012) Treatment with Abeta42 binding D-amino acid peptides reduce amyloid deposition and inflammation in APP/PS1 double transgenic mice. *Adv Protein Chem Struct Biol* **88**, 133-152.

[96] van Groen T, Kadish I, Funke SA, Bartnik D, Willbold D (2013) Treatment with D3 removes amyloid deposits, reduces inflammation, and improves cognition in aged AbetaPP/PS1 double transgenic mice. *J Alzheimers Dis* **34**, 609-620.

[97] Herdegen T, Böhm R, Culman J, Gohlke P, Luippold G (2013) *Kurzlehrbuch Pharmakologie und Toxikologie*, Thieme.

[98] Wehling M, Diener HC (2005) *Klinische Pharmakologie*, Thieme.

[99] Fox SC (2014) *Remington Education Pharmaceutics*, Pharmaceutical Press.

[100] Hein L (2011) Pharmakokinetik In *Pharmakotherapie in der Anästhesie und Intensivmedizin*, Tonner PH, Hein L, eds. Springer Berlin Heidelberg, Berlin, Heidelberg, pp. 3-14.

[101] Lüllmann H, Mohr K, Hein L (2008) *Taschenatlas Pharmakologie*, Thieme.

[102] Freissmuth M, Offermanns S, Böhm S (2012, 2016) *Pharmakologie und Toxikologie - Von den molekularen Grundlagen zur Pharmakotherapie*, Springer.

[103] Kwon Y (2007) *Handbook of Essential Pharmacokinetics, Pharmacodynamics and Drug Metabolism for Industrial Scientists*, Springer US.

[104] Hladky SB (1990) *Pharmacokinetics*, Manchester University Press.

[105] Pahnke J, Langer O, Krohn M (2014) Alzheimer's and ABC transporters--new opportunities for diagnostics and treatment. *Neurobiol Dis* **72 Pt A**, 54-60.

[106] Storck SE, Meister S, Nahrath J, Meissner JN, Schubert N, Di Spiezio A, Baches S, Vandenbroucke RE, Bouter Y, Prikulis I, Korth C, Weggen S, Heimann A, Schwaninger M,

Bayer TA, Pietrzik CU (2016) Endothelial LRP1 transports amyloid-beta(1-42) across the blood-brain barrier. *J Clin Invest* **126**, 123-136.

[107] Van Dorpe S, Bronselaer A, Nielandt J, Stalmans S, Wynendaele E, Audenaert K, Van De Wiele C, Burvenich C, Peremans K, Hsuchou H, De Tre G, De Spiegeleer B (2012) Brainpeps: the blood-brain barrier peptide database. *Brain Struct Funct* **217**, 687-718.

[108] Stalmans S, Bracke N, Wynendaele E, Gevaert B, Peremans K, Burvenich C, Polis I, De Spiegeleer B (2015) Cell-Penetrating Peptides Selectively Cross the Blood-Brain Barrier In Vivo. *PLoS One* **10**, e0139652.

[109] Bickel U (2005) How to measure drug transport across the blood-brain barrier. *NeuroRx* **2**, 15-26.

[110] Blasberg RG, Fenstermacher JD, Patlak CS (1983) Transport of alpha-aminoisobutyric acid across brain capillary and cellular membranes. *J Cereb Blood Flow Metab* **3**, 8-32.

[111] Muir ER, Shen Q, Duong TQ (2008) Cerebral blood flow MRI in mice using the cardiac-spin-labeling technique. *Magn Reson Med* **60**, 744-748.

[112] Weidman EK, Foley CP, Kallas O, Dyke JP, Gupta A, Giambrone AE, Ivanidze J, Baradaran H, Ballon DJ, Sanelli PC (2016) Evaluating Permeability Surface Area Product as a Measure of Blood Brain Barrier Permeability in a Murine Model. *AJNR Am J Neuroradiol* **37**, 1267-1274.

[113] Singh SS (2006) Preclinical pharmacokinetics: an approach towards safer and efficacious drugs. *Curr Drug Metab* **7**, 165-182.

[114] Pardridge WM (2016) CSF, blood-brain barrier, and brain drug delivery. *Expert Opin Drug Deliv* **13**, 963-975.

[115] Jiang N, Frenzel D, Schartmann E, van Groen T, Kadish I, Shah NJ, Langen KJ, Willbold D, Willuweit A (2016) Blood-brain barrier penetration of an Abeta-targeted, arginine-rich, d-enantiomeric peptide. *Biochim Biophys Acta* **1858**, 2717-2724.

[116] Futaki S, Goto S, Sugiura Y (2003) Membrane permeability commonly shared among arginine-rich peptides. *J Mol Recognit* **16**, 260-264.

[117] Vives E, Brodin P, Lebleu B (1997) A truncated HIV-1 Tat protein basic domain rapidly translocates through the plasma membrane and accumulates in the cell nucleus. *Journal of Biological Chemistry* **272**, 16010-16017.

[118] Stalmans S, Gevaert B, Wynendaele E, Nielandt J, De Tre G, Peremans K, Burvenich C, De Spiegeleer B (2015) Classification of Peptides According to their Blood-Brain Barrier Influx. *Protein Pept Lett* **22**, 768-775.

[119] Van Dorpe S, Adriaens A, Polis I, Peremans K, Van Bocxlaer J, De Spiegeleer B (2010) Analytical characterization and comparison of the blood-brain barrier permeability of eight opioid peptides. *Peptides* **31**, 1390-1399.

[120] Morris RG, Garrud P, Rawlins JN, O'Keefe J (1982) Place navigation impaired in rats with hippocampal lesions. *Nature* **297**, 681-683.

X. Druckgenehmigungen

3.1 Preclinical Pharmacokinetic Studies of the Tritium Labelled D-Enantiomeric Peptide D3 Developed for the Treatment of Alzheimer's Disease → <u>open access</u>

3.2 Pharmacokinetic Properties of a Novel D-Peptide Developed to be Therapeutically Active Against Toxic beta-Amyloid Oligomers

SPRINGER NATURE LICENSE TERMS AND CONDITIONS

Jan 23, 2018

This Agreement between Research Center Juelich GmbH, ICS -- Elena Schartmann ("You") and Springer Nature ("Springer Nature") consists of your license details and the terms and conditions provided by Springer Nature and Copyright Clearance Center.

License Number	4274830795167
License date	Jan 23, 2018
Licensed Content Publisher	Springer Nature
Licensed Content Publication	Pharmaceutical Research
Licensed Content Title	Pharmacokinetic Properties of a Novel d-Peptide Developed to be Therapeutically Active Against Toxic β-Amyloid Oligomers
Licensed Content Author	Leonie H. E. Leithold, Nan Jiang, Julia Post et al
Licensed Content Date	Jan 1, 2015
Licensed Content Volume	33
Licensed Content Issue	2
Type of Use	Thesis/Dissertation
Requestor type	academic/university or research institute
Format	print and electronic
Portion	full article/chapter
Will you be translating?	no
Circulation/distribution	<501
Author of this Springer Nature content	yes
Title	Prof.
Instructor name	Dieter Willbold
Institution name	Forschungszentrum Juelich GmbH
Expected presentation date	Mar 2018
Portions	full article
Requestor Location	Research Center Juelich GmbH, ICS-6 Wilhelm-Johnen-Straße Juelich, NRW 52426 Germany Attn: Research Center Juelich GmbH, ICS-6
Billing Type	Invoice
Billing Address	Research Center Juelich GmbH, ICS-6 Wilhelm-Johnen-Straße Juelich, Germany 52426 Attn: Research Center Juelich GmbH, ICS-6
Total	0.00 EUR

Terms and Conditions

Springer Nature Terms and Conditions for RightsLink Permissions

Springer Customer Service Centre GmbH (the Licensor) hereby grants you a non-exclusive, world-wide licence to reproduce the material and for the purpose and requirements specified in the attached copy of your order form, and for no other use, subject to the conditions below:

1. The Licensor warrants that it has, to the best of its knowledge, the rights to license reuse of this material. However, you should ensure that the material you are requesting is original to the Licensor and does not carry the copyright of another entity (as credited in the published version).

   If the credit line on any part of the material you have requested indicates that it was reprinted or adapted with permission from another source, then you should also seek permission from that source to reuse the material.

2. Where **print only** permission has been granted for a fee, separate permission must be obtained for any additional electronic re-use.

3. Permission granted **free of charge** for material in print is also usually granted for any electronic version of that work, provided that the material is incidental to your work as a whole and that the electronic version is essentially equivalent to, or substitutes for, the print version.

4. A licence for 'post on a website' is valid for 12 months from the licence date. This licence does not cover use of full text articles on websites.

5. Where '**reuse in a dissertation/thesis**' has been selected the following terms apply: Print rights for up to 100 copies, electronic rights for use only on a personal website or institutional repository as defined by the Sherpa guideline (www.sherpa.ac.uk/romeo/).

6. Permission granted for books and journals is granted for the lifetime of the first edition and does not apply to second and subsequent editions (except where the first edition permission was granted free of charge or for signatories to the STM Permissions Guidelines http://www.stm-assoc.org/copyright-legal-affairs/permissions/permissions-guidelines/), and does not apply for editions in other languages unless additional translation rights have been granted separately in the licence.

7. Rights for additional components such as custom editions and derivatives require additional permission and may be subject to an additional fee. Please apply to Journalpermissions@springernature.com/bookpermissions@springernature.com for these rights.

8. The Licensor's permission must be acknowledged next to the licensed material in print. In electronic form, this acknowledgement must be visible at the same time as the figures/tables/illustrations or abstract, and must be hyperlinked to the journal/book's homepage. Our required acknowledgement format is in the Appendix below.

9. Use of the material for incidental promotional use, minor editing privileges (this does not include cropping, adapting, omitting material or any other changes that affect the meaning, intention or moral rights of the author) and copies for the disabled are permitted under this licence.

10. Minor adaptations of single figures (changes of format, colour and style) do not require the Licensor's approval. However, the adaptation should be credited as shown in Appendix below.

Appendix — Acknowledgements:

For Journal Content:
Reprinted by permission from **[the Licensor]**: **[Journal Publisher** (e.g. Nature Springer Palgrave)] **[JOURNAL NAME] [REFERENCE CITATION** (Article name, Author(s) Name), **[COPYRIGHT]** (year of publication)

For **Advance Online Publication papers:**
Reprinted by permission from **[the Licensor]**: **[Journal Publisher** (e.g. Nature Springer Palgrave)] **[JOURNAL NAME] [REFERENCE CITATION** (Article name, Author(s) Name), **[COPYRIGHT]** (year of publication), advance online publication, day month year (doi: 10.1038/sj.[JOURNAL ACRONYM])

For Adaptations/Translations:
Adapted/Translated by permission from **[the Licensor]**: **[Journal Publisher** (e.g. Nature Springer Palgrave)] **[JOURNAL NAME] [REFERENCE CITATION** (Article name, Author(s) Name), **[COPYRIGHT]** (year of publication)

Note: For any republication from the British Journal of Cancer, the following credit line style applies:

Reprinted/adapted/translated by permission from **[the Licensor]**: on behalf of Cancer Research UK: : **[Journal Publisher** (e.g. Nature Springer Palgrave)] **[JOURNAL NAME] [REFERENCE CITATION** (Article name, Author(s) Name), **[COPYRIGHT]** (year of publication)

For **Advance Online Publication** papers:
Reprinted by permission from The **[the Licensor]**: on behalf of Cancer Research UK: **[Journal Publisher** (e.g. Nature Springer Palgrave)] **[JOURNAL NAME] [REFERENCE CITATION** (Article name, Author(s) Name), **[COPYRIGHT]** (year of publication), advance online publication, day month year (doi: 10.1038/sj.[JOURNAL ACRONYM])

For Book content:
Reprinted/adapted by permission from **[the Licensor]**: **[Book Publisher** (e.g. Palgrave Macmillan, Springer etc) **[Book Title]** by **[Book author(s)]** **[COPYRIGHT]** (year of publication)

X. Druckgenehmigungen

3.3 Pharmacokinetic properties of tandem D-peptides designed for treatment of Alzheimer's disease

Copyright Clearance Center RightsLink®

Home | Create Account | Help

Title: Pharmacokinetic properties of tandem d-peptides designed for treatment of Alzheimer's disease

Author: Leonie H.E. Leithold,Nan Jiang,Julia Post,Nicole Niemietz,Elena Schartmann,Tamar Ziehm,Janine Kutzsche,N. Jon Shah,Jörg Breitkreutz,Karl-Josef Langen,Antje Willuweit,Dieter Willbold

Publication: European Journal of Pharmaceutical Sciences

Publisher: Elsevier

Date: 30 June 2016

© 2016 Elsevier B.V. All rights reserved.

LOGIN

If you're a copyright.com user, you can login to RightsLink using your copyright.com credentials. Already a RightsLink user or want to learn more?

Please note that, as the author of this Elsevier article, you retain the right to include it in a thesis or dissertation, provided it is not published commercially. Permission is not required, but please ensure that you reference the journal as the original source. For more information on this and on your other retained rights, please visit: https://www.elsevier.com/about/our-business/policies/copyright#Author-rights

BACK | CLOSE WINDOW

Copyright © 2018 Copyright Clearance Center, Inc. All Rights Reserved. Privacy statement. Terms and Conditions.
Comments? We would like to hear from you. E-mail us at customercare@copyright.com

3.4 Blood-brain barrier penetration of an Aβ-targeted, arginine-rich, D-enantiomeric peptide

Copyright Clearance Center RightsLink®

Home | Create Account | Help

Title: Blood-brain barrier penetration of an Aβ-targeted, arginine-rich, d-enantiomeric peptide

Author: Nan Jiang,Daniel Frenzel,Elena Schartmann,Thomas van Groen,Inga Kadish,N. Jon Shah,Karl-Josef Langen,Dieter Willbold,Antje Willuweit

Publication: Biochimica et Biophysica Acta (BBA) - Biomembranes

Publisher: Elsevier

Date: November 2016

© 2016 Elsevier B.V.

LOGIN

If you're a copyright.com user, you can login to RightsLink using your copyright.com credentials. Already a RightsLink user or want to learn more?

Please note that, as the author of this Elsevier article, you retain the right to include it in a thesis or dissertation, provided it is not published commercially. Permission is not required, but please ensure that you reference the journal as the original source. For more information on this and on your other retained rights, please visit: https://www.elsevier.com/about/our-business/policies/copyright#Author-rights

BACK | CLOSE WINDOW

Copyright © 2018 Copyright Clearance Center, Inc. All Rights Reserved. Privacy statement. Terms and Conditions.
Comments? We would like to hear from you. E-mail us at customercare@copyright.com

X. Druckgenehmigungen

3.5 The Aβ oligomer eliminating D-enantiomeric peptide RD2 improves cognition without changing plaque pathology → open access

3.6 Comparison of blood-brain barrier penetration efficiencies between linear and cyclic all-D-enantiomeric peptides developed for the treatment of Alzheimer's disease

Copyright Clearance Center RightsLink®

Home | Create Account | Help

Title: Comparison of blood-brain barrier penetration efficiencies between linear and cyclic all-d-enantiomeric peptides developed for the treatment of Alzheimer's disease

Author: Elena Schartmann,Sarah Schemmert,Tamar Ziehm,Leonie H.E. Leithold,Nan Jiang,Markus Tusche,N. Joni Shah,Karl-Josef Langen,Janine Kutzsche,Dieter Willbold,Antje Willuweit

Publication: European Journal of Pharmaceutical Sciences

Publisher: Elsevier

Date: 1 March 2018

© 2017 Elsevier B.V. All rights reserved.

LOGIN

If you're a copyright.com user, you can login to RightsLink using your copyright.com credentials. Already a RightsLink user or want to learn more?

Please note that, as the author of this Elsevier article, you retain the right to include it in a thesis or dissertation, provided it is not published commercially. Permission is not required, but please ensure that you reference the journal as the original source. For more information on this and on your other retained rights, please visit: https://www.elsevier.com/about/our-business/policies/copyright#Author-rights

BACK | CLOSE WINDOW

Copyright © 2018 Copyright Clearance Center, Inc. All Rights Reserved. Privacy statement. Terms and Conditions.
Comments? We would like to hear from you. E-mail us at customercare@copyright.com

3.7 Development and validation of an UHPLC-ESI-QTOF-MS method for quantification of the highly hydrophilic amyloid-β oligomer eliminating all-D-enantiomeric peptide RD2 in mouse plasma

Copyright Clearance Center RightsLink®

Home | Create Account | Help

Title: Development and validation of an UHPLC-ESI-QTOF-MS method for quantification of the highly hydrophilic amyloid-β oligomer eliminating all-D-enantiomeric peptide RD2 in mouse plasma

Author: Michelle Hupert,Anne Elfgen,Elena Schartmann,Sarah Schemmert,Brigitte Buscher,Janine Kutzsche,Dieter Willbold,Beatrix Santiago-Schübel

Publication: Journal of Chromatography B

Publisher: Elsevier

Date: 15 January 2018

© 2017 Elsevier B.V. All rights reserved.

LOGIN

If you're a copyright.com user, you can login to RightsLink using your copyright.com credentials. Already a RightsLink user or want to learn more?

Please note that, as the author of this Elsevier article, you retain the right to include it in a thesis or dissertation, provided it is not published commercially. Permission is not required, but please ensure that you reference the journal as the original source. For more information on this and on your other retained rights, please visit: https://www.elsevier.com/about/our-business/policies/copyright#Author-rights

BACK | CLOSE WINDOW

Copyright © 2018 Copyright Clearance Center, Inc. All Rights Reserved. Privacy statement. Terms and Conditions.
Comments? We would like to hear from you. E-mail us at customercare@copyright.com